TOWARD THE NEUROCOMPUTER: GOAL-DIRECTED LEARNING IN EMBODIED CULTURED NETWORKS

A Dissertation
Presented to
The Academic Faculty

by

Zenas C. Chao

In Partial Fulfillment
of the Requirements for the Degree
Doctor of Philosophy in the
School of Bioengineering/Biomedical Engineering

Georgia Institute of Technology
December 2007

TOWARD THE NEUROCOMPUTER: GOAL-DIRECTED LEARNING IN EMBODIED CULTURED NETWORKS

Approved by:

Dr. Steve Potter, Advisor
School of Biomedical Engineering
Georgia Institute of Technology

Dr. Robert Butera
School of Biomedical Engineering
Georgia Institute of Technology

Dr. Bob Lee
School of Biomedical Engineering
Georgia Institute of Technology

Dr. Dieter Jaeger
School of Biology
Emory University

Dr. Thomas DeMarse
School of Biomedical Engineering
University of Florida

Date Approved: October 10, 2007

To my parents and my sister

ACKNOWLEDGEMENTS

These couple nights when I had my cigarettes during the breaks between finishing up this thesis, I was trying to remember what has happened during the past six years. Everything seems to be a contradiction, I loved it as much as I hated it. But tonight, I suddenly realized that it's a beautiful contradiction, just like Muse's lyric, and I want to thanks those who made it beautiful.

I would like to start by thanking my advisor, Steve Potter. I came to the Neurolab almost a year before he did, and that was a year of confusion. The cultural shock and the language barrier kept me from reaching out to other people. Without any specific project at hand, I was hardly in the lab, and my desk was literally occupied by half a dozen undergrads. I remember how nervous I was having the first telephone interview with Steve when he was still at Caltech. What I said on the phone was no way near any complete grammatically-correct sentence, but he embraced it with understanding. That is Steve, open minded and encouraging. I also remember Steve asked about my life outside the lab in several occasions, and advised me to have a balanced life by sharing his own experiences. Of course, he sent me brochures and emails about quit-smoking programs. Even though I'm too weak to quit, I still deeply appreciate that kindness and warmness. Academically, Steve creates an atmosphere of tremendous freedom in the lab, which is the only air I can breathe. When I was struggling to continue in the Animat project, Steve agreed to let me pursue the simulation approach, which later led to a successful breakthrough. When I was stuck and made little progress, he was patient. I remember during one lab meeting, he firmly said, if not yelled, that nobody should judge other

people's progress in this lab. That is his respect for science, and is my respect for him. With his guidance, my writing finally can break free from the level of "did you write it in Taiwanese and then translate it into English by some software?". I think in the future when I look back into my years as a graduate student, Steve's smiling face will emerge from the back of my head, like a overprint on a postage stamp, along with his suspenders and fluorescent t-shirts.

It also has been a pleasure working with other people in the Potter group. There is no way I could have graduated without Radhika Madhavan, who reminded me to register every semester. Her dedication to science inspired me and made me rethink the meaning of being a scientist. I remember the first day I met her, she put a huge pile of papers on my desk (still occupied by undergrads), and gave me a deadline to read them. That was the first and only time I hated her. Besides, she was the only one who noticed every time I had a new piercing. Douglas Bakkum is an American version of me, or almost. We wrote papers together like conjoined twins. I can communicate with him, sometimes through telepathy, without any language barrier, and this makes me feel more like my real self. Also, his laidback attitude made my laidback attitude look normal, and I thank him for that. I also want to thank Tom DeMarse, who talked me out of quitting my PhD when I drove him to rent his tuxedo; John Rolston, Douglas Swehla, and Daniel Wagenaar who all helped me improve my research with their intelligence; Peter, Komal, Mark, Blythe, Nathan, Chu, and Yixiao for their invaluable friendships.

During my graduate years, I didn't really know too many people outside the Potter group. Among those few, I would like to thank Dr. Rob Butera, who praised my final term project of my very first semester to the next year students. This sadly did boost

my self-confidence, even though it might have been just a rumor. Also Dr. Bob Lee, our natural problem solver, who helped me in the PBL class and really improved my communication skills. I also thank Gelsy, Murat, Luke, and Laveeta for their wonderful company.

Finally, I'd like to thank Remus Chang, who has urged and supported me to complete my PhD since the day we met (on the internet). Even being separated by thousands of miles, even with our constant arguments, she balances and stabilizes me. I want to dedicate this work to her and to my family, my irreplaceable harbor.

Zenas 趙陳 懷

Atlanta, August 3rd, 2007.

TABLE OF CONTENTS

LIST OF TABLES

LIST OF FIGURES

LIST OF ABBREVIATIONS

BAM	Burst activity matrix
CA	Center of activity
CAT	Center of activity trajectory
CAT-ELS	Center of activity trajectory with electrode locations shuffled
CPS	Context-control probing sequence
CR	Column-row
CW	Center of weights
CWT	Center of weights trajectory
dAP	Direct electrically-evoked action potentials
FR	Firing rate
FRH	Firing rate histogram
IPI	Inter-pulse interval
JPSTH	Joint peri-stimulus time histogram
LIF	Leaky integrate-and-fire
LTD	Long-term depression
LTF	Long-term facilitation
LTP	Long-term potentiation
MASC	Mean absolute synaptic change
MEA	Multi-electrode array
MI	Mutual information
PTS	Patterned training stimulation
RBS	Random background stimulation

RPS	Random probing sequence
SBS	Shuffled background stimulation
SCCC	Shift-predictor corrected cross-correlogram
STC	Spatiotemporal complexity
STDP	Spike-timing-dependent plasticity
WIO vector	Whole-input-output vector

LIST OF SYMBOLS

C/D	Change-to-drift ratio
$PTS_{\Delta t}$	Inter-pulse interval of a PTS
PTS-E1	First electrode in a PTS
PTS-$E2_k$	Second electrode in a PTS

SUMMARY

Brains display very high-level parallel computation, fault-tolerance, and adaptability, all of which are properties that we struggle to recreate in engineered systems. The *neurocomputer* (an organic computer built from living neurons), where a complicated language is naturally programmed and organized in the system, seems possible and may lead to a new generation of computing device that can operate in a brain-like manner. Cultured neuronal networks on multi-electrode arrays (MEAs) provide a complex network connectivity pattern and greater freedom to manipulate and to access the dynamics of groups of neurons, and become one of the best candidates for the next neurocomputer.

I explored the possibility of the neurocomputer by studying whether we can show *goal-directed learning*, one of the most fascinating behavior of brains, in cultured networks. Inspired by the brain, which needs to be embodied in some way and interact with its surroundings in order to give a purpose to its activities, we have developed tools for closing the sensory-motor loop between a cultured network and a robot or an artificial animal (an animat). This embodied hybrid neural-robotic system is termed a "*hybrot*". Unlike in the brain, sensory-motor mappings in a hybrot are defined by the experimenters. In order to efficiently find an effective closed-loop design among infinite potential mappings, I constructed a biologically-inspired simulated network, which exhibits similar activity dynamics found in the cultured networks. By using this simulated network, I designed a statistic that can effectively and efficiently *decode* network functional plasticity better than some other existing statistics. Furthermore, in order to *encode*

sensory information about the interactions between a hybrot and its environment, I designed several stimulation protocols and an adaptive training algorithm that worked cooperatively to direct network plasticity, and thus the hybrot's behavior toward a user-defined goal. By closing the sensory-motor loop with these decoding and encoding designs, we successfully demonstrated a simple adaptive goal-directed behavior: learning to move in a user-defined direction, and further showed that multiple tasks could be learned simultaneously. These results suggest that even though a cultured network lacks the 3-D structure of the brain, it still can be functionally shaped and show meaningful behavior. Moreover, this demonstrates the possibility of utilizing living neurons for an engineering purpose (e.g., control a robot to achieve a goal).

To our knowledge, this is the first demonstration of promising goal-directed learning in a hybrot controlled by cultured neurons. Extending from these findings, I further proposed a research plan to search for mappings that could help verify the maximal learning capacity (or even true intelligence) of the cultured network, which can help elucidate the possibility of the neurocomputer as the agent to future intelligent machines. Knowledge gained from effective closed-loop designs also provides insights about learning and memory in the nervous system, which could influence the design of future artificial neural networks, more effective neuroprosthetics, and even the use of the networks themselves as a biologically-based control system.

CHAPTER 1

INTRODUCTION

1.1 Overview

Brains display very high-level parallel computation, fault-tolerance, and adaptability, all of which are properties that we struggle to recreate in engineered systems. Scientists and engineers have made attempts to incorporate ideas from neuroscience into computing in order to build machines that operate in a brain-like manner. The *neurocomputer* (an organic computer built from living neurons), where a complicated language is naturally programmed and organized in the system, seems possible and may lead to a new generation of computing devices. The first neurocomputer consisted of two leech neurons, which could successfully perform arithmetic sums by encoding numbers in the injected currents (Chase and York, 1999). However, the range of numbers that the system could encode was limited; it was believed that this could be solved by recruiting more neurons with a more complex connectivity pattern (Garcia et al., 2001).

Advances in the biocompatibility of materials and electronics have allowed neurons to be grown directly on devices called multi-electrode arrays (MEAs), through which it is possible to stimulate and record neuronal electrical activity at the network level (Gross et al., 1977; Pine, 1980; Blum et al., 1991). Cultured neuronal networks on MEAs provide not only a much more complex connectivity pattern but also a much greater freedom to manipulate and to access the dynamics of groups of neurons, and become one of the best candidates for the next neurocomputer. Besides the access of electrodes, the cultured network's activity can be recorded with microscopic imaging (Bonhoeffer and Staiger, 1988; Parsons et al., 1989; Parsons et al., 1991; Potter, 1996); and stimulation can be administered by optical (Bucher et al., 2001; Suzurikawa et al., 2007) and pharmacological (Segal, 1983; Gibbs et al., 1997; Baruchi and Ben-Jacob,

2007) means. These versatilities further elevate the role of cultured networks in neurocomputer development.

The cultured network model used in this work was dissociated rat cortical neurons grown on MEAs (Figure 1.1). Compared to cultured brain slices, dissociated cultures provide an additional flexibility, where the network's size and connectivity pattern can be controlled (Corey et al., 1991; Maher et al., 1999; Kam et al., 2001). Our dissociated cultures are obtained from E18 rat embryos by mechanical and enzymatic dissociation (Banker and Goslin, 1998b; Potter and DeMarse, 2001). Usually around 50,000 cells (including neurons and glia) are plated onto an MEA. Teflon-sealed dishes (Potter and DeMarse, 2001) are placed in an incubator, which allows us to have a stable and infection-free environment. Our custom-made stimulator (Wagenaar et al., 2004) is capable of stimulation at 59 electrodes, which allows us to deliver stimuli with complex spatiotemporal patterns and record the activity at the same time. This system provides long-term (up to months) accessibility and controllability in the highly-interconnected neuronal network, from which a more complex computational capability, than arithmetic summation, might emerge.

The objective of this work is to explore the possibility of the neurocomputer by demonstrating one of the most important features of the brain, goal-directed learning, in our MEA cultures. Goal-directed learning involves modification of a network's input-output function, or stimulus-response transformation, which leads to changes in responses toward a desired outcome, and was found occur in the animal cortex (Balleine and Dickinson, 1998; Corbit and Balleine, 2003). However, to our knowledge, no study has yet promisingly shown goal-directed learning in cultured networks. Similar to how the brain needs to be embodied in some way and interact with its surroundings in order to give a purpose to its activities, learning in the cultured network cannot be evaluated when disconnected from a body or isolated from the environment. We have developed a closed-loop paradigm (Potter et al., 1997; DeMarse et al., 2001; Potter et al., 2006) consisting of

a sensory-motor loop between a dissociated culture and a robot or an artificial animal (an animat) (Meyer and Wilson, 1991) in order to study sensory processing, memory formation, and behavioral control. This embodied hybrid neural-robotic system is termed a "*hybrot*" (Figure 1.2) (Potter et al., 2006). Compared to animal models, the dissociated cultured network is a simpler and more controllable system to investigate basic network computations; confounding factors such as sensory inputs, attention, and behavioral drives are absent, while diverse and complex activity patterns remain (Gross and Kowalski, 1999; Shefi et al., 2002; Wagenaar et al., 2006c; Rolston et al., 2007). However, this also implies that the sensory-motor loop that re-embodies the dissociated culture needs to be defined artificially by the experimenters. Designing a sensory-motor loop that allows the embodied network to interact with the environment in a meaningful way, such as learning to reach a specific goal, becomes extremely challenging, since the connectivity in a dissociated cultured network is not predictable.

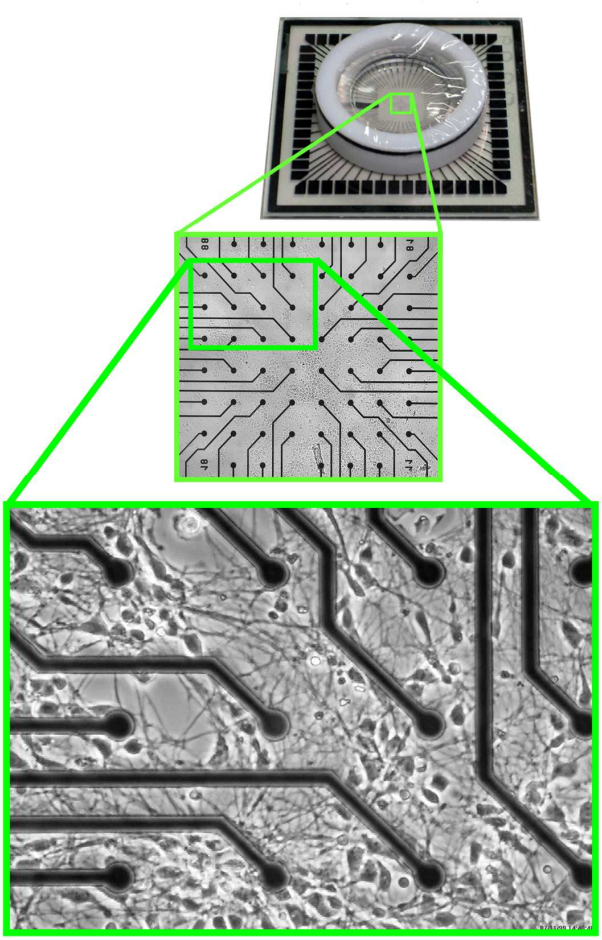

Figure 1.1. Dissociated cortical culture on multi-electrode arrays (MEAs): An MEA (**Top**), with an 8 by 8 grid of electrodes (**Middle**), and neurons (**Bottom**).

This work is focused on finding an effective closed-loop design among infinite potential mappings in order to show goal-directed learning behaviors in embodied dissociated cultures. Finding effective mappings not only enables the utilization of living neurons for engineering purposes (e.g., control a robot to achieve a goal), but is also the step toward evaluating the learning capacity (or even true intelligence) of the embodied culture, which can help elucidate the possibility of the neurocomputer as the future of intelligent machines. Even though there is still a huge gap between demonstrating cultured networks' ability for goal-directed learning and actually constructing an organic computer applicable to solving problems that we use artificial intelligence for these days,

I believe that this is the necessary first step. Furthermore, the knowledge gained from effective mappings also provides insights about learning and memory in the nervous system, which could further lead to direct development of an electronic computer, or new artificial intelligence, based on the operational principles of biological brains.

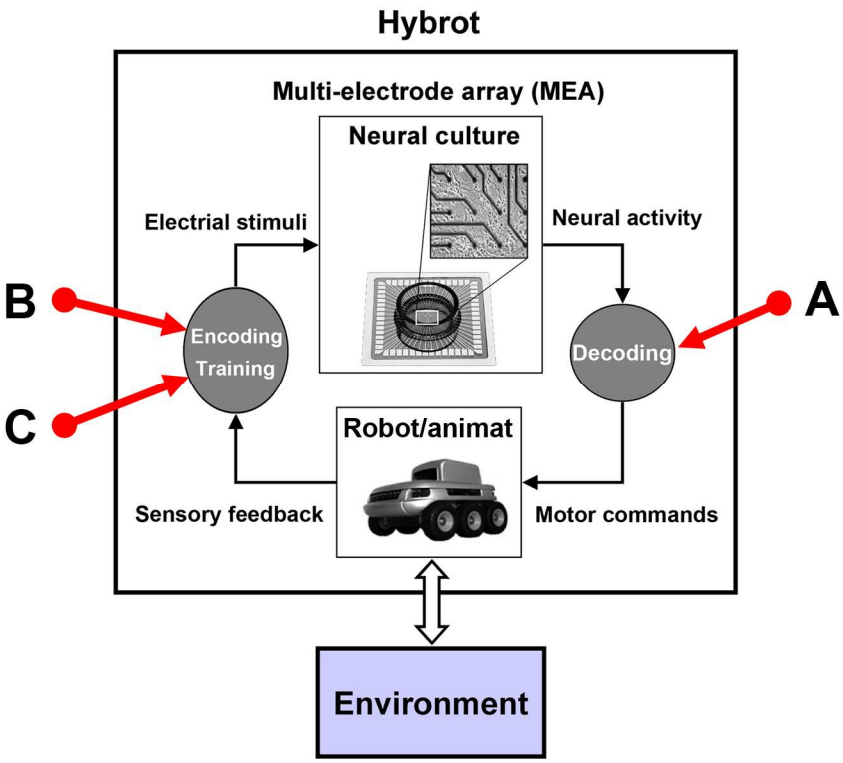

Figure 1.2. The components of a hybrot, an embodied hybrid neural-robotic system: A hybrot consists of a cultured neuronal network, a robot, and a sensory-motor loop. In order to embody a cultured network for goal-directed learning, four fundamental elements are needed for closing the sensory-motor loop: **A.** Decoding: network activity recorded from the cultured network is transformed into the robot's motor commands. **B.** Encoding: the interaction between the robot and its environment is detected by the robot's sensors and transformed into an electrical stimulation fed back to the cultured network. **C.** The behavioral performance is also transformed into stimulation based on a training algorithm.

1.2 Plasticity in disembodied cultured networks

Previous studies have demonstrated the potential for disembodied cultured networks on MEAs to achieve functional plasticity (see Table 1.1). This neural plasticity provides a potential learning capability to cultured networks. Jimbo et al. used a localized

tetanic stimulus to induce long-lasting changes in the network responses that could be either potentiated or depressed depending on the electrode used to evoke the responses (Jimbo et al., 1999). Moreover, we and others previously found that such tetanus-induced plasticity was spatially localized and asymmetrically distributed (Ruaro et al., 2005; Chao et al., 2007c). By delivering two different tetanic stimulation patterns, Ruaro et al. trained a cultured network to discriminate the spatial profiles of the stimuli. Furthermore, by stimulating the network at two sites with different frequencies, Eytan et al. found that network responses adapted selectively to different stimulation frequencies: attenuated responsiveness to the more frequent (> 0.1 Hz) input and increased responsiveness to the rarely delivered (< 0.1 Hz) stimuli. More importantly, this selective adaptation was a reversible process (Eytan et al., 2003). Bakkum et al. showed a different form of plasticity, where the timing of non-synaptic responses changed and adapted to different spatiotemporal patterns of paired stimuli (Bakkum et al., 2007). Long-term plasticity (hours to days) in the spontaneous activity was also discovered, where new spontaneous activity patterns were imprinted or erased after a tetanus (Madhavan et al., 2007b) or after a chemical stimulation (Baruchi and Ben-Jacob, 2007). These results indicate that different stimulation patterns and protocols can shape diverse functional connectivity in cultured networks. Further understanding of the rules that govern plasticity in embodied cultured networks might lead to effective methods to “program” living neurons in order to learn a desired task.

Table 1.1. Overview of functional plasticity in dissociated cultures

Reference	Inducing method	Measures	Principal results
(Maeda et al., 1998a)	Tetanization (> 20Hz)	Stimulus-evoked responses	Increased probability of stimulus-evoked bursting.
(Jimbo et al., 1999)			Pathway-specific plasticity.
(Ruaro et al., 2005)			Enhanced discrimination between two spatial profiles of the stimuli.
(Chao et al., 2007c)			Region-specific plasticity.
(Madhavan et al., 2007b)		Spontaneous bursts	Changes in the spatiotemporal pattern of spontaneous bursts.
(Eytan et al., 2003)	Paired electrical stimulation	Stimulus-evoked responses	Responses to "slow" stimuli enhanced, to "fast" stimuli reduced (reversible).
(Bakkum et al., 2007)			Stimulation-pattern-dependent changes in the timing of presynaptic responses.
(Baruchi and Ben-Jacob, 2007)	Chemical stimulation	Spontaneous and evoked bursts	New bursting patterns imprinted for days.

1.3 Learning in embodied cultured networks

Cultured networks have been embodied previously (see Table 1.2). An embodied cultured network's ability to control an animat or a mobile robot was demonstrated without a specifically defined goal (DeMarse et al., 2001; Martinoia et al., 2004). In another case, animats were designed to avoid obstacles (Cozzi et al., 2005) or follow objects (Bakkum et al., 2004), but deterministically and without learning. By using an acute slice of a lamprey brainstem to control a mobile robot, Mussa-Ivaldi et al. demonstrated the embodied *in vitro* network's tendency to compensate the sensory imbalance caused by artificially altering the sensitivity of the sensors at one side of the robot. Without a pre-defined goal and external training stimulation, long-term changes in

behavior in response to the sensory imbalance were found in embodied lamprey brainstems (Reger et al., 2000), however, the changes were unpredictable (Karniel et al., 2005). With feedback training and a simple user-defined goal, Shahaf and Marom showed unidirectional learning in an isolated (not embodied) MEA culture, where the culture was trained to induce an electrode-specific increase in response. This simple form of learning was achieved by a binary training: to stop a periodic stimulation at one electrode when the desired response level at the target electrode was obtained (Shahaf and Marom, 2001). The same training induced underlying changes in network functional connectivity, which resulted in a different synchrony of spontaneous activities (Li et al., 2007). These results demonstrate the feasibility to shape or to rewire embodied cultured networks, particularly, to direct this change. However, in order to scale to more complex behaviors, we need to create more structured training stimuli and detailed activity metrics, and to incorporate a more realistic interaction between the embodied network and its environment.

1.4 Toward more complex goal-directed learning behaviors

A more complex goal-directed learning in embodied cultured networks was demonstrated using the closed-loop hybrot design described by Novellino et al. (2007), where the performance of an object-avoidance task in an embodied dissociated culture was improved by a binary training (also see Table 1.2). Detailed comparisons between Novellino's model and the closed-loop design proposed in this work are shown in Table 1.3. The details of this comparison will be explained in subsequent chapters. In summary, the advantages of our closed-loop design are: (1) using a detailed decoding statistic that can detect network functional plasticity effectively and efficiently; (2) continuously delivering stimulation to mimic continuous sensory inputs and ongoing processing in the brain; and (3) more variety of training stimulation delivered contingent on the behavioral performance.

1.4.1 Detailed decoding statistics

Inspired by the differential firing rate statistic described by Wagenaar et al. (2006), I designed a statistic called the center of activity trajectory (CAT) to detect network functional plasticity in living MEA cultures (Chao et al., 2007c). This statistic is more capable of revealing the functional plasticity of a network than other existing statistics, including the firing rate measure used in Novellino's model, and thus is a better indicator of learning. Furthermore, CAT incorporates population activity recorded at *all* electrodes, rather than the single electrode activity used in Novellino's model, which is a more robust coding strategy with computationally desirable properties, such as mechanisms for noise removal (Pouget et al., 2000).

Table 1.2. Overview of embodied cultured network systems and feedback training

Reference	System	Emb.	Training algorithm	Goal	Principal results
(DeMarse et al., 2001)	Dissociated cultures	Animat	—	—	Development of the framework for the bi-directional interface.
(Martinoia et al., 2004)		Robot	—	—	
(Bakkum et al., 2004)		Robot	—	Follow a moving object.	Successful utilization of deterministic input-output functions in networks to achieve the goals.
(Cozzi et al., 2005)		Robot	—	Avoid objects.	
(Novellino et al., 2007)		Robot	Binary training: Tetanization at the electrode corresponding to collision side after the robot hits an obstacle.	Avoid objects.	One example showing an improvement of performances during the obstacle-avoidance task.
(Reger et al., 2000)	Lamprey brainstem	Robot	—	Phototactic behavior.	Adaptive compensation to sensory imbalance.

Table 1.3. Comparisons between two models for more complex goal-directed learning

		Design by Novellino et al. (2007)	Design in this work
Environment		2-D circular arena with several objects.	2-D circular arena divided into four quadrants.
Hybrot		Robot + MEA culture.	Animat + MEA cultures.
Sensory inputs		Distance measures from two sensors (left/right).	Sense of which quadrant animat is in / sense of being in or outside the circular arena.
Motor outputs		Speeds of two wheels (left/right).	2-D incremental movement.
User-defined goal		Avoid objects.	Move toward and stay close to the center of the arena.
Sensory-motor loop	**Decoding**	Instantaneous firing rates at two recording electrodes with winner-takes-all (WTA) mechanism.	Center of activity (CA) of population responses at all electrodes.
	Encoding	If sensory input reaches a threshold, deliver a stimulus (max frequency 1Hz); else, no stimulation.	Deliver one of the four context-control probing sequences (CPSs) based on sensory input.
	Training algorithm	Apply 20Hz tetanus at the electrode used to encode movement for the collision side if the robot hits an obstacle.	Adaptive algorithm to select random background stimulation (RBS) if the animat moves closer to the center of the arena, or a patterned training stimulation (PTS) if not.
Reaction time		1 Hz	0.2 Hz
Results		Preliminary: improvement of performances during the object-avoidance task for one example, with no proper control and statistical tests.	Quadri-task learning in simulated networks, uni-task learning in living networks.

1.4.2 Continuous stimulation to maintain a more steady level of responses

Our closed-loop design consists of continuous stimulation with an aggregate frequency of 3 Hz, which is analogous to continuous sensory inputs and ongoing processing in the brain. Continuous external inputs reduced the occurrence of network-wide synchronize bursts (Chao et al., 2005; Wagenaar et al., 2005), which are the most dominant pattern of spontaneous activity in MEA cultures (Gross et al., 1993a; Wong et

al., 1993; Kamioka et al., 1996; Gross and Kowalski, 1999). This maintains a more steady level of firing in the network, where changes in network responses can more directly reflect neural learning induced by training. The significant difference in spatiotemporal structures and magnitudes between spontaneous activity and stimulus-evoked responses might create an artifact in instantaneous firing rates, which might bias the encoding process in Novellino's model, where the object-avoidance behavior of the robot depended more on the on/off of the stimulation, but less on the training-induced changes in network responses.

1.4.3 Variety of training stimulation with adaptive selection

Because the connectivity in a cultured network is not predictable, the effects of a given training stimulation cannot be known a priori. Delivering any training stimulation when the performance is undesired cannot guarantee the network is shaped toward a desired state. Therefore, unlike in Novellino's model where fixed training stimulation was used, we delivered training stimulation contingent on the behavioral performance in order to direct changes in network connectivity and shift the behavior toward the desired behavior.

By incorporating the designs of decoding, encoding, and training, we successfully demonstrate goal-directed learning in simulated networks (Chao et al., 2007a), and living networks (Chao et al., 2007b). This approach could be applied with different and more complex goal-directed behaviors, which may provide a useful *in vitro* model for studying sensory-motor mappings, learning, and memory in the nervous system. This could further lead to direct development of more advanced artificial neural networks, more robust computing methods, and even the use of neurally-controlled animats themselves as biologically-based control systems.

1.5 Toward the neurocomputer

By using a hybrid system, we successfully demonstrated a simple adaptive goal-directed behavior: learning to move in a user-defined direction (Chao et al., 2007b). We further showed that multiple tasks could be learned simultaneously (Chao et al., 2007a). These results suggest that even though a cultured network lacks the 3-D structure of the brain, it still can be functionally shaped and show meaningful behavior. However, whether the cultured network could only express these simple behaviors or also achieve a complex a goal remains unknown.

In order to evaluate the possibility of developing the neurocomputer by using cultured networks, I believe it is necessary, although not sufficient, to understand what capacity cultured networks have for being intelligent. The closed-loop design described above is just a subset of infinite possibilities, and the behavior derived from it does not represent the true capabilities of the embodied cultured network. Therefore, not only do we need to find the "optimal" sensory-motor mappings, but also the optimal body. This is analogous to our brains, which are optimized through evolution to control our bodies, which are also optimized to be controlled by the brain. My future work will focus on finding the optimal combinations of a body and sensory-motor mappings, in order to verify the maximal learning capacity (or even true intelligence) of the embodied cultured network.

1.6 Dissertation overview

In order to efficiently find an effective closed-loop design among infinite potential mappings, I first embodied a biologically-inspired simulated network to explore many different possible sensory-motor mappings and training algorithms. The simulated network provides savings in preparation time and an accessibility to the detailed properties of the network that cannot be directly measured from our experimental setups. The details of the simulated network will be described in Chapter 2. The rest of the

dissertation is organized by the approaches described in Section 1.4. In the last chapter, I summarize our findings and discuss the gap from these findings to my own vision of the neurocomputer, and propose a research plan to narrow this gap. The overview of chapters and appendices are shown in Table 1.4.

Table 1.4. Dissertation overview

Chap.	Contents	Related appendices
2	Design of the biologically-inspired simulated network, and its validation.	**A.** Model details.
3[i]	The center of activity (CAT): an activity statistic that decodes network functional plasticity.	**B.** Calculation of other existing statistics for comparison. **C.** Experimental setups for MEA cultures.
4[ii]	Random background stimulation (RBS): a stimulation protocol that stabilizes stimulus-induced changes in network synaptic connectivity.	**F.** Stabilizing effects in living MEA cultures[iii].
5[iv]	Multi-task goal-directed learning in the simulated network.	**G.** Effects of context-control probing sequence (CPS) stimulation. **H.** Effects of patterned training stimulation (PTS).
6[v]	Goal-directed learning in living MEA cultures, and its application to neurorehabilitation.	
7	Conclusions and future work: A research proposal for evaluating the maximal learning capability of embodied cultured networks.	**I.** Future study of plasticity-inducing stimuli with different spatiotemporal complexity.

[i] Adapted from: Zenas C. Chao, Douglas J. Bakkum, and Steve M. Potter (2007): *Region-specific network plasticity in simulated and living cortical networks: comparison of the Center of Activity Trajectory (CAT) with other metrics*. J. Neural Eng. **4**, 294-308.
[ii] Adapted from: Zenas C. Chao, Douglas J. Bakkum, Daniel A. Wagenaar, and Steve M. Potter (2005): *Effects of random external background stimulation on network synaptic stability after tetanization: a modeling study*. Neuroinformatics **3:3**, 263–280.
[iii] To be submitted as: Radhika Madhavan, Zenas C. Chao, and Steve M. Potter (2007): *Electrical control of population bursting aids functional plasticity in cortical networks*.
[iv] Under review as: Zenas C. Chao, Douglas J. Bakkum, and Steve M. Potter (2007): *Shaping embodied neural networks for adaptive goal-directed behavior*. PLoS Computational Biology.
[v] To be submitted as: Zenas C. Chao, Douglas J. Bakkum, and Steve M. Potter (2007): *Feedback training of electrical stimuli in a cortical network: learning and neurorehabilitation*. The first two authors contributed equally.

In addition, network plasticity in other different forms, and the possible underlying mechanisms, are described in the following two appendices:
D. Network plasticity in spontaneous bursts[vi].
E. Network plasticity in the timing of direct electrically-evoked action potentials (dAPs)[vii].

[vi] Adapted from: Radhika Madhavan, Zenas C. Chao, and Steve M. Potter (2007): *Plasticity of recurring spatiotemporal activity patterns in dissociated cortical networks*. Physical Biology, **4**, 181-193.
[vii] Under review as: Douglas J. Bakkum, Zenas C. Chao,and Steve M. Potter (2007): *Long-term activity-dependent plasticity of action potential propagation in cortical networks*. PLoS One.

CHAPTER 2

BIOLOGICALLY-INSPIRED SIMULATED NETWORKS

Neuronal networks cultured on multi-electrode arrays (MEAs) are helpful model systems to understand brain functions because they reduce the brain's overwhelming complexity. In order to find an effective closed-loop design among infinite potential mappings, I introduced a biologically-inspired simulated network, where detailed properties of individual neurons and synapses could be measured and manipulated. The simulation also provides the ease of experimental setups, where possible closed-loop design candidates can be evaluated in a systematic and controllable way. In order to make the simulated network useful for helping closed-loop design in embodied MEA cultures, the simulated network was constructed to mimic the biological properties in living MEA cultures. The simulated network successfully demonstrated various known properties of the MEA cultures found in our lab and others, and predicted several other complex properties that were further validated in living MEA cultures. This demonstrates its usefulness for studying network dynamics that are difficult to access and control in living networks.

2.1 Introduction

For studying the long-term network-level dynamics in dissociated cultures, a multi-electrode array (MEA) is advantageous over patch-clamp or sharp electrodes since recording and stimulation can be performed at multiple locations for months. By applying MEA technology, researchers are able to record and electrically stimulate cultured networks at multiple spatial locations (Gross et al., 1993b; Tateno and Jimbo, 1999; Shahaf and Marom, 2001). However, recording and stimulation techniques on living nervous systems still have certain limitations, especially for large networks, such as limited accessibility of membrane potential of every neuron and limited controllability of stimulation on specific group of neurons. In order to overcome these limitations, computational network models have been introduced.

Network-level properties have been studied on randomly connected network models (Mongillo and Amit, 2001; Aviel et al., 2003), locally connected network models (Latham et al., 2000a; Mehring et al., 2003), hippocampal slice models (Ermentrout and Kopell, 1998; Biswal and Dasgupta, 2002), and cortical slice models (Marinaro and Scarpetta, 2004). Moreover, the activity-dependent self-organization of neurons has been studied in a detailed large network model consisting of 10,000 neurons (Izhikevich et al.,

2004; Izhikevich, 2005). A complex brain-based model (Darwin X), which included 90,000 neurons to incorporate detailed anatomy and physiology of the hippocampus, was embodied with a real robot to perform navigation tasks, where functional hippocampal pathways for spatial memory were studied (Krichmar et al., 2005). These network models were built to mimic the biological properties of living neuronal networks in order to study unknown underlying mechanisms, instead of for engineering applications of traditional artificial neural networks. The advantages of using simulated network models to study nervous systems are: (1) the accessibility of quantities hard to measure in actual experiments; (2) the controllability of experimental conditions hard or impossible to control and/or maintain in actual experiments; (3) the ease of experimental manipulations; (4) cheaper; (5) ability to repeat experiments exactly, with the same random seed, with only one small change; and (6) capability to do more experiments in less time.

Here, I constructed a simulated network to mimic the properties of the living dissociated cortical network cultured on an MEA. An impressive fidelity between this simulated model and MEA cultures was found in several validation experiments. The detailed features of this simulated model are described in following sections, and their detailed implementations are listed in Appendix A.

2.2 Model features

2.2.1 Overview

The Neural Circuit SIMulator (CSIM) (Natschlager et al., 2003)[viii] was modified to produce artificial neural networks with the following features. 1,000 leaky integrate-and-fire (LIF) neurons with a total of 50,000 synapses were placed randomly in a 3 mm by 3 mm area (see Figure 2.1B). All synapses were frequency-dependent (Markram et al.,

[viii] http://www.lsm.tugraz.at/csim/index.html

1998b; Izhikevich et al., 2004) to model synaptic depression; the synaptic efficacy was determined by the probability of release of neurotransmitters depending on the mechanism of frequency dependence. 70% of the neurons were excitatory, with STDP (Song et al., 2000) at all excitatory synapses. The other neurons were inhibitory (30%) (Marom and Shahaf, 2002). The distribution of the synaptic connection distances followed the distribution found by Segev and Ben-Jacob (Segev and Ben-Jacob, 2000): neurons tend to make many short synaptic connections but a few long ones as well. The number of synaptic connections per neuron followed a Gaussian distribution and each neuron had 50 ± 15 synapses onto other neurons. The conduction delay was proportional to the synaptic connection distance, and the conduction velocity was set to be 0.3 m/s (Kawaguchi and Fukunishi, 1998). Gaussian random noise was introduced into each neuron independently as fluctuations in membrane voltage: 30% of the neurons ("self-firing neurons") had variance at a high enough level to initiate spikes (Latham et al., 2000a; Latham et al., 2000b), while the rest exhibited only subthreshold fluctuations. An 8 by 8 grid of electrodes with 333 μm inter-electrode spacing was included. All electrodes could be used for stimulation, while 60 of these, except corner electrodes 11, 18, 81 and 88 in column-row (CR) number, were used for recording (Figure 2.1D).

Some differences between the simulated neural network and our living network should be noted. In the simulated network, external stimulation was set to generate activity only on nearby neurons' "cell bodies"; an electrode affected about 76 neurons (see Section 2.2.2.4). However, electrical stimulation applied to our cultured neurons by an MEA could also evoke action potentials on axons (McIntyre and Grill, 2002; Wagenaar et al., 2004), generating spikes on neurons that may be far from the electrode, directly without synaptic transmission. Furthermore, little experimental evidence exists for the number of neurons or the range that one stimulus electrode could affect in cultured living networks.

2.2.2 Detailed features

The exponential Euler method was used for numerical integration (Hochbruck et al., 1998). The values of parameters and their implementations in CSIM are described in Appendix A. Most of the parameters in the simulated network were approximated from studies of acute slices (Markram et al., 1998b; Song et al., 2000), retinal networks (Yang and Masland, 1992), and from the simulation of neocortical networks (Froemke and Dan, 2002; Izhikevich et al., 2004; Izhikevich, 2005), others were determined in various validation experiments.

2.2.2.1 Neuron model

1,000 neurons were placed randomly in a 3 mm by 3 mm area (Figure 2.1B). In real MEAs, we plate rat cortical neurons in an area larger than the dimension of the electrode grid, which is 1.4 mm by 1.4 mm (Figure 2.1A), to ensure every electrode has neurons around it. The 3 mm by 3 mm area for the simulated network is an estimation.

2.2.2.1.1 Leaky integrate-and-fire (LIF) neuron

A standard LIF neuron model was implemented where the membrane potential V_m of a neuron is given by:

$$\tau_m \cdot \frac{dV_m}{dt} = -(V_m - V_{rest}) + R_m \cdot (I_{syn} + I_{noise}) \qquad \text{[Equation 2.1]}$$

V_m: membrane potential

R_m: membrane resistance

τ_m: the membrane time constant, (= C_m∗R_m), where C_m: membrane capacitance

I_{syn}: the current supplied by the synapses

I_{noise}: a Gaussion random variable with zero mean and a given variance noise

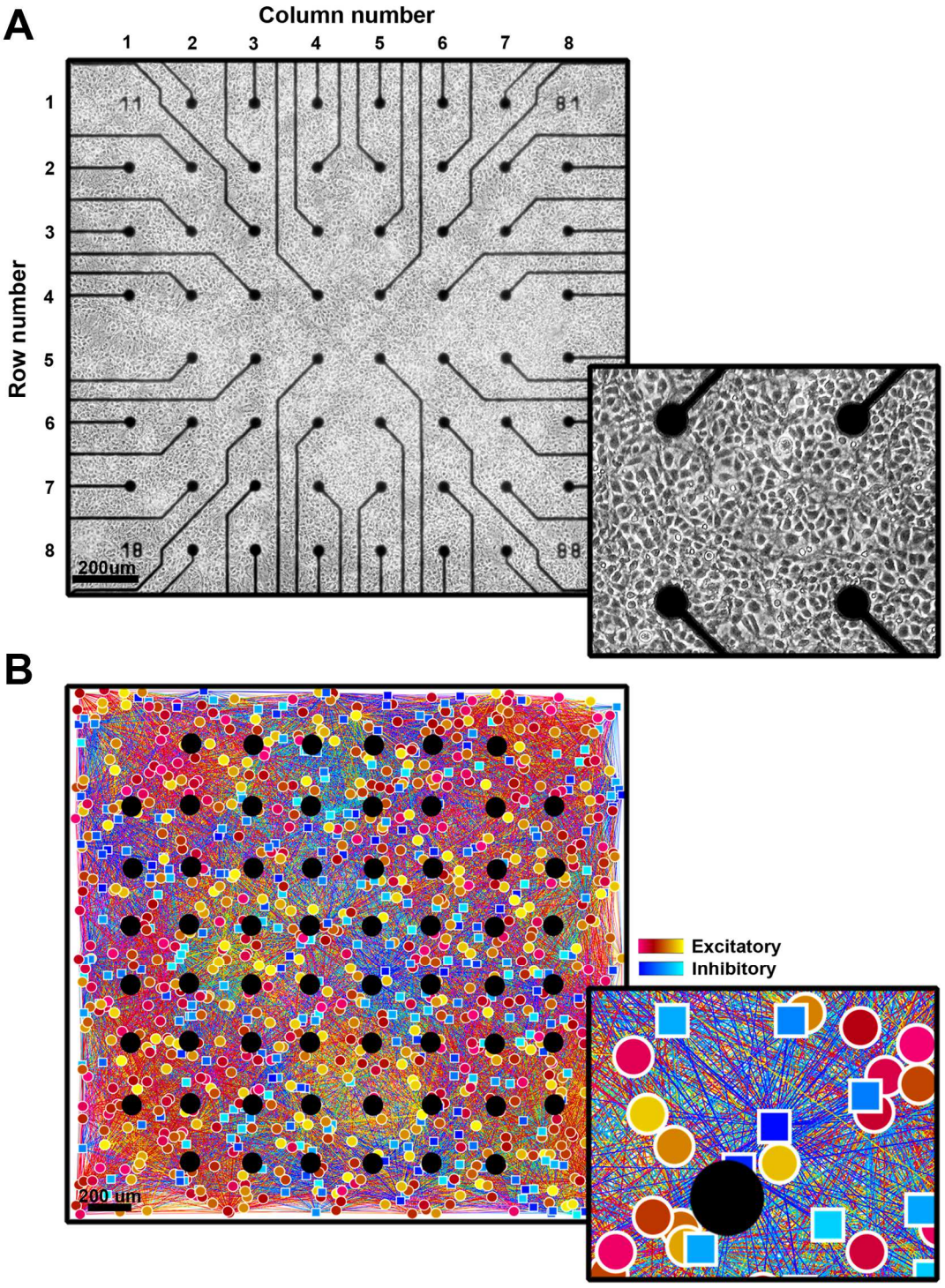

Figure 2.1. Living MEA culture vs. simulated network: The simulated neural network and stimulation electrodes were constructed to mimic the dissociated cultured network and MEA setup. **A.** A view of a living MEA culture with 59 electrodes. **B.** The structure of a simulated network with 1,000 LIF neurons located in a region of 3 mm by 3 mm. The reddish circles indicate the excitatory neurons, the bluish squares indicate the inhibitory neurons, the reddish lines represent the excitatory synapses, and the bluish lines represent the inhibitory synapses (see colorbars). All neurons and synapses are shown. The locations of electrodes are shown in black circles.

At time t= 0, V_m is set to V_{init}. If V_m exceeds the threshold voltage V_{thresh}, it is reset to V_{reset} and hold there for the length $T_{refract}$ of the absolute refractory period. An example of the postsynaptic current and the membrane potential of a neuron receiving several action potentials is shown in Figure 2.1.

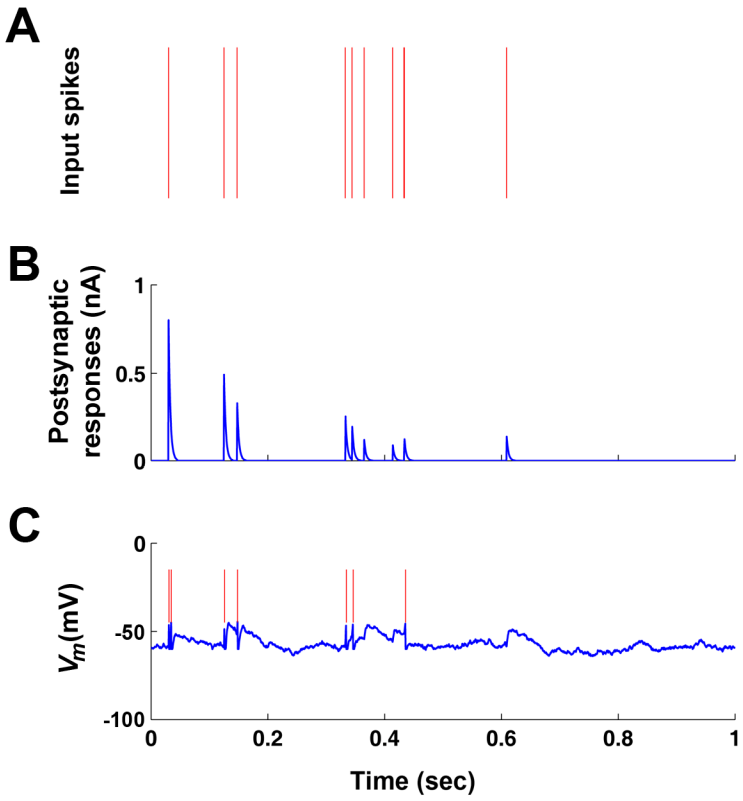

Figure 2.2. Evoked spikes in a LIF neuron: Spikes from another neuron (**A**) evoked synaptic currents at the postsynaptic neuron (**B**), which increase the membrane potential (V_m) in the postsynaptic neuron. A spike (red vertical lines) is evoked at the neuron, when V_m is higher than a threshold (**C**).

2.2.2.1.2 Self-firing

30% of the neurons (self-firing neurons) had I_{noise} (see Equation 2.1) with variance at a high enough level to initiate spikes (Latham et al., 2000a; Latham et al., 2000b), while the rest exhibited only subthreshold fluctuations. Different levels of the standard deviation of I_{noise} introduced to the self-firing neurons caused different spontaneous activity patterns: the rate of synchronized spontaneous bursting (see Section

2.3.1), increased as the standard deviation of I_{noise} increased (Figure 2.3). The bursting rate found in living cortical cultures is generally between 1 to 10 bursts per minute. In order to obtain the similar result, the standard deviation of 30 nA was added at each integration time step for self-firing neurons, and 10 nA was added for non-self-firing neurons according to the results shown in Figure 2.3.

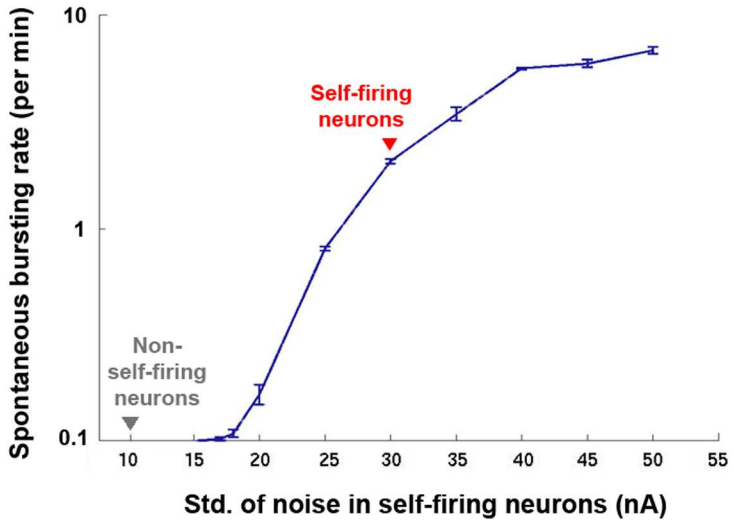

Figure 2.3. Determination of noise levels in self-firing and non-self-firing neurons: The spontaneous bursting frequency increases as the standard deviation of the Gaussian noise added at each integration time step increases. For the non-self-firing neurons, the noise level was set at 10 nA, where the neurons only exhibited subthreshold fluctuation without spontaneous firing. For the self-firing neurons, the noise level was set at 30 nA, where spontaneous network bursting occurred at 1 to 10 bursts per minute, which is similar to the frequency found in living MEA cultures.

2.2.2.2 Synapse model

2.2.2.2.1 Excitatory vs. inhibitory

70% of the neurons were excitatory, which connected to other postsynaptic neurons with excitatory synapses, and the other neurons were inhibitory (30%) (Marom and Shahaf, 2002). The setup of excitatory and inhibitory synapses is described later in Section 2.2.2.5. The relations between several properties of spontaneous bursting and the proportion of inhibitory neurons are shown in Figure 2.4. We observed at most 15%

GABAergic neurons in our cultures (Madhavan et al., 2007a), which were within the 0-30% range where the burst frequency, which is reversely proportional to the inter-burst interval (Figure 2.4A), and the burst duration (Figure 2.4B) remained at constant levels.

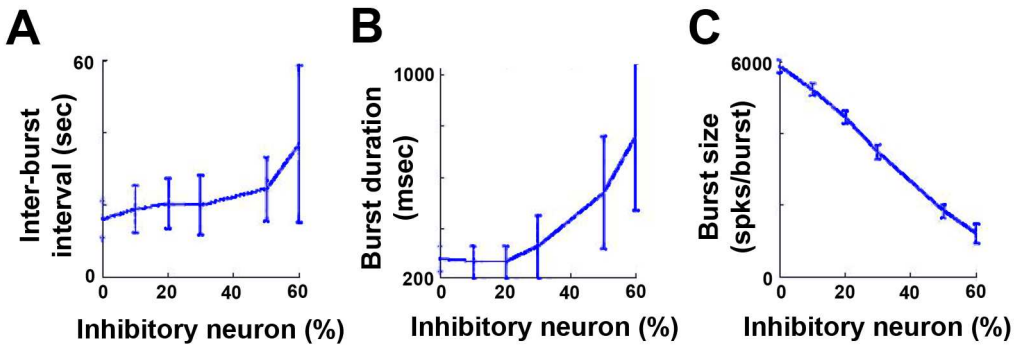

Figure 2.4. The size of inhibitory neuron population affected spontaneous bursting properties: Spontaneous bursts were observed in the simulated network even without inhibitory neurons (100% excitatory neurons). The proportion of inhibitory neurons affected the interval between two consecutive bursts (**A**), the duration of a burst (**B**), and the number of spikes within a burst (**C**).

2.2.2.2.2 Frequency-dependent dynamics

All synapses were frequency-dependent (Markram et al., 1998b; Izhikevich et al., 2004) to model synaptic depression; the synaptic efficacy was determined by the probability of release of neurotransmitters depending on the mechanism of frequency dependence (del Castillo and Katz, 1954; Betz, 1970). The model is based on earlier concepts of the refractoriness of the release process (Zucker, 1989), which can be rephrased by stating that the fraction (U) of the synaptic efficacy used by an action potential (AP) becomes instantaneously unavailable for subsequent use and recovers with a time constant of D. The fraction of available synaptic efficacy is termed R. The running value of U is referred to as u, where U remains a parameter that applies to the first AP in a train. u decays with a single exponential, τ, to its resting value U. The frequency-dependent dynamics are governed by the following equations:

$$R_1 = 1 - U$$

$$R_{n+1} = R_n \cdot (1 - u_{n+1}) \cdot \exp\left(\frac{-isi}{D}\right) + 1 - \exp\left(\frac{-isi}{D}\right)$$

$$u_{n+1} = u_n \cdot \exp\left(\frac{-isi}{\tau}\right) + U \cdot \left(1 - u_n \cdot \exp\left(\frac{-isi}{\tau}\right)\right) \qquad \text{[Equations 2.2]}$$

$$EPSP_n = W \cdot \exp\left(\frac{-\Delta t}{\tau}\right) \cdot R_n \cdot U$$

R_n: the fraction of available synaptic efficacy at time step n

U: utilization of synaptic efficacy

u_n: and the running value of U at time step n

isi: the time between nth and $(n+1)th$ APs

D: time constant of recovery from the depression

$EPSP_n$: excitatory postsynaptic potential and time step n

W: the synaptic weight

Δt: the time from previous arrival of AP to the simulation time

τ: the time constant of decay of responses

Intuitively, the excitatory postsynaptic potential (EPSP) of the synapse is proportional to the synaptic weight (W), the available synaptic efficacy (R_n), and the initial capacity (U); and is increased when a presynaptic spike hits the synapse, otherwise decays exponentially with the time constant τ.

2.2.2.2.3 Spike-timing-dependent plasticity (STDP)

Both long-term potentiation (LTP) and long-term depression (LTD) of synapses are induced through STDP: firing of a postsynaptic neuron immediately after a presynaptic neuron results in LTP of synaptic transmission, and the reverse order of firing results in LTD (Desmond and Levy, 1983; Gerstner et al., 1996; Markram et al., 1997; Bi

and Poo, 1998). Here, several advanced features were incorporated in the basic model (see below). The resulting STDP rule that governed the modification of synaptic weights between two monosynaptically connected neurons is shown in Figure 2.5.

(1) Basic model:

The basic STDP rule describes how a synaptic weight is modified by the timing between pre- and postsynaptic APs. In modeling studies, the basic rule is described as (Song et al., 2000):

$$dw = \begin{cases} W \cdot A_+ \cdot \exp(\Delta t/\tau_+) & if\ \Delta t < 0 \\ W \cdot A_- \cdot \exp(-\Delta t/\tau_-) & if\ \Delta t \geq 0 \end{cases} \qquad \text{[Equation 2.3]}$$

dw: the normalized change of the synaptic weight (= dW/W)

A_+ / A_-: the maximum amounts of synaptic modification, which occur when Δt is close to zero (both> 0)

Δt: pre-to-postsynaptic inter-spike intervals

τ_+ / τ_-: time constants of exponential decay of positive/negative learning window

Intuitively, presynaptic APs that follow postsynaptic APs ($\Delta t < 0$) produce long-term weakening of synapses ($dw < 0$), and APs arriving at the synapse with reverse order ($\Delta t > 0$) produce the opposite effect ($dw > 0$). The largest changes in synaptic efficacy (A_+ or A_-) occur when the time difference between pre- and postsynaptic APs is small, and there is a sharp transition from strengthening to weakening as this time difference passes through zero. The effects of weakening and strengthening decrease as the time difference increases by time constants τ_- and τ_+, respectively (see Figure 2.5).

(2) Saturation model:

In order to prevent synaptic weights increasing or decreasing to unrealistic values, an upper bound and a lower bound were set. The updating functions (the first term on the right-hand side of Equation 2.4) were added to attenuate synaptic changes as a synapse approaches the upper or lower boundary of the allowed range.

$$dw = \begin{cases} (W_{\max} - W)^{\mu_+} \cdot A_+ \cdot \exp(\Delta t / \tau_+) \ \ if\ \Delta t < 0 \\ (W - W_{\min})^{\mu_-} \cdot A_- \cdot \exp(-\Delta t / \tau_-) if\ \Delta t \geq 0 \end{cases} \qquad \text{[Equation 2.4]}$$

W_{max} / W_{min}: the maximal/minimal weight of the synapse

μ_+ / μ_-: the extended multiplicative positive/negative update (Gutig et al., 2003)

If μ_+ and μ_- equal 1, then the updating functions linearly attenuate positive and negative synaptic weights when approaching W_{max} and W_{min}, respectively; otherwise, faster or slower nonlinear attenuation occurs. This prevents synaptic efficacies from becoming unnaturally excitatory or inhibitory and removing the problems caused by artificially clipping synaptic weights at their maxima.

(3) Suppression model:

The context of spike trains also affects how STDP operates. In visual cortical slices, the contribution of each pre- or postsynaptic spike pair to synaptic modification depends not only on the interval between the pair, but also on the timing of preceding spikes (Froemke and Dan, 2002). That is, activity-induced synaptic modification depends not only on the relative spike timing between the neurons, but also on the spiking pattern within each neuron. The firing history of each neuron influences the efficacy (e_{pre} / e_{post}) of subsequent APs, and further affects the role of each AP plays in STDP. This phenomenon is modeled as follow:

$$\begin{cases} e_{pre} = 1 - \exp(-\Delta t_{pre} / \tau_{pre}) \\ e_{post} = 1 - \exp(-\Delta t_{post} / \tau_{post}) \end{cases}$$

$$W_{n+1} = W_n \cdot (1 + e_{pre} \cdot e_{post} \cdot dw)$$

[Equations 2.5]

e_{pre} / e_{post}: the efficacy of the presynaptic/postsynaptic AP

Δt_{pre} / Δt_{post}: the time intervals between APs for calculating STDP and their previous APs in presynaptic/postsynaptic neurons

τ_{pre} / τ_{post}: the suppression time constant for presynaptic/postsynaptic neurons (Froemke and Dan, 2002)

The synaptic change (dw) is "suppressed" by the efficacy of corresponding pre- and postsynaptic APs, which depends only on the interval from the preceding AP in the same neuron.

(4) Overall modified model:

Combining the standard STDP model with saturation constraints and the AP efficacy, the STDP synapse model was modified and governed by the following equations:

$$dw_n = \begin{cases} (W_{\max} - W_n)^{\mu_+} \cdot A_+ \cdot \exp(\Delta t / \tau_+) \ \ if\ \Delta t < 0 \\ (W_n - W_{\min})^{\mu_-} \cdot A_- \cdot \exp(-\Delta t / \tau_-) if\ \Delta t \geq 0 \end{cases}$$

$$\begin{cases} e_{pre} = 1 - \exp(-\Delta t_{pre} / \tau_{pre}) \\ e_{post} = 1 - \exp(-\Delta t_{post} / \tau_{post}) \end{cases}$$

$$W_{n+1} = W_n \cdot (1 + e_{pre} \cdot e_{post} \cdot dw_n)$$

[Equations 2.6]

The relation between dW/W (= dw) and Δt is shown in Figure 2.5.

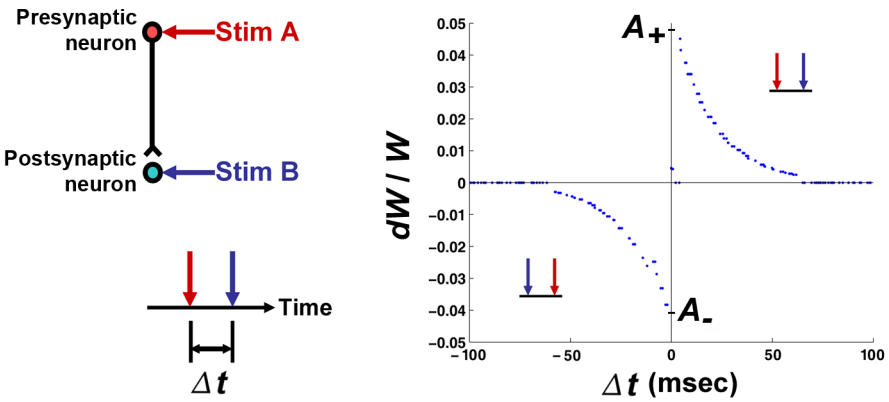

Figure 2.5. STDP synapse between two LIF neurons: By varying the time interval (Δt) between spike inputs at two synaptically-connected neurons A and B, the normalized change in the synaptic weight of A to B followed the STDP rule. A_+ and A_- represent the maximum amounts of synaptic potentiation and depression, respectively.

2.2.2.3 Axon model

The axons in the simulated network connected neurons located at different locations, conducted APs traveling in the network with different propagation delays depending on the distance between neurons. For each axon, APs only travel one way. Two-way communications were allowed between two neurons using two separate axons, but no multiple axons connected one neuron to another in the same direction.

2.2.2.3.1 Conduction velocity

The conduction delay was proportional to the distance between two connected neurons, and the conduction velocity was set to be 0.3 m/s (Kawaguchi and Fukunishi, 1998).

2.2.2.3.2 Connectivity

The distribution of the connection distances followed the distribution found by Segev and Ben-Jacob (Segev and Ben-Jacob, 2000): neurons tend to make many short

connections but a few long ones as well (Figure 2.6). The number of connections per neuron followed a Gaussian distribution and each neuron had 50 ± 15 synapses onto other neurons.

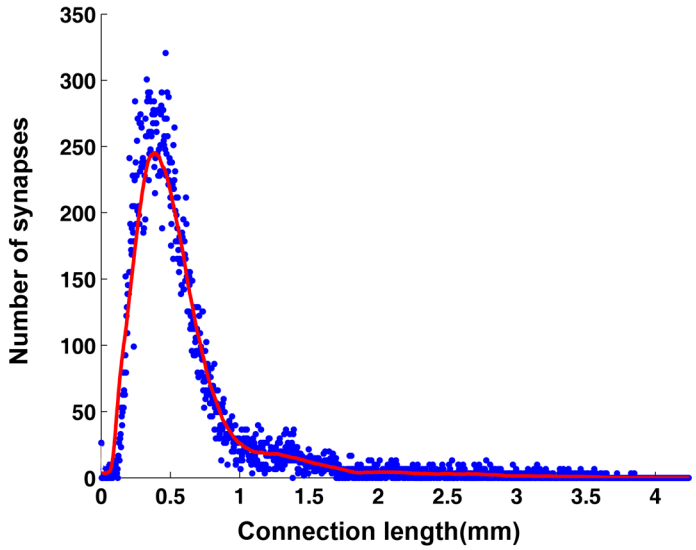

Figure 2.6. Distribution of synaptic connection lengths: Neurons connected by axons tended to make many short connections but a few long ones as well. The longest connection was close to 4.24 mm, which is the length of the diagonal of the 3 mm by 3 mm area where the neurons were located.

2.2.2.4 Electrode model

An 8 by 8 grid of electrodes with 333 µm inter-electrode spacing was included. The inter-electrode spacing, which was larger than the inter-electrode spacing of 200 µm in MEAs, was selected so that the distance from each peripheral electrode to the edge of the network were also the inter-electrode spacing. This difference showed no significance in validity tests (Section 2.3). All electrodes could be used for stimulation, while 60 of these (except corner electrodes CR11, CR18, CR81 and CR88) were used for recording (Figure 2.1B). In real MEAs, electrode CR15 is the large ground electrode and is not used for recording/stimulation (not shown in Figure 2.1A). In the simulated network, each electrode recorded 5 ± 1 of the closest neurons, and stimulated 76 ± 12 of the closest

neurons. These parameters were tweaked and optimized in various validation experiments (described in Section 2.3), since little experimental evidence exists for the number of neurons recorded or the range that one stimulus electrode could affect in cultured living networks.

2.2.2.5 Simulation setup

All excitatory synaptic weights were initially set to 0.05 and could vary between zero and 0.1 due to STDP. At the maximal weight, each spike would have a 50% probability of evoking a spike in the postsynaptic neuron, due to its summation with intrinsic noise (Figure 2.7). The synaptic weights for the inhibitory connections were fixed at -0.05. The networks were run for 2 hours in simulated time until the synaptic weights reached the steady state, which took 3 to 4 hours in compute time (MATLAB 7.0, AMD Athlon processor, 2.08 GHz, 512 MB RAM). Most of the excitatory synaptic weights (93 ± 2%) were less than 0.01 or greater than 0.09 (Figure 2.8). This bimodal steady-state distribution of weights arose from the STDP rule, as previously observed by Song et al. (2000), and Izhikevich and Desai (2003). The set of synaptic weights after 2 hours, which stabilized without external stimuli, was used for the subsequent simulation experiments as the initial state.

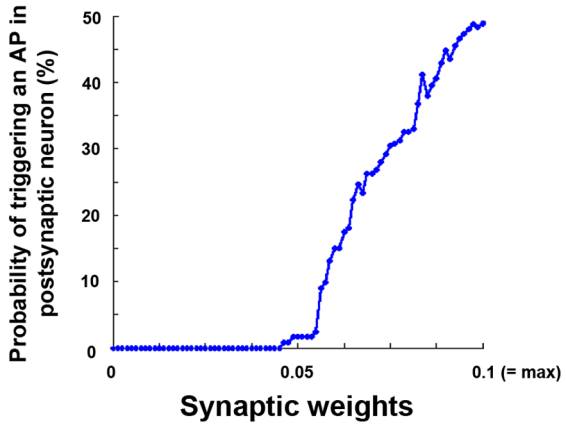

Figure 2.7. Relation between the synaptic weight and the firing probability of the postsynaptic neuron: By varying the synaptic weight between two neurons, the probability of triggering an AP in the postsynaptic neuron was measured. At the maximal weight (0.1), each presynaptic spike would have a 50% probability of evoking a spike in the postsynaptic neuron, due to fluctuations in the postsynaptic neuron's membrane potential.

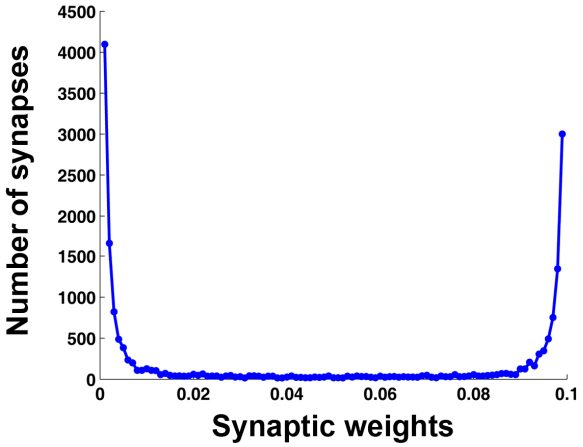

Figure 2.8. Bimodal distribution of network synaptic weights in equilibrium: The network synaptic weights of excitatory synapses reached equilibrium with a bimodal distribution after 2 hours in simulation time. Most of the excitatory synaptic weights (93 ± 2%) were less than 0.01 or greater than 0.09.

2.3 Validation

In order to show that the simulated networks exhibit similar properties observed in living cultures of rat cortical neurons, the results from the following validity tests in simulated networks were compared to the experimental data collected in MEA cultures prepared as in Appendix C. In several cases, simulated networks even predicted and helped determine the experimental parameters.

2.3.1 Spontaneous activity

The most dominant pattern of spontaneous activity in MEA cultures is global dish-wide bursting (Gross et al., 1993a; Wong et al., 1993; Kamioka et al., 1996; Gross and Kowalski, 1999). The artificial networks are able to produce the similar synchronized activity pattern (Figure 2.9).

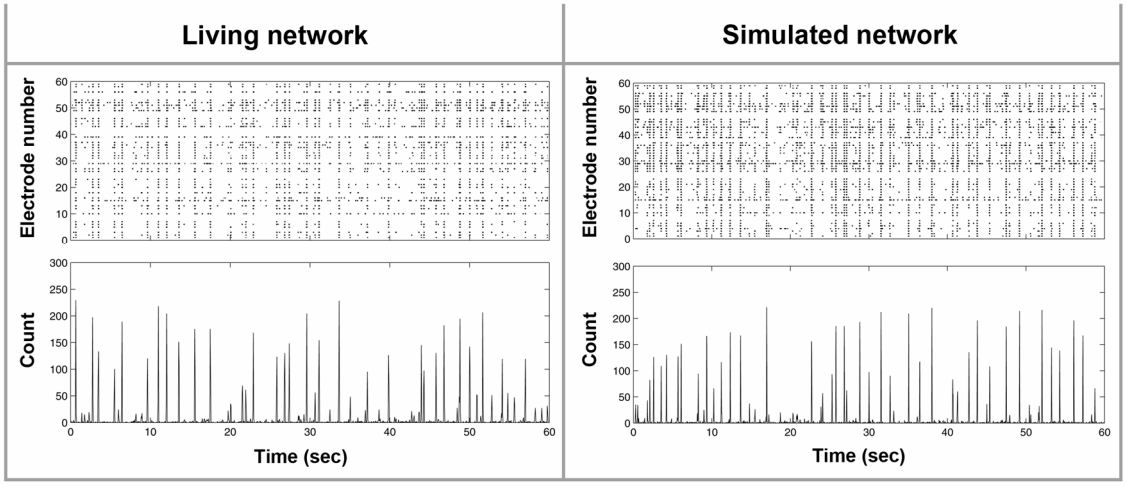

Figure 2.9. Comparison of the network spontaneous activities: Simulated spontaneous activity resembles the experimentally recorded data. One minute of spontaneous activity was recorded from a living network by a 60-electrode MEA (**Left**), and in simulation (**Right**) for comparison. The upper panels are spike raster plots. The lower panels are firing rate histograms, with bin sizes of 100 msec.

2.3.2 Stimulus-evoked responses

Evoked responses are observed when electrical stimuli are delivered into MEA cultures. By repeating the same stimulus, the evoked responses with a specific delay pattern were usually observed, called direct electrically-evoked action potentials (dAPs, see more in Appendix E) shown in Figure 2.10.

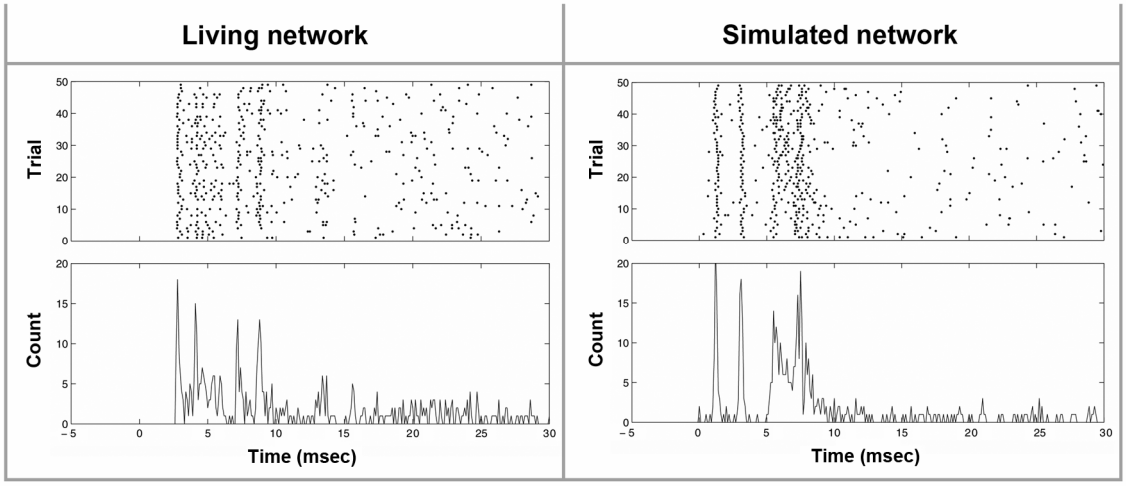

Figure 2.10. Comparison of the network evoked responses: Simulated evoked responses resemble the experimentally recorded data. Fifty trials of evoked responses recorded by one electrode in a living network (**Left**), and in simulation (**Right**) are shown for comparison. The upper panels are spike raster plots. The lower panels are firing rate histograms, with the bin size of 0.1 msec. The timings of stimuli for each trial are aligned at time zero. For the living network, the activity 2 msec immediately after the stimulation was removed by a stimulus artifact suppression algorithm (Wagenaar and Potter, 2002).

2.3.3 Frequency-dependent property

By delivering paired stimulus pulses at two different electrodes in an MEA culture, the network response to the second stimulus pulse was inhibited when the inter-pulse interval (IPI) was around 100 msec (Shkolnik, 2003). The relation between IPI and network responses (Figure 2.11A) suggests a network-level refractory period, which is also found in the simulated networks implemented with frequency-dependent synapses (Figure 2.11B).

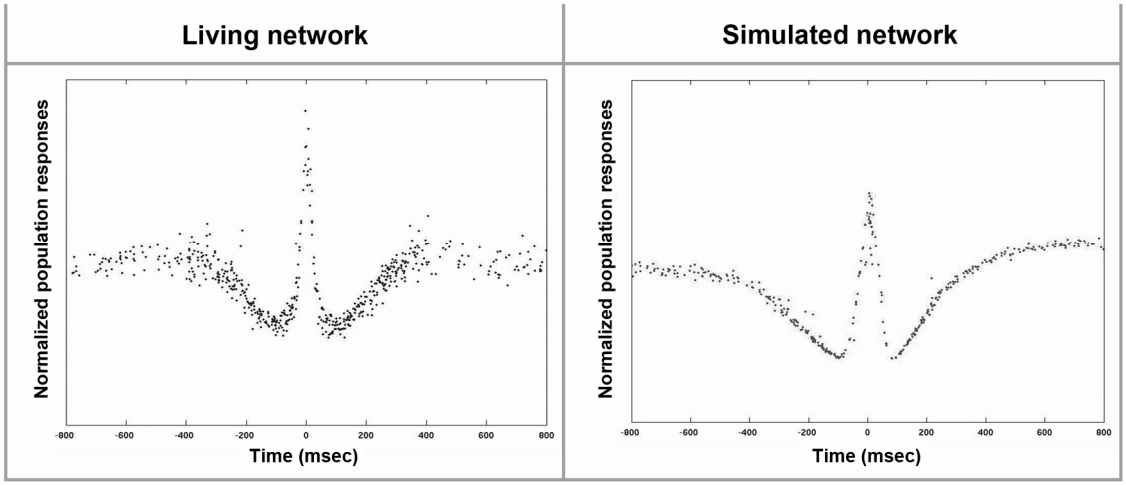

Figure 2.11. Comparison of the network responses to different IPIs: The IPI curve from simulation resembles the experimental results. The normalized network responses to the second stimulus pulse were plotted versus the range of IPIs. The IPI curve obtained from a living network (**Left**) is compared to the one from simulation (**Right**).

The study was expanded from one IPI between two stimulus pulses into two IPIs between three stimulus pulses. By measuring the network response to the third stimulus pulse, the results of this 3-electrode IPI experiment are shown in Figure 2.12A. The simulated networks were able to predict the results and help determine the experimental parameters (Figure 2.12B).

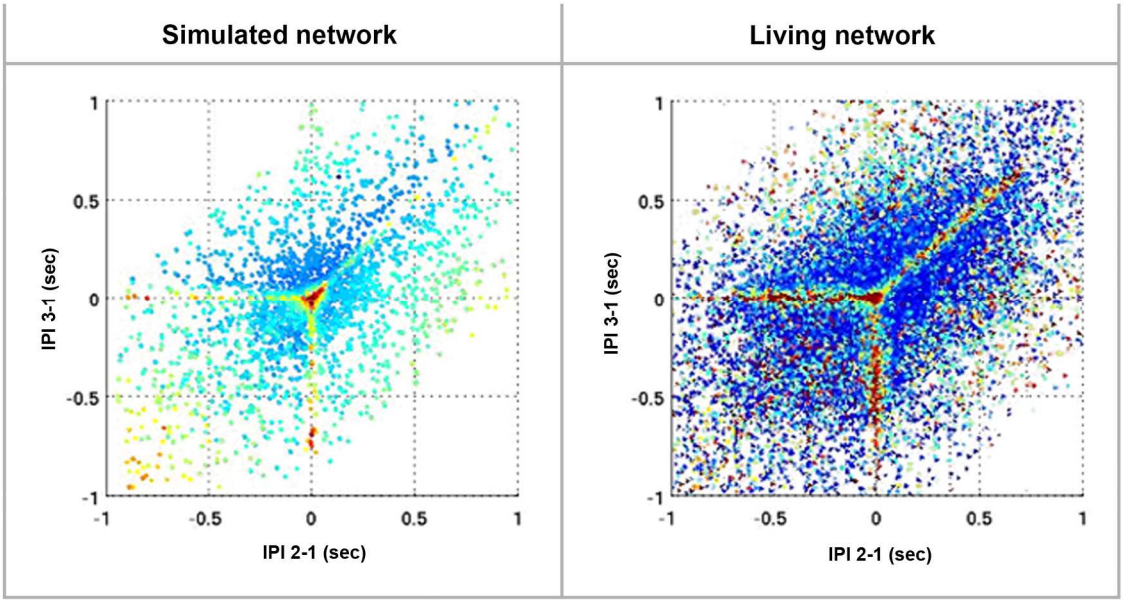

Figure 2.12. Prediction and comparison of the network responses to different IPIs in 3-channel experiment: The results of 3-electrodel IPI experiment from simulation resemble the experimental results (obtained by Bakkum). The normalized network responses to the third stimulus pulse were plotted (color coded) versus the IPI between the first and the second pulses (x-axis) and the IPI between the first and the third pulses (y-axis). The result from simulation (**Left**) is compared to the one from a living network (**Right**).

2.3.4 Spontaneous bursts quieting

The number of spontaneous bursts were suppressed by sequentially stimulating multiple locations in MEA cultures (Wagenaar et al., 2005) (see more in Appendix F). The ability of multi-site stimulation to "quiet" the spontaneous bursts in living neuronal networks was also found in simulated networks (Figure 2.13).

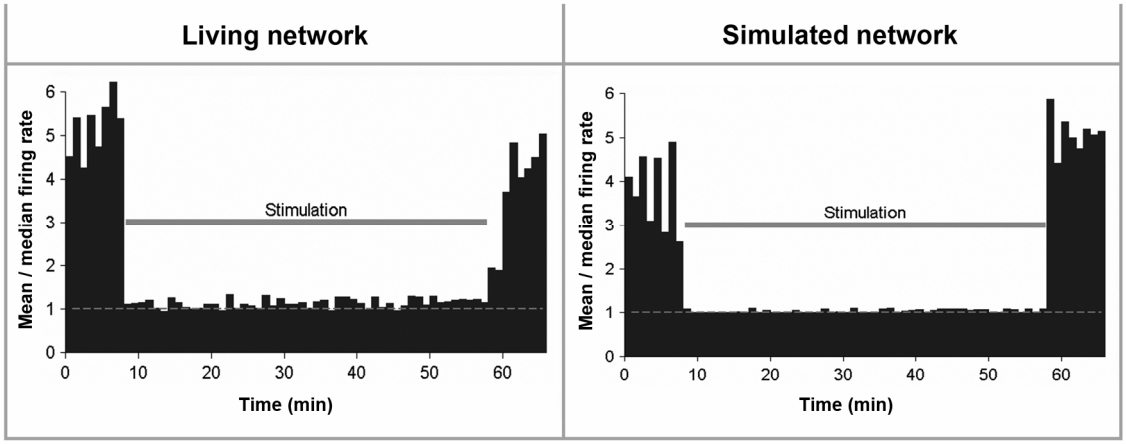

Figure 2.13. Comparison of the effect of spontaneous bursts quieting: The quieting of spontaneous bursts by multi-site stimulation was similar in experimental data (carried out by Wagenaar) (**Left**) and simulation (**Right**). The measure of the mean firing rate over median firing rate (y-axis) is calculated in1-minute sliding window, is plotted vs. time (x-axis) during spontaneous activity and multi-site stimulation (indicated by gray bars). The multi-site stimulation was applied on 8 electrodes at an aggregate rate of 8Hz.

2.3.5 Superbursts

Population-wide bursts in MEA cultures were found spontaneously clustered into sequences of 5 to 12 members with a highly stereotyped spatiotemporal pattern that lasted up to 30 seconds (Wagenaar et al., 2006b). These bursts of bursts, termed "superbursts" (Figure 2.14A), were found in a minority of cultures. In the simulated networks, a superburst-like activity structure was found by increasing the density of connectivity from 50 synapses per neuron to 100 synapses per neuron (~ 10,000 synapses in a network) (Figure 2.14.B).

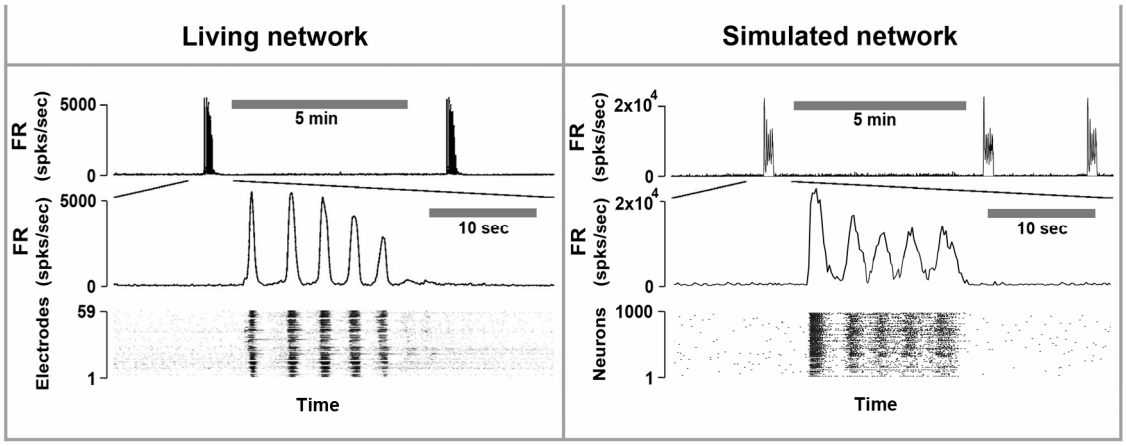

Figure 2.14. Comparison of the structure of superbursts: The temporal structure of superbursts was similar in experimental data (carried out by Wagenaar) (**Left**) and simulation (**Right**). The top panels are firing rate histograms of a 10-min data. The middle panels are firing rate histograms of a superburst, whose spike raster plots are shown in the bottom panels.

2.4 Discussion

Without detailed dynamics exhibited in some other more complex neuron models, such as Hodgkin-Huxley neuron model (Hodgkin and Huxley, 1990) and Izhikevich neuron model (Izhikevich, 2004), 1,000 LIF neurons demonstrated an impressive fidelity to living MEA cultures in various comparisons. Since little is known about how the STDP rule scales to the network level, the STDP algorithm in the simulated network could only be examined between two synaptically-connected neurons (Figure 2.5). By

delivering plasticity-inducing stimulation, such as a tetanus (Bliss and Lømo, 1973), changes in the network spontaneous activity pattern observed in the simulated network were similar to those in living cultures (Figure E.1). This indirectly validates the long-term plasticity mechanism implemented in the simulated networks. For the short-term plasticity mechanism, frequency-dependent depression provided the network-level refractoriness found in living cultures (Figures 2.10 and 2.11). Without the frequency-dependent dynamics, spontaneous bursts exhibited an abnormally long duration, or even without termination.

This biologically-inspired simulated network successfully predicted several complex properties that were further validated in MEA cultures (Chapters 3 to 6), which shows its usefulness for studying network dynamics that are difficult to access and control in living networks.

CHAPTER 3

ACTIVITY STATISTIC TO DETECT NETWORK PLASTICITY: CENTER OF ACTIVITY TRAJECTORY (CAT)[ix]

Electrically-interfaced cortical networks cultured *in vitro* can be used as a model for studying the network mechanisms of learning and memory. Lasting changes in functional connectivity have been difficult to detect with extracellular multi-electrode arrays (MEAs) using a standard firing rate statistic. We used both simulated and living networks to compare the ability of various statistics to quantify functional plasticity at the network level. Using the simulated leaky integrate-and-fire (LIF) neural network (described in Chapter 2), we compared 5 established statistical methods to one of our own design, called center of activity trajectory (CAT). CAT, which depicts dynamics of the location-weighted average of spatiotemporal patterns of action potentials across the physical space of the neuronal circuitry, was the most sensitive statistic for detecting tetanus-induced plasticity in both simulated and living networks. By reducing the dimensionality of multi-unit data while still including spatial information, CAT allows efficient computation of spatiotemporal activity patterns which is useful for real-time closed-loop systems. Thus, CAT is a excellent candidate for decoding network activity for demonstrating learning behavior in embodied cultured networks, and will be useful for studies *in vivo* or *in vitro* in which the locations of recording sites on multi-electrode probes are important.

3.1 Introduction

Modification of connectivity between cortical neurons plays an important role in the processes of learning (Ahissar et al., 1992; Buonomano, 1998) and memory (Merzenich and Sameshima, 1993). Connectivity at the synaptic level has been studied by administering stimuli while simultaneously recording neural activity, and then quantifying plasticity by analyzing the stimulus-response relationships. Culturing on multi-electrode arrays (MEAs) was introduced to help understand connectivity and plasticity in networks of neurons (Gross, 1979; Pine, 1980). This allows long term (months), non-invasive observation of the electrical activity of multiple neurons simultaneously (Potter and DeMarse, 2001) in a system with less experimental

---

[ix] Adapted from: Zenas C. Chao, Douglas J. Bakkum, and Steve M. Potter (2007): *Region-specific network plasticity in simulated and living cortical networks: comparison of the Center of Activity Trajectory (CAT) with other metrics*. J. Neural Eng. **4**, 294-308.

complexity and greater control than preparations *in vivo*. External factors such as sensory inputs, attention, and behavioral drives are absent, while many aspects of complex spatiotemporal spike patterns observed in animals remain (Gross and Kowalski, 1999; Shefi et al., 2002).

Many activity statistics have been used to quantify stimulus-response relationships from simultaneous recordings of multiple neurons (Brown et al., 2004). Most analyze the dependencies between spike trains, such as the maximum likelihood method (Chornoboy et al., 1988; Okatan et al., 2005), product-moment correlation coefficient (Kudrimoti et al., 1999), and functional holography (Baruchi and Ben-Jacob, 2004), etc. However, only a few were applied for measuring network plasticity. The most common of these was firing rate (FR), which showed plastic modifications of network response induced by tetanic stimulation in cortical cultures (Reich et al., 1997; Jimbo et al., 1998b; Maeda et al., 1998b; Jimbo et al., 1999; Wagenaar et al., 2006a), and dopamine-regulated plasticity in anaesthetized rats (Rosenkranz and Grace, 1999). Firing rate histogram (FRH) uses firing rates integrated over successive sequential latency epochs to add detailed temporal information, and was applied to demonstrate adaptable image processing and pattern recognition through the training of tetanic stimulation in MEA cultures (Ruaro et al., 2005). Mutual information (MI) characterized the statistical dependence between neuron pairs, exposing the strength of coupling between neurons and the functional connectivity among cortical areas (David et al., 2004). Cross-correlation histograms (CCH) from pairs of neurons showed functional plasticity in the auditory cortex of behaving monkeys (Ahissar et al., 1998), and the more advanced shift-predictor corrected cross-correlogram (SCCC) was used to quantify receptive field plasticity in the rat auditory cortex (Bao et al., 2003). Joint peri-stimulus time histogram (JPSTH) characterized the causality of firing between neuron pairs, and successfully demonstrated long-term facilitation of neural activity involved in respiratory control (Morris et al., 2003). Robust neuronal computation and encoding is believed to involve

the distribution of information over populations of neurons and synapses in a combination of spatial and temporal domains. Observing only pairs of neurons (MI, CCH, SCCC, and JPSTH), neglecting temporal information (FR), and neglecting spatial information (all) limit the ability of these to measure the complex plasticity of the brain.

We recently devised a statistic called the center of activity trajectory (CAT), which incorporates both the physical locations of the recording sites and the timing of neural activity in order to depict dynamics of the population activity in the *neuronal circuitry space* (first described in Chao et al., 2005, upon which Chapter 4 is based). The neuronal circuitry space is defined by the physical locations of the neurons, in our case being the MEA's 2-dimensional plane. The center of activity (CA) component is analogous to the center of mass, in that the mass at an electrode location is determined by the recorded firing rate. CAT is the sequence of CAs over successive time intervals. We discuss how the inclusion of spatial and temporal information improved the detection of neural network plasticity. The importance of the spatial location of neural activity has been widely emphasized in other studies. For example, spatiotemporal dipole models were used to represent the spatial distribution of underlying focal neural sources producing electroencephalographic (EEG) and magnetoencephalographic (MEG) signals (Scherg, 1990; Leahy et al., 1998).

We used the simulated network of Chapter 2 to compare CAT's ability to detect network plasticity to the alternative statistics: FR, FRH, MI, SCCC, and JPSTH. No ground truth about network plasticity in living networks exists, because neuronal connectivity cannot be measured for more than a few pairs of neurons simultaneously. Therefore, we could only cross-validate the amount of plasticity detected by each statistic in a simulated network, in which the weights of *all* synapses were observable. In simulation, we modulated neural plasticity in a controlled manner, and quantified the ability of each statistic to reveal underlying changes in functional synaptic connectivity.

In simulation, CAT showed the ability to detect smaller changes in the distribution of network synaptic weights than did FR, FRH, MI, SCCC or JPSTH. CAT also detected more pronounced changes in the network following tetanus than the alternate statistics in living MEA cortical cultures.

By applying a shuffling method to the CAT analysis to erase spatial information about recording location in its calculation, we found that changes in activity patterns recorded from neighboring electrodes were not independent and contributed to the better performance of CAT to detect plasticity. The network plasticity was *region-specific*: despite the apparent random connectivity of neurons, plasticity was not symmetrically distributed, and the location of neurons played a role in stimulus-induced plasticity.

3.2 Methods

3.2.1 Simulation

3.2.1.1 Simulated network

For simulation experiments, we used five 1,000-LIF-neuron simulated networks, as described previously in Chapter 2, each with a different connectivity.

3.2.1.2 Setup of networks with different synaptic states

Synaptic state of a network was determined by its connections and synaptic weight distribution. In order to generate different synaptic states, we used 5 simulated networks with different connectivity as reference networks. We ran the networks for 5 hours in simulated time until the synaptic weights reached a steady state (see Section 2.2.2.5). The set of synaptic weights stabilized after 5 hours of spontaneous activity, without external stimuli, and was used as the initial state for the corresponding reference network.

For each reference network, we applied simulated tetanization at two randomly picked electrodes at 20 Hz, and a series of subsequent networks (snapshots of their different synaptic states) were collected after different tetanus durations (1, 2, 5, 10, 15, 20, 30 sec, and 1, 2, 5 min). That is, starting from a reference network (S_0), S_1 was the network with the synaptic state at 1 sec after the start of tetanization, S_2 at 2 sec, and so forth. Therefore, for each pair of randomly chosen tetanization electrodes, 10 new networks with different synaptic states were obtained. This process was repeated for each reference state using 10 different tetanization electrode pairs. By altering the 5 reference networks in this manner, a total of 500 new networks with different synaptic states was obtained.

Tetanic stimulation induces long-lasting changes in synaptic transmission (Bliss and Lømo, 1973), which shapes how neural circuits process information and is involved in behavioral modifications, including simple forms of learning in motor control (Fisher et al., 1997). Administration of 20 Hz tetanization, as in our study, was widely used to induce long-term facilitation (LTF) of postsynaptic potentials at crayfish neuromuscular junctions (Wojtowicz and Atwood, 1985; Delaney et al., 1989), short-term synaptic plasticity in anesthetized fish (Fortune and Rose, 2000), long-term potentiation (LTP) in hippocampal slices (Miles and Wong, 1987), and modification of synaptic strength in cortical cultures (Jimbo et al., 1999). In our simulated networks, tetanization induced both LTP and long-term depression (LTD) of synapses through STDP: firing of a postsynaptic neuron immediately after a presynaptic neuron results in LTP of synaptic transmission, and the reverse order of firing results in LTD (Desmond and Levy, 1983; Gerstner et al., 1996; Markram et al., 1997; Bi and Poo, 1998).

3.2.1.3 Simulations with random probing sequence (RPS)

For each network, we ran ten simulations with different 10-min random probing sequences (RPSs). Therefore, a total of 5050 simulations were performed separately on

505 networks (500 new networks and 5 reference networks). The probe stimuli were applied to all 60 electrodes, one at a time, with inter-stimulus intervals on a given electrode drawn from independent exponential distributions with a mean of 60 seconds. Thus, each electrode stimulated the simulated network with different random sequences, averaging 1 pulse per second for the whole array.

In each simulation, there were 10.0 ± 3.1 (mean and standard deviation) stimuli delivered at each electrode. The same Gaussian noise, introduced into neurons as fluctuations in membrane voltage, was used for each simulation to control the effects of self-firing or of sub-threshold fluctuation of membrane potential on activity. In order to ensure the statistics calculated from the same network correspond to the same synaptic state, the STDP algorithm was turned off throughout the simulation to prevent ongoing activity from changing the network state.

3.2.1.4 Plasticity statistics

Five commonly used statistics and the center of activity trajectory (CAT) were measured from each simulation (see Figure 3.6). The 5 commonly used statistics were firing rate (FR), firing rate histogram (FRH), mutual information (MI), shift-predictor corrected cross-correlogram (SCCC) and joint peri-stimulus time histogram (JPSTH). The details and sources of these statistics are given in Appendix B.

3.2.1.5 Center of activity trajectory (CAT)

CAT represents spatiotemporal patterns of network-wide population activity. As applied here, it is a spatially-weighted measure of temporally binned responses to single-electrode stimuli in neuronal circuitry space. During each simulation, stimuli at each electrode occurred multiple times (10.0 ± 3.1 times) in one RPS. FRH from recording electrode E_k to the stimulus at electrode P_i, $FRH_{E_k}^{P_i}$, was defined as the average number of spikes counted in a 5 msec moving time bin with 500 μsec time step over trials.

$FRH_{E_k}^{P_i}(n)$ represents the value of $FRH_{E_k}^{P_i}$ in the *n*th bin, and $Col(E_k)$ and $Row(E_k)$ are the column number and the row number of electrode E_k, respectively. For example, the electrode in column number 2 and row number 8 is 28 (see Figure 2.1). The value of the center of activity (CA) in the *n*th bin for stimulation electrode P_i has X and Y components, which are defined as:

$$[CA_X^{P_i}(n), CA_Y^{P_i}(n)] = \frac{\sum_{k=1}^{60} FRH_{E_k}^{P_i}(n) \cdot [Col(E_k) - R_{col}, Row(E_k) - R_{row}]}{\sum_{k=1}^{60} FRH_{E_k}^{P_i}(n)}$$

[Equation 3.1]

where R_{col} and R_{row} are the coordinates of a reference point (the physical center of the 8 by 8 grid of electrodes, in our case). CA was calculated with electrode number in the neuronal circuitry space, which is equivalent to using the physical location since the inter-electrode spacing is constant. The corresponding X and Y components for CAT are defined as:

$$\begin{aligned} CAT_X^{P_i} &= [CA_X^{P_i}(1), CA_X^{P_i}(2), ...CA_X^{P_i}(n), ...CA_X^{P_i}(N)] \\ CAT_Y^{P_i} &= [CA_Y^{P_i}(1), CA_Y^{P_i}(2), ...CA_Y^{P_i}(n), ...CA_Y^{P_i}(N)] \end{aligned}$$

[Equation 3.2]

where *N* is the total number of bins in $FRH_{E_k}^{P_i}$. Intuitively, CA is analogous to the center of mass, where the "mass" at an electrode location is determined by the recorded firing rate. CAT is the sequence of CAs over successive time intervals.

CA reflects spatial asymmetry of neural activity about the reference point (the center of the dish), and CAT represents the dynamics of CA. That is, if the network is

firing symmetrically, the CA will be at the center of the dish, whereas if the network fires mainly in one corner then the CA will be found off-center toward that corner. CA reduces the dimensionality from 60 to 2, and it is not an injective (information-preserving) function of activity distribution.

3.2.1.6 Evaluating the performances of different statistics

Performance of a statistic was defined by how small a change in network synaptic weights could be detected as significant. To evaluate performance, in each simulation, we evaluated the statistic for evoked responses to all 60 stimulation electrodes and joined together into a large vector representing the whole stimulus-response information (input-output function) of the network. We called this joint vector the whole-input-output (WIO) vector of the statistic. Figure 3.1 demonstrates the calculation of the WIO vector for CAT. A visualization of the change in WIO vectors for CAT from S_0 to S_1- S_{10} appears in Figure 3.2.

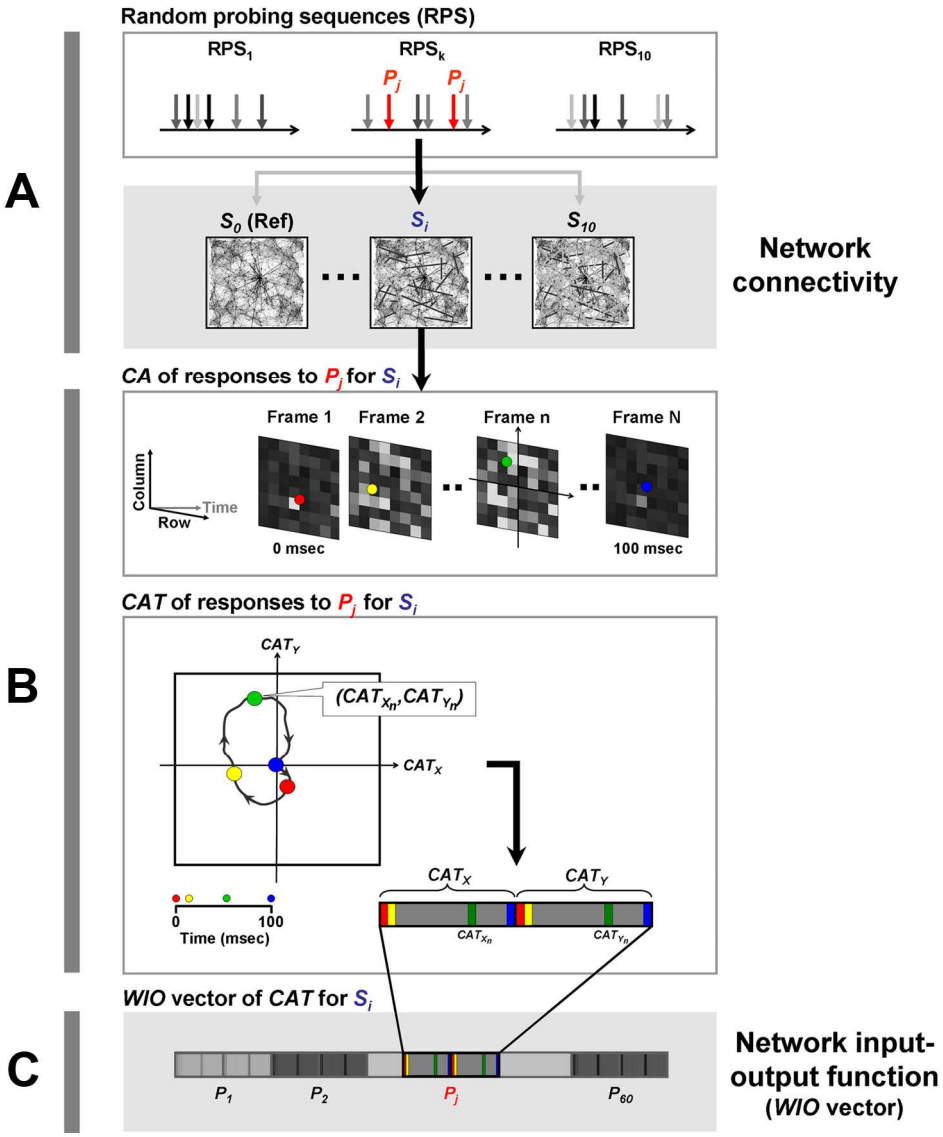

Figure 3.1. Whole-input-output (WIO) vectors for analyzing performances of different statistics: WIO vectors calculated from each statistic were used to represent network input-output function. As an example, the WIO vector of CAT calculated from probe responses to one RPS at one network state is demonstrated. **A.** An RPS, RPS_k, was delivered into a network with synaptic state S_i. **B.** CA was calculated for evoked responses to stimulation electrode P_j (j= 1 to 60). Each frame indicates the firing rate over a 5 msec moving time window (with 500 μsec time step) on an 8 by 8 grid of electrodes averaged over multiple stimuli at P_j (RPS_k might have multiple stimuli delivered at P_j, see A). The 2-D trajectory of CAs from Frame 1 to Frame N (from 0 to 100 msec after the stimuli), CAT, can be represented by a 1-D vector by joining CAT_X and CAT_Y. This vector represents CAT of responses to stimuli P_j at network state S_i. **C.** CATs for responses to 60 different stimulation electrodes (P_1 to P_{60}) were jointed together to form the WIO vector. This WIO vector represents the input-output function, in terms of CAT, of network state S_i. For each statistic, each synaptic state has one corresponding WIO vector to describe its input-output function. The statistic that is sensitive to changes in network synaptic states should be able to show significantly different WIO vectors from different synaptic states. One WIO vector was constructed for each RPS (RPS_k, k= 1 to10) in each network state (S_i, i= 0 to 10). Therefore, for each statistic, 5050 WIO vectors were obtained (= (500+5)∗10. 505: 500 new networks + 5 reference networks; 10: number of RPSs delivered on each network).

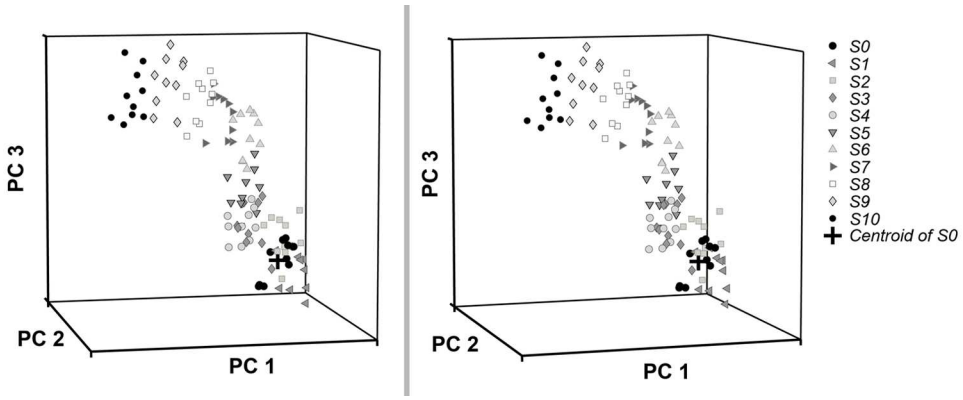

Figure 3.2. Multi-dimensional WIO vectors measured in different synaptic states in simulated networks: The WIO vectors measured from different synaptic states were different. This is a *cross viewing 3-D stereogram* of an example of the WIO vectors for CATs from the simulations at S_0 to S_{10} (generated by the same tetanization electrodes). Principal components analysis (PCA) was applied on the WIO vectors to visualize the data. Each symbol represents the first 3 principal components (PC1- PC3) of the WIO vector of a CAT from one simulation. Each synaptic state S_i has 10 corresponding symbols, which represent the results from 10 different simulations (with different RPSs). The distance of each symbol from the centroid of S_0 (shown as a cross) indicates amount of change in CATs between the corresponding synaptic state and the reference state. CATs obtained from the synaptic states generated by longer tetanizations were further from CATs obtained from S_0 than those from shorter tetanizations, indicating longer tetani cause greater plasticity.

We measured the Euclidian distances $E(S_i)$ between 10 WIO vectors (from 10 simulations with different RPSs) calculated at S_i to the centroid calculated at S_0 (shown as a cross in Figure 3.2). We then compared $E(S_i)$ for S_1- S_{10} to $E(S_0)$ separately, and the p-values (n= 10 RPSs, Wilcoxon signed rank test, which tests the magnitudes of the differences between paired observations without assumptions about the form of the distribution of the measurements) were computed to quantify the significance of differences. For each state, the relation between the mean p-values (n= 50, from 5 reference networks and 10 tetanization electrode pairs per reference network) and the mean absolute synaptic change (MASC) was quantified:

$$MASC(S_i) = \frac{1}{N} \cdot \sum_{k=1}^{N} \frac{\left\| W_k(S_i) - W_k(S_0) \right\|}{0.5} \cdot 100\% \qquad \text{[Equation 3.3]}$$

where N is the number of excitatory synapses and $W_k(S_i)$ represents the synaptic weight of the kth excitatory synapse at network S_i. We normalized the absolute change in each synapse by the possible range, 0 to 0.5, for excitatory synapses. We determined the performance of different statistics as the minimum MASC for p-values below a significance threshold of 0.05; this is termed "detectable MASC". The smaller the MASC a statistic can detect, the better the statistic's performance.

Successful performance can be artificially enhanced if a statistic mistakes some non-significant changes as being significant. Therefore, analyzing sensitivity (ability to detect significant plasticity) and specificity (ability to discount insignificant plasticity) can further determine the quality of a statistic. *Sensitivity* was defined as the probability that a statistic indicated significant difference when calculated from two significantly different network synaptic states (probability of a true positive). *Specificity* was defined as the probability that a statistic showed no significant difference when calculated from networks with no significant difference in synaptic state (probability of a true negative). Together, sensitivity and specificity described the accuracy of a statistic.

For each reference network, the 500 new states (S_1 to S_{10}) were individually evaluated to determine whether their synaptic weights distributions were significantly different than the distribution of the reference state (two-sample Kolmogorov-Smirnov test, which tests whether the two samples have the same distribution, two-tailed, $\alpha = 0.05$). If a statistic showed a significant difference (p-value< 0.05; see previous section) for a state that was significantly different than the reference state (according to Kolmogorov-Smirnov test), then the result was classified as being a true positive (*TP*). Conversely, if it showed no significance, then the result was considered a false negative (*FN*). If a statistic showed significance when calculated from a state that was not significantly different than the reference state, then the result was considered a false positive (*FP*). If it showed no significance, then the result was considered a true negative (*TN*). The numbers of *TP*, *FN*,

FP, and *TN* were counted for the 500 new networks, and the sensitivity and specificity were defined as:

$$Sensitivity = \frac{TP}{TP + FN} \times 100\%$$

$$Specificity = \frac{TN}{FP + TN} \times 100\% \qquad \text{[Equation 3.4]}$$

3.2.2 Experiments in living cultures

3.2.2.1 Culture and experimental protocol

Dense networks of dissociated cortical neurons (~ 7000 cells/mm^2) were prepared and cultured as described by Potter and DeMarse (Potter and DeMarse, 2001). The details of cell culture protocol used in this work are described in Appendix C.

Six experiments were performed on 5 cultures from 4 dissociations. Culture ages ranged from 1 to 3 months (Potter and DeMarse, 2001). We delivered biphasic stimuli (monopolar) at 500 mV and 400 us per phase by using our custom-made stimulator (Wagenaar et al., 2004; Wagenaar and Potter, 2004). Data acquisition, visualization, artifact suppression (Wagenaar and Potter, 2002), and spike detection were performed using Multichannel Systems hardware and our publicly available acquisition and analysis software, Meabench (Potter et al., 2006). Experiments were conducted in an incubator to control environmental conditions.

Each experiment consisted of a 2-hr period of RPS followed by a 15 minute tetanic stimulation followed by another 2 hour period of RPS (Wagenaar et al., 2006a). In six experiments, the RPS periods consisted of 6 electrodes stimulated in random order at an aggregate frequency of 0.5 Hz (In one experiment, the RPS periods consisted of only 4 probe electrodes). Prior to an experiment, every electrode was stimulated in random order

20 times, and electrodes with the 6 (or 4) highest responses (the total number of spikes counted within 100 msec latency after stimuli over recording electrodes) were selected as probe electrodes. The tetanus electrodes were randomly chosen from these. Fewer electrodes were used in RPS for living networks than simulated networks because not every electrode was able to evoke responses. Two of these electrodes were used for the tetanic stimulation: 150 trains of 20 paired pulse stimuli with 10 msec intervals between paired pulses, 50 msec intervals between pairs, and 6 s intervals between the start of each train.

3.2.2.2 Measures of CAT, FR, FRH and SCCC

We used evoked responses within 100 msec after the stimuli of RPS for statistics calculations (see Appendix B).We measured CAT from the evoked responses in the cultured networks and compared these to the three most commonly used statistics: FR, FRH and SCCC. MI was not measured, due to its poor performance in detecting network plasticity in simulations (see Section 3.3.1). JPSTH was not measured because of its high dimensionality and computation time (see Figure 3.6 and Appendix B).

3.2.2.3 Statistics

For each statistic, we calculated one WIO vector every 240 seconds (a "block") for the experiments with 6 probe stimulation electrodes, and every 160 seconds for the experiments with 4 probe stimulation electrodes. Thus, there were 19.9 ± 4.2 (mean and standard deviation) stimuli delivered at each electrode for each WIO vector. Three periods were used for statistics: *Pre1*, *Pre2* and *Post1* (see Figure 3.8A). Each period had a duration of 52.5 minutes, and the intervals between *Pre1* and *Pre2* and between *Pre2* and *Post1* were 15 minutes. The 15-min interval between *Pre2* and *Post1* was the tetanization. For each statistic, the mean distance of the WIO vectors in *Pre1* to the centroid of the WIO vectors in *Pre2* (*C*) was compared to the mean distance to their own

centroid (*D*). The ratio of change to drift, *C/D*, was used to quantify the change from *Pre1* to *Pre2* before the tetanus (no change if this ratio ~ 1). A similar measure between *Pre2* and *Post1* was used to quantify the change across the tetanus. The performance of each statistic to detect the tetanus-induced change was quantified by comparing the two *C/Ds* (n= 6 experiments, Wilcoxon signed rank test).

3.3 Results

We tested the performances of six network plasticity statistics in simulated networks: FR, FRH, MI, SCCC, JPSTH and CAT (all acronyms are shown on pages xvii-xix). We then applied the statistic with the highest performance for detecting changes in simulated network synaptic weights to *living cultures* on MEAs to detect tetanus-induced functional plasticity.

3.3.1 Network simulation: CAT showed the highest performance and sensitivity for detecting changes in network synaptic state

In simulation, the synaptic connectivity can be easily controlled and monitored, and the way(s) changes in synaptic connectivity affect a statistic's value can be directly studied. Various statistics were used to study functional connectivity in simulated networks under different synaptic states. The performance of different activity statistics to small differences in network synaptic connectivity was evaluated by measuring the statistical significance of the change in each statistic under different network synaptic states, altered gradually by simulated tetanic stimulation with spike-timing dependent plasticity (STDP).

Our 1,000-neuron LIF model and the living networks expressed similar spontaneous and evoked activity patterns, demonstrating the ability of the LIF model to represent the activity of biological networks. Raster plots and firing rate histograms of spontaneous activity and evoked responses obtained from both MEA cultures and

simulated networks are shown together for comparison, and demonstrate a remarkable similarity of activity patterns (Figure 3.3) (see other comparisons between the simulated network and the living MEA cultures in Section 2.3). For example, the rates of bursts (the ongoing synchronized barrages of action potentials) were 0.70 Hz and 0.73 Hz, and the proportions of spikes in bursts were 76% and 71%, in spontaneous activity of living and simulated networks respectively.

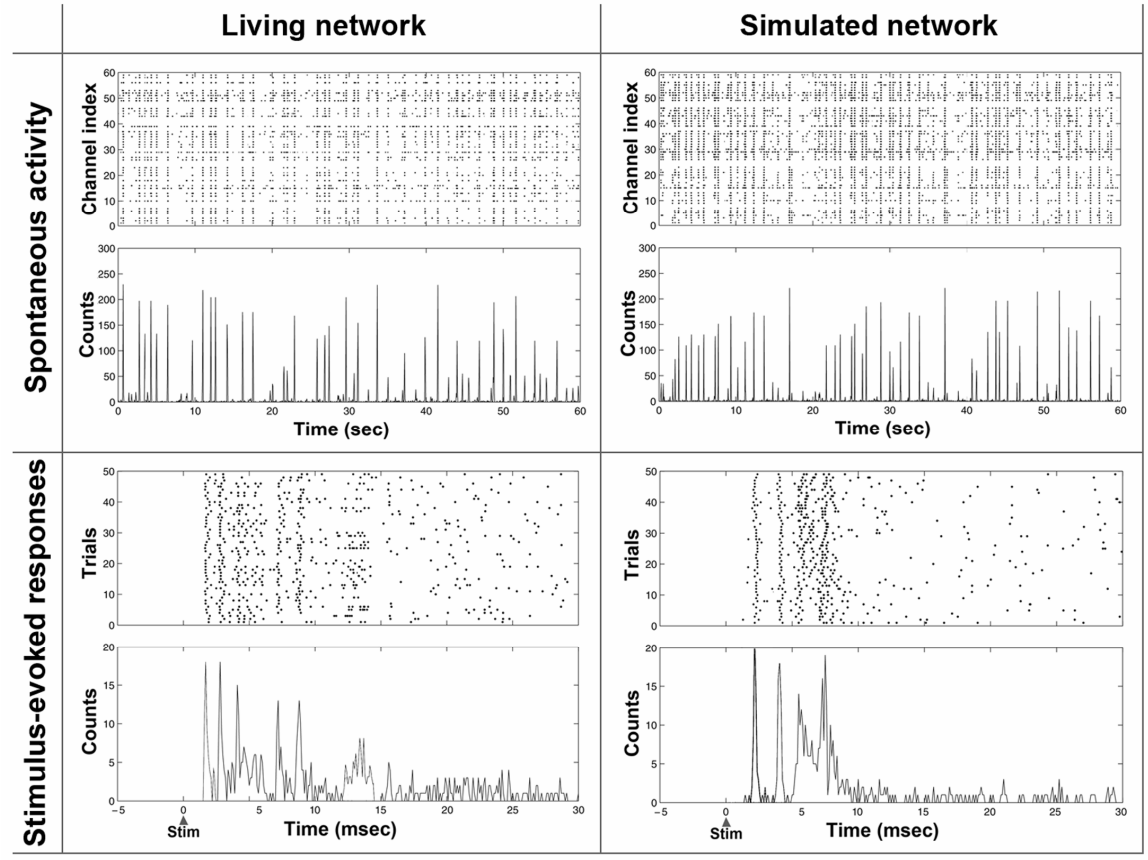

Figure 3.3. Comparison of the network activities from a MEA culture and a simulated network: Simulated spontaneous activity and evoked responses resemble the experimentally recorded data. **First row:** One minute of spontaneous activity was recorded from a living network by a 60-channel MEA and in simulation for comparison. The upper panels are spike raster plots. The lower panels are firing rate histograms, with bin sizes of 100 msec. **Second row:** Fifty trials of evoked responses recorded by one electrode in a living network and in simulation are shown for comparison. The upper panels are spike raster plots. The lower panels are firing rate histograms with a bin size of 0.1 msec. The timings of stimuli for each trial were aligned at time zero. In the simulation, each electrode recorded the activities occurring within 100 μm. (same data as for Figures 2.8 and 2.9)

A set of simulated networks with different synaptic states was created after tetanizations by using different electrode pairs and durations. In order to verify that different tetanization electrode pairs with different durations changed the synaptic weight distribution in the simulated networks, the centers of weights (CWs, see details in Section 4.2.2.5 and Equations 4.1 and 4.2) (Chao et al., 2005) that were found for network states (S_0 to S_{10}) were calculated and are shown in Figure 3.4A.

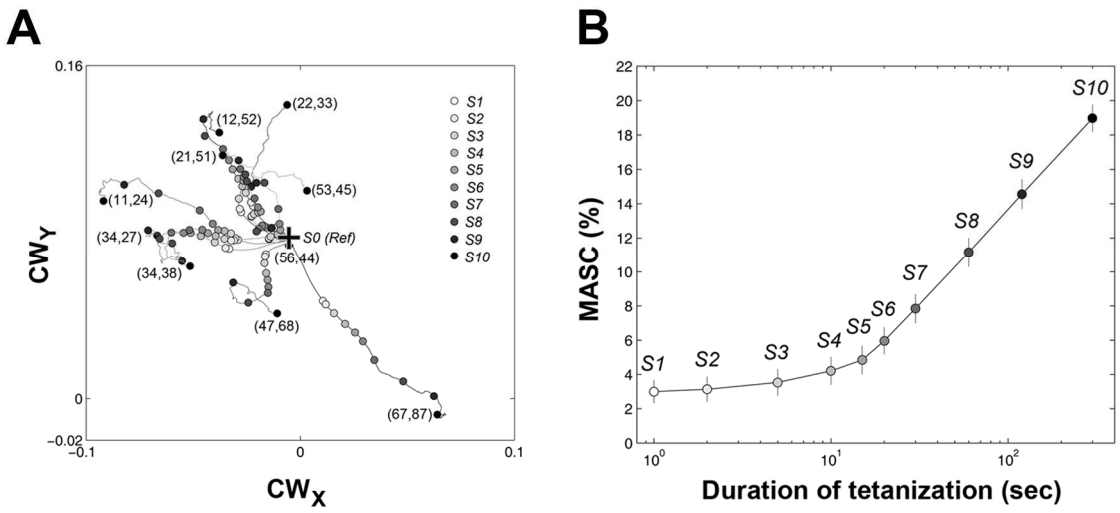

Figure 3.4. Setup of different synaptic states in simulation: A series of networks with different synaptic states were obtained by tetanization at different electrode pairs and with different durations from the reference network. From each reference network S_0, 10 tetani at different electrode pairs were delivered. For each tetanization electrode pair, 10 synaptic states were obtained after different durations. A**.** Different tetanization electrode pairs caused different changes in synaptic weight distribution. The center of weights (CW) was used to visualize how the symmetry of the network synaptic weight distribution changed over time. Each curve represents CWs corresponding to a tetanization electrode pair (the column-row numbers of the electrodes are shown at the end of each curve). Synaptic states (S_1 to S_{10}) "collected" at different tetanization durations and the corresponding reference state S_0 are shown as dots. **B.** The relation between mean absolute synaptic change (MASC) and the duration of tetanization (note log scale) from 5 reference networks. The means and the standard deviations of MASCs are shown (n= 50 networks: from 5 reference networks, each with 10 different tetani).

CW represents the spatial asymmetry of the network *synaptic weights* distribution. The CW changed differently for different initial network synaptic weight distributions, for different tetanization electrode pairs, and for different tetanization durations. Therefore, the various networks provide a basis to test the ability of various activity

statistics to discriminate between synaptic states. The mean absolute synaptic change (MASC) of all different states (S_1 to S_{10}) relative to the initial S_0 is shown in Figure 3.4B. For each tetanization duration, the mean and standard deviation of MASC were calculated (n= 50 networks, from 5 reference networks and 10 tetanization electrode pairs per reference network). Even with significantly different CWs, the MASCs from different networks "collected" at the same tetanization duration were similar in magnitude (standard deviation< 1%, n= 50), suggesting the magnitude of plasticity was dependent mainly on tetanus duration, as opposed to network structure.

Simulations with random probing sequences (RPSs) were performed on simulated networks with different synaptic weights distributions. The various activity statistics of evoked responses to the RPS were calculated from each simulation. An activity statistic with good discrimination of underlying synaptic states should show different results in different networks, even with only small differences in distribution of synaptic weights.

CAT demonstrated the highest performance in detecting changes in state among the 6 statistics. The performances of the statistics are shown in Figure 3.5. For each state S_i, the Euclidian distances $E(S_i)$ between each whole-input-output (WIO) vector of the statistic from S_i to the centroid of the WIO vectors from the corresponding S_0 were measured. Ten $E(S_i)$, measured from 10 RPSs in the same network with the same tetanization electrode pair, were compared to 10 corresponding $E(S_0)$, and the p-value was calculated (n= 10 RPSs, Wilcoxon signed rank test). For each state S_i, 50 p-values and 50 MASCs were collected from 50 networks (5 reference networks with 10 different tetanization electrode pairs per reference network). The mean and standard deviation of the p-values were plotted versus the corresponding MASC averaged across the networks (n= 50 networks). The detectable MASCs for CAT, JPSTH, SCCC, FRH, MI and FR were 4.68, 6.65, 6.75, 9.3, 11.7 and 15.7% respectively. CAT detected the smallest MASC and is therefore the best statistic.

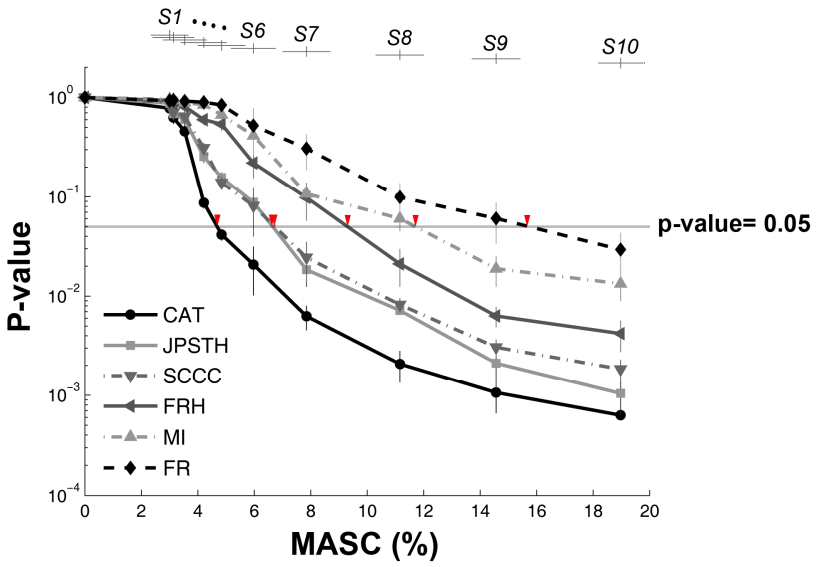

Figure 3.5. Evaluating the performances of different statistics: CAT showed the highest performance to detect changes in synaptic state among 6 statistics. The performance of different statistics to detect changes in synaptic state was evaluated by finding the "detectable MASC" at the point the p-values reach a threshold of 0.05 (shown as red arrows). For each state S_i, 50 p-values and 50 MASCs were collected from 50 networks (5 reference networks with 10 different tetanization electrode pairs per reference network, see Results). The mean and standard deviation of the p-values (n= 50 networks) were plotted versus the corresponding MASC averaged across the networks (n= 50 networks). The mean and standard deviation of MASCs (n= 50 networks) are shown on the top of the figure (with vertical offsets for clarity). The performance of the statistic to detect the difference in MASC shown in descending order is: CAT, JPSTH, SCCC, FRH, MI and FR.

The relative performance (the smaller the detectable MASC, the higher the performance), average compute time, and dimensionality are shown in Figure 3.6. The performance of the statistic shown in descending order is: CAT, JPSTH, SCCC, FRH, MI and FR. The dimensionality of each statistic from one stimulation electrode is described in Appendix B. The average compute times for CAT, FR, FRH, MI, SCCC and JPSTH were 31.8 sec, 1.2 sec, 30.6 sec, 3.9 min, 26.4 min and 70.4 min per simulation respectively (MATLAB 7.0, AMD Athlon processor, 2.08 GHz, 512 MB RAM). Among all 6 statistics, only FR and FRH had shorter compute time than CAT, and only FR had smaller dimensionality than CAT. However, CAT showed significantly higher performance than FR and FRH.

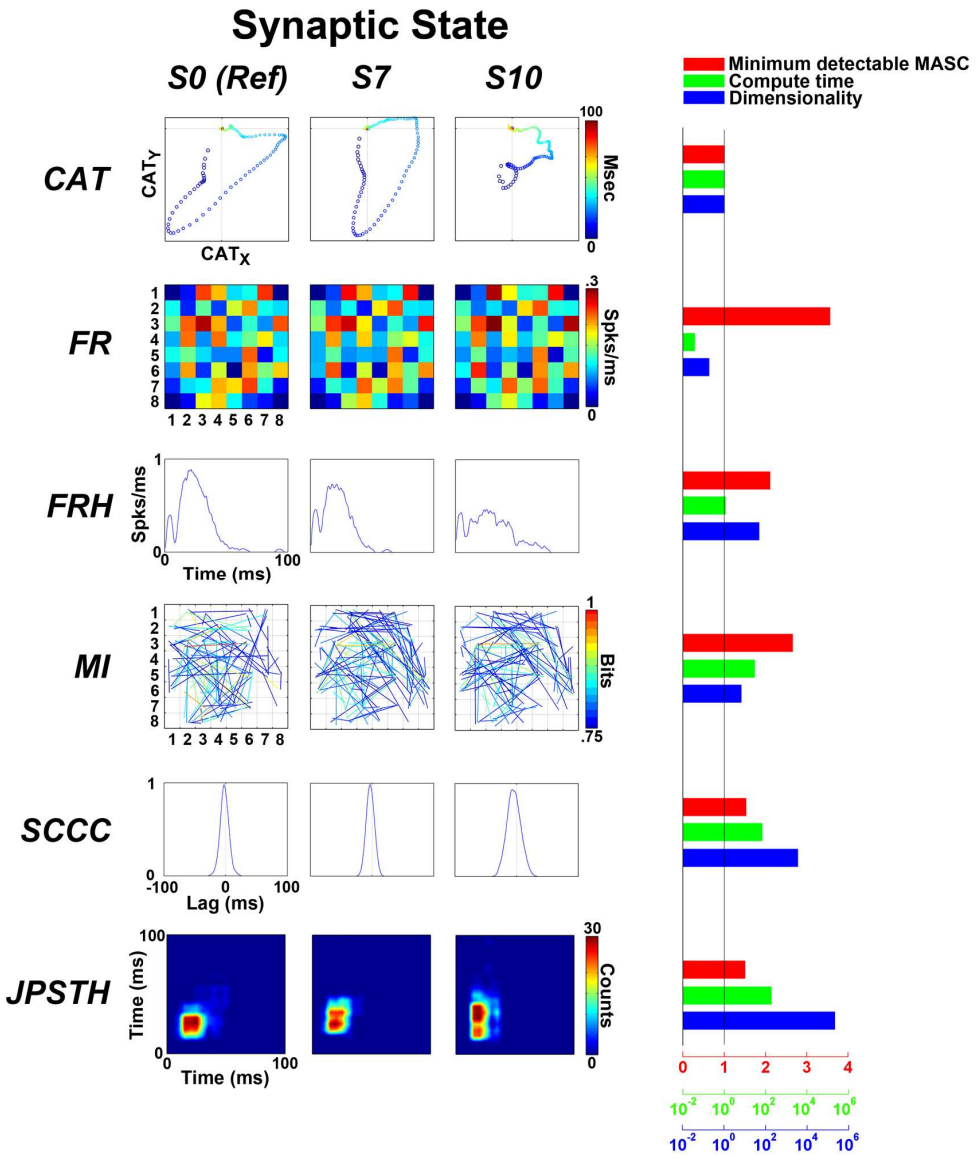

Figure 3.6. Comparison of the 6 different statistics: CAT was the most sensitive activity statistic and was highly efficient. Examples of 6 statistics calculated from the same RPS during 3 synaptic states are shown: S_0 (reference network), S_7 (network with ~ 50% of the maximal MASC, see Figure 3.4B) and S_{10} (network with the maximal MASC). All statistics were obtained from the same randomly chosen stimulation electrode. **CAT:** CATs are plotted as CAT_X vs. CAT_Y from blue to red. **FR:** Number of spikes per msec at each recording electrode is displayed according to the corresponding location in the 8 by 8 grids. **FRH:** FRHs, in the unit of number of spikes per msec, from a randomly chosen recording electrode are plotted. **MI:** MIs above 0.75 bits are plotted as colored lines between the corresponding electrode pairs. **SCCC:** SCCCs above zero from a randomly chosen pair of recording electrodes are plotted. **JPSTH:** JPSTH from the same randomly chosen pair of recording electrodes are shown. The performance (quantified by detectable MASC), compute time, and dimensionality, normalized by the values for CAT, are shown on the right. The axes for detectable MASC, compute time, and dimensionality are shown on the bottom in red, green, and blue respectively (the latter two are with logarithmic scales). Among all 6 statistics, only FR and FRH had shorter compute time than CAT, and only FR had smaller dimensionality than CAT. However, CAT had significantly smaller detectable MASC than FR and FRH. CAT showed significantly higher performance to detect the difference in network synaptic state than other statistics.

Table 3.1 shows the occurrences of true positives, false negatives, false positives, true negatives, and the sensitivity and specificity (see Section 3.2) of each statistic. CAT showed a sensitivity of 88.7%, the highest among all, with a specificity of 82.4%, comparable to JPSTH and SCCC. FRH, MI, and FR showed high specificity, which was an artifact of their low sensitivities. Sixty-eight out of the 500 new network states were found to not have significantly different distributions of network synaptic weights as compared to their original reference states (two-sample Kolmogorov-Smirnov test, two-tailed, $\alpha = 0.05$).

Table 3.1. Sensitivity vs. specificity in simulated networks

Statistic	*CAT*	*JPSTH*	*SCCC*	*FRH*	*MI*	*FR*	*CAT-ELS* (10 shuffles)
True positive (%)	77.6	70.4	68.0	47.4	44.0	27.2	30.6
False negative (%)	8.8	16.0	18.4	39.0	42.4	59.2	55.8
True negative (%)	11.2	11.0	11.2	12.2	13.6	13.6	12.6
False positive (%)	2.4	2.6	2.4	1.4	0	0	1.0
Sensitivity (%)	88.7	83.8	78.7	54.9	50.9	31.5	35.4
Specificity (%)	82.4	81.2	82.4	90.6	100	100	92.9

By evaluating the performance, sensitivity, specificity, and compute time, CAT was found to be most sensitive and highly efficient at detecting synaptic changes in simulated networks.

The alternative statistics are often used in spike-sorted data. Spike sorting is used to distinguish the spike trains of individual neurons (Ahissar et al., 1998; Jimbo et al., 1998a; Jimbo et al., 1999; Celikel et al., 2004), and can aid studies of neural populations (Lewicki, 1998), especially for neural computations that use spike timing. In simulated networks, activity of individual neurons can be directly observed. The analysis in Figure 3.5 was repeated using sorted neurons to investigate if the performance of the alternative statistics would improve. In the 5 reference simulated networks constructed, 4.1 ± 1.8

neurons were recorded per electrode, and the six statistics were re-calculated based on about 250 neurons instead of 60 electrodes. CAT remained unchanged as the sorted spikes were spatially summed as before (see Equation 3.1 in Section 3.2). Despite improved performance and sensitivity of the other 5 statistics, CAT *still* detected the most plasticity. JPSTH, SCCC, FRH, MI and FR improved 11.1, 17.6, 11.0, 35.0, and 31.2% in performance, respectively (Figure 3.7), and improved 1.9, 5.2, 9.7, 27.7, and 62.5% in sensitivity (see Table 3.2).

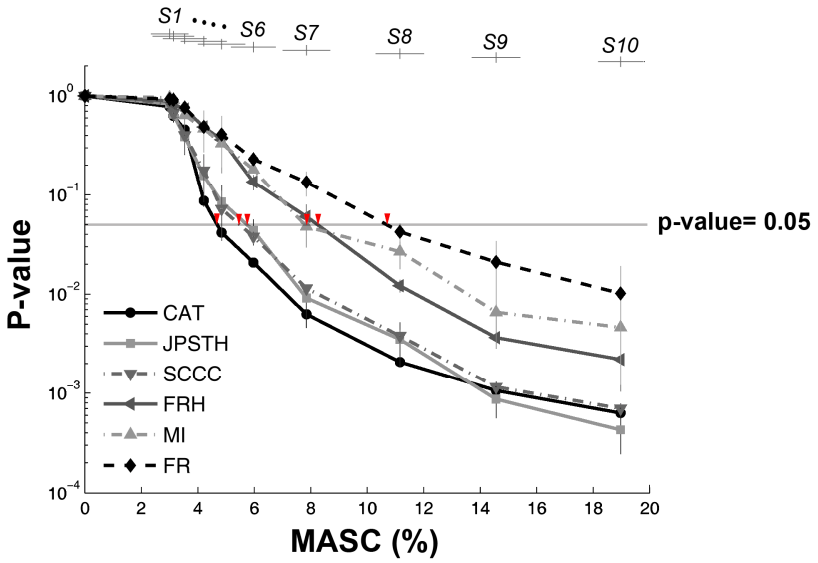

Figure 3.7. The performances of the statistics improved after spike sorting: The same figure representation is used as in Figure 3.6

Table 3.2. The sensitivities and specificities of the statistics after spike sorting

Statistic	*CAT*	*JPSTH*	*SCCC*	*FRH*	*MI*	*FR*
Sensitivity (%)	88.7	85.4	82.8	60.2	65.0	51.2
Specificity (%)	82.4	77.9	77.9	85.3	95.6	100

3.3.2 Experiments in living cultures: CAT revealed tetanus-induced long-term plasticity significantly better than the other statistics

CAT was measured from the evoked responses to RPS in 6 experiments on living cultured cortical networks and compared to the three most commonly used statistics: FR, FRH and SCCC. For visualization purposes, principal components analysis (PCA) was applied to the series of multi-dimensional WIO vectors to capture the largest variances and graphically demonstrate trends in changes. The first two principal components were normalized by subtracting their means and then dividing their standard deviations. The normalized first principal component (PC1) was plotted versus the normalized second principal component (PC2). An example comparing CAT, FR, FRH and SCCC is shown in Figure 3.8A. The corresponding CATs before and after tetanization from every block (a 240-sec window, see Section 3.2) and the average CATs are shown in Figure 3.8B. CATs from all experiments are shown in Figure 3.9.

The change across the tetanus was significantly greater than the drift before the tetanus for CAT (p-value< 1e-4, Wilcoxon signed rank test), FRH (p-value< 0.01) and SCCC (p-value< 0.01), but not for FR (p-value= 0.013). The *C/D* was used to quantify the change before the tetanus and the change across the tetanus (if the change is small, *C/D* ~ 1). The statistics of *C/D* from 6 experiments are shown in Figure 3.8C.

We did not perform spike sorting for experiments in living cultures. Standard spike sorting methods sort neural signals based on variations in spike waveform. In MEAs, local field potentials and overlapping action potentials distort the waveform to an extreme degree, and the electrodes are too far apart to allow triangulating common signal sources. Spike sorting was attempted, but proved to be unreliable.

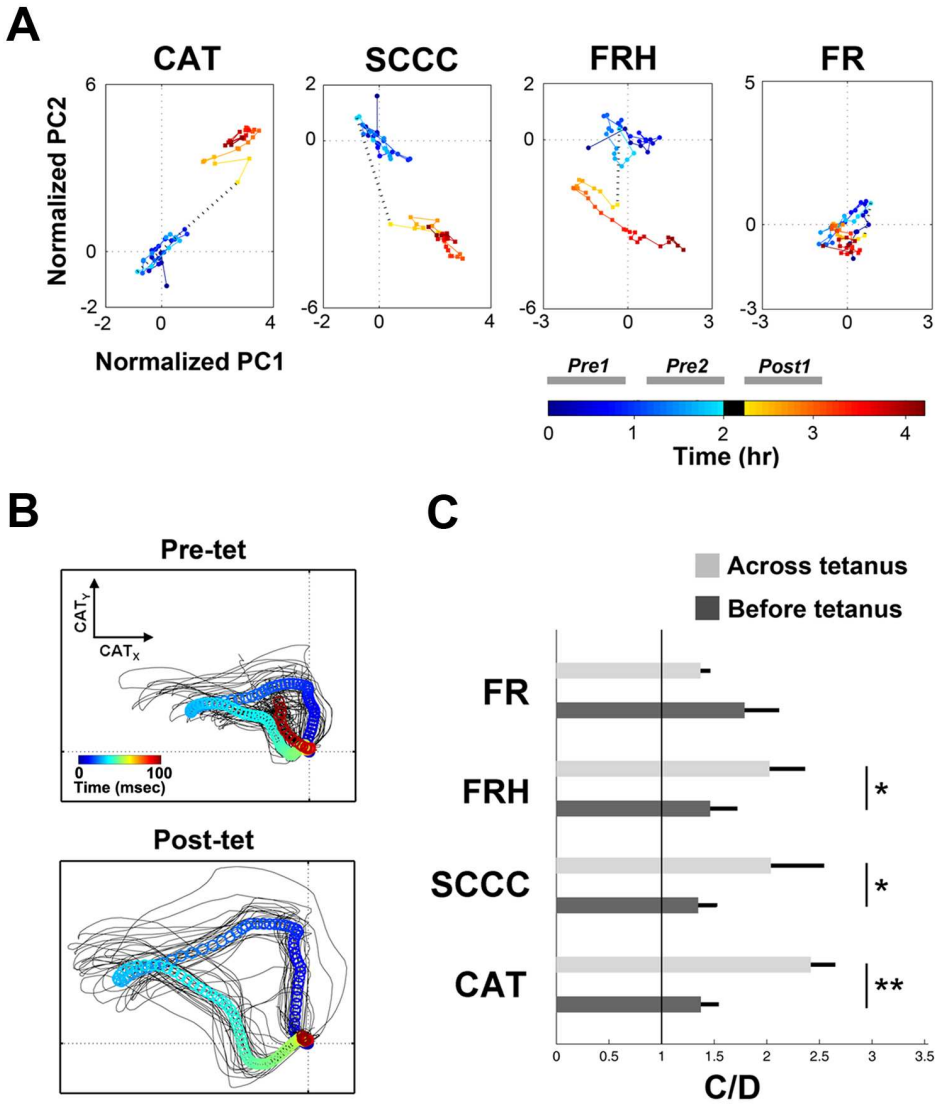

Figure 3.8. Comparison of the changes in CAT, FR, FRH and SCCC across tetanization in living MEA cultures: A. An example of comparison of CAT, FR, FRH and SCCC (from evoked responses to RPS in one experiment) before and after tetanization is shown. Principal components analysis (PCA) was applied on multi-dimensional WIO vectors for visualization purposes. The normalized principal component was obtained by removing its mean and then dividing through by its standard deviation. The normalized first principal component (PC1) was plotted versus the normalized second principal component (PC2). Each dot represents the statistic calculated from every block (a 240-sec window), and the color indicates the corresponding time (shown in the colorbar). The black dashed line represents the tetanus. The separation between Pre-tetanization cluster (bluish dots) and Post-tetanization cluster (reddish dots) indicates the change of the statistic across the tetanus. **B.** Different patterns of CATs were observed before and after tetanization. CATs from an example experiment were overlaid (black trajectories), and the average CATs were shown by series of circles (from blue to red across 100 msec probe response). **C.** The statistics of *C/D* from 6 experiments showed that the change across the tetanus was significantly greater than the drift before the tetanus for CAT (**, p-value< 1e-4, Wilcoxon signed rank test), FRH (*, p-value<0.01) and SCCC (*, p-value<0.01), but not for FR (p-value= 0.013). The p-values indicate that CAT was more capable of detecting the change over the drift than FRH, SCCC and FR.

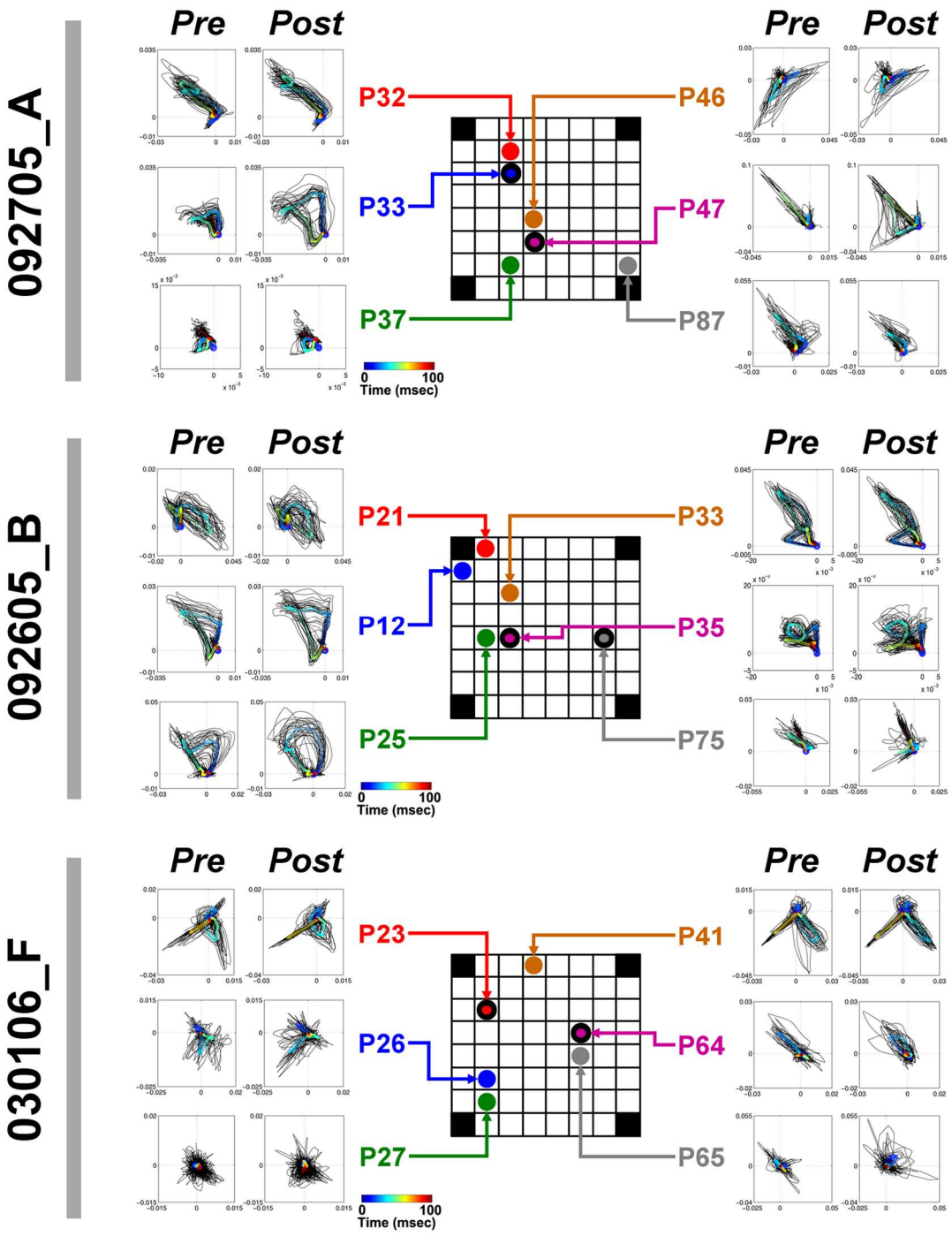

Figure 3.9. CATs in six experiments with MEA cultures: Different patterns of CATs were obtained before and after tetanization from 6 experiments in MEAs. CATs obtained before tetanization (*Pre*) and after tetanization (*Post*) for each probe electrode are shown. The column-row numbers of corresponding probe electrodes are shown in the 8 by 8 MEA grids shown in the middle. The tetanization electrodes are depicted by thick black circles. For each probe, CATs calculated for each "block" (see Section 3.2) are shown in black lines and overlaid. The averaged CATs are shown in colored circles (from blue to red).

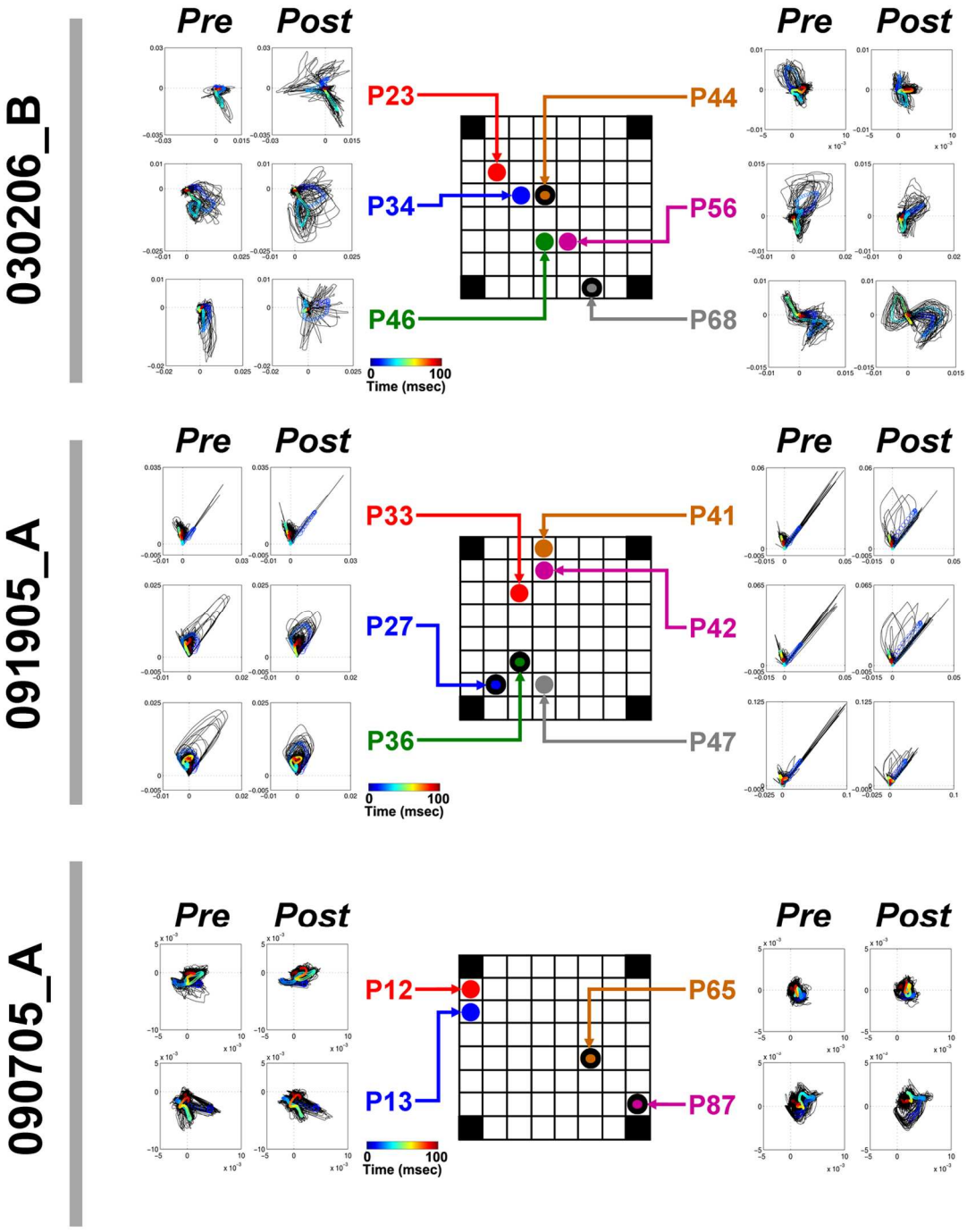

Figure 3.9. (continued) CATs in six experiments with MEA cultures

3.3.3 Electrode shuffling demonstrates the importance of electrode locations shown by CAT

In order to get some idea of the degree of localization of function in cultured cortical networks, the performance of CAT statistic with electrode locations shuffled (CAT-ELS) was calculated (see Appendix B). In CAT-ELSs, the information about the physical locations of the recording electrodes was removed. In both simulations and experiments in living cultures, the electrode locations were shuffled 10 times, and 10 different corresponding CAT-ELSs were generated. The performance of these CAT-ELSs was evaluated and compared to the original CAT.

CAT, unlike the other statistics, incorporates the physical locations of the recording electrodes. This is the primary difference between methods, and we attribute CAT's superior performance in both living and simulated networks to this feature. For simulated networks, the comparison of the performance between CAT-ELS and original CAT is shown in Figure 3.10A. The detectable MASC (threshold p-value= 0.05) for Mean CAT-ELS was 10.8%, which was greater than CAT (4.68%). The decrease in performance (increase in detectable MASC) indicates that electrode locations significantly affect performance of CAT in simulated networks. Furthermore, the sensitivity of CAT-ELS was 35.4%, significantly smaller than CAT's 88.7% (see Table 3.1).

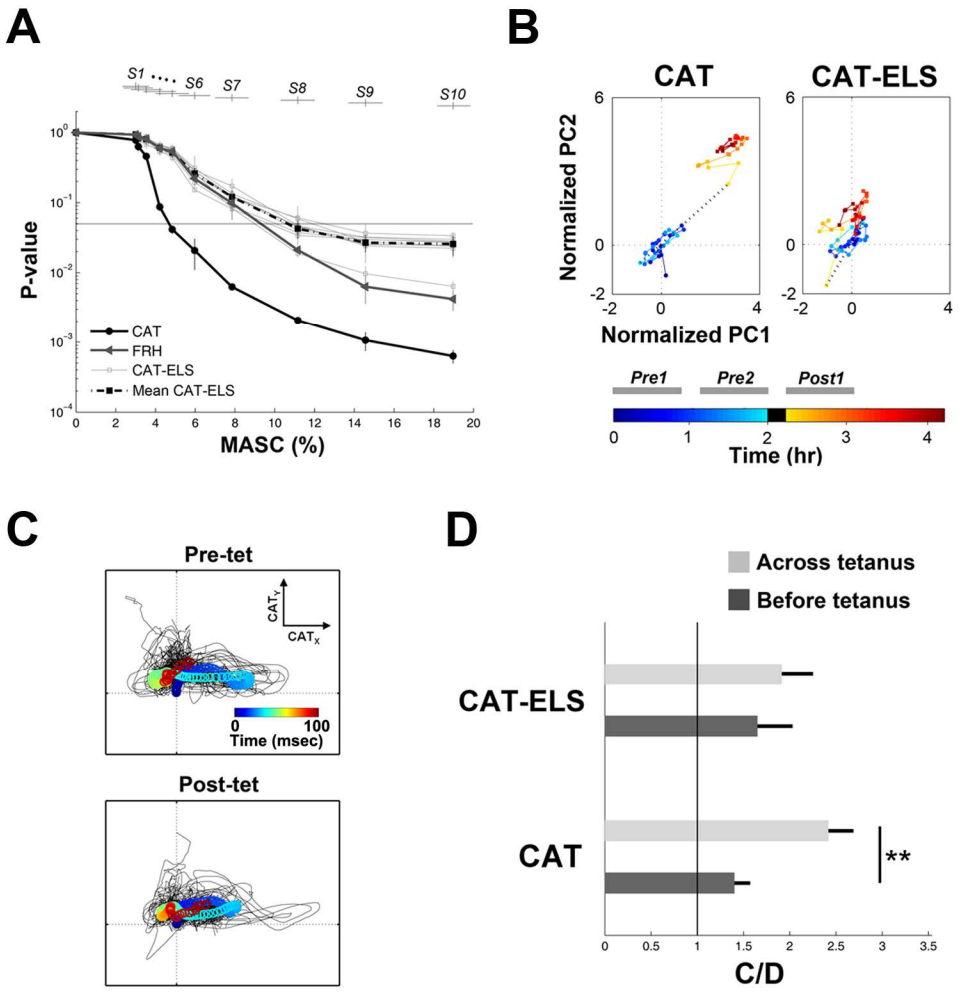

Figure 3.10. Comparison of CAT and CAT-ELS in simulated and living networks: A. A comparison of the performance of CAT and CAT-ELS in simulated networks (the representation is the same as Figure 6). Ten performance curves corresponding to different random shuffled electrode locations (CAT-ELS) and the mean of the ten curves (Mean CAT-ELS) are shown. The performance curve of FRH is also shown for comparison. The detectable MASC (threshold p-value= 0.05) for Mean CAT-ELS was 10.8%, which was greater than CAT (4.68%). The decrease in performance (increase in detectable MASC) indicates the importance of physical electrode locations in the performance of CAT in simulated networks. **B.** An example comparison of CAT and CAT-ELS in a living MEA culture before and after tetanization (the data used and representation are the same as in Figure 3.8A). The difference between Pre-tetanization (bluish dots) and Post-tetanization cluster (reddish dots) was reduced by shuffling electrode locations in CAT-ELS. **C.** The electrode locations shuffling "collapsed" the patterns of CAT-ELSs before and after tetanization in a living MEA culture. The difference between before and after tetanization trajectories (compared to Figure 3.8B) was reduced in CAT-ELS. **D.** The statistics of *C/D* for CAT-ELS in living networks (n= 60, 6 experiments, 10 shuffles for each experiment). The change across the tetanus was not significantly different than the drift before the tetanus (p-value= 0.19, Wilcoxon signed rank test), unlike CAT (**, p-value< 1e-4). Thus, for both simulated and living networks, the shuffling of signals from different electrodes greatly reduces the performance of CAT for detecting stimulus-induced synaptic change over a background of continual synaptic drift.

For living MEA cultures, one example of the comparison between CAT and CAT-ELS is shown in Figure 3.10B. The corresponding CAT-ELSs before and after tetanization from every block are shown in Figure 3.10C. The electrode location shuffling "collapsed" the patterns of CAT-ELSs before and after tetanization (compare to Figure 3.8B). The difference between Pre-tetanization and Post-tetanization clusters found in CAT was also reduced in CAT-ELS (Figure 3.10B).

The statistics of *C/D* for CAT-ELS (n= 60, 6 experiments, 10 shuffles for each experiment) are shown in Figure 3.10D. The change across the tetanus was significantly greater than the drift before the tetanus for CAT (p-value< 1e-4, Wilcoxon signed rank test), but not for CAT-ELS (p-value= 0.19).

3.4 Discussion

3.4.1 Statistics of functional plasticity in extracellular multi-electrode recording

While comparing firing rates shows plasticity in intracellular recordings of monosynaptically connected neurons, more detailed statistics are necessary for spatiotemporal population activity patterns in extracellular multi-electrode recordings. Electrode spacing on the order of hundreds of microns means that any induced or observed plasticity will span pathways of multiple neurons instead of neighboring monosynaptic neurons (Jimbo et al., 1999). Intracellularly, synaptic strength is directly observable by stimulating a presynaptic neuron while recording from an adjacent postsynaptic neuron. Extracellularly, synaptic noise across a chain of neurons and convergent pathways will obscure firing rate measures of stimulus-induced plasticity.

Alternatively, by incorporating the timing and spatial flow of activity, spatiotemporal patterns have been found both *in vivo* and *in vitro*. Spike sequences, imposed upon the network by behavioral manipulations, recur spontaneously during subsequent sleep episodes (Nádasdy et al., 1999; Nádasdy, 2000; Lee and Wilson, 2002).

Calcium imaging of cortical slices reveals re-activation of sequences of neurons, "cortical songs", with distinct spatiotemporal structures over tens of seconds (Ikegaya et al., 2004). Robust recurrent spike patterns were also found in a detailed cortical simulation (Izhikevich et al., 2004) and in living slices (Fellous et al., 2004). CAT provides a new and simple statistic to detect spatiotemporal patterns in networks and extends the previous studies by quantifiably demonstrating its ability to discern plasticity.

3.4.2 Region-specific plasticity

Although FRH included detailed temporal information about the activity dynamics at all electrodes, it was less capable of capturing network plasticity than CAT, which has the same temporal resolution as the FRH but "condenses" the spatial dimension by linear combination (see Equation 3.1). We hypothesize this was due to the inclusion of spatial information of the electrode locations. The performance and the sensitivity of CAT with electrode locations shuffled was significantly worse than unshuffled CAT, both in simulation (the detectable MASC increased from 4.68% to 10.8%, and the sensitivity decreased from 88.7% to 35.4%) and in living networks (the change across the tetanus was significantly greater than the drift before the tetanus for CAT, but not for CAT-ELS) (see Figure 3.10 and Table 3.1). This indicates that activity varied systematically with electrode location, and also suggested that the observed network plasticity was *region-specific*: the plasticity was not symmetrically distributed throughout the network. This further suggests that despite the apparent random connectivity of cultured neurons, neuron location played a role in tetanus-induced plasticity.

Region-specificity was not limited to plasticity induced by tetanization. In simulation, we also altered the weights of randomly-selected synapses in reference networks to different degrees to generate different new network states. CAT still showed the highest sensitivity to changes in MASC, and furthermore, the sensitivity of CAT-ELS

was still significantly lower (data not shown). Despite the synaptic plasticity not being region specific, the spatiotemporal flow of neural activity was region dependent, effectively making the plasticity of neural activity region specific. This result supports the notion of synfire chains or braids of neural activity (Ikegaya et al., 2004), where information is transmitted in a pipeline of neighboring pathways as opposed to a single string of connections. In this study, tetanization was used to obtain different synaptic states since it provided a more realistic form of plasticity, and a more straight-forward comparison to our study of local functional plasticity in living networks.

A common misconception regarding dissociated cultures is that they are random, homogenous, and lack structure, and thus cannot support stable changes to synaptic weight associated with memory formation. While plated from a random cell suspension, microscopic observation reveals that a heterogeneous arrangement develops over time (Gross and Kowalski, 1999; Segev et al., 2003). Although very different than structures found *in vivo*, the ability of neurons and glia to interact remains and a network having a diverse array of activity patterns arises spontaneously (Wagenaar et al., 2006c). Altering sensory input of thalamic relays to cortical areas has demonstrated that the cortex develops structure according to the type of the sensory input (Sur et al., 1988), which suggests an important relationship between neural structure and function. CAT demonstrates that structure is also relevant to neural function in a cultured network, and that tetanic stimulation alters network function. Future experiments will incorporate closed-loop sensory-motor feedback and optical imaging to investigate the network mechanisms of our cultures to functionally and structurally adapt to environmental interaction (Potter et al., 2006).

3.4.3 CAT vs. population coding

It is important to note that CAT is distinct from the population vector description of neural activity (Georgopoulos et al., 1986; Caminiti et al., 1990). Population coding,

which is widespread in the brain and in invertebrate nervous systems, has been found in the motor cortex (Georgopoulos, 1994), premotor cortex (Caminiti et al., 1990), hippocampus (Wilson and McNaughton, 1993a) and other cortical areas. It demonstrates how the firing rates of a group of broadly tuned (e.g., to a direction of arm movement) neurons, taken together, provide an accurately tuned representation. With population codes, a fixed-weight linear combination of neuronal activity is projected in a sensory input space or a motor output space (Carmena et al., 2003). In contrast, CAT incorporates information about the physical recording locations into its linear combination calculation, and projects neuronal activities recorded at different sites into the actual neuronal location space in order to depict the dynamics of the population activity. Furthermore, the linear combination of activities in CAT is normalized by the total firing rate across all electrodes (see Equation 3.1).

CA is a measure of the asymmetry of the spatial activity distribution, and CAT is a measure of its dynamics. Incorporating information of electrode locations in the calculation of CAT was inspired by the differential firing rate statistic described by Wagenaar et al. (2006), where differences between firing rates from electrodes located at different quadrants of an MEA were used to describe the dynamics of spontaneous bursts. A similar measure of population activity flow was applied in a human study to quantify the trajectory patterns of the traveling electroencephalographic alpha waves across the scalp (Manjarrez et al., 2007).

3.4.4 Plasticity vs. spontaneous bursting

Without external stimulation, the most prominent feature of spontaneous activity found in MEA cultures and in simulated networks is synchronous bursting (Wong et al., 1993; Kamioka et al., 1996; Gross and Kowalski, 1999; Van Pelt et al., 2004; Wagenaar et al., 2005), and bursts were found to have effects on tetanus-induced synaptic plasticity in cortical neurons (Maeda et al., 1998b). In simulation, the network synaptic state after

tetanization was found to change gradually due to the presence of spontaneous bursts, which makes quantifying tetanus-induced plasticity difficult (Chao et al., 2005). In the 6 experiments we performed on living MEA cultures, 8.57 ± 3.33 spontaneous bursts per minute and 16.06 ± 4.55 stimulus-evoked bursts per minute were observed. Even with the presence of the spontaneous bursts, the tetanus-induced plasticity was still detected by using CAT. By controlling the level of bursting in MEA cultures with multi-site stimulation (Wagenaar et al., 2005), we used CAT measure to demonstrate that a network's ability to induce and/or maintain tetanus-induced plasticity could be enhanced by reducing the degree of bursting (Madhavan et al., 2007c) (also see Appendix F).

3.5 Conclusion

CAT's superior performance, sensitivity, and low computational load make it an attractive method for real-time applications. CAT can also be applied to *in vivo* multi-electrode or optical recording studies for neural activity aligned to behavioral or sensory cues. As techniques for observing distributed activity become faster and more fine-grained, studying the details of the spatial flow of activity through neuronal networks will reveal more and more about processes of learning and memory.

CHAPTER 4

STABILIZING EFFECTS OF RANDOM BACKGROUND STIMULATION (RBS) ON NETWORK PLASTICITY[x]

We constructed a simulated spiking neural network model to investigate the effects of random background stimulation (RBS) on the dynamics of network activity patterns and tetanus induced network plasticity. RBS was used to re-afferent the sensory-deprived MEA cultures by continuous electrical stimulation, which is analogous to continuous sensory inputs and ongoing processing in the brain. To help visualize activity patterns and plasticity in our simulated model, we introduced new population measures called the center of activity (CA) and center of weights (CW) to describe the spatiotemporal dynamics of network-wide firing activity and network-wide synaptic strength, respectively. Without RBS, the network synaptic weights were unstable and often drifted after tetanization. In contrast, with RBS, the network synaptic weights remained close to their values immediately after tetanization. The simulation suggests that the effects of tetanization on network synaptic weights were difficult to control because of ongoing synchronized spontaneous bursts of action potentials. RBS helped maintain network synaptic stability after tetanization by reducing the number and thus the influence of spontaneous bursts. We used our simulated network to model the interaction between ongoing neural activity, external stimulation, and plasticity, and to guide our choice of sensory-motor mappings for adaptive behavior in hybrid neural-robotic systems or "hybrots." We also propose a potential paradigm for hybrot control with RBS and tetanization in order to show goal-directed learning behavior.

4.1 Introduction

In vitro model systems are helpful to understand brain functions because they reduce the brain's overwhelming complexity. However, having been severed from the intact brain, they lack the rich sensory inputs the brain received continuously. In unanesthetized animals, cortical neurons display a combination of spontaneously generated and sensory-experience-dependent activity (Riva Sanseverino et al., 1973; Legendy and Salcman, 1985), which endows the brain with an ability to accommodate to dynamically changing inputs during development and throughout life (Katz and Shatz, 1996). Sensory feedback in the brain also plays a critical role in learning *in vivo*. This has

---

[x] Adapted from: Zenas C. Chao, Douglas J. Bakkum, Daniel A. Wagenaar, and Steve M. Potter (2005): *Effects of random external background stimulation on network synaptic stability after tetanization: a modeling study*. Neuroinformatics **3:3**, 263–280.

been widely demonstrated in learning and maintaining of accurate vocalizations, where various perturbations of auditory feedback elicited disruptions of the sequencing and timing of ongoing vocalization in humans (Lee, 1950; Houde and Jordan, 1998) and in songbirds (Sakata and Brainard, 2006). Sensory experience also modulates spine formation, plasticity, and maintenance, where a decrease in spine density was observed in the primary visual cortex of mice raised from birth in total darkness (Valverde, 1967; Nimchinsky et al., 2002) and in the rat hippocampus after entorhinal cortex lesions (Parnavelas et al., 1974). In order to study learning using *in vitro* neuronal networks (which are usually sensory-deprived), this evidence suggests the importance of incorporating continuous sensory input, or re-afferentation.

Spontaneous bursting, a transient increase in the population firing rate, is a characteristic activity pattern in sensory-deprived neuronal networks. Reduced inputs from other brain areas result in large-scale synchronized bursting, such as bursting in mammalian thalamus during drowsiness, sleep, or anaesthesia (Steriade et al., 1993; Krahe and Gabbiani, 2004). Bursts of synchronized firings occur in the developing retina in the dark (Meister et al., 1991; Wong et al., 1993), and disappear after the retina becomes mature and visually responsive (Demas et al., 2003). *In vivo* cortical slabs isolated from thalamic and cortical inputs exhibit spontaneous oscillations of population firings (Timofeev et al., 2000), whereas intact and awake cerebral cortex displays activity patterns in a much richer spectrum (Steriade et al., 1993; Steriade, 1996). Spontaneous population bursts were also widely observed in *in vitro* networks prepared from the cortex (Murphy et al., 1992; Gross et al., 1993a; Kamioka et al., 1996; Canepari et al., 1997; Latham et al., 2000b; Wagenaar et al., 2006c), hippocampus (Garaschuk et al., 1998), spinal cord (O'Donovan et al., 1998; Tscherter et al., 2001), and retina (Meister et al., 1991). Furthermore, the bursting activity pattern could disrupt long-term potentiation (LTP) in hippocampal slices (Moore et al., 1993; Hu et al., 2005). This suggests that

spontaneous bursts in sensory-deprived networks might alter previous stimulus-induced changes in synaptic strengths.

Activity-dependent modification of synaptic strengths plays a central role in the processes of learning and memory in the central nervous system (Bliss and Collingridge, 1993). In cultured cortical networks, those changes have been experimentally induced by a strong electrical stimulation called a tetanus. Jimbo and co-workers have shown that these cellular plasticity mechanisms scale to the network level, studied in cultured neurons on multi-electrode arrays (MEAs) (Jimbo et al., 1999). In their studies both LTP and long-term depression (LTD) were observed, though the change could not be predicted nor controlled. This lack of predictability and controllability makes it difficult to create effective learning protocols for hybrots (see Chapter 1). We hypothesize that the effects of a tetanus on network synaptic strengths are difficult to control because the synaptic weights are also being altered by spontaneous bursts. This could be avoid by reducing the occurrence of spontaneous bursts by re-afferentation.

In order to restore sensory input to cultured MEA networks to obtain more controllability over stimulus-induced plasticity, we designed a stimulation protocol called random background stimulation (RBS). With random stimuli distributed over all electrodes at an aggregate frequency of 1 Hz in the simulated networks of Chapter 2, tetanus-induced changes in network synaptic weights were stabilized. We hypothesized that RBS negated "attractors" in network synaptic weight distributions caused by spontaneous bursts, and prevented network synaptic weights from drifting to such attractors after inducing plasticity with electrical stimulation. This is consistent with results from another simulation study of 1,000 excitatory neurons, where random activation counterbalanced degradation of synaptic weights and maintained the basins of attraction of all memories (Horn, 1998).

In a different approach, a burst-control stimulation protocol consisting of a group of electrodes cyclically, not randomly, stimulated with an aggregated frequency of 50 Hz

was found to completely eliminate spontaneous bursts in dissociated cortical cultures (Wagenaar et al., 2005). Similar to RBS, the burst-control stimulation stabilized tetanus-induced plasticity in dissociated cortical cultures (Madhavan et al., 2007c). However, different mechanisms might be involved. RBS evoked network-wide responses with unbiased spatiotemporal structure, while the burst-control stimulation desynchronized spontaneous activity into spatially-localized and temporally-dispersed responses.

Here, we demonstrate the stabilizing effects of RBS on stimulus-induced plasticity, and propose a potential paradigm for hybrot control with RBS and tetanization in order to show goal-directed learning behavior, which became the precursor of our closed-loop design described later in Chapters 5 and 6.

4.2 Methods

4.2.1 Living cultured neuronal network model

4.2.1.1 Cell culture, recording and stimulation system

Dense cultures of dissociated neocortical neurons (2500 cells/mm^2) were prepared as described before (Potter and DeMarse, 2001). The details of cell culture protocol used in this work are also described in Appendix C.

4.2.1.2 Stimulation protocol

Random background stimulation (RBS) was performed on one cultured network. For all 53 usable electrodes, 53 trains of 1/53 Hz stimulation generated by a Poisson process were applied. The spatiotemporal structure of RBS is identical to random probing sequence (RPS) described in Chapter 3 (Section 3.2.1.3), where each usable electrode stimulated the network with different random sequences, averaging 1 pulse per second for the whole array (also see RBS in simulated networks in Section 4.2.2.1). However, the purpose of RPS was to evaluate network instantaneous input-output properties in a

short period of 10 minutes, whereas RBS was continuously delivered as an artificial sensory input to the sensory-deprived network.

4.2.2 Artificial neural network model

For simulation experiments, we used five 1,000-LIF-neuron simulated networks, as described previously in Chapter 2, each with a different connectivity.

4.2.2.1 Artificial neural network initialization and stimulation protocol

All excitatory synaptic weights were initially set to 0.05 and could vary between zero and 0.1 due to STDP. At the maximal weight, each spike would have a 50% probability of evoking a spike in postsynaptic neuron, due to its summation with intrinsic noise (Figure 2.7). The synaptic weights for the inhibitory connections were fixed at -0.05. The networks were run for 2 hours in simulated time until the synaptic weights reached the steady state. Most of the excitatory synaptic weights (93 ± 2%) in 5 simulated networks were less than 0.01 or greater than 0.09 (Figure 2.8). This bimodal steady-state distribution of weights arose from the STDP learning rule, as previously observed by Song et al. (Song et al., 2000), and Izhikevich et al. (Izhikevich et al., 2004). The set of synaptic weights after 2 hours, which stabilized without external stimuli, was used for the subsequent simulation experiments as the initial state.

Two types of electrical stimuli were delivered to the simulated networks, *tetanization* and *background* stimuli. Tetanization was applied simultaneously at two stimulation electrodes (electrode 33 and 66, in column-row number, see Figure 2.1) at 20 Hz for either 10 seconds or 5 minutes; tetanization was used to induce change in the network synaptic weights (as described in Chapter 3). The background stimuli were applied to all 64 electrodes, one at a time, with random intervals generated by Poisson processes, at an average rate of 1/64 Hz per electrode. Thus, each electrode stimulated the

simulated network with different random sequences, averaging 1 pulse per second for the whole array.

Four experiments were performed on each of five simulated networks to investigate how the tetanization and the random multi-site background stimulation affected the network synaptic weights:

1. **"Short"**: Spontaneous activity was recorded for 10 minutes (pre-tetanization period), before a short tetanization was applied for 10 seconds. After tetanization, spontaneous activity was recorded for an additional 50 minutes (post-tetanization period).
2. **"Long"**: Same as "Short", but the tetanization period was 5 minutes instead of 10 seconds.
3. **"Short+Background"**: Same as "Short", but with random multi-site background stimulation turned on during the whole simulation.
4. **"Long+Background"**: Same as "Long", but with random multi-site background stimulation turned on during the whole simulation.

4.2.2.2 Measures of network activity and network synaptic weight

To help visualize activity patterns and plasticity in the artificial neural network, we used the center of activity (CA) (described in Section 3.2.1.5 and Equation 3.1) and center of weight (CW) (analogous to center of gravity) to describe the spatiotemporal dynamics of the network-wide firing activity and network-wide synaptic strength in our simulated networks, respectively.

4.2.2.3 Calculation center of activity trajectory (CAT)

Center of activity trajectory (CAT) was used to quantify the spatiotemporal patterns of network-wide population activity. The definition, implementations and properties of CAT are described in Section 3.2.1.5 and Equations 3.1 and 3.2.

4.2.2.4 Spontaneous burst detection and clustering of burst CATs

Spontaneous bursts in simulated networks were classified into different clusters according to their CATs. A firing rate histogram was obtained by counting the number of spikes network-wide in 10 msec bins. Bins with more than 20 spikes were considered a part of a burst. The length of the burst was defined as the time span of consecutive bins with a number of spikes over this threshold. CATs were calculated for each burst and aligned to each other at the peaks of the corresponding firing rate histograms. This alignment had similar results but operated more efficiently compared to shifting the lag on one trajectory to gain the highest cross-correlation with another. The beginnings and/or the ends of the CATs of shorter than maximum length were padded with zeros. Each same-length CAT then was reshaped into a one-dimensional vector by appending the y values of its CAT to the x values. Clustering was performed with the k-means algorithm, run multiple times for different k values. The best of the clustering results was selected by choosing the k value with best Davies-Bouldin validity index (Davies and Bouldin, 1979).

4.2.2.5 Calculation of center of weights (CW) and center of weights trajectory (CWT)

Plastic changes in the simulated networks' functional architecture can be represented by the trajectory of the center of weights (CW). Let W be a 1 by N vector, where N is the total number of excitatory synapses, representing the weights of every synapse at time t. Let X_i and Y_i indicate the horizontal and vertical distances from the postsynaptic neuron of the ith synapse to the center of the dish. Then, the CW of time t is a two dimensional vector:

$$[CW_X(t), CW_Y(t)] = \frac{\sum_{i=1}^{N} W_i(t) \cdot [X_i, Y_i]}{\sum_{i=1}^{N} W_i(t)} \qquad \text{[Equation 4.1]}$$

The CWT from time t_0 to t_1 with time step Δt is defined as:

$$CWT_X(t_0, t_1) = [CW_X(t_0), CW_X(t_0 + \Delta t), ...CW_X(t), ...CW_X(t_1)]$$
$$CWT_Y(t_0, t_1) = [CW_Y(t_0), CW_Y(t_0 + \Delta t), ...CW_Y(t), ...CW_Y(t_1)] \qquad \text{[Equation 4.2]}$$

Note that while the CAT describes the spatiotemporal patterns of signal propagation in typically brief time intervals, the CWT shows the dynamics of connection strengths changing over a typically larger time scale. In our case, the CA represented the neural activity flowing during a burst while the CW described the network's plasticity over the duration of a simulation.

4.3 Results

Our leaky integrate-and-fire (LIF) model networks and the living networks expressed similar activity patterns and input-output properties (see Section 2.3).

4.3.1 Tetanus-induced plasticity in the spatiotemporal pattern of spontaneous bursts

In order to investigate the effects of tetanization on patterns of spontaneous activity, the CATs were calculated for every spontaneous burst in the artificial neural networks. 2387 bursts were detected in the "Long" experiment on the network represented in Figures 4.4 and 4.5. The CATs of these bursts were calculated and classified by the k-means clustering algorithm (see Section 4.2), and eleven clusters were found (Figure 4.1A).

The simulated network's spontaneous activity was changed by a 5-min tetanization (Figure 4.1B). Some types of bursts happened mostly in the 10-min pre-

tetanization period, such as clusters *5*, *9* and *11*, while different bursts happened in the post-tetanization period, such as clusters *1*, *3*, *7*, *8* and *10*. Most of the clustered bursts ceased to occur for some minutes after tetanization and reappeared later. For example, cluster *2* reappeared around $t = 25$ min, sooner than cluster *4*, which reappeared around $t = 40$ min. Some clusters were transient, such as cluster *1* being highly concentrated around $t = 30$ min. A similar tetanus-induced change in the spatiotemporal structure of spontaneous bursts was observed in living MEA cultures (see Figure E.1).

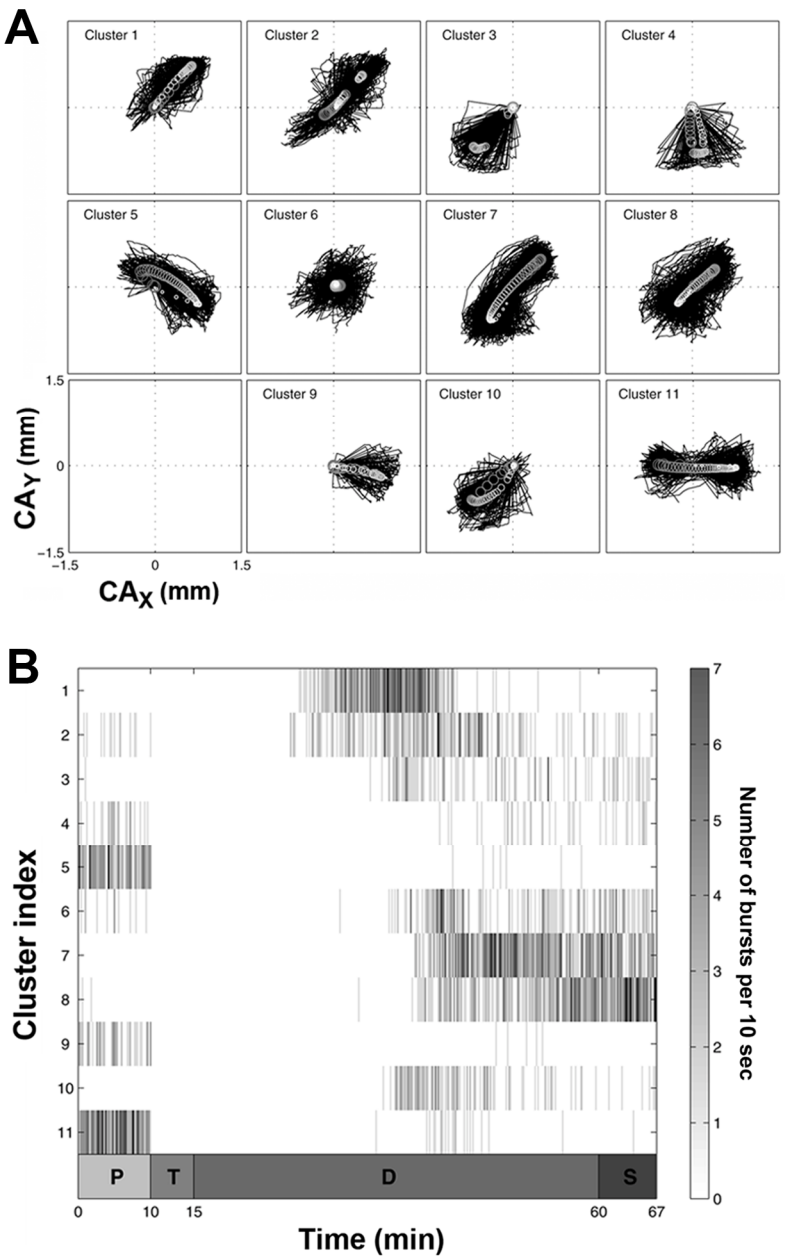

Figure 4.1. CAT of spontaneous bursts in a "Long" experiment in one network: Different kinds of spontaneous bursts occurred in different periods. **A.** Different classes of CATs of spontaneous bursts. A total of 2387 bursts were detected. The CATs of these bursts were classified by the k-means clustering algorithm, and eleven classes were found. The CATs for different clusters were plotted separately. The coordinate shown in the lower-left corner represents the 3mm by 3mm area of the "dish". The trajectories belonging to the same cluster are overlaid together. The averaged trajectories of each cluster are shown by a trace of circles, dark and large for the start of the trajectory, lighter and smaller towards the end. **B.** The occurrences of different types of spontaneous bursts. The x-axis represents time in minutes, and the y-axis indicates the cluster index that corresponds to the index shown in A. The shading represents the frequency of occurrences of the spontaneous bursts measured in every 10 seconds; the corresponding grayscale is shown at right. Notice that there is no spontaneous activity during tetanization (from 10-15 min). Marked periods are: *P*, Pre-tetanization; *T*, Tetanization; *D*, Post-tetanization (drifting) and *S*, Post-tetanization (steady) (see Section 4.3 and Figure 4.2B)

4.3.2 RBS stabilized tetanus-induced changes in network synaptic weights

We studied the changes in synaptic weights that might underlie the differences in spontaneous barraging activity before and after tetanization. The CWT of the simulated synaptic weights, shown in the "Long" experiment in Figure 4.2B, was calculated and sampled at 2 Hz over the entire 67 minute simulation. The trajectory was divided into four periods (Figure 4.1B):

1. **Pre-tetanization** (*P*): from $t = 0$ min to $t = 10$ min, the CWT remained within a localized area we termed a "steady state".
2. **Tetanization** (*T*): from $t = 10$ min to $t = 15$ min, the CW was driven away from the steady state of period *P*. No spontaneous bursts occurred during this period.
3. **Post-tetanization drifting** (*D*): from $t = 15$ min to $t = 60$ min, after the tetanization, the CW drifted for about 45 minutes without external stimulation. As shown in Figure 4.1B, different types of spontaneous bursts gradually appeared and disappeared during this period.
4. **Post-tetanization steady-state** (*S*): after $t = 60$ min, the CW arrived at a new steady state where it remained.

We compared the effects of 10-sec and 5-minute tetanizations by investigating the CWTs between the "Short" and the "Long" experiments (Figures 4.5A and 4.5B), and the "Short+Background" and the "Long+Background" experiments (Figures 4.5C and 4.5D). All drove the CW away from the pre-tetanization steady state (light grey). The CW distance between the centroid of the pre-tetanization steady state and the tetanization end point was used to quantify the effects of tetanization in changing network synaptic weights. This distance and standard error of the mean (SEM) (n = 5 simulated networks) was 79.5 ± 6.0 μm in the "Long" experiments, significantly greater than 28.9 ± 2.5 μm in the "Short" experiments (p-value $< 10^{-4}$, two-tailed t-test); and was 75.7 ± 5.2 μm in the

"Long+Background" experiments, significantly greater than 32.8 ± 2.8 μm in the "Short+Background" experiments (p-value < 10^{-4}) (Figure 4.3A).

In previous studies to model the restoration of sensory input to our living *in vitro* networks, we applied multi-site background stimulation. This decreased or eliminated the occurrence of spontaneous bursts when delivered at an aggregated frequency of ≥ 20 Hz (Wagenaar et al., 2005). Here, using our simulated networks, we investigated the influences of simulated random multi-site background stimulation on the short and long tetanizations by quantifying the differences in CWTs with or without low-frequency 64-electrode RBS (averaging 1 Hz) (Figure 4.2). With RBS, the CW did not move back to the pre-tetanization steady state even after only 10 seconds of tetanization, unlike without RBS (Figure 4.2C). The CW distance between the centroids of pre- and post-tetanization steady states was used to quantify the difference between the "Short" and the "Short+Background". The distance was 7.17 ± 1.01 μm (n = 5 simulated networks) in the "Short" experiments, much shorter than 56.2 ± 10.5 μm in the "Short+Background" experiments (p-value < 0.001) (Figure 4.3B).

In addition to preventing "turning-back" of the CW after a 10-sec tetanization, background stimulation also reduced "drifting-away" of the CW after a 5 minute tetanization. CWTs of a "Long" and "Long+Background" experiment from the same network are shown in Figure 4.2. With RBS, the CW stayed near its value immediately after tetanization (Figure 4.2D). Without random multi-site background stimulation, the CW drifted and came to rest at a new steady state (Figure 4.2B). The CW distance between the centroid of the post-tetanization steady state and the turn-off point of the tetanization (large "X") was used to quantify the drifting of the CW after the tetanization. This distance was 77.6 ± 15.2 μm (n = 5 simulated networks) in the "Long" experiments, much longer than 24.0 ± 7.1 μm in the "Long+Background" experiments (p-value < 0.01) (Figure 4.3B).

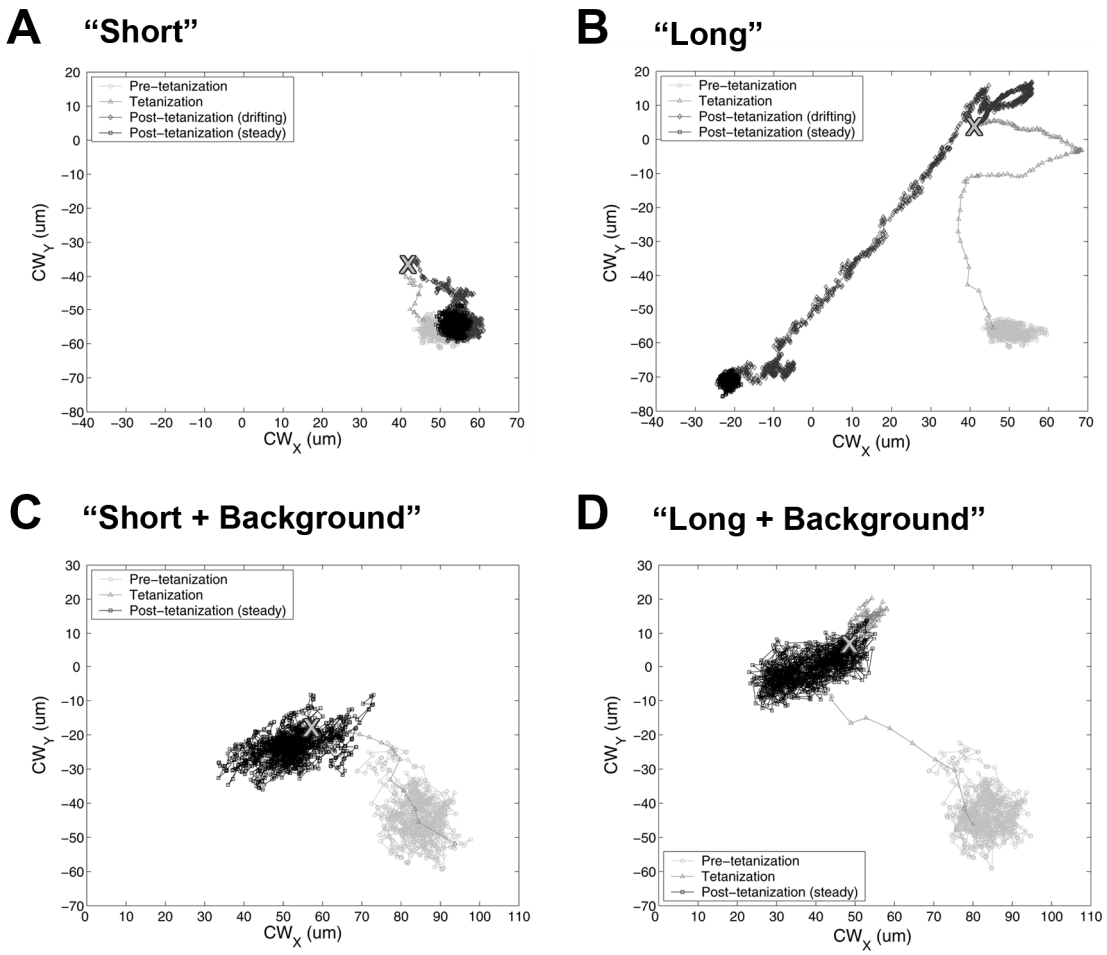

Figure 4.2. Comparison of CWTs from four experimental conditions on a simulated networks: Random multi-site background stimulation maintained the network synaptic stability by reducing the "turning-back" and "drifting-away" of the CWTs after 10-sec and 5-min tetanizations respectively. CWTs, sampled at 2 Hz, are shown for one of the five networks for the "Short" experiment (**A**), the "Long" experiment (**B**), the "Short+Background" experiment (**C**) and the "Long+Background" experiment (**D**). The light-gray circles, mid-gray triangles, dark-gray diamonds and black squares represent the Pre-tetanization period, Tetanization period, Post-tetanization drifting period (in A and B only) and Post-tetanization steady period respectively. The turn-off points of tetanization are marked with "X". Notice that with RBS, the CWT stayed near the point where the short tetanization was turned off without turning back toward the Pre-tetanization steady state (compare A and C). For long tetanizations, the random multi-site background stimulation kept the CWT near the point where the tetanization was turned off without drifting away (compare B and D).

Although background stimulation stabilized the network against large CW drift, small CW variations in the pre- and post-tetanization steady states were higher with the background stimulation than those without background stimulation (Figure 4.2). The mean distance of individual CWs in the pre-tetanization steady state from their centroids

was used to quantify the spread of the CW. The spread was 2.9 ± 0.2 μm (n = 5 simulated networks) without background stimulation, smaller than 9.8 ± 0.8 μm with background stimulation (p-value < 10^{-4}). This spread was compared to the change of CW caused by tetanization, which was quantified by the CW distance between the centroid of the pre-tetanization steady state and the tetanization end point. Without background stimulation, the spread was significantly smaller than the short tetanization-induced change (p-value < 10^{-6}) and significantly smaller than long tetanization-induced change (p-value < 10^{-6}). With background stimulation, the spread was significantly smaller than the short tetanization-induced change (p-value < 10^{-4}) and also significantly smaller than long tetanization-induced change (p-value < 10^{-5}) (Figure 4.3A).

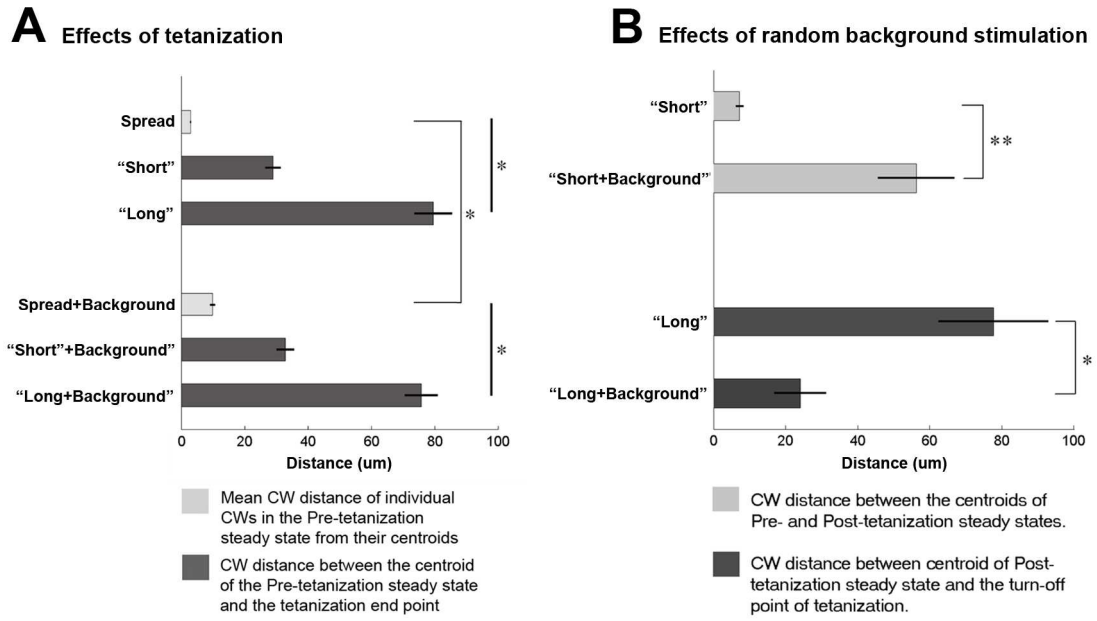

Figure 4.3. Statistics of CWTs from 5 simulated networks: RBS did not affect the amount of CW change induced by tetanization, and had a stabilizing effect on CWT after tetanization. **A.** The change of CW after tetanization was significantly greater than the spread of CW in Pre-tetanization period. The spread of CW without background stimulation was significantly smaller than with background stimulation (marked *, n = 5 simulated networks, p-value < 10^{-4}). This spread was compared to the change of CW caused by tetanization (see Section 4.3). Without background stimulation, the spread was significantly smaller than both the tetanization-induced changes in the "Short" experiments (p-value < 10^{-6}) and the "Long" experiments (p-value < 10^{-6}). With background stimulation, the spread was significantly smaller than both the tetanization-induced changes in the "Short+Background" experiments (p-value < 10^{-4}) and the "Long+Background" experiments (p-value < 10^{-5}). The CW change induced by long tetanization was greater than that induced by short tetanization, both without background stimulation (p-value < 10^{-4}) and with background stimulation (p-value < 10^{-4}). Vertical bars represent significant differences between values (marked *, p-values < 10^{-4}). **B.** The CW distance between centroids of Pre- and Post-tetanization steady states was used to quantify "turning-back" of the CWT after 10-sec tetanization (Figure 4.2A). With RBS, the CW of the Post-tetanization steady state stayed significantly farther from the Pre-tetanization steady state after the short tetanization (marked **, p-value< 0.001). The CW distance between the centroid of the Post-tetanization steady state and the turn-off point of the tetanization was used to quantify the "drifting-away" of the CW after the 5-min tetanization (Figure 4.2B). With RBS, the CW of the Post-tetanization steady state drifted significantly less after the long tetanization than without (marked *, p-value< 0.01).

4.4 Discussion

4.4.1 Effects of random multi-site background stimulation in simulated and living networks

RBS helped maintain the stability of network synaptic weights after tetanization in simulated networks. The CW plots (Figure 4.2) showed that the network synaptic

weights tend towards a localized set of values, and that tetanization moves the network synaptic weights away. In the absence of background stimulation, the CW returned to near its previous locus after a short tetanization, suggesting this locus served as an attractor. After a long tetanization, the CW drifted for some time before settling on a new attractor, suggesting the tetanization effect is not stable. With background stimulation, a short tetanization *can* change the network synaptic weights (Figures 4.5 and 4.6); to use a mechanical analogy, the 'elastic' change becomes a 'plastic' change. A long tetanization will drive the network to a new locus, where it remains without drifting. The observation of attractors in synaptic weight space suggests that a form of self-organization or homeostasis exists in the interaction of synaptic weights and network activity; however, much remains to be studied about the mechanisms of this interplay.

We hypothesized that the network synaptic weights drifted after a tetanization because of the ongoing spontaneous activity, consisting of mostly spontaneous bursts (Figure 4.1B). Spontaneous activity and network synaptic weights interacted with each other until reaching a stationary set of patterns (trajectories) in CA space and an attractor in CW space. With RBS, spontaneous activity was reduced, and so the network synaptic weights were mainly affected by stimulus-evoked activity. Since background stimulation, and consequently the evoked activity, was random spatially and temporally, these stimuli had an unbiased randomizing effect on changing network synaptic weights. Thus, the size of CW attractors was greater with the background stimulation than without it (Figures 4.5 and 4.6). In summary, while the background stimulation stabilized the network synaptic weights by preventing the directional drift caused by influences of transient spontaneous bursts after tetanization, the randomizing effect also increased the variation of network synaptic weights isotropically.

In both simulated networks and living cultured networks, spontaneous bursts were reduced by RBS and stimulus-evoked activity became dominant. Random multi-site background stimulation was applied to living neural networks also, and neural activity

was recorded and compared to that of the simulated neural network (Figure 4.4). In a typical one-minute recording, the ratio of the number of evoked bursts versus spontaneous bursts was 41:1 in the living network compared to 42:3 in the simulated network. Moreover, the spontaneous burst rate was reduced from 0.70 Hz to 0.017 Hz (1 burst in 1 minute) in the living network and was reduced from 0.73 Hz to 0.05 Hz (3 bursts in 1 minute) in the simulated network (see Figure 2.9).

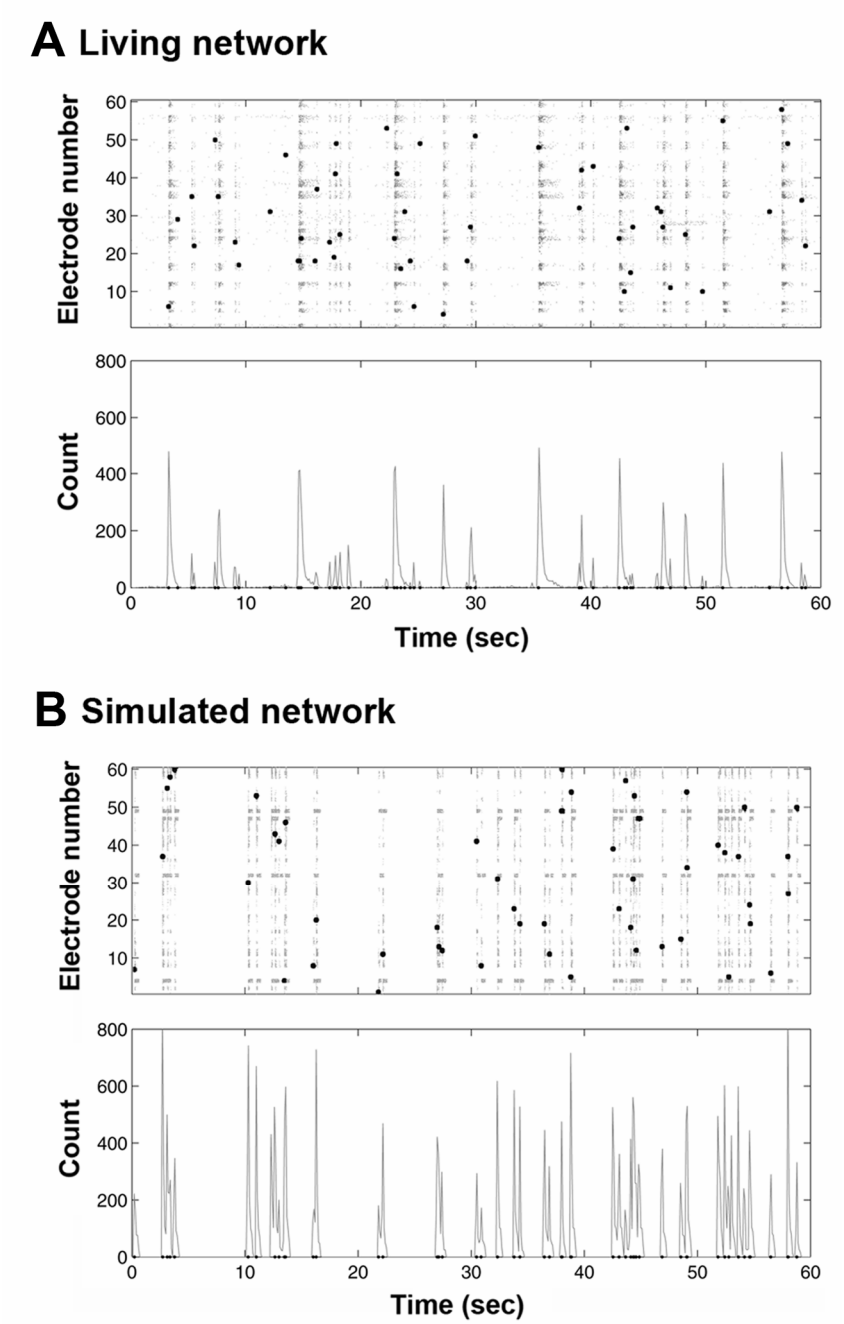

Figure 4.4. Comparison of network activity with RBS in living and simulated networks: In the presence of background stimulation, the network activity consisted mostly of evoked responses, both in living networks and simulated networks. **A.** A 1-minute recording from a living network with background stimulation by 60-channel MEA is shown in a rasterplot (upper panel, spikes recorded in the *i*-th electrode were randomly spread out in the interval [*i*-0.5 *i*+0.5] on the y-axis for clarity) and the corresponding firing rate histogram (lower panel, bin size is 100 msec). **B**. A 1-minute simulation with background stimulation is shown as a raster plot (upper panel) and the corresponding firing rate histogram (lower panel). The timings and channels of applied stimuli are shown as black dots in the raster plots and on the x-axes in the histograms. The ratio of the number of evoked bursts versus spontaneous bursts was 41:1 in the living network compared to 42:3 in the simulated network. Moreover, the spontaneous burst rate was reduced from 0.70 Hz to 0.017 Hz (1 burst in 1 minute) in the living network and was reduced from 0.73 Hz to 0.05 Hz (3 bursts in 1 minute) in the simulated network (see Figure 2.9).

4.4.2 Stability in other systems

Long-term stability of spontaneous activity patterns was found in cortical slice cultures (Beggs and Plenz, 2004; Ikegaya et al., 2004), suggesting these recurrent patterns could be used by cortical circuits to store information for memories. Our simulation results support this hypothesis by showing that for an attractor in CW space, a finite set of clustered CATs recurs. The results also show that tetanizations changed the network to different attractors, and RBS eliminated CW drift after a tetanization. This suggests the tetanization altered the contents of the memory stored in the network, and that RBS reduced spontaneous transients, allowing a greater control over network plasticity. Results of tetanization on living networks support this view (Wagenaar et al., 2005; Madhavan et al., 2007c) (also see Appendix F).

4.4.3 Control of network synaptic weights and implementation in hybrots

The use of MEAs in hybrots provides a model system to simultaneously study behavior and detailed neuronal function, including plasticity underlying adaptation or learning. In our experiments, a tetanus was used to induce plasticity. By adding background stimulation, the plasticity remained while the stability needed for memory was provided.

We created motor mappings to control the behaviors of a robot based on the activity in a real neuronal network, and sensory mappings to stimulate the network based on the sensory input from a hybrot (Bakkum et al., 2004). The first step to demonstrate learning behavior, begun in this simulated modeling study, is to search for the relationship between the network synaptic weights and the network spatiotemporal activity patterns. We demonstrated that tetanization drives the network from one attractor to another. This is promising for hybrots, because if we can induce the network synaptic weights to change, we can show the behaviors of a robot changing from one mode to another mode to demonstrate adaptive learning.

A potential mapping for hybrot control is to use the CAT of the responses to RBS as motor commands (Figure 4.5). Different forms of tetanization have different effects on network synaptic weights (such as long vs. short tetanization, Figures 4.5 and 4.6) and can serve as the feedback to a living network representing different sensory inputs. In this case, network synaptic weights change during each tetanization, and the changes are stabilized by continuous random background stimulation. Therefore, the behavior pattern of the hybrot would change after each sensory feedback and remain steady until the next feedback. In this study we used the CWTs and the occurrence of spontaneous bursts with different CATs to illustrate network plasticity in model networks. However, these two quantities cannot be easily applied in living networks. First, the synaptic weights of a living culture are not directly measurable by the extracellular electrodes of our MEAs. Second, background stimulation reduces the frequency of spontaneous bursts in living networks; thus, not enough spontaneous bursts occur to reliably cluster their CATs nor to provide instant reaction for generating motor commands. Thus we expect the responses to background stimuli to be the better parameter for hybrot control.

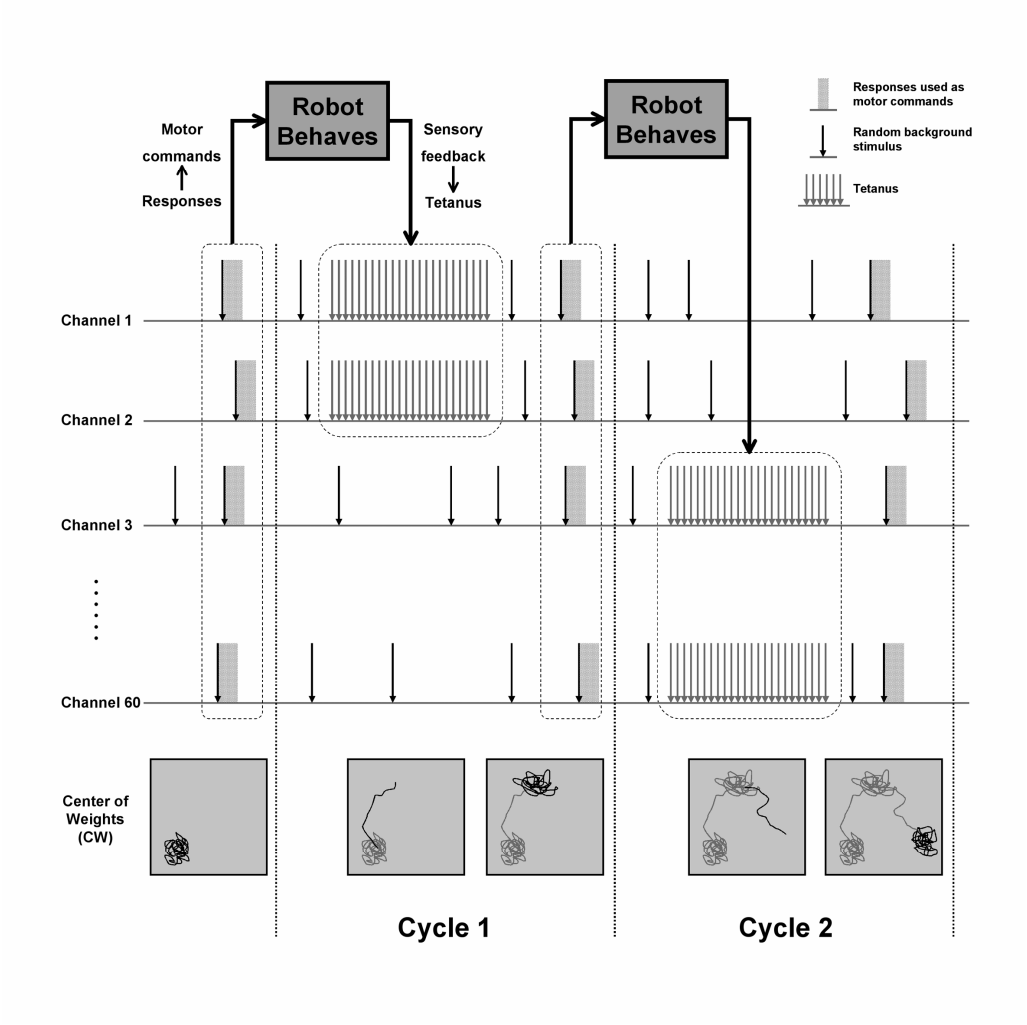

Figure 4.5. A potential paradigm for hybrot control with RBS and tetanization: Two and a half command cycles are depicted above, separated by vertical dotted lines. Each cycle consists a tetanus at two channels and continuous random background at all 60 channels. The CATs of the responses to the most recent background stimulus at each channel in one cycle could be transformed into motor commands for a robot. The sensory feedback from the robot could be transformed into different forms of tetanization in the next cycle (in this figure, two different tetanizations are applied at two different pairs of electrodes). Based on our model, we expect the network synaptic weights to change in different ways depending on the sensory feedback since different tetanizations could have different effects. The continuous random background stimulation is expected to stabilize the weight changes (a series of hypothesized CWTs are shown in the bottom row). As a result, the behavior pattern of the hybrot would change after each sensory feedback and remain steady until the next feedback.

4.4.4 CAT and CWT

Finding structure in the complexity of multiple time-varying neural signals is difficult and likely requires the creation of new mathematical tools (Pesaran et al., 2002; Baruchi and Ben-Jacob, 2004; Beggs and Plenz, 2004; Brown et al., 2004). The CA and

the CW were designed to map multiple spatiotemporal signals into a more comprehensible form while retaining enough detail to discriminate network states. The CAT and CWT give summary statistics about the network-wide properties as opposed to statistics on individual neurons. Note that the shapes of the trajectories are independent of the selection of the trajectory origin or of the spatial center of the network since they are linear summations of neural locations.

Most current methods for neural spike train data analysis, such as the cross-correlogram, cross intensity function, and joint peri-stimulus time histogram, yield information only about associations between pairs of neurons (Brown et al., 2004). To give information on the whole network, these methods would require large computational power to go through every possible pair of neurons and require further statistics to compare more than two recordings. Although a CAT cannot provide detailed information about individual neurons, it has the advantage of depicting the spatiotemporal dynamics of the whole network (see Chapter 3).

4.5 Conclusion

Using artificial neural networks to control robots is an active area of research and, in addition to directing studies in living neural networks, holds the potential for many promising products (Brooks, 1999; Krichmar and Edelman, 2002; 2004; Schaal et al., 2004). Most work in AI and robotic systems faces limitations in the ability to adapt to novel situations in real-time. By contrast, it is clear that biological neural systems excel at this. Much can be learned from the activity, morphology, and connectivity of biological neural networks to inform the design of future artificial networks. If future research on living networks demonstrates that directed functional changes can be obtained by stimulating the network, then we expect to find corresponding morphological changes. Imaging neuronal networks using time-lapse multiphoton microscopy (Potter, 2000; Potter et al., 2001) is compatible with many-neuron electrophysiology. We are building a

dedicated 2-photon/MEA microscope (Rambani et al., 2005). The "brain" of the hybrot system, unlike an animal's brain, holds still during behavior, and can be imaged in its entirety (Bakkum et al., 2004).

We have explored the effects of multi-site background stimulation on networks (Wagenaar et al., 2005; Madhavan et al., 2007c). We are applying a synergy of modeling simple networks, and multi-unit experimentation on substantially more complex living ones. Simulated network studies help suggest new experiments for studying learning *in vitro*, while the experimentation helps us come up with better simulated models for the network-level properties of neural circuits. By embodying *in vitro* networks with hybrots in closed-loop systems, we can more easily observe the cellular and network mechanisms of learning while it happens than with *in vivo* models, and ensure that any changes induced by the stimuli have functional consequences on hybrot behavior. The closed-loop paradigm proposed in Figure 4.5 further became the precursor of our closed-loop design for goal-directed learning described later in Chapters 5 and 6.

CHAPTER 5

CLOSING THE LOOP: ADAPTIVE GOAL-DIRECTED BEHAVIOR WITH SIMULATED NETWORKS[xi]

The acts of learning and memory are considered to emerge from the modifications of synaptic connections between neurons, as guided by sensory feedback during behavior. However, much is unknown about how such synaptic processes can sculpt and are sculpted by neuronal population dynamics and an interaction with the environment. Here, we embodied a biologically-inspired simulated network with an artificial animal (an animat) through a sensory-motor loop, a refined design from the paradigm proposed previously (see Section 4.4.3). The application of training stimuli contingent on behavioral performance directed network plasticity and shaped the network to learn various multi-task goals. An individual network had the flexibility to achieve different multi-task goals, and the same goal behavior could be exhibited with different sets of network synaptic strengths. When training stimuli were replayed to the same network (a non-contingent control), behavior did not reach the goal, demonstrating the importance of feedback. Additionally, the closed-loop training algorithm was verified in a living cortical culture. While lacking the characteristic layered structure of *in vivo* cortical tissue, these monolayer networks, when incorporated in a closed-loop system, could tune their activity in behaviorally relevant manners, demonstrating that *in vitro* neural networks have an innate ability to process information. This closed-loop hybrid system is a useful tool to study the network properties intermediating synaptic plasticity and behavioral adaptation. The training algorithm provides a stepping stone towards designing future hybrid control systems, whether with artificial neural networks or living ones.

5.1 Introduction

One of the most important features of the brain is the ability to adapt or learn to achieve a specific goal, which requires continuous sensory feedback about the success of its motor output in a specific context. Previously, an embodied cultured network's ability to control an animat or a mobile robot was demonstrated without a specifically defined goal (DeMarse et al., 2001; Martinoia et al., 2004) (see the summary of previous studies on embodied cultured networks in Table 1.2). In other studies, animats were designed to avoid obstacles (Cozzi et al., 2005) or follow objects (Bakkum et al., 2004), but deterministically and without learning. Without a pre-defined goal, Mussa-Ivaldi et al.

[xi] Under review as: Zenas C. Chao, Douglas J. Bakkum, and Steve M. Potter (2007): *Shaping embodied neural networks for adaptive goal-directed behavior*. PLoS Computational Biology.

(Mussa-Ivaldi and Miller, 2003) showed adaptive phototactic behavior in an embodied lamprey brainstem without additional external training stimulation. In order to further understand the learning capability of an embodied cultured network for goal-directed behavior, we need to investigate how the network can be shaped and rewired, and how to direct this change.

Previous studies have demonstrated the potential for disembodied cultured networks to achieve functional plasticity (see Table 1.1 and Appendices E and F). This neural plasticity provides a potential learning capability to cultured networks. Jimbo et al. used a localized tetanic stimulus to induce long-lasting changes in the network responses that could be either potentiated or depressed depending on the electrode used to evoke the responses (Jimbo et al., 1999). Moreover, we and others previously found that such tetanus-induced plasticity was spatially localized and asymmetrically distributed (Ruaro et al., 2005; Chao et al., 2007c) (also see Chapter 3). By delivering two different tetanic stimulation patterns, Ruaro et al. trained a cultured network to discriminate the spatial profiles of the stimuli. These results suggest that different stimulation patterns can shape diverse functional connectivity in cultured networks. By incorporating closed-loop feedback, Shahaf and Marom (Shahaf and Marom, 2001) showed unidirectional learning: to induce an electrode-specific increase in response. This simple form of learning was achieved by a binary training: to stop a periodic stimulation at one electrode when the desired response level at the target electrode was obtained. In order to scale to more complex behavior, we need to create more structured training stimuli and detailed activity metrics to investigate whether an embodied cultured network can learn multiple tasks simultaneously.

Unlike *in vivo* systems, the sensory-motor mapping and training algorithm in an embodied cultured network are defined by the experimenters. In order to efficiently find an effective closed-loop design among infinite potential mappings, we first embodied a biologically-inspired simulated network to study an adaptive goal-directed behavior in an

animat: learning to move toward and stay within a user-defined area in a 2-D plane. We used the simulated network described in Chapter 2 to express spontaneous and evoked activity patterns similar to those of living MEA cultures (Chao et al., 2005). A similar but larger simulated network showed that localized coherent input resulted in shifts of receptive and projective fields similar to those observed *in vivo* (Izhikevich et al., 2004). Simulated networks are therefore useful for analyzing biological adaptation with various closed-loop designs.

The closed-loop design we discuss here consists of four novel elements:

1. Patterned stimulation to induce network plasticity. This low-frequency training stimulation differs from most studies of cultured networks, where plasticity was induced by high frequency tetanic stimulation (Jimbo et al., 1999; Ruaro et al., 2005).
2. Continuous low-frequency background stimulation to stabilize accumulated plasticity (Chao et al., 2005) (Chapter 4), which is analogous to continuous sensory inputs and ongoing processing in the brain.
3. Population coding for motor mapping. Population coding is considered a robust means to represent movement directions in the primary motor cortex (Georgopoulos et al., 1986). We used a novel population coding scheme, the center of activity (CA) (Chapter 3), to instruct movement outputs.
4. Adaptive selection of training stimulation. Because the connectivity in a cultured network is not predictable, the effects of a given training stimulation cannot be known a priori. Thus we delivered training stimulation contingent on the animat's performance in order to direct changes in network connectivity that further shift the animat's behavior toward the desired behavior.

We demonstrate adaptive goal-directed behavior in the simulated network, where multiple tasks are learned simultaneously. The desired behavior could only be achieved

when the feedback was contingent on the network activity and the animat's behavior. This suggests that even though a 2-D cultured network lacks the 3-D structure of the brain, it still can be functionally shaped and show meaningful behavior. We also validated the closed-loop design in a living cortical culture on a multi-electrode array (MEA). The proposed design is not restricted to a particular sensory-motor mapping, and could be applied with different and more complex goal-directed behaviors, which may provide a useful *in vitro* model for studying sensory-motor mappings, learning, and memory in the nervous system.

5.2 Methods

5.2.1 Simulation

5.2.1.1 Animat

5.2.1.1.1 Environment

The animat was controlled by a simulated network (see Chapter 2) to move in a plane within a circle of 50 units radius, which was divided into four quadrants (Q1: northeast, Q2: northwest, Q3: southwest, and Q4: southeast, see Figure 5.1A). The animat was put back to a random location within a smaller concentric circle of 5 units radius if it moved outside the outer circle.

5.2.1.1.2 Multi-task goal

The goal of the animat was to move and stay within a smaller concentric circle of 5 units radius. This goal consisted of *four different sub-tasks*, which were to move in four different desired directions in different quadrants.

5.2.1.1.3 Sensory system and motor capability

The sensory inputs of the animat were one of four discrete values representing which quadrant it was in (Q1- Q4) and whether the performance was desired (desired or undesired). The movement of the animat was implemented by population network responses to stimulation determined by the sensory input (see Closed-loop algorithm section below). The sensory input was evaluated to generate a movement every 5 seconds.

5.2.1.2 Simulated network

The animat was connected to a simulated network through a sensory-motor loop (Figure 5.1A). We produced three artificial neural networks, as described in Chapter 2, with different connectivity.

5.2.1.3 Closed-loop algorithm

5.2.1.3.1 Stimulation protocols

We used three classes of stimulation protocols for three different purposes: (1) Four *context-control probing sequences (CPSs)* (CPS_{Q1}- CPS_{Q4}) were used to encode 4 sensory inputs (current location= Q1- Q4) that also evoked neural activity used as motor commands for the animat. (2) Four "pools" of *patterned training stimulation (PTS)* (PTS_{Q1}- PTS_{Q4}), each also assigned to Q1- Q4, were used to induce network plasticity to train the animat. (3) *Random background stimulation (RBS)* was used to stabilize accumulated plasticity, as shown in Chapter 4 to stabilize network synaptic weights (Chao et al., 2005).

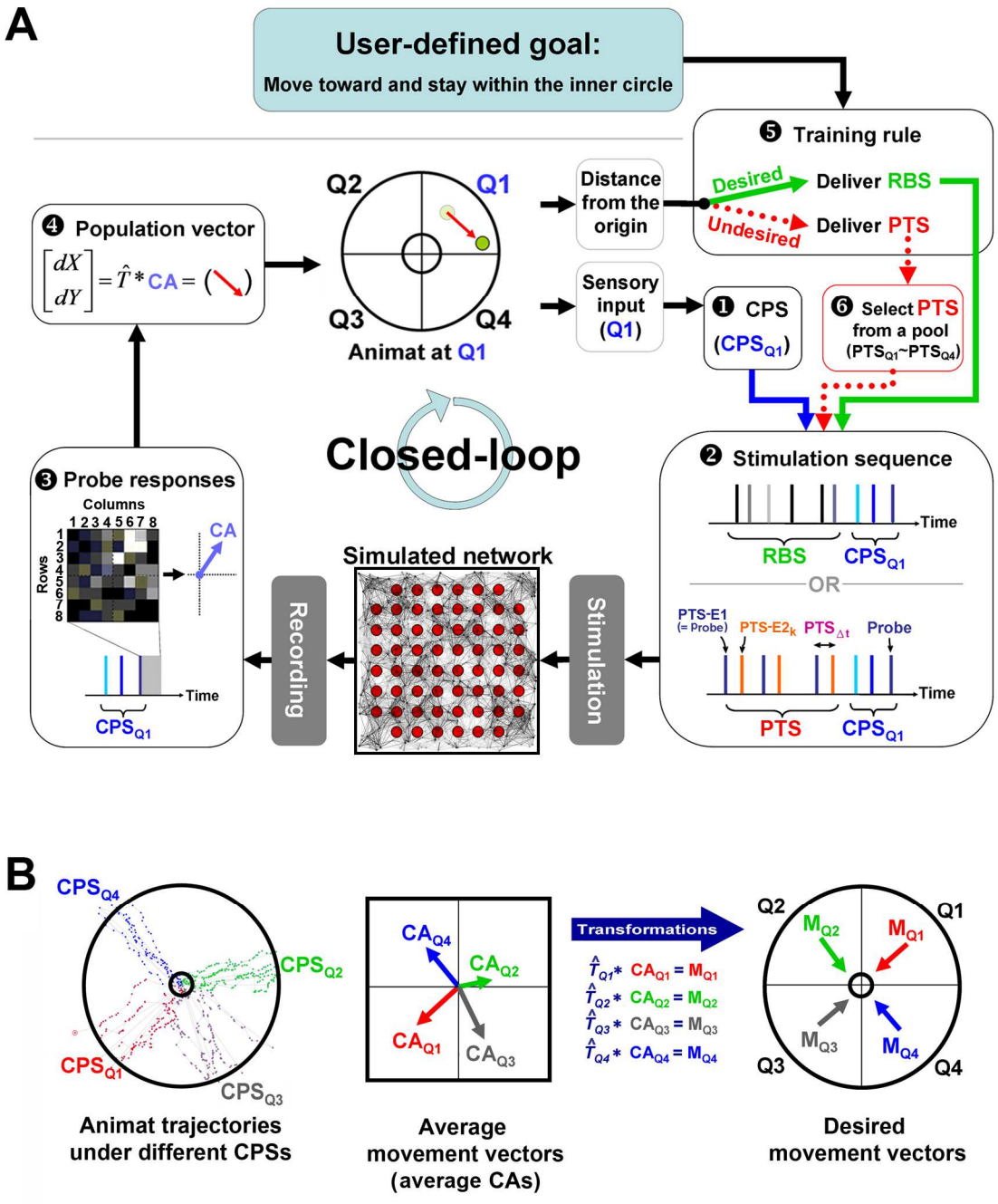

Figure 5.1. Closed-loop algorithm: A. Closed-loop design: the sensory mapping (❶- ❷), the motor mapping (❸- ❹), and the training feedback (❺- ❻). **B.** Transformation for motor mapping. Refer to Section 5.2 for a detailed explanation.

1. Context-control probing sequence (CPS)

Four stimulation sequences were used (CPS_{Q1}- CPS_{Q4}). Each CPS consisted of a sequence of 3 stimulation pulses, one from each of 3 randomly selected electrodes with inter-pulse intervals randomly selected between 200 and 400 msec (Figure 5.1A). The last stimulus, termed probe, was unique to each CPS. For each experiment, the CPSs were fixed throughout.

Each CPS (CPS_{Q1}- CPS_{Q4}) was delivered every 5 seconds, when the corresponding sensory input (Q1- Q4) was evaluated. We used the evoked action potentials from the last stimulus (probe responses) to generate motor commands to control the animat. The context before the probe stimulus was found to influence the probe response (Darbon et al., 2002). Therefore, in order to directly quantify learning by changes in movement, we sought to reduce the variability in the probe response due to recent neural activity and stimulation history, such that changes in probe responses were due mainly to changes in network connectivity. We found that by controlling the stimulation context (the first two stimuli of a CPS) before the probe with inter-pulse intervals between 200 to 400 msec, the variability of the probe responses was minimized. Data supporting this in both simulated and living networks are shown in Appendix G.

2. Patterned training stimulation (PTS)

Four pools of PTSs (PTS_{Q1}- PTS_{Q4}) were used, each associated with its corresponding quadrant. A PTS consisted of repetitive stimulation at two electrodes. The location of the first electrode (PTS-E1) was chosen as the probe electrode used in the preceding CPS (for PTS_{Q1}, it was the last stimulus in CPS_{Q1}). The two parameters varied among different PTSs in a pool were: the location of the second electrode ($PTS\text{-}E2_k$), and the relative timing from the first electrode (inter-pulse interval, $PTS_{\Delta t}$) (see Figure 5.1A). $PTS\text{-}E2_k$ was chosen from one of the 60 electrodes (k= 1- 60), and $PTS_{\Delta t}$ was chosen from one of 11 values: -100, -80, -60, -40, -20, 0, 20, 40, 60, 80, and 100 msec. Therefore,

each pool consisted of 660 (= 60∗11) PTSs. Paired stimuli with different spatiotemporal structures induced different network synaptic plasticity (shown in Appendix H). Thus, the pool of 660 PTSs provides a variety of options to shape the network dynamics.

During training, a PTS was delivered repetitively at the pair of electrodes with random inter-PTS-intervals between 400 to 800 msec. Paired stimulation of monosynaptically connected neurons evokes STDP dependent on the stimulation interval (Bi and Poo, 1998), and paired stimulation of two electrodes has the potential to induce STDP throughout any shared activation pathways in the network.

3. Random background stimulation (RBS)

RBS was delivered randomly at 60 electrodes, one at a time, with random inter-pulse-intervals ranging from 200 to 400 msec (see Figure 5.1A). RBS of an aggregated frequency of 1 Hz was shown in Chapter 4 to have stabilizing effects on network synaptic weights in a simulated network after stimulus-induced plasticity (Chao et al., 2005). Thus we delivered RBS to maintain the network synaptic weights if the desired behavior was observed. In this study, the aggregated stimulation frequency of RBS was increased to 3 Hz so that amounts of stimulation in RBS and PTS were comparable.

The closed-loop system consisted of three parts (see Figure 5.1A): the sensory mapping, the motor mapping, and the training feedback.

5.2.1.3.2 Sensory mapping

One CPS (CPS_{Q1}, CPS_{Q2}, CPS_{Q3}, or CPS_{Q4}) was delivered every 5 seconds based on which sensory input was received (Q1, Q2, Q3, or Q4) (❶ and ❷ in Figure 5.1A).

5.2.1.3.3 Motor mapping

1. Center of activity (CA)

After delivering a CPS, the number of spikes within 100 msec after the probe were measured at 60 recording electrodes, and the center of activity (CA) was calculated (❸ in Figure 5.1A) (Equation 3.1). CA represents the spatial asymmetry of the activity, which is analogous to the center of mass.

2. Population coding and motor mapping transformation:

We instructed incremental movement of the animat [*dX*, *dY*] by using a population vector calculated from CA (❹ in Figure 5.1A):

$$[dX, dY] = \hat{T} * CA \qquad \text{[Equation 5.1]}$$

where $\hat{T}$ is a transformation matrix that transformed CAs in the four quadrants into desired movements toward the center with average 1 unit moving distance, as described below.

In the beginning of each experiment, CPS_{Q1} was continuously delivered every 5 seconds with RBS in between. If the animat reached the outer circle, it was moved back to the inner circle, and CPS_{Q2} was delivered, then CPS_{Q3} and CPS_{Q4}. The whole process was repeated 5 times, and the average CAs from probe responses to each CPS were calculated (shown as CA_{Q1}- CA_{Q4} in Figure 5.1B). The average CAs represent the average movements from each CPS. The transformations $\hat{T}$ for each CPS were created so that the average movement in each quadrant would be the desired movement (M_{Q1}-M_{Q4}; pointing to the center of the inner circle) with a magnitude of 1 unit (see Figure 5.1B). For example, for CA_{Q1}= [$CA_{Q1,X}$, $CA_{Q1,Y}$] and the desired movement

$M_{Q1}=[-\sqrt{2},-\sqrt{2}]$, the transformation $\hat{T}_{Q1}$ consisted of two scaling numbers α_{Q1}, *and* β_{Q1} that satisfied:

$$\hat{T}_{Q1} * CA_{Q1} = [\alpha_{Q1} \cdot CA_{Q1,X}, \beta_{Q1} \cdot CA_{Q1,Y}] = M_{Q1} \qquad \text{[Equation 5.2]}$$

Thus, for a CPS_{Q1} delivered with no neural plasticity, the animat will move on average at a -135° angle by 1 unit distance. For each experiment, the transformations ($\hat{T}_{Q1}$ - $\hat{T}_{Q4}$) were calculated first, and then fixed for the duration of the experiment.

5.2.1.3.4 Training feedback

If the animat's performance was desirable (moving inward), then RBS was delivered for 5 seconds until the next sensory input was evaluated (❺ to ❷ in Figure 5.1A). If the animat's performance was not desired (moving outward), then training was applied (❺ in Figure 5.1A): a PTS was randomly selected from the corresponding pool; if the previous CPS was CPS_{Q1}, then the PTS was selected from PTS_{Q1} (❻ in Figure 5.1A) and delivered for 5 seconds (❷ in Figure 5.1A). If the performance of the animat was improved but still not desirable after the PTS (still moving outward but at a slower rate), then the same PTS would be used for the next training. Initially, the probability of choosing a PTS from a pool was identical (1/660). Every time a PTS improved the performance of the animat after the next probe, a copy was added into its pool. Thus the size of the pool increased, and the probability of this "favorable" PTS being chosen later was increased. In contrast, if that PTS worsened the performance of the animat (moving outward faster), it was removed from the pool, unless only one PTS of this specific type remained.

To summarize, if the animat was moving correctly, RBS was delivered to stabilize the corresponding network synaptic state. Otherwise, PTS was delivered to change the

network synaptic weights. Also, the probability of specific PTS patterns being chosen was constantly updated according to the performance of the animat.

5.2.1.4 Simulation experiments

We used three simulated networks with different connectivity, each with 5 different sets of CPSs (randomly selected CPS_{Q1}- CPS_{Q4}). Therefore, a total of 15 experiments with different sensory-motor mappings was performed in the three networks.

5.2.1.4.1 Sensory mapping switch with feedback training

We investigated the networks' ability to learn a user-defined goal behavior by "switching" the sensory mapping. This would be analogous to placing an animal into a different environment, or imposing a new task. As described previously, the sensory-motor mapping was set up so that the animat would move toward the center as desired. We quantified the animat's ability to adapt to a switch of the sensory mapping, that is, the ability to restore desired behavior under a different sensory mapping.

The transformation, $\hat{T}$, allowed the animat to move correctly, on average, and after 10 minutes the sensory mapping was switched by exchanging CPS_{Q1} and CPS_{Q3} while CPS_{Q2} and CPS_{Q4} remained unchanged. That is, if the animat was at Q1, CPS_{Q3} was delivered instead of CPS_{Q1}, and vice versa. The simulation was stopped when either the simulation time exceeded 4 hours without reaching the goal or the animat stayed within the inner circle 90% of the time (reached the goal) for 10 minutes. If the animat was able to adapt to the new sensory mapping and learn the desired behavior, the network was considered successfully rewired.

5.2.1.4.2 Non-contingent training

In order to verify the importance of behavior-based training feedback on the performance of the animat, we recorded the whole training stimulation sequence (PTS and RBS) for each successfully adapted experiment and replayed it into the same network

with the same initial state and with the same sensory-motor mapping. In the replayed-training simulation, a different random seed for fluctuations in neurons' membrane potentials and synaptic currents was used. Thus, responses to CPSs in the replayed-training simulation were not identical to those in the original successful learning simulation, and hence the trajectory of the animat rapidly diverged from that of the original simulation. The replayed training stimulation was delivered open-loop, that is, regardless of whether the movement was desired or not. Therefore, the training stimulation soon became no longer contingent on the network activity.

5.2.1.5 Analyses

5.2.1.5.1 Mutual information

We used mutual information between stimuli and responses to quantify the stability of the input-output function of the network; that is, the stability of the animat's movement under the same sensory input. Mutual information measures the reduction in uncertainty about the stimulus after a response is observed. We used CPSs for the sensory input and the animat's movement angles for the output. The animat's movement angles (-180°- 180°) and sensory inputs (1, 2, 3, or 4 for Q1, Q2, Q3, or Q4, respectively) were recorded and the mutual information was calculated in 5-min moving time windows with a time step of 5 seconds using the histogram-based mutual information methods (Moddemeijer, 1989).

5.2.2 Experiments on living networks

5.2.2.1 Cell culture and experimental setups

We have developed techniques to maintain neuronal cultures and conduct experiments for many months (Potter and DeMarse, 2001). The details are described in Appendix C.

5.2.2.2 Experimental protocol

We tested whether a living network could learn to control movement of an animat in a desired direction under just one sensory input. That is, we only delivered one CPS, and investigated whether a single pre-defined desired moving direction could be learned, and if so, whether the animat could adapt to switched desired moving directions (see Section 5.4). Prior to the closed-loop experiment, RBS was applied in an open-loop manner for 2 hours to acclimate the culture to being stimulated. The transformation, $\hat{T}$, was calculated from CAs collected during the last 30 minutes of this acclimatization period. However, spontaneous activity during a no-stimulation period between finding the transformation and beginning the closed-loop experiment caused CA to drift, creating a movement bias. The bias was calculated at the beginning of the experiment and subtracted from the original trajectory and distributions of movement angles.

5.3 Results

In order to investigate how external training stimuli can shape a network into a desired state, we used the biologically-inspired simulated network of Chapter 2 to study multi-task goal-directed behavior by embodying the network with an animat. We then validated (explored) some aspects of our closed-loop system in a living network. All acronyms are shown on pages xvii- xix.

5.3.1 Random background stimulation (RBS) helped maintain the network input-output function

In Chapter 4, we showed that RBS helped stabilize network synaptic weights after stimulus-induced plasticity in a simulated network (Chao et al., 2005). Here we further verified how this effect on network synaptic weights affected the stability of the network input-output function, that is, the stability of the animat's movement under the same sensory input. The animat was run with RBS between CPSs without training (no PTS) for

one hour. We compared this to the animat's performance without RBS (CPSs only). The initial network state, the random seed for fluctuations in neurons' membrane potentials and synaptic currents, and the sensory-motor mapping were not varied.

An example of the time course of the animat's distance from the origin is shown in Figure 5.2A. In this example, the animat moved in desired directions in each quadrant and thus stayed within the inner circle for the entire hour when RBS was applied, whereas it moved outward after 10 minutes when no RBS was applied. The animat was commanded to move every 5 seconds, and in order to stay within the inner circle, movement needed to remain towards the desired directions in each quadrant. The mutual information between the movement angle and the sensory input is shown in Figure 5.2B. When the animat started moving outward in an undesired direction, the mutual information decreased significantly.

The mutual information during the last 10 minutes (*P2* period in Figure 5.2B) was compared to the mutual information during the first 10 minutes (*P1*) in the 15 simulations (3 networks, 5 different selections of CPSs each) (Figure 5.2C). With RBS, the mutual information in *P2* was 1.42 ± 0.15 bits (mean ± SEM, n= 1800 measures, 15 networks, 120 measures in 10 minutes per network), which was comparable to 1.53 ± 0.09 bits in *P1* (p-value= 0.77, Wilcoxon signed-rank test). Without RBS, the mutual information in *P2* was 0.14 ± 0.10 bits, which was significantly lower than 1.40 ± 0.24 bits in *P1* (p-value< 1e-4). This indicates that RBS of aggregated frequency of 3 Hz maintained the stability of the network input-output function, validating the use of RBS to maintain desired behavior in the animat.

The results also suggested the CPSs did not affect the animat's behavior. In 15 experiments, the stability of the network input-output function was not altered by different sequences of CPSs delivered. Every stimulus that evoked responses induced plasticity more or less; however, the results indicate that repetitive CPSs alone were unable to induce enough plasticity to systematically alter the animat's behavior.

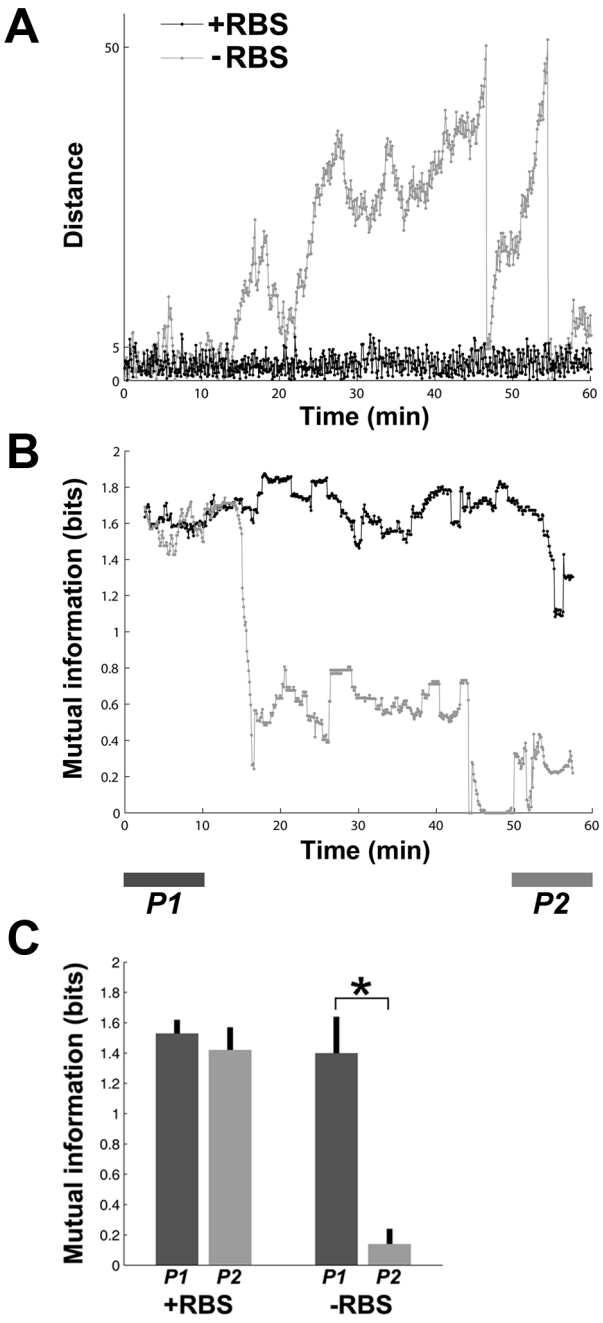

Figure 5.2. RBS stabilized the network input-output function: A. An example of the time course of the distance between the animat and the origin. The animat stayed within the desired area (the inner circle of 5 units radius) for more than 95% of an hour when RBS was applied. When no RBS was applied, the animat moved outward after 10 minutes. When the animat reached the outer circle of 50 units radius, it was put back to a random location within the inner circle, which is shown as vertical downward lines. **B.** The mutual information between the movement angle and the sensory input. When no RBS was applied, the mutual information decreased significantly when the animat started moving outward. **C.** Comparison between the mutual information during the last 10 minutes (light gray, *P2* period shown in B) and that during the first 10 minutes (dark gray, *P1*) for the 15 simulations (3 networks, 5 different selections of CPSs each). With RBS, the mutual information in *P2* was comparable to that in *P1* (p-value= 0.77). Without RBS, the mutual information in *P2* was significantly lower than that in *P1* (p-value< 1e-4, shown as an asterisk).

5.3.2 Adaptation to switching of the sensory mapping

We investigated the networks' ability to learn a user-defined goal behavior by "switching" the sensory mapping. Initially, the sensory-motor mapping was set up so that the animat exhibited the desired behavior. This sensory mapping was later switched, so that the desired behavior was no longer displayed. Learning was then quantified by the animat's ability to adapt and to restore desired behavior under a different, fixed sensory mapping.

Ten simulations, out of 15, showed successful adaptation to the switch, and the average time for the adaptation was 88.6 ± 12.2 minutes (n= 10 simulations). One successful simulation is shown in Figure 5.3A, and all 15 simulations are shown in Figure 5.4. Immediately after the switch, as expected the animat moved outward in Q1 and Q3. Training feedback began to shape the network synaptic weights, and the desired behavior was restored. An unsuccessful simulation is shown in Figure 5.3B. In 5 unsuccessful simulations, explained in the Section 5.4, the animat kept moving outward and was repeatedly put back into the inner circle after reaching the outer circle. The training feedback was unable to restore the desired behavior throughout 4 hours in simulation. In Figure 5.3B, only the first 90 minutes are shown for clarity.

Additional aspects of another successful learning example are shown in Figure 5.5. The corresponding learning curve is shown in Figure 5.5C. Immediately after the switch, the probability of successful behavior dropped, but generally kept increasing afterward due to the training. Among all successful-learning simulations, the average probability of successful behavior before the switch was 63.3 ± 3.5% (n= 10 simulations), dropped significantly to 9.8 ± 1.1% after the switch (p-value< 5e-4, Wilcoxon signed-rank test), and increased significantly back to 53.6 ± 3.5% after 88.6 ± 21.9 minutes when the desired behavior was restored (p-value< 5e-4) (Figure 5.5D). The probability of learning successful behavior after the switch was comparable to that before the switch (p-value=

0.09). The training history from the same example is shown in Figure 5.5E, which showed that not just one PTS, but a certain *sequence* of PTSs was needed in order to restore the desired behavior.

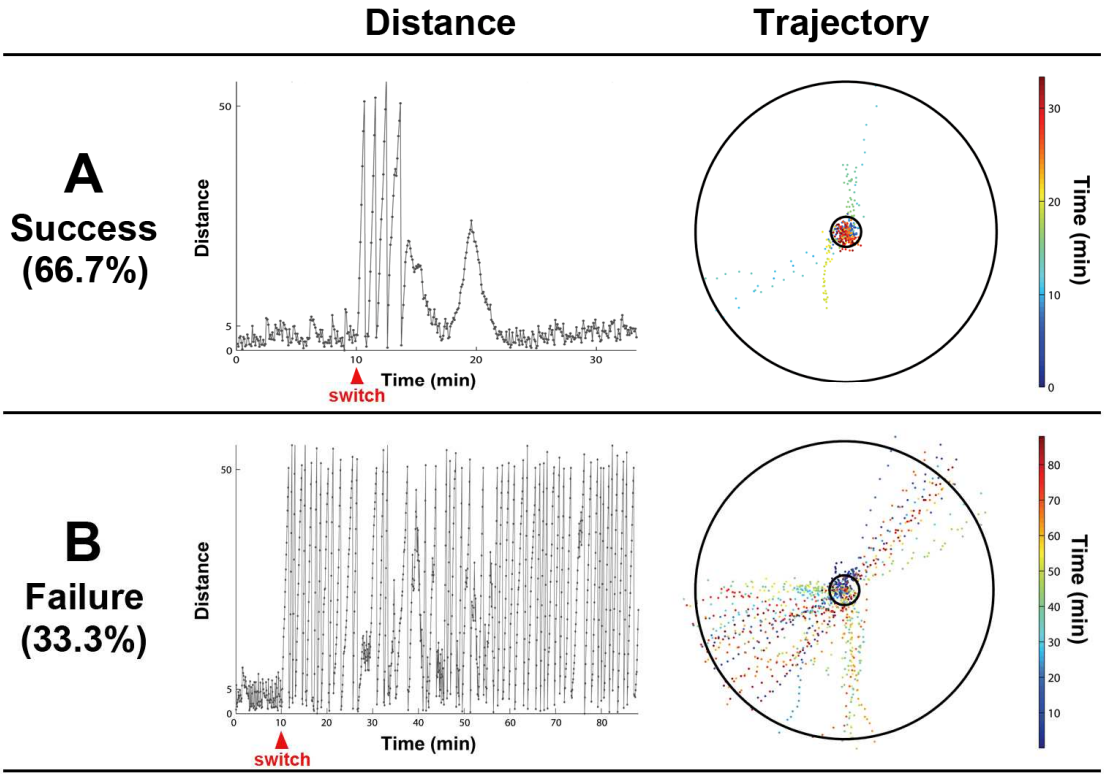

Figure 5.3. Adaptation to a new sensory mapping: The animat's learning ability was quantified by its ability to restore desired behavior after a sensory mapping switch. **A.** An example of successful learning. The distance between the animat and the origin is shown in the left panel. The animat maintained the desired behavior before the sensory mapping switch between quadrants Q1 and Q3 at 10 minutes into the simulation. Immediately after the switch, the animat started moving outward (the trajectory is shown in the right panel). Eventually, the animat adapted to the switch and restored the desired behavior to stay within the inner circle. Ten simulations (out of 15) showed successful adaptation to the switch. **B.** An example of unsuccessful learning. The animat kept moving outward and was repeatedly returned to the inner circle after reaching the outer circle. The training feedback was unable to restore the desired behavior throughout 4 hours of experiment. Only the first 90 minutes are shown for clarity. One-third of the simulations showed unsuccessful learning.

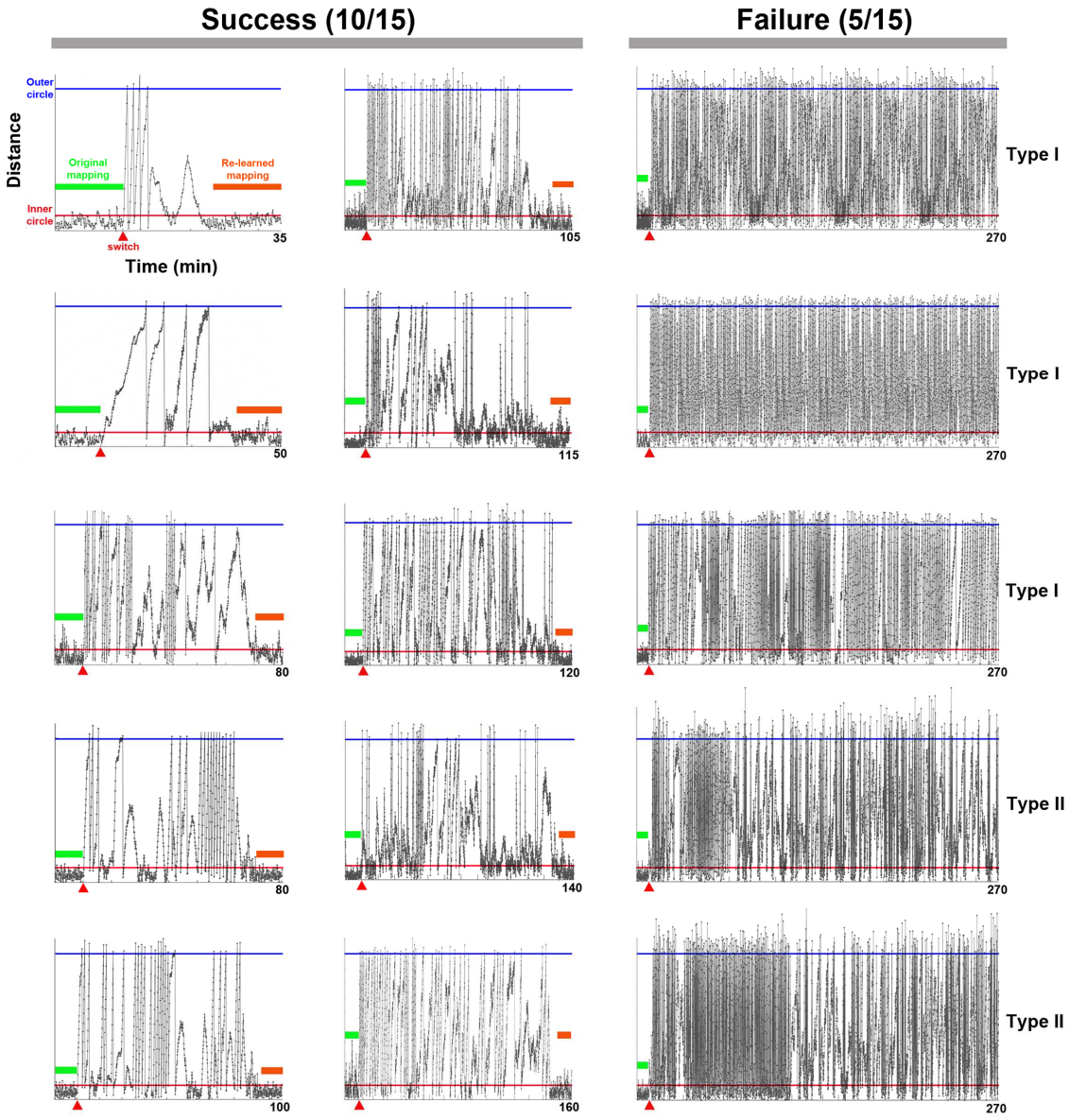

Figure 5.4. Successful and failed adaptation to a new sensory mapping: The distances between the animat and the origin in all 15 simulations are shown. The animat maintained the desired behavior before the sensory mapping switch (red triangle) between quadrants Q1 and Q3 at 10 minutes into the simulation (green bar). Immediately after the switch, the animat started moving outward. In 10 simulations, the animat adapted to the switch and restored the desired behavior to stay within the inner circle (orange bar). For other 5 unsuccessful learning, the animat kept moving outward and was repeatedly returned to the inner circle after reaching the outer circle. The training feedback was unable to restore the desired behavior throughout 4 hours of experiment (only the first 3 hours are shown for clarity). Type I and Type II failures are indicated (see Section 5.4.1).

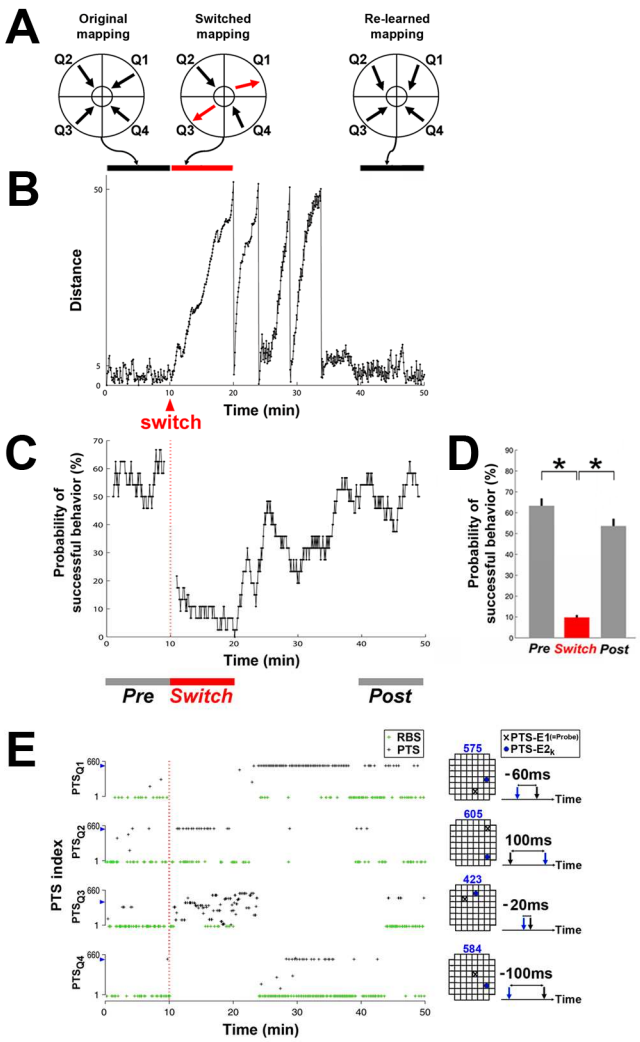

Figure 5.5. A successful adaptation required not only one PTS but a certain sequence of PTSs: A. Desired moving directions in the switched quadrants were restored by training. Average moving directions in each quadrant (shown as arrows) were measured in three 10-min periods (horizontal bars). The average moving directions in the switched quadrants immediately after the switch are shown in red. **B.** The distance between the animat and the origin. **C.** The corresponding learning curve, defined as the change in probability of successful behavior over time. The frequency of the desired behavior was measured during 2-min moving time windows with a time step of 5 seconds. Immediately after the switch, the probability of successful behavior dropped, but generally increased afterward due to the training. **D.** The average probabilities of successful behavior in three different periods in 10 successful learning experiments. These periods are shown in C (*Pre*: the 10 minutes before the switch; *Switch*: the 10 minutes immediately after the switch; and *Post*: the last 10 minutes). The average probability of successful behavior dropped significantly after the switch (p-value< 5e-4), and increased significantly back after the desired behavior was restored (p-value< 5e-4). The probability of successful behavior learned after the switch (*Post*) was comparable to that before the switch (*Pre*) (p-value= 0.09). **E.** The corresponding training stimuli. PTSs delivered from four different pools (PTS_{Q1}- PTS_{Q4}) are shown as black crosses, and the occurrences of RBS are shown as green crosses. From the 660 possible PTSs, the index of PTSs delivered most frequently in Q1, Q2, Q3, and Q4 were 575, 605, 423, and 584, respectively. The electrode locations and $PTS_{\Delta t}$ of these four PTSs are shown on the right. For each pool, the location of the first electrode (PTS-E1, also the probe electrode, see Section 5.2 and Figure 5.1) is shown as a black X in the grids of 60 electrodes, and the second electrode ($PTS\text{-}E2_k$) is shown as a blue dot. $PTS_{\Delta t}$ between the PTS-E1 (black arrow) and $PTS\text{-}E2_k$ (blue arrow) is also indicated for these four PTSs.

5.3.3 Training feedback contingent on behavior was required for successful learning

In order to investigate the importance of the training feedback for successful learning, we recorded the whole training stimulation sequence (PTS and RBS) for each successfully adapted case and replayed it into the same network with the same initial state and same sensory-motor mapping. Different random seeds for fluctuations in neurons' membrane potentials and synaptic currents (see Section 2.2.2.2) were used between the successful learning simulations and the replayed training simulations. This difference would lead to different network responses, and thus different movement trajectories and different CPS sequences. However, the effect of CPSs on shaping the network was insignificant, as shown in Figure 5.2. Therefore, whether the network could adapt to the new sensory mapping solely depended on the effect of training stimulation. The replayed training stimulation was no longer contingent on whether or not desired movement occurred. In ten stimulation-replay experiments, the animat was unable to show successful adaptation with replayed training stimulation (shown as "non-contingent" in Figure 5.6) that had been successful with behavior-contingent training feedback (shown as "contingent").

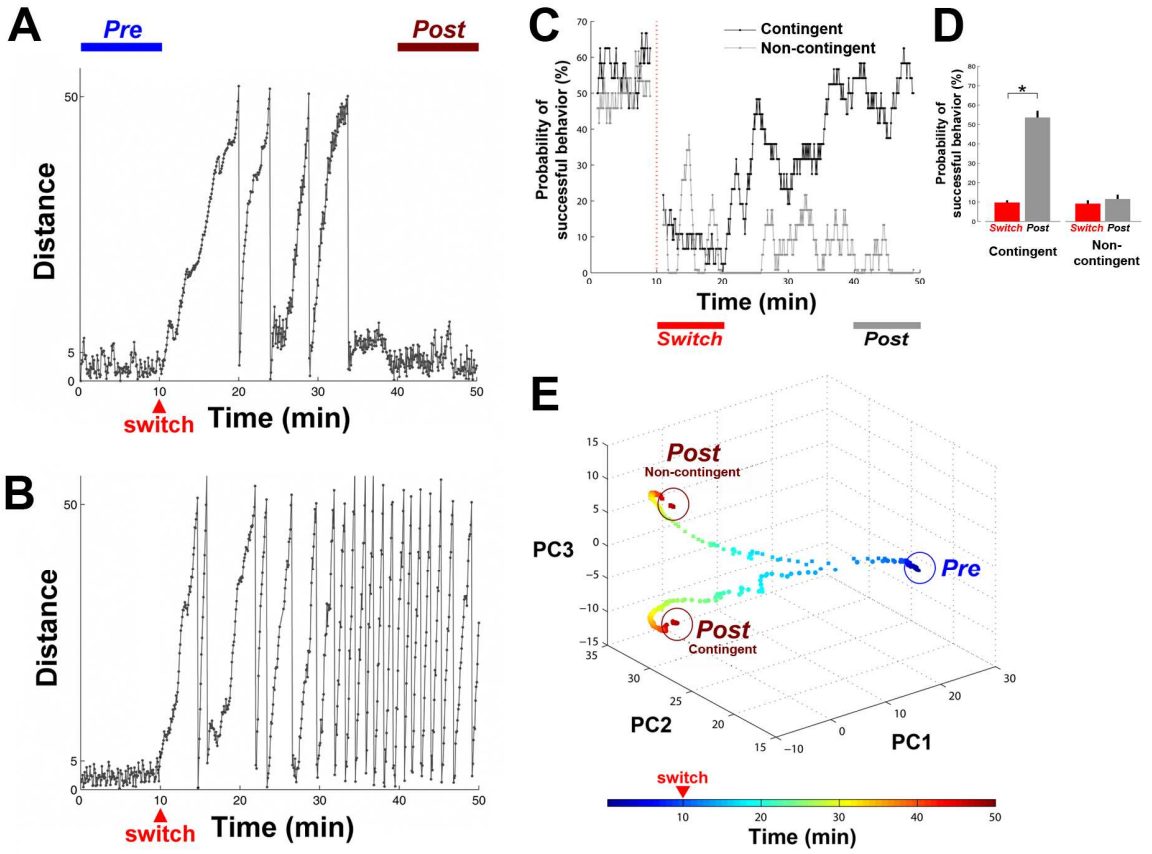

Figure 5.6. Behavior-contingent training feedback was necessary for successful learning: A comparison between experiments with behavior-contingent training feedback and with replayed training stimulation (non-contingent). **A.** With real-time behavior-contingent training feedback, the animat was able to adapt to a sensory mapping switch and reach the desired behavior: moving in desired directions in each quadrant and staying within the inner circle. **B.** The adaptation was absent in the non-contingent experiment. **C.** The comparison of the learning curves (black, grey). **D.** The average probabilities of successful behavior in the 10 successful learning experiments and the corresponding non-contingent experiments. With behavior-contingent training feedback, the average probability of successful behavior in the last 10 minutes of the simulations (*Post* period shown in C) was significantly greater than that measured within 10 minutes after the switch (*Switch* period in C) (p-value< 5e-4). In non-contingent experiments, the average probability of successful behavior in *Post* was comparable to that in *Switch* (p-value= 0.47). **E.** The changes in all synaptic weights were visualized by Principal components analysis (PCA). The first three components (PC1 to PC3) of the network synaptic weights in the same example are plotted over time. Starting from the same initial synaptic weights, the network diverged to different synaptic weight distributions as the training became progressively less contingent on the network activity and the animat's performance. The circled periods, *Pre* and *Post*, are indicated at the top of A.

A comparison of the learning curves is shown in Figure 5.6C. With contingent training feedback, the average probability of successful behavior in the last 10 minutes of the simulations was 53.6 ± 3.5% (n= 10 successful learning simulations), which was significantly greater than 9.8 ± 1.1% measured within 10 minutes after the switch (p-value< 5e-4). With replayed training stimulation, the average probability of successful behavior in the last 10 minutes of the simulations was 11.6 ± 2.2%, which is comparable to 9.2 ± 1.8% measured within 10 minutes after the switch (p-value= 0.47) (see Figure 5.6D).

In order to understand how successful and replayed training stimulation shaped the network differently, we visualized the changes in weights of all synapses by using principal components analysis (PCA). The first three components (PC1 to PC3) of the network synaptic weights for contingent training simulation (Figure 5.6A) and non-contingent training simulation (Figure 5.6B) are plotted over time (Figure 5.6E). Starting from the same initial synaptic weights, the network diverged to different synaptic weights distributions as the training became progressively less contingent on the network activity and the animat's performance.

5.3.4 The "solution" is not unique

After the network adapted to a switching of the sensory mapping, the original sensory mapping was returned to see whether the network could re-adapt to the original mapping (Figure 5.7). After the switch-back, the behavior-contingent training feedback was able to restore the desired behavior under the original sensory mapping (Figure 5.7A), but with a different set of network synaptic weights (Figure 5.7B). This indicates that multiple synaptic configurations, or "solutions", existed for the desired behavior.

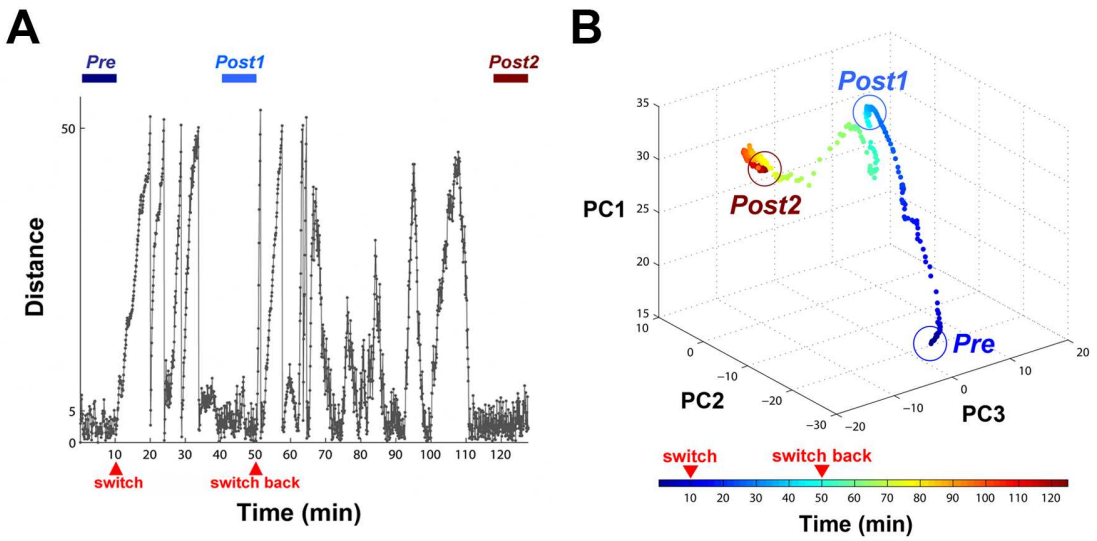

Figure 5.7. The "solution" is not unique: The network re-adapted to reapplication of the original sensory mapping via different state of network synaptic weights. **A.** After the network adapted to a switch of the sensory mapping (*Post1* period), the sensory mapping was switched back to see whether the network could re-adapt to the original sensory mapping. One example is shown. The animat was able to restore the desired behavior (*Post2*) after the switch-back. **B.** After adaptation to the switch-back, the animat showed the same desired behavior under the same sensory mapping, but with a different set of network synaptic weights. Multiple solutions existed for the desired behavior.

5.4 Discussion

We demonstrate that an embodied simulated network, despite lacking the structure present in the brain, can be shaped into desirable states capable of expressing meaningful behavior. We applied a switching of the sensory mappings and measured the network's ability to rewire itself in order to restore the desired behavior under a new mapping. Previous studies have shown that functional visual projections routed into non-visual structures can change the modality of the cortex (Sur et al., 1988; Sharma et al., 2000). This rewiring process was also found to restore function in the olfactory bulb following injury or neurological disease (Costanzo, 2000). Successful rewiring observed in the random network suggests that cultured networks could be a useful model to investigate functional reorganization in cortical circuits after deafferentation or changes in sensory contingencies.

We exploited structured stimuli and detailed activity metrics (Chapter 3) (Chao et al., 2007c) incorporating spatial information to show that with training contingent on the animat's behavior, the network was capable of associating multiple sensory inputs to the desired motor outputs. Figure 5.5 shows that a successful adaptation required not only one PTS but a certain sequence of PTSs. This indicates that for training feedback to lead to the "solution", the interaction between training stimulation and ongoing changes in the network were important. This could be achieved only through real-time feedback (Figure 5.6). We also found that the learned solution for a desired behavior was not unique (Figure 5.7) and could be achieved through different paths of training. These results shed light on the complexity and flexibility of the learning process in neural networks.

5.4.1 Hypotheses for unsuccessful learning

One-third of the simulations showed unsuccessful learning but were nevertheless informative (see Figure 5.4). Two typical behaviors were observed in these five unsuccessful experiments:

5.4.1.1 Type I failure

The animat showed no sign of improving behavior in the quadrant(s) where the switch of the sensory mapping was performed (Q1 and/or Q3) (see Trajectory in Figure 5.8A). In those cases, CPS_{Q1} and/or CPS_{Q3} evoked activity in neurons localized mainly at one quadrant of the network. We hypothesized that this localization reduced or eliminated the ability of the responses to shift the movement toward a different direction. Compared to more spatially homogeneous or symmetric responses, a localized response results in a larger magnitude in CA (see Equation 5.1 in Section 5.2). The maximum of CA_{Q1} and CA_{Q3} (average CAs to CPS_{Q1} and CPS_{Q3}), $Max(CA_{Q1}, CA_{Q3})$, quantified the level of localization in responses to CPS_{Q1} and CPS_{Q3}. This measure indicates the change needed for the directions of CAs to CPS_{Q1} and CPS_{Q3} to be "reversed".

5.4.1.2 Type II failure

The animat showed signs of improving by changing moving direction(s) in the quadrant(s) where the switch was performed (Q1 and/or Q3). However, the movement direction in an un-switched quadrant (Q2 and/or Q4) became undesired (Figure 5.8B). In those cases, neurons activated by different CPSs had large degrees of overlap. We hypothesized that the training stimuli caused correlated changes in multiple CPSs. The degrees of overlap between the responses of different pairs of CPSs quantified this effect. Assume that N_{Q1} is the set of neurons activated by CPS_{Q1}, and N_{Q2} is the set of neurons activated by CPS_{Q2}. Then the degree of overlap between responses to CPS_{Q1} and CPS_{Q2} was defined as:

$$Overlap(CPS_{Q1}, CPS_{Q2}) = \frac{\left\| N_{Q1} \cap N_{Q2} \right\|}{\left\| N_{Q2} \right\|} \cdot 100\% \qquad \text{[Equation 5.3]}$$

where $\|\cdot\|$ represents the number of elements in the set. This value indicates the proportion of neurons activated by CPS_{Q1} that were also activated by CPS_{Q2}, which quantifies how much the training in Q1 (a switched quadrant) might affect the behavior in Q2 (un-switched). The maximum of all possible overlaps between a switched quadrant and an un-switched quadrant was found:

$$\begin{aligned} \textit{Max overlap} = \max\{ & \textit{Overlap(}CPS_{Q1}, CPS_{Q2}\textit{)}, \\ & \textit{Overlap(}CPS_{Q1}, CPS_{Q4}\textit{)}, \\ & \textit{Overlap(}CPS_{Q3}, CPS_{Q2}\textit{)}, \\ & \textit{Overlap(}CPS_{Q3}, CPS_{Q4}\textit{)}\} \end{aligned} \qquad \text{[Equation 5.4]}$$

Max overlap is plotted versus *Max(CA_{Q1}, CA_{Q3})* in Figure 5.8C, which shows that smaller overlap, smaller CA_{Q1} and smaller CA_{Q3} were found in all 10 successful learning experiments. Also, as hypothesized, Type I failure showed large *Max(CA_{Q1}, CA_{Q3})* and Type II failure showed large *Max overlap*.

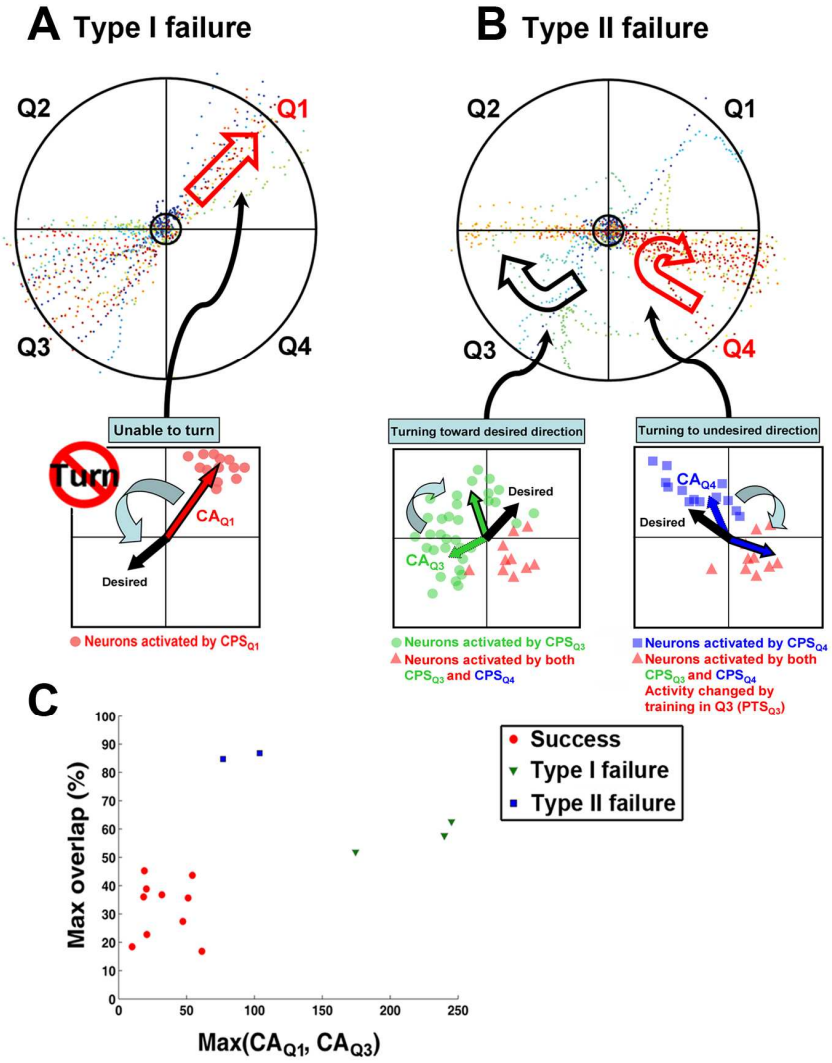

Figure 5.8. Hypotheses about the reasons for failed learning: One-third of the experiments showed unsuccessful learning. Two types of learning failures were found, and examples are shown. **A.** Type I failure: the animat showed no sign of improving behavior in the quadrant(s) where the switch of the sensory mapping was performed (Q1 and/or Q3). Using the trajectory in Q1 as an example, the animat kept going outward without turning (indicated as a hollow red arrow). In those cases, CPS_{Q1} and/or CPS_{Q3} evoked activity in neurons localized mainly at one quadrant of the network. The localization of neurons activated by CPS_{Q1} is illustrated in the cartoon. We hypothesize that this localization reduced or eliminated the ability of the responses to shift the CA from the original direction (shown as a solid red arrow) toward the desired direction (shown as a black arrow). **B.** Type II failure: the animat showed signs of improving by changing movement direction(s) in the quadrant(s) where the switch was performed (Q1 and/or Q3). However, the original desired movement direction(s) in the un-switched quadrant(s) (Q2 and/or Q4) was/were changed into undesired ones(s). Using the trajectory in Q3 and Q4 as an example, the animat was able to turn in Q3 (shown as a hollow black arrow) but the desired direction in Q4 was later altered (shown as a hollow red arrow). In those cases, neurons activated by different CPSs had large degrees of overlap. The neurons activated both by CPS_{Q3}, CPS_{Q4}, and both are illustrated in the cartoon. We hypothesize that the training stimuli in Q3 caused correlated changes in the overlapped neurons (shown as red dots), which caused undesired change in responses to CPS_{Q4}. **C.** The degree of overlap (quantified by *Max overlap*, see Section 5.4) is plotted versus the degree of localization (quantified by $Max(CA_{Q1}, CA_{Q3})$), which shows that smaller overlap, smaller CA_{Q1} and smaller CA_{Q3} were found in all 10 successful cases. Also, Type I failure showed large $Max(CA_{Q1}, CA_{Q3})$ and Type II failure showed large *Max overlap*.

Therefore, in order to obtain successful learning, the stimulation used to encode sensory inputs should evoke neither overly localized nor largely overlapped responses. Localization reduced the possibility to improve moving directions in switched quadrants, and overlap caused unwanted changes in un-switched quadrants. These results suggest a certain level of independence is required between responses to stimulation used to encode different sensory inputs, which could be achieved by using smaller and distinct recording areas to determine movement, or by offsetting the CA through the motor mapping transformation so that the probability of a CA to point in different directions is more uniform. Furthermore, correlated changes in responses to different sensory inputs could also be avoided by using training stimulation that only causes localized plastic changes. These findings could instruct the designs of implant electrodes and feedback stimulation in prosthetics to achieve a more efficient and effective adaptation.

In order to further verify the hypotheses, we calculated the $Max(CA_{Q1}, CA_{Q3})$ and *Max overlap* for additional 85 randomly-generated sets of CPSs from the 3 simulated networks. The $Max(CA_{Q1}, CA_{Q3})$ and *Max overlap* of these 85 sets and the 15 sets used previously, a total of 100 sets, are shown in Figure 5.9A. A cluster with small $Max(CA_{Q1}, CA_{Q3})$ (< 150) and small *Max overlap* (< 50%) was observed (the shaded area in Figure 5.9A). Therefore, we hypothesized that Type I and Type II learning failures could be avoided by selecting CPSs within this cluster:

1. Type I failure can be prevented by choosing CPS_{Q1} and CPS_{Q3} that each evoke responses which are not too localized, (criterion: $Max(CA_{Q1}, CA_{Q3}) < 150$).
2. Type II failure can be prevented by choosing CPSs that evoke responses without too much overlap, (criterion: *Max overlap*< *50%*).

Sixty-four, out of 100, sets of CPSs satisfied the criteria of $Max(CA_{Q1}, CA_{Q3}) < 150$ and *Max overlap*< *50%*. By using 10 randomly-selected sets of CPSs that satisfied the criteria, we found that successful learning could be achieved (Figure 5.9B). The

success rate was improved from 66.7% (from the 15 original simulations, see Figure 5.4) to 100% (from the 10 new simulations, Figure 5.9B). The chance that randomly selecting 10 CPSs that all satisfy the criteria from the 100 randomly-generated sets is less than 0.01 ($C_{10}^{64} / C_{10}^{100} = 0.0088$). This supports the hypotheses and indicates that a higher success rate of adaptations can be achieved by selecting CPSs with smaller *Max(CA_{Q1}, CA_{Q3})* and smaller *Max overlap*. The average time for the adaptation in these additional simulations was 71.8 ± 10.7 minutes (n= 10 simulations), which was comparable to 88.6 ± 12.2 minutes in the 10 successful learning simulations shown previously (p-value= 0.43, Wilcoxon rank sum test). Furthermore, 64 out of 100 random selections of CPSs (64%) satisfied the criteria (see Figure 5.9A), which was comparable to the success rate (66.7%) from the previous 15 simulations with CPSs selected randomly without the criteria.

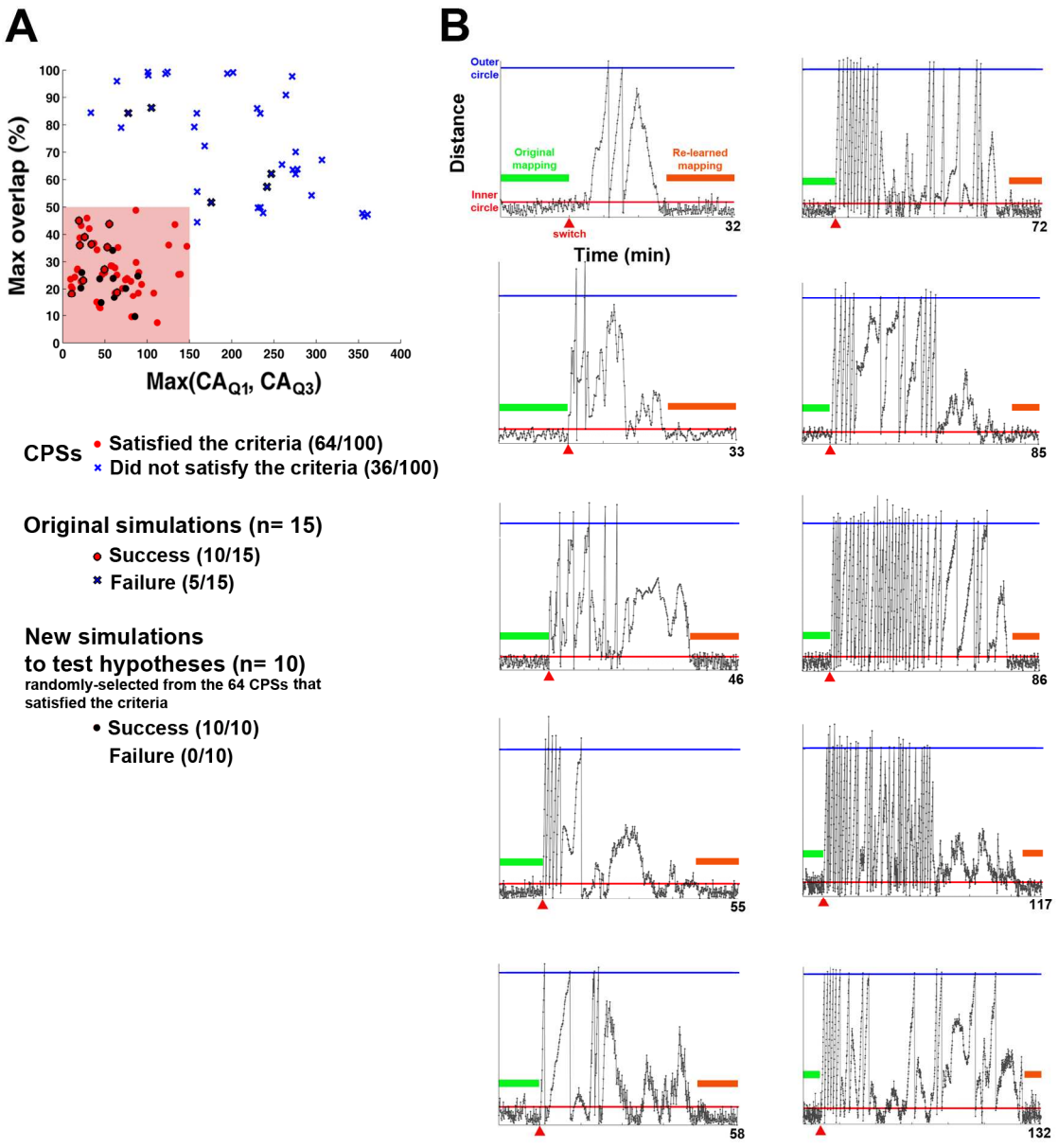

Figure 5.9. Improve learning by selecting CPSs based on the hypotheses: Successful adaptations can be achieved by selecting CPSs with small *Max(CAQ1, CAQ3)* and small *Max overlap*. **A.** *Max(CAQ1, CAQ3)* and *Max overlap* from 100 randomly-selected sets of CPSs in the three simulated networks. The 15 sets of CPSs used in the previous simulations are indicated as dots and crosses with black outlines. Among the 100 sets, 64 sets satisfied the criteria of *Max(CAQ1, CAQ3)< 150* and *Max overlap< 50%* (red dots). **B.** Successful learning was achieved by using 10 randomly-selected sets of CPSs that satisfied the criteria (the selections are indicated as black dots in A). The success rate was improved from 66.7% (10/15, see Figure 5.4) to 100% (10/10). The same representations are used as in Figure 5.4.

5.4.2 Successful adaptive goal-directed behavior in a living cultured network with one sensory-motor mapping

In order to find out whether the learning ability found in the simulated network can also be found in living cultured networks, we tested our closed-loop algorithm in a cortical network cultured over an MEA. The simulated network showed that the animat was able to learn to move toward a user-defined area. In order to achieve this, the animat had to change its movement direction from 45 ± 45° (immediately after the switch) to -135 ± 45° in Q1, and from -135 ± 45° to 45 ± 45° in Q3, while maintaining the desired movement directions in Q2 and Q4. To simplify the goal for living networks and avoid Type II failure, we tested whether a living network could learn to control movement of an animat in a desired direction under just one sensory input. That is, we only delivered one CPS, and investigated whether a single pre-defined desired moving direction could be learned, and if so, whether the animat could adapt to the switching of desired moving directions. Inspired by the learning failures in the simulation results (see above), we removed any directional bias through the motor mapping transformation. Thus, a CA had a uniform probability to point in all directions, and Type I failure could be avoided. An example of a series of successful adaptations in a living network is shown in Figure 5.10.

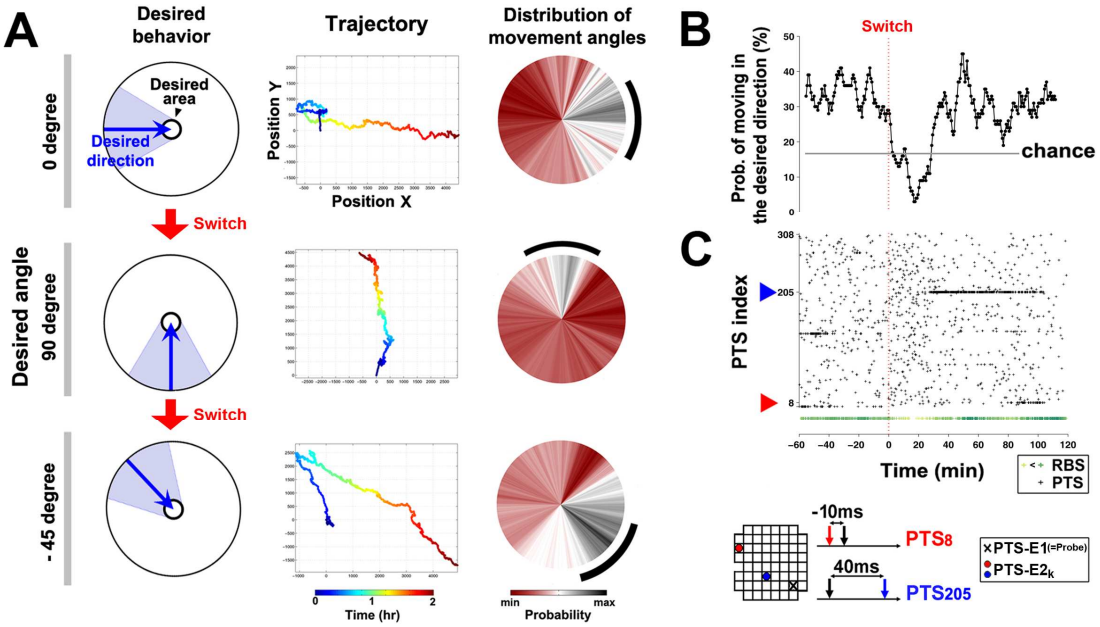

Figure 5.10. Adaptive goal-directed behavior in a living MEA culture: We tested the proposed closed-loop algorithm in a cortical network grown over an MEA with a simplified goal: moving in desired directions under just one sensory input. Furthermore, we tested whether the animat could adapt if we switched the desired movement direction after adapting to a previous one. Inspired by the learning failures in the simulation results (see Section 5.4), we used the motor mapping transformation to remove any directional bias. Thus, a CA had uniform probability to point in all directions, and Type I failure could be avoided. **A.** The trajectory (center column) and the distribution of movement angles (right column) demonstrated that the animat learned to move in the desired direction (left column). A desired angle of 0° was first applied for 2 hours and switched to 90° and then -45°, each for 2 hours (blue to red in time). Successful behavior was considered to be movement within the desired angle ± 30° (right column, black arcs). The probability distribution of movement angles during the last 10 minutes of a 2-hr period was found to match the pre-defined desired angles, which indicated that the animat was able to adapt to the switch of desired angle. **B.** The learning curve across the switch from desired angle of 90° to -45°. An animat moving randomly would give a 16.67% chance that the movement was within the ± 30° range of the desired angle (60°/360°), which is indicated as a horizontal line. The same presentation is used as in Figure 5.5C. **C.** The corresponding training stimuli. The two most frequent PTSs are indicated. The same presentation is used as in Figure 5.5E. For clarity, each RBS was colored based on its occurrence frequency (low to high: yellow to green). Similar to the results found in simulation, not only one PTS, but a complex sequence of PTSs was needed in order to achieve the desired behavior.

We switched between 3 desired angles every 2 hours, and successful learning was judged by network's ability to control an animat to move to new desired angles. We found that after training, the animat was able to move toward the pre-defined desired angles, and the distribution of movement angles converged to the desired angle. The living cultured network was able to show adaptive goal-directed behavior with one sensory-motor mapping. Our future work is to study whether multiple sensory-motor

mappings also can be learned simultaneously in living cultured networks, allowing them to control more complex animat behaviors.

5.4.3 Effects of random background stimulation (RBS) in simulated and living cortical networks

RBS was hypothesized to negate "attractors" in network synaptic weight distributions caused by spontaneous activity (mainly network-wide synchronized bursts of activity), and to prevent network synaptic weights from drifting to such attractors after inducing plasticity with electrical stimulation (Chao et al., 2005) (also see Chapter 4). RBS with an aggregated frequency of 1 Hz reduced the occurrence of spontaneous bursts by at least 10 times in the simulated network and dissociated cortical cultures (Chao et al., 2005). By reducing the occurrence of spontaneous bursts, the network synaptic weights were mainly affected by activity evoked by RBS. Since RBS was random spatially and temporally, the evoked activity had an unbiased randomizing effect on changing network synaptic weights. In a different approach, a burst-control stimulation protocol consisting of a group of electrodes cyclically stimulated with an aggregated frequency of 50 Hz was found to completely eliminate spontaneous bursts (Wagenaar et al., 2005). Similar to RBS, the burst-control stimulation stabilized tetanus-induced plasticity in dissociated cortical cultures (Madhavan et al., 2007c). However, different mechanisms might be involved. RBS evoked network-wide responses with unbiased spatiotemporal structure, while the burst-control stimulation desynchronized spontaneous activity into spatially-localized and temporally-dispersed responses.

In this study, the aggregated stimulation frequency of RBS was increased from 1 to 3 Hz so that the amount of stimulation in RBS and PTS were comparable. RBS did stabilize network synaptic weights (the network synaptic weights were clustered in *Pre* period in Figure 5.6E) and also stabilized the network input-output function (see Figure 5.2).

5.5 Conclusion

The simulated network was used to explore many different possible sensory-motor mappings and training algorithms (not described here) because of savings in preparation time and an ability to monitor all synaptic weights. The described algorithm successfully demonstrated adaptive goal-directed behavior with multiple sensory-motor mappings. This closed-loop algorithm is not restricted to a particular type or a particular number of sensory-motor mappings. Studying a living neuronal network's basic computational properties, such as parallel signal processing and learning, by working with *in vitro* networks could lead to direct development of more advanced artificial neural networks, more robust computing methods, and even the use of neurally-controlled animats themselves as biologically-based control systems.

CHAPTER 6

CLOSING THE LOOP: ADAPTIVE GOAL-DIRECTED BEHAVIOR WITH LIVING CORTICAL NETWORKS [xii]

The closed-loop algorithm described in Chapter 5 successfully showed adaptive goal-directed behavior with multiple sensory-motor mappings in embodied simulated networks. In order to obtain more consistent and faster learning, we modified the designs of patterned training stimulation (PTS) and random background stimulation (RBS), and implemented a better training algorithm. By using the modified closed-loop design, we demonstrated the capability of living cultures to learn to modulate their dynamics and achieve pre-determined activity states within tens of minutes through training. *A priori* knowledge of functional connectivity was not necessary. Instead, effective training sequences were continuously discovered and refined based on real-time feedback based on performance. We found that the short-term dynamics in response to training became engraved in the network, requiring fewer training stimuli later in time to achieve the same results. After 2 hours of training, plasticity was significantly greater than baseline for 80 minutes (p-value< 0.01). Interestingly, a given sequence of stimuli did not induce plasticity, let alone desired activity, when replayed to the network and no longer contingent on behavioral performance. Our results encourage an *in vivo* investigation of how targeted electrical stimulation of the brain, contingent on the activity of the body or even of the brain itself, could treat neurological movement disorders by re-linking neuronal activity to a goal movement.

6.1 Introduction

A life's experiences spur the brain to continuously rewire itself to best achieve behavioral goals. However, errors can occur when injury or a pathological condition causes aberrant neural activity, and often a disconnection arises between the activity of the brain and that of the body. Treating movement disorders using physical therapy has been shown to modify neural activity, and a range of studies have shown electrically stimulated neuronal tissue exhibits neuronal plasticity (see below). Thus theoretically, electrically-induced plasticity could allow the brain to be rewired to achieve a more desired behavioral state. Here in a preliminary experiment, we investigated how a neocortical network could learn to modulate its dynamics and achieve user-defined

---

[xii] To be submitted as: Zenas C. Chao, Douglas J. Bakkum, and Steve M. Potter (2007): *Feedback training of electrical stimuli in a cortical network: learning and neurorehabilitation*. The first two authors contributed equally.

activity states through the feedback training with electrical stimuli. Besides elucidating potential therapeutic roles for artificial stimulation of the brain, these experiments give insight into how the processes underlying learning and memory are expressed in and induced by network activity (Chao et al., 2007a).

Electrical stimulation has been extensively used to artificially induce neuronal plasticity and study learning and memory. For example, cellular plasticity has been observed in a variety of functions, including in synaptic efficacy (Bliss and Lømo, 1973; Bi and Poo, 1998), intrinsic neuronal excitability (Daoudal and Debanne, 2003; Zhang and Linden, 2003), neuronal (Uesaka et al., 2007) and glial (Fields, 2005; Ishibashi et al., 2006a) morphology, action potential propagation (Bakkum et al., 2007), and neurogenesis (Kempermann, 2002). A much-needed progression in the field is determining how cellular plasticity scales and integrates to influence neuronal network dynamics. In primate motor cortex, a neuron was repetitively stimulated 5 msec after the occurrence of an action potential on a different neuron using an electronics implant (Jackson et al., 2006); after halting the stimulation, subsequent activity of the recorded neuron caused an increase in the firing rates in the vicinity of the stimulated neuron. This "pathway-specific" plasticity (Jimbo et al., 1999) and also a "region-specific" variation in the flow of neuronal activity (Chao et al., 2007c) have been observed in our cultured networks. Thus electrical stimulation can sculpt the flow of neuronal information through a variety of mechanisms, and holds promise for either retraining or bypassing malfunctioning neuronal circuits.

Therapeutic techniques used to treat neurological disorders create links between neuronal activity and behavior via the use of directed attention or perceptible feedback signals, and a lot of practice. Physical therapy, including treadmill training and robotic-assisted or neuromuscular (functional) electrical stimulation (NMES / FES) -induced limb movement, has been used to combine natural motion with proprioceptive feedback (Dobkin et al., 2004; Sheffler and Chae, 2007). The feedback activates motor circuits,

improving the control of paretic limbs. Further incorporating visual and aural cues, such as targets for foot steps or beats to maintain walking gaits, and also mental imagery of movement have been used to improve training by priming motor circuits in a top-down (cortical origin) manner (Morrison et al., 2000). Biofeedback therapy uses visual, aural, or tactile displays to improve performance by making underlying physiological or cognitive processes perceptible (Huang et al., 2006). These examples all re-link neuronal activity to a movement, and moreover, physical therapies have led to cortical plasticity: improved hand movements after constraint-induced movement therapy was accompanied by an increased representational area in the motor cortex, observed by transcranial magnetic stimulation (Liepert et al., 2000) and fMRI (Johansen-Berg et al., 2002). However, while helpful; (1) benefits from these techniques are not guaranteed among different individuals or different disorders; (2) optimal therapeutic protocols have not been established; and (3) the relationship with neuronal plasticity is unclear (Dobkin et al., 2004; Huang et al., 2006). Adaptive electrical stimulation may improve therapeutic results by directly treating the abnormal neuronal circuits and related pathways themselves.

Additionally, electrical stimulation inside the brain has successfully managed pathological symptoms, but without re-linking neural activity and behavior (more of a *treatment* rather than *rehabilitation*). Deep brain stimulation (DBS) has been used to treat severe cases of essential tremor, dystonia, Parkinson's disease, Tourette syndrome, clinical depression, and epilepsy (Perlmutter and Mink, 2006). However, its functional mechanisms are debated, and whether or not plasticity plays a key role in DBS therapy is unclear: effects depend on continual stimulation, which causes serious side effects including attentional and learning impairments (Jahanshahi et al., 2000). Other methods to reduce epileptic seizures have been used, including repetitive vagus nerve stimulation (Prater, 1998; Schachter and Saper, 1998) or electrical pulses at or near seizure foci applied prior to a predicted seizure onset (Martinerie et al., 1998), but their consequences

on neuronal plasticity are not known. Therefore, designing an adaptive algorithm to select appropriate training stimuli, contingent on neuronal output, could optimize the effect of a treatment while also avoiding extraneous side effects from excessive stimuli.

We hypothesize that electrical training stimuli contingent on neuronal or motor output could provide a therapy by taking advantage of existing neural plasticity mechanisms to re-link the body with the brain. Many steps are required to reach this ambition, including quantifying the ability and limitations of electrical stimulation to induce functional or adaptive changes in neural activity. Here, we developed an adaptive training algorithm which reshaped the activity of a neocortical network into different desired motor outputs within tens of minutes through the application of patterned training stimulation (PTS) using an extracellular multi-electrode array (MEA). A priori knowledge of connectivity was not necessary. Instead, effective sequences of PTSs were continuously discovered and refined based on real-time performance. The short-term dynamics in response to PTSs became engraved in the network, requiring fewer PTS applications later in time to achieve the same results. Interestingly, a given training sequence did not induce plasticity, let alone desired motor output, when it was replayed to the network and no longer contingent on neural activity. Reducing the amount of stimulation would be expected to reduce the incidence of side effects if applied in patients, and, with enough training, allow the removal of stimulation hardware. Results from our controlled in vitro model encourage an in vivo investigation of how targeted electrical stimulation of the brain, contingent on the activity of the body, could treat aberrant neural activity.

6.2 Methods

6.2.1 Cell culture

We have developed techniques to maintain neuronal cultures and conduct experiments for many months (Potter and DeMarse, 2001). The details are described in Appendix C.

6.2.2 Closed-loop training algorithm

To train a cortical network to achieve a desired motor output, a feedback loop from neural activity to electrical stimulation needs to be created (Figure 6.1). The closed-loop design in this study was similar to the design described in Chapter 5 (Section 5.4.2), but with several modifications, which are summarized in Table 6.1 and explained in the following sections.

First, sequences of neuronal action potentials were transformed into movements. Understanding how such sequences encode movement and information in general is a subject of much scientific inquiry. Population coding is a candidate motor mapping found to occur in the motor cortex (Georgopoulos, 1994), premotor cortex (Caminiti et al., 1990), hippocampus (Wilson and McNaughton, 1993b), and other cortical areas: the firing rates of a group of broadly tuned neurons taken together provide an accurately tuned representation (e.g., to a preferred direction of arm movement). We used a related population coding to instruct motor output, termed the center of activity (CA) (Chapter 3). For training, plasticity was induced by repetitive stimulation of a set of electrodes, termed patterned training stimulation (PTS). If the correct movement occurred, a shuffled background stimulation (SBS) was used instead, which balanced overall stimulation rates. The difference between SBS and random background stimulation (RBS), which was delivered after correct movement in the closed-loop design of Chapter 5, are decribed later in Section 6.2.3.1.

Table 6.1. Differences between closed-loop designs with living cultures in Chapters 5 and 6

Modification	Chapter 5 (Section5.4.2)	Chapter 6	Purpose
Plasticity-inducing stimulation	308 patterned training stimulations (PTSs) with different electrode pairs and inter-pulse intervals (IPIs). (= 28 usable electrodes ∗ 11 IPIs)	100 PTSs, each consisting of 6 stimuli with fixed IPIs of 10 msec. (Section 6.2.3.1)	To induced more pronounced plasticity by including more stimuli.
Plasticity-maintaining stimulation	Random background stimulation (RBS) with random electrodes and random IPIs between 200 and 400 msec.	Shuffled background stimulation (SBS) with the similar spatial structure as the 100 PTSs but with randomly-shuffled temporal order. (Section 6.2.3.1)	To maintain more comparable overall firing rate in probe responses as with PTS. (Section 6.2.3.1)
Probing sequence	Context-control probing sequence (CPS) consisted of 3 stimuli.	CPS consisted of 7 stimuli. (Section 6.2.3.1)	
Training algorithm	Adding desired PTS into the pool to increase its probability being selected later.	Updating the probability of each PTS being selected based on a pre-defined function. (see Section 6.2.2.2)	To include "punishment" on undesired PTSs, instead of only rewarding the desired ones.
Stimulation voltage	± 500 mV	± 300 mV	To localize evoked activity in order to obtain more control and higher resolution in stimulus-induced plasticity. (see Section 6.2.3.1)

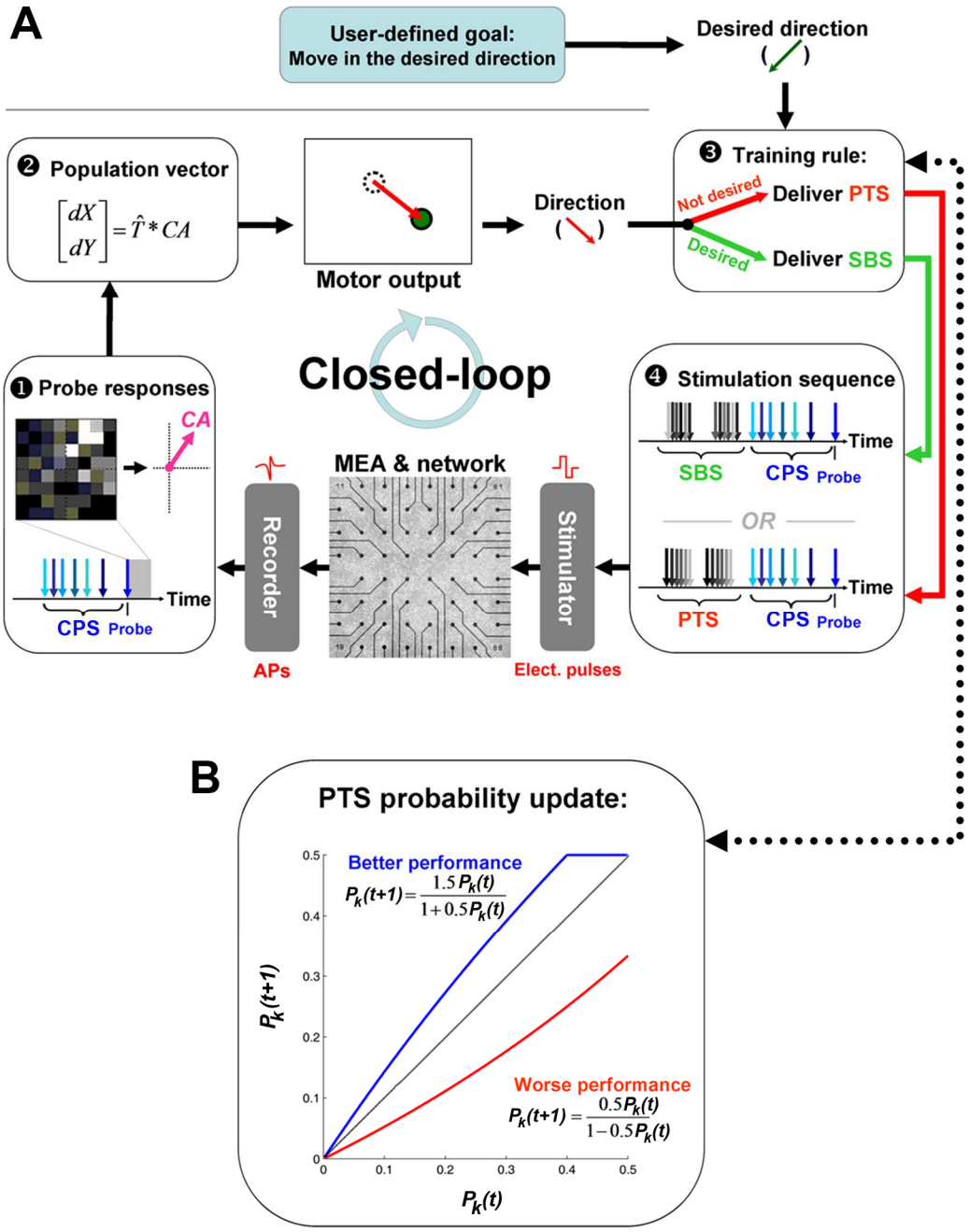

Figure 6.1. Schematic of the closed-loop feedback and adaptive training: See Section 6.2 for details. **A.** ❶ A context-control probing sequence (CPS) was repetitively delivered every 6 seconds. After each last stimulus in CPS, a probe, 100 msec of evoked responses was recorded to form the 2-D center of activity (CA) vector. ❷ The CA was transformed ($\hat{T}$) into incremental movement [*dX*, *dY*]. ❸ If movement was within ± 30º of the user-defined desired direction, a shuffled background stimulation (SBS) was delivered. Otherwise, a set of patterned training stimulation (PTS) was delivered. ❹ CPS was delivered after SBS or PTS to reduce variability in the probe response from ongoing activity. **B.** For unsuccessful movement, a PTS (PTS_k) was selected from a pool of 100 possibilities. The probability of each PTS ($P_k(t)$) being chosen later ($P_k(t+1)$) increased (blue) or decreased (red) depending on the success of the motor output (see Equations 6.1 and 6.2).

6.2.2.1 Motor mapping

Action potentials evoked by repetitive stimulation (1/6 Hz) of a single electrode, termed probe, were recorded for 100 msec following each pulse on the remaining electrodes of an MEA. The *same* probe electrode was used throughout an experiment. A population code, CA, mapped the activity into incremental motor output [*dX*, *dY*], described in Chapter 5 (Equation 5.1) (Figure 6.1A❶ and 6.1A❷). The CA was normalized by a fixed transformation matrix, $\hat{T}$, to remove any directional bias arising from different distributions of neurons in different MEAs (Figure 6.1A❷): the transformation centered the distribution of CAs to (0, 0) to allow movement in all possible directions with equal magnitudes (offsets and scalings in X and Y directions, respectively). This could avoid Type I learning failure, which is described in Chapter 5 (Section 5.4.1.1).

6.2.2.2 Training algorithm

For unsuccessful movement, plasticity of the probe response is desired. Paired stimulation of monosynaptically connected neurons evokes spike-timing dependent synaptic plasticity (STDP) dependent on the stimulation interval (Bi and Poo, 1998). Repetitive PTS, a stimulation sequence with a specific spatiotemporal structure (see below), applied using the extracellular electrodes of an MEA has the potential to induce STDP throughout any shared activation pathways. When movement was within ±30º of the desired direction and no training was required, SBS, which contains no specific temporal structure as in PTS (see below), was used instead (Figure 6.1A❸ and ❹). Neurons at different electrodes can be connected through multiple neurons and pathways; some PTSs may give a desired neuronal plasticity while others may give the opposite or none. Therefore we compiled a pool of 100 possible PTSs, each with a different spatial stimulation sequence (see details below). Initially, each PTS had an equal probability of being chosen. If the current PTS (PTS_k) improved the performance, then the probability

of PTS_k ($P_k(t)$) being chosen later ($P_k(t+1)$) increased, and the probability of other PTSs ($P_i(t+1)$) being chosen decreased (Figure 6.1B):

$$\begin{cases} P_k(t+1) = \dfrac{1.5 \cdot P_k(t)}{1 + 0.5 \cdot P_k(t)}, & k = current \quad PTS \\ P_i(t+1) = \dfrac{P_i(t)}{1 + 0.5 \cdot P_k(t)}, & for \quad i \neq k \end{cases} \qquad \text{[Equation 6.1]}$$

Otherwise, if PTS_k worsened the performance, than $P_k(t+1)$ decreased from $P_k(t)$ and $P_i(t+1)$ for other PTSs increased:

$$\begin{cases} P_k(t+1) = \dfrac{0.5 \cdot P_k(t)}{1 - 0.5 \cdot P_k(t)}, & k = current \quad PTS \\ P_i(t+1) = \dfrac{P_i(t)}{1 - 0.5 \cdot P_k(t)}, & for \quad i \neq k \end{cases} \qquad \text{[Equation 6.2]}$$

In this manner, neuronal plasticity could be directed. A maximum probability of 0.5 was set so that a high probability for one PTS would not saturate the pool of possible choices. A minimum probability of 0.002 was set to ensure each PTS remained available in the future. This allowed the flexibility to adapt to ongoing changes in neuronal network dynamics.

6.2.3 Experiment design

6.2.3.1 Determining PTS, SBS, and CPS

Before every experiment, biphasic voltage stimuli (Wagenaar et al., 2004) of ±300 mV, 400 μs per phase were delivered randomly at the 59 usable electrodes on our MEAs for 30 minutes, one at a time, with random inter-stimulus-intervals between 200

and 400 msec. An electrode that evokes synaptic activity at multiple electrodes is capable of revealing changes in network-level synaptic connectivity, and one was selected as the probe electrode. Six electrodes that evoked only short responses (< 20 msec latency) were selected for "context" stimuli. They were stimulated in order, prior to the probe stimuli, with inter-stimulus intervals between 200 and 400 msec in order to provide a consistent context: these intervals were found to minimize the variability of subsequent evoked responses (Appendix G), and moreover in a simulated network, the block-context set did not cause plasticity themselves (Chao et al., 2007a) (see Chapter 5). Once the spatiotemporal structure of the 6 context stimuli and the probe was determined, it was fixed throughout the experiment and used to sample the network state every 6 seconds to collect movement data. This stimulation sequence is termed a context-control probing sequence (CPS) (see Section 5.2.1.3.1 and Appendix G).

The remaining electrodes that evoked activity were used as candidates for constructing PTS and SBS. The CPS electrodes were not used in PTS nor SBS. Each PTS consisted of 6 stimuli randomly selected from the candidate electrodes (repeated electrodes allowed). The inter-pulse-interval (IPI) between two consecutive stimuli was fixed at 10 msec. When training was required, a PTS was repetitively delivered until the beginning of the next context block, with an inter-PTS-interval between 200 and 400 msec. The design of PTS with 6 stimuli was different from the paired stimulation design described in Chapter 5, since we hypothesized that more pronounced network plasticity could be induced by including more stimuli. Furthermore, since a PTS included 6 stimuli, the design of varying the inter-stimulus-interval of PTS described in Chapter 5 would result in too many combinations. Therefore, the inter-stimulus-intervals were fixed at 10 msec, which was found to be in the range that could induce the most pronounced network plasticity in simulated networks (see Appendix H). When training was not required, SBS consisted of repetitively delivering one randomly selected PTS with inter-SBS-intervals again between 200 and 400 msec, but with randomly-shuffled electrode order each time,

delivered before the next CPS. The randomized order in SBS maintained comparable overall rates and distribution of stimuli as in PTS, while removing the repeating spatiotemporal pattern of neural activation. The probe-evoked response's overall firing rates, and in turn their distribution of CAs, depended on the amount and spatial distribution of stimulation (data not shown). Therefore, any changes in motor output would stem from changes in network connectivity. RBS, which was used to maintain correct movement in the closed-loop design described in Chapter 5, lacked the spatiotemporal structure of hexa-pulse clusters as in the PTS design in this study. This resulted in a significant difference between overall firing rates of probe responses after an RBS and after a PTS (data not shown).

Stimulation voltages of ± 300 mV were lower than those in our previous investigations of plasticity magnitude (Chao et al., 2007c; Chao et al., 2007a; Madhavan et al., 2007b) in order to better localize evoked activity and PTS-induced plasticity. This and only a few seconds of training stimulation at a time were intended to induce plasticity incrementally with enough resolution to reach desired network states and minimize overshoot.

6.2.3.2 SBS-only stimulation

At the beginning of an experiment and prior to each closed-loop training, CPS and probe stimuli were delivered with SBS interspersed for 6 hours. This allowed 2 hours for the network to habituate to the presence of electrical stimulation and another 4 hours for calculating baseline plasticity without training.

6.2.3.3 Closed-loop experiments with different desired movement directions

One closed-loop experiment consisted of four 2-hr training periods, each with a different desired direction of four possible directions (45º, 135º, -135 º, or -45 º), and 2-hr SBS-only periods in between. After a training period, the duration of plasticity was

measured during the 2-hr SBS-only period. The transformation matrix for each training period, $\hat{T}$, was calculated during the last 30 minutes in the preceding SBS-only period. Six closed-loop experiments to learn 4 desired directions each were performed on 5 different cultures from 3 dissociations such that 23 training periods (trials) were analyzed (= 6∗4 minus 1 where a technical error caused a loss of data). Two experiments were performed on one culture, with 13 days in between and different CPS and PTSs.

6.2.3.4 Open-loop stimulation experiments

To test if the improvement in performance was an artifact of the electronics or electrode chemistry arising from a particular stimulation sequence, the stimulation sequence recorded from each closed-loop experiment was replayed to the same network about a day later. Since the same transformation might not successfully offset the CAs if activity changed, the transformations were recalculated as before. However, the particular transformation used does not affect the calculations of plasticity of motor output (Figure 6.5) or of neuronal activity (Figure 6.6). Moreover, the transformation offsets between closed-loop and open-loop trials were found not significantly different (p-value= 0.34, Wilcoxon sign rank test, n= 23 trials ∗ 2 directions; scaling transformations do not affect movement direction).

6.3 Results

6.3.1 Training contingent on motor output shifted neural activity towards the desired activity

We designed a closed-loop algorithm to train cultured networks to learn user-defined motor outputs: moving ± 30º within a pre-defined direction. The closed-loop training algorithm was tested in 5 cortical networks grown over MEAs. Action potentials evoked by repeating probe stimuli, at a single fixed electrode, commanded motor output,

and electrical stimuli were fed back as training signals. The probability of selecting a PTS was updated based on how its application influenced the network's short-term activity dynamics during the following motor output (see Section 6.2). Four goals were applied sequentially to a network, that is, the desired movement direction was changed ± 90º or 180º three times. Overall success was judged by the ability of the network to crystallize successful short-term changes into long-term plasticity and also by its ability to adapt to new desired motor outputs. We found that with training, motor output was able to head toward the predefined desired directions (one representative experiment is shown in Figure 6.2A). The learning curves show that a greater proportion of movements were in the desired direction as training progressed (Figure 6.2C). Since a correct movement meant applying SBS instead of PTS, fewer training stimuli were needed in time, suggesting the network was learning the appropriate input/output function to allow successful behavior.

Learning curves for all experiments are shown in Figure 6.3. A random movement would give a 16.67% chance (horizontal line) of movement within ± 30° of the desired direction (60°/360°). In 5 out of 23 trials (21.7%), the learning curves were below the 16.67% chance in the last 10 minutes of training (black arrows in Figure 6.3). This suggests that a more optimal training algorithm may exist. For example, using a different set of possible PTSs might improve success rates by inducing a different plasticity. The average normalized learning curve of closed loop experiments showed the success rate increased by a factor of 2.88 ± 0.08 (mean ± SEM) times after 2 hours of training for each desired direction (n= 23 trials, from 6 experiments) (Figure 6.4).

The stimulation sequence delivered during a closed-loop experiment was recorded and replayed to the same network the next day. This ruled out artifactual changes in network responses due to non-biological causes, such as electrochemistry or electronic noise, and ensured that neuronal plasticity was responsible for the observed learning. With open-loop training, motor output was unable to move toward the desired directions

(the motor outputs and the learning curves of the corresponding open-loop experiment of the closed-loop experiment shown in Figure 6.2A and 6.2C are shown in Figure 6.2B and 6.2D, respectively). The average learning curve of open-loop experiments was significantly lower than in closed-loop experiments (p-value= 9.9e-54, n= 23 trials, Wilcoxon signed rank test) (Figure 6.4). Changes in movement direction were distributed across a wider range of angles than with closed-loop training (compare Figures 6.2B and 6.2A). Therefore, we concluded that the successful learning reflected biological plasticity in the neuronal networks, and required closed-loop training in which stimuli were contingent on behavior.

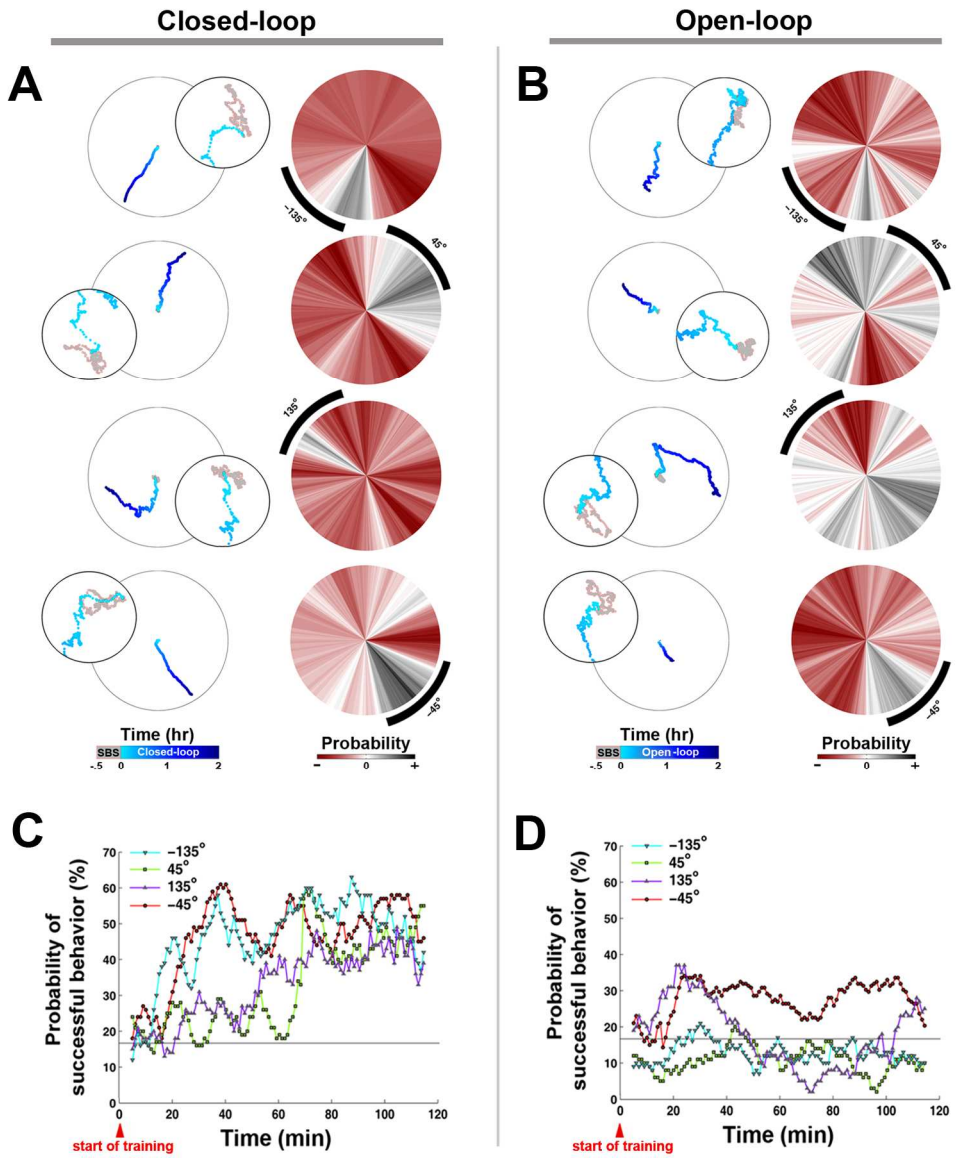

Figure 6.2. Neural response to closed-loop and open-loop training: A. Closed-loop training: Movement trajectory (left column) and the change in the probability distribution of movement directions (right column) demonstrated the motor output adapted to the desired direction (black arcs). Desired directions of -135º, -45º, 135º, and 45º were applied in random order for 2-hr periods (light to dark blue in time) interspersed by 2-hr SBS-only periods (see Section 6.2). Successful motor output was considered to be movement within ± 30º of the desired direction. The smaller trajectory circle is a zoom-in of the beginning of the experiment and the 30-min SBS-only period (gray) used to calculate the transformation, $\hat{T}$. The probability distribution of movement directions during 10 minutes at the start of experiments was subtracted from that during the final 10 minutes, thus allowing negative values (red). **B.** Open-loop training: The closed-loop stimulation sequence was recorded and replayed to the same network. Movement trajectories (scaled to match the corresponding closed-loop experiment) changed but not necessarily towards the desired direction. The distribution of movement directions also changed but in a more distributed manner. Learning curves of (**C**) closed-loop and (**D**) open-loop examples shown in A and B: A learning curve was defined as the probability of movement in the desired direction within a 10-min moving time window (time step= 1 min). The probability of successful motor output increased in time when training was contingent on motor output. A random movement would give a 16.67% chance (horizontal line) of movement within ± 30° of the desired direction (60°/360°).

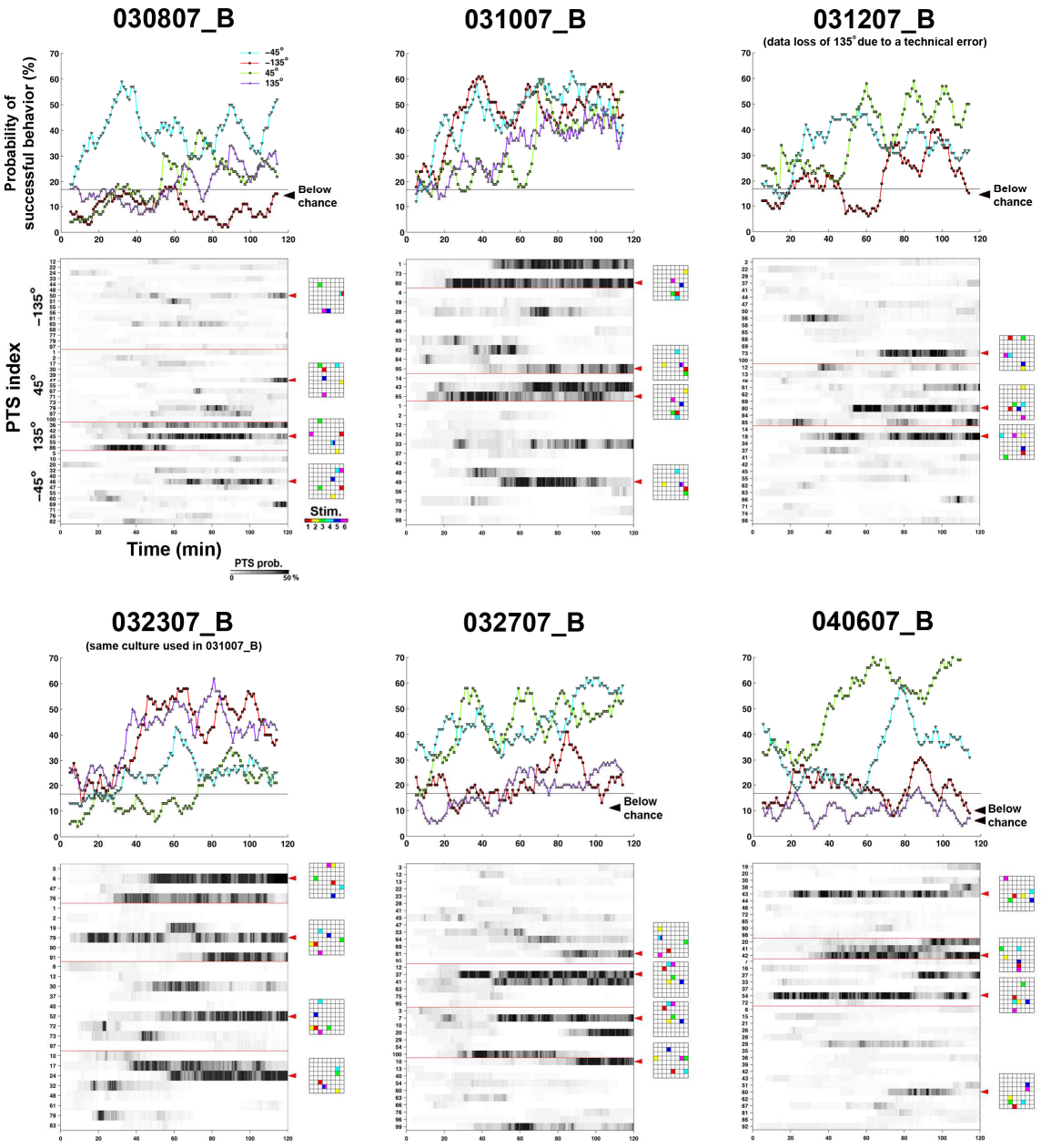

Figure 6.3. Learning curves for all closed-loop experiments: For each experiment, the learning curves and the time courses of different PTS probabilities are shown. See more about the PTS probability in Section 6.3.3 and Figure 6.7B. In 5 out of 23 trials (21.7%), the learning curves were below the 16.67% chance in the last 10 minutes of training (black arrows).

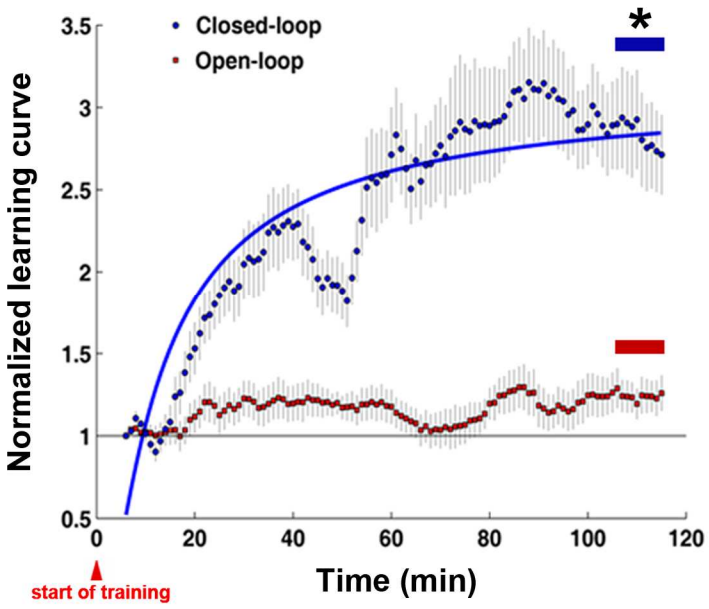

Figure 6.4. Average normalized learning curves of all closed-loop and open-loop experiments: To compare trends among different experiments, each learning curve was normalized by dividing by the probability of successful motor output when training began. The average normalized learning curve in the last 10 minutes of closed loop experiments was 2.88 ± 0.08 (mean ± SEM) times higher than at the start, which was significantly higher than 1.24 ± 0.03 for open-loop experiments (p-value= 9.9e-54, n= 23 trials from 6 experiments, Wilcoxon signed rank test). An exponential curve fit gives a time constant of 10.6 minutes and a learning curve asymptote of 3.13 (SSE= 2.95, R-square= 0.7814).

6.3.2 Changes in motor output arose from neuronal plasticity, not an elastic dependency on stimulation history

The improved performance could be due to plastic changes in the neuronal network or, alternatively, due to an elastic dependency on the recent stimulation history. An elastic change in the neurons' responsiveness to stimuli was observed in dissociated cortical cultures, where the sensitivity of neurons selectively adapted to stimulation with different frequencies, and this change in the sensitivity faded away within several minutes after stimulation was removed (Eytan et al., 2003). In order to characterize the plasticity, we followed the motor output after switching closed-loop training back to the SBS-only stimulation, and quantified whether the learned movement was maintained, and if so, for how long.

By sampling the distribution of movement angles every 10 minutes from 1 hour before to 2 hours after the closed-loop experiment, we found that: (1) the movement angle gradually converged to the desired directions during closed-loop training, and (2) the learned directions were maintained after training during SBS-only stimulation. Results from the experiment used in Figure 6.2 are shown in Figure 6.5A. The distribution of the 10-min SBS-only period immediately before (*Pre*) closed-loop training was significantly different than that immediately after (*Post*) closed-loop training (histograms on the right side of Figure 6.5A). This training-induced plasticity led to desired motor outputs in 18 out of 23 trials (78.3%) (see Figure 6.3). This demonstrated that closed-loop training successfully directed network plasticity, that directed plasticity had occurred (Figure 6.5C). Moreover, the distributions were not significantly different between the last 10 minutes of the training and the next 10 minutes of the SBS-only control (Figure 6.5D). This indicated that motor outputs were preserved in the SBS-only period after training was turned off, and further demonstrated that the improved performance was due to network plasticity, not an elastic response to particular stimuli or to non-biological causes (such as stimulation artifacts of PTS).

In order to investigate the duration of training-induced plasticity, the change-to-drift ratio (C/D, see the definition in Section 3.2.2.3) between CAs in different 10-min periods after training (*Post*, see Figure 6.5) moving with 1-min time steps and CAs in a 10-min reference period immediately before training (*Pre*) was calculated. The mean and SEM of C/D across closed-loop and open-loop periods (n= 23 trials) was compared to C/D across equivalent periods of SBS-only stimulation conducted before training (n= 12 closed-loop and open-loop experiments) (Figure 6.6A). C/D across closed-loop period for each trial is also shown (Figure 6.6B). Closed-loop training-induced plasticity was significantly greater than background plasticity (termed “drift”, measured before training) for 80 minutes (Wilcoxon rank sum test, $\alpha = 0.01$) (Figure 6.6C). Replayed open-loop stimulation did not induce significant plasticity. The decrease in C/D beginning about 70

minutes after closed-loop training indicates that CAs returned back to the distribution before training, and so did movement directions. The return could be due to an active "re-habituation" to the SBS-only stimulation. SBS, while less structured than PTS, still has a spatiotemporal structure and the ability to induce plasticity.

For replayed open-loop stimuli, the distribution of movements was less focused (Figure 6.5B; also see Figure 6.4B), and no significant changes in motor output (Figure 6.5C) or neuronal activity (Figure 6.6) occurred for most of the experiments. Desired movement directions were found in 4 out of 23 open-loop trials (17.4%) during the last 10 minutes (see -45º trial in Figure 6.2B), which was close to the 16.67% chance but significantly lower than the 78.3% success rate for closed-loop experiments. Interestingly, despite having an identical stimulation sequence, the PTSs in open-loop training could not cause noticeable plasticity. When contingent on neural activity, the set of PTSs were able to incrementally shift network dynamics until a significant functional change was detectable.

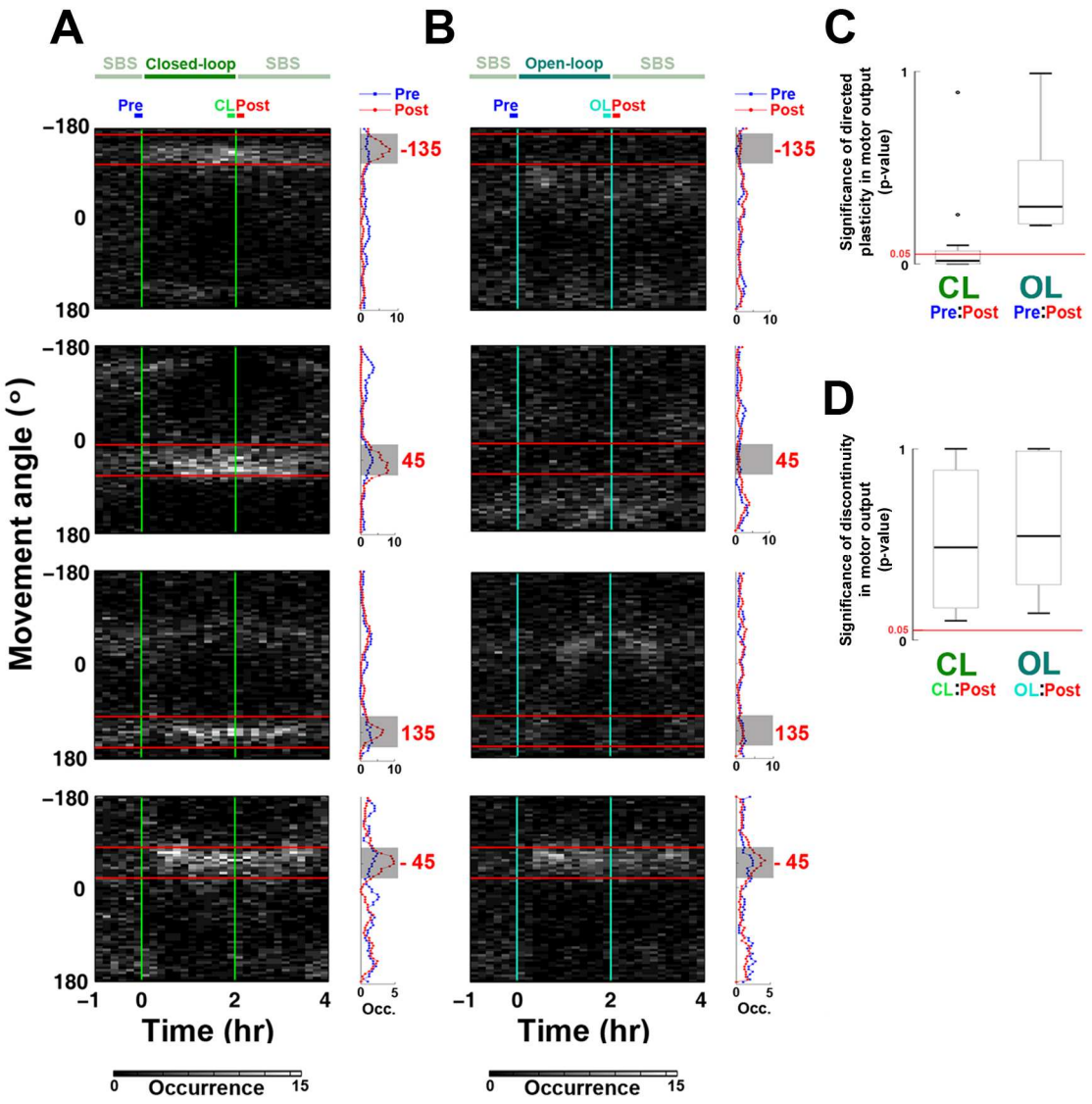

Figure 6.5. Long-term plasticity of movement direction: A. Movement directions became concentrated within ± 30º of the desired direction (red numbers and horizontal lines) during closed-loop training (*CL*) and persisted into the SBS-only periods. Data is from the same representative experiment as in Figures 6.2. The distribution of movement angles was sampled every 10 minutes from 1 hour before to 2 hours after the closed-loop experiment (gray scale). The distributions of the occurrence of different movement angles during 10-min SBS-only periods immediately before (*Pre*) and immediately after (*Post*) closed-loop training are shown in the histograms (right). **B.** Changes in movement direction were not observed in the corresponding open-loop experiment (*OL*). **C.** The distribution of movement angles in *Pre* periods was significantly different than that in *Post* periods for closed-loop training, suggesting directional plasticity occurred. This did not occur for replayed open-loop stimulation suggesting plasticity was not a stimulation artifact. P-values of the difference in movement angle distributions for 23 desired directions (two-sample Kolmogorov–Smirnov test, two-tailed) are represented in box plots showing the first (lower) quartile, the median, and the third (upper) quartile. Outliers are indicated as black dots, and the largest and smallest non-outlier observations are indicated as tic marks (whiskers). The median p-value for closed-loop experiments was below a significance level of 0.05 (0.016 median). **D.** The distribution of movement angles between the last 10 minutes in closed-loop (or open-loop trials; *CL*, *OL*) and that during the next 10 minutes of SBS-only (*Post*) were not significantly different, demonstrating the directed plasticity was not an artifact of PTS history.

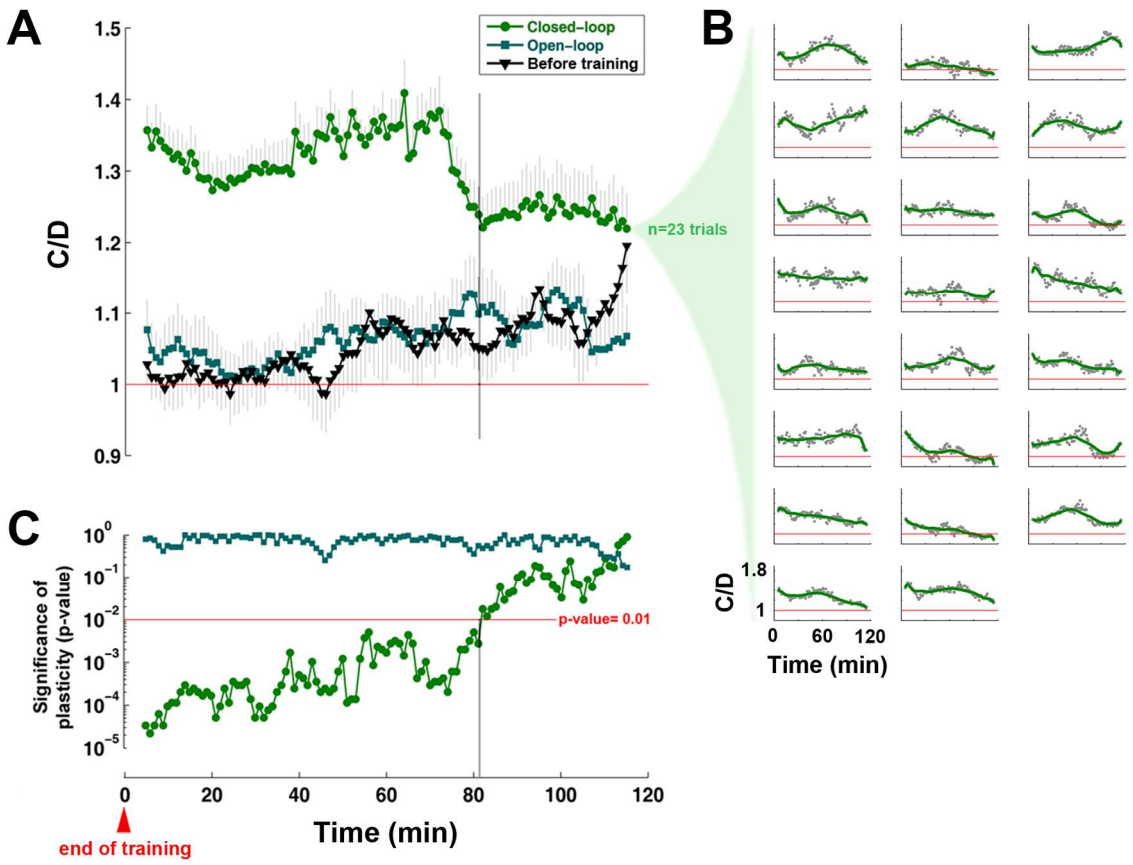

Figure 6.6. Plasticity of neuronal activity induced by closed-loop training lasted for 80 minutes: Plasticity induced by closed-loop training was significantly greater than background plasticity before training, for 80 minutes on average for all experiments, but not for replayed open-loop stimulation. **A.** The change-to-drift ratio (C/D, see the definition in Section 3.2.2.3) between CAs in different 10-min periods after training (*Post*, see Figure 6.5) moving with 1-min time steps and CAs in a 10-min reference period immediately before training (*Pre*) was calculated. The mean and SEM of C/D across closed-loop and open-loop periods (n= 23 trials) was compared to C/D across SBS-only periods during the first 6 hours of SBS-only stimulation (Before training, n= 12 closed-loop and open-loop experiments). **B.** C/D across closed-loop period for each trial. In each subplot, C/D of each 10-min period is indicated as a gray dot, and the overall trend is shown by a smoothed time course, a moving average with 30-point span, of C/D (green curve). **C.** Closed-loop training-induced plasticity was significantly greater than background plasticity measured before training for 80 minutes. Time course of p-values were calculated by comparing C/D of closed-loop and open-loop experiments to C/D before training (shown in A). Plasticity in closed-loop experiments was significantly greater than background plasticity for 80 minutes (Wilcoxon rank sum test, $\alpha = 0.01$).

6.3.3 Training required different PTS at different times

A neural network is continuously plastic, being modified by both stimulus-evoked and spontaneous activity. The same PTS may therefore have different effects at different points in time, and successful adaptation to a desired motor output would require

application of PTSs in a certain sequence. This is what we observed (Figure 6.7B), in agreement with our preliminary results from Chapter 5 (Figure 5.4E for a simulated network and Figure 5.8C for a living culture). Additionally, logic dictates that a finite amount of plasticity is needed to achieve the desired motor output. A given PTS could induce appropriate plasticity initially, but continued application of the PTS could be maladaptive.

We also found that fewer PTSs were needed across a training period to maintain successful motor output (Figure 6.7C). The trend of the PTS-delivering frequency was measured by counting successful PTSs in a 10-min moving time bin with 1-min time step and normalized by its maximum value. We defined a successful PTS as one that improved performance at least one time, and found that the occurrence of successful PTSs monotonically decreased over the last hour (Spearman correlation of means, one-tailed, rho= -0.89, p-value= 1.2e-31, n= 231 successful PTSs in 23 trials). This suggests that the training stimuli which were successful in the first hour were less often or no longer required during the last hour to maintain a high rate of correct motor outputs (see average closed-loop learning curve in Figure 6.4).

Although the training algorithm increased the probability of occurrence of a PTS based on the success of short-term "elastic" responses after the next probe stimuli, the elastic responses became consolidated as long-term plastic changes in time. This is demonstrated by the stability of the distribution of movement directions into the SBS-only period following training (Figure 6.5), the learning curves (Figure 6.4), maintenance of the plasticity of neuronal activity (Figure 6.6), and progressively fewer PTSs being needed to maintain desired movement (Figure 6.7C). At the start of training, the changes in the probe responses were indeed initially short-term elastic responses because they were not maintained, requiring reapplication of PTSs.

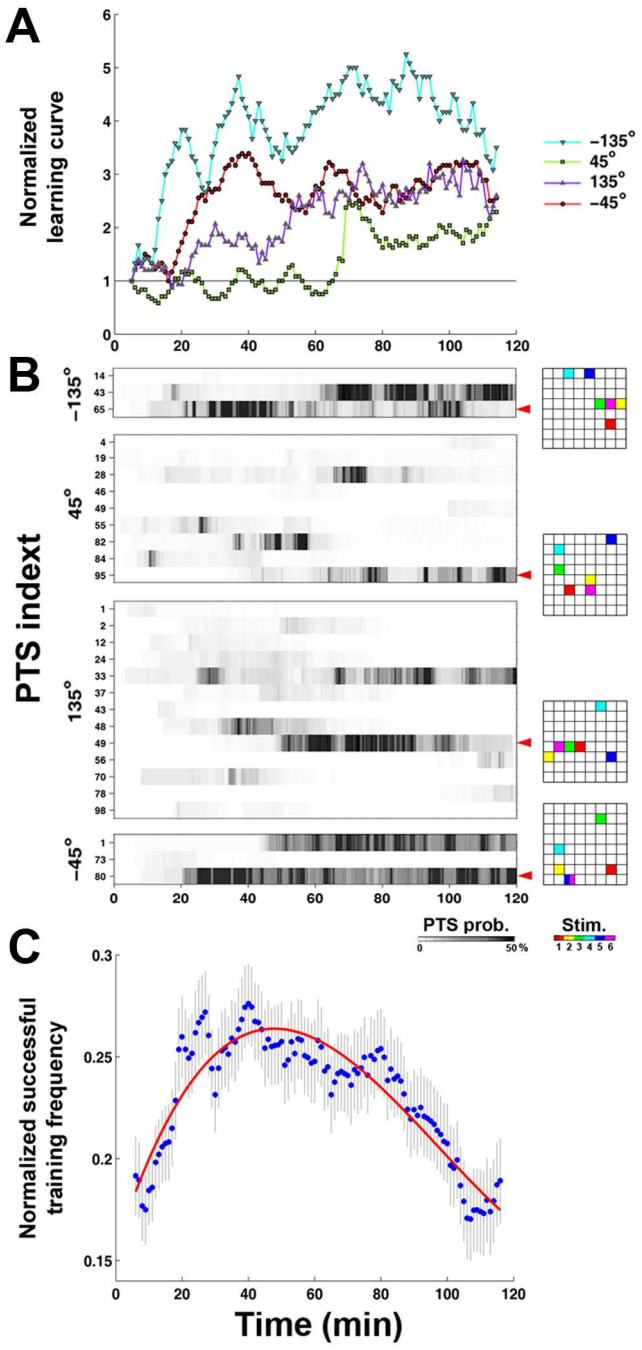

Figure 6.7. Training required different PTS at different times: A. A normalized version of the learning curve shown in Figure 6.2C. **B.** PTS probability in time for different desired directions, color coded to match A. Various series of PTS were needed to induce appropriate neural plasticity and successful motor output. For clarity, the PTS with lower probabilities were not plotted. Electrode locations and order (right) for the PTS indicated by red arrows are shown in 8 by 8 grids of electrode locations. **C.** Across the 23 trials, fewer PTS were needed in time to maintain successful motor output. The frequency of occurrence of a PTS was measured by a 10-min moving time bin with 1-min time step and normalized by its maximum value (set to 1). The initial rise occurred while appropriate PTSs were searched. PTS occurrence monotonically decreased over the last hour (Spearman correlation of means (dots), one-tailed, rho= -0.89, p-value= 1.2e-31, n= 231 successful PTSs in 23 trials). A successful PTS was defined as one that improved performance at least one time. A cubic polynomial (red) was fit to the data to better visualize the trend.

6.4 Disccusion

Following a footpath over a mountain range is quicker and more energy efficient than digging straight through middle. We hypothesize that directing plasticity using training stimuli contingent on the motor output is more efficient than blindly forcing plasticity, for example, via a large tetanic stimulation or open-loop DBS. Moreover, since neuronal activity is continuously plastic, each electrical stimulus and ongoing spontaneous activity alter the landscape, and routes cannot be plotted in advance. Learning is an ongoing and continuous process. Our training algorithm allowed the probabilities of the PTS pool to change, and "solutions" to achieve desired motor outputs were explored in real-time.

The learning curves increased (Figure 6.4), but success did not approach 100%, and some trials showed no learning (Figure 6.3). A more optimal training algorithm may exist, although learning may have continued if training was not stopped after 2 hours. Using a larger set of possible PTSs could improve success rates by inducing a greater range of plasticity; the tradeoff is potentially longer training to find an appropriate sequence of PTSs. Different spatiotemporally structured PTSs, e.g. using more or fewer stimulation electrodes and different temporal arrangements, could also produce different performance. Furthermore, the 0.5 maximum criterion on the probability of selecting a PTS allows randomly-applied inappropriate PTS to produce setbacks. In addition, the 0.002 minimum may keep unhelpful PTSs in the loop. Different optimization rules, such as evolving the PTS pool with a genetic algorithm, or introducing a PID controller to govern the duration of training could improve performance. Future work includes further characterizing the abilities and limitations of electrical stimuli to induce neuronal plasticity, optimizing training parameters, and applying closed-loop algorithms to achieve multiple simultaneous desired motor outputs (Chao et al., 2007a).

6.5 Conclusion

For neurological disorders, targeted electrical stimulation of the brain contingent on the activity of the body or even of the brain itself could direct neuronal plasticity to bypass or accommodate aberrant neural activity. Initial candidate pathologies include those with (1) a focal neural source or related pathway at which to insert an MEA for electrical training and (2) a measurable physical manifestation from which to gather feedback on performance. As an example, to treat movement disorders, such as after stroke, electrical modification of motor areas could be guided by physical measurements of changes muscle activity using electromyography. Directly measuring motor output negates the need for context and probe stimuli to sample neuronal activity, allowing training to be a continuous process. Ongoing afferent input from different brain areas would be expected to negate the need for SBS. Re-linking the body and the brain with electrical training stimuli would give existing brain mechanisms the potential to overcome neurological disorders.

CHAPTER 7

CONCLUSIONS AND FUTURE WORK

7.1 Summary

Brains display very high-level parallel computation, fault-tolerance, and adaptability, all of which are properties that we struggle to emulate in engineered systems. Scientists and engineers have made attempts to cross-fertilize ideas from neuroscience into computing in order to build machines that operate in a brain-like manner. The neurocomputer, where a complicated language is naturally programmed and organized in the system, seems possible and may lead to a new generation of computing devices. Advances in the biocompatibility of materials and electronics have allowed neurons to be cultured directly on metal or silicon substrates, through which it is possible to stimulate and record neuronal electrical activity. The dissociated neuronal culture is one of the best candidates for the neurocomputer because of its: (1) Functional merits: dissociated cultured networks preserve many aspects of complex spatiotemporal activity patterns observed in the brain (Gross and Kowalski, 1999; Shefi et al., 2002; Wagenaar et al., 2006c; Rolston et al., 2007) and can self-organize to be "shaped" by manipulations from experimenters (Jimbo et al., 1999; Shahaf and Marom, 2001; Kudoh and Taguchi, 2005; Baruchi and Ben-Jacob, 2007; Chao et al., 2007a, b; Li et al., 2007; Madhavan et al., 2007c, b; Novellino et al., 2007). (2) Technical merits: the cultured network system provides high flexibility and accessibility. For flexibility, the dissociated cultured network's size and connectivity pattern can be controlled (Corey et al., 1991; Maher et al., 1999; Kam et al., 2001). For accessibility, the cultured network's activity can be recorded with imaging (Bonhoeffer and Staiger, 1988; Parsons et al., 1989; Parsons et al., 1991; Potter, 1996) and electrodes (Gross et al., 1977; Pine, 1980) and stimulation can be

administered by electrical (Jimbo and Kawana, 1992; Gross et al., 1993b), optical (Bucher et al., 2001; Suzurikawa et al., 2007) and pharmacological (Segal, 1983; Gibbs et al., 1997; Baruchi and Ben-Jacob, 2007) means.

By embodying cultured networks on multi-electrode arrays (MEAs) with a virtual robot (an animat), we successfully demonstrated one of the most important features of the brain: *goal-directed learning*. We showed a simple adaptive goal-directed behavior: learning to move in a user-defined direction in living MEA cultures (Chapters 5 and 6), and showed that multiple tasks could be learned simultaneously in simulated networks (Chapter 5). These results suggest that even though a cultured network lacks the 3-D structure of the brain, it still can be functionally shaped and show meaningful behavior. This provides a stepping stone towards designing future neurocomputers with cultured networks. Here I will first summarize the major advances of findings described in the previous chapters, and discuss some possible next steps to continue from them. Then I will briefly discuss how far we are from realizing the neurocomputer and what hurdles remain. In the end, I will propose a detailed future project to reach further toward a neurocomputer.

7.2 Major advances of findings and the next steps

7.2.1 Biologically-inspired simulated networks

The simulated network of 1,000 leaky integrate-and-fire (LIF) neurons exhibited similar activity patterns to those found in living MEA cultures (Chapter 2), and successfully helped with the design of the closed-loop system (Chapters 3 to 5). However, the LIF model is a simplified model for spiking neurons with no capability of showing the rich dynamics observed in cortical networks. By using a more realistic neuron model,

more realistic network properties might emerge. The Izhikevich neuron model[xiii] is one of the best candidates for replacing LIF neurons in my simulated network, since it exhibits a wide spectrum of different dynamics found in biological neurons. Moreover, the Izhikevich model only requires twice the number of "FLOPs" (an approximate number of floating point operations, such as addition, multiplication, etc., needed to simulate the model) as the LIF model, whereas the Hodgkin-Huxley model, another realistic model, requires 240 times more FLOPs (Izhikevich, 2004). In addition to replacing LIF neurons with Izhikevich neurons, moving the simulated network to other more popular simulators, such as NEURON[xiv] and GENESIS[xv], will make it more useful to other researchers. Furthermore, adding the capability for the simulated network to interact with experimenters or the physical environment in real-time will also be useful for future closed-loop designs.

7.2.2 Network activity decoding

Center of activity trajectory (CAT) could detect more subtle stimulus-induced plasticity than several other commonly-used statistics (Chapter 3). It also revealed the region-specific property of stimulus-induced plasticity in dissociated cortical cultures, which demonstrated the important role of neuron location in network functional plasticity (Chapter 3). In order to verify the network mechanisms of long-term region-specific plasticity in dissociated cortical cultures, optical imaging may aid the investigation by acquiring detailed information about stimulus-induced functional and structural changes.

A similar measure of population activity flow, as in CAT, was applied in a human study to quantify the trajectory patterns of the traveling electroencephalographic alpha

---

[xiii] http://vesicle.nsi.edu/users/izhikevich/publications/whichmod.htm
[xiv] http://www.neuron.yale.edu/neuron/
[xv] http://www.genesis-sim.org/GENESIS/

waves across the scalp, but with no learning task involved (Manjarrez et al., 2007). In order to evaluate the usefulness of CAT as a functional indicator of behavioral learning, CAT can be applied to analyze *in vivo* data from animals performing learning tasks. Furthermore, using CAT to analyze data from cultured slices, which preserve some of the morphological structures in the brain, will be helpful to evaluate whether region-specific distributed plasticity also exists in the brain.

7.2.3 Re-afferentation in cultured networks

Random background stimulation (RBS) with an aggregated frequency of 1 Hz was used to restore sensory input to cultured MEA networks to obtain more controllability over stimulus-induced plasticity (Chapter 4). With an aggregated frequency of 3 Hz, RBS further demonstrated its ability to stabilize the network input-output function (Chapter 5). However, these studies were performed in simulated networks, and thus require further validation in living MEA cultures. Furthermore, it is also useful to verify the effects of RBS with different aggregated frequencies on stabilizing network plasticity, and to explore the gap between low frequencies (e.g. 1 Hz and 3 Hz) and the high frequencies (e.g. 50 Hz) used in the burst-control stimulation protocol (Wagenaar et al., 2005). If an optimal frequency exists, it might shed light on how the nervous system utilizes sensory inputs or inputs from different brain areas for memory consolidation.

7.2.4 Multi-task goal-directed learning in simulated networks

Multi-task goal-directed learning could be achieved in the simulated networks, where four sensory-motor mappings could be learned simultaneously (Chapter 5). However, to date, only learning with single-task goals was evaluated in living MEA cultures (Chapters 5 and 6). By using only one probe, corresponding to only one sensory-motor mapping, Type II learning failure can be avoided (see Section 5.4.1) since no

overlap of probe responses exists. However, the closed-loop algorithm in Chapter 5 is not restricted to a particular type or a particular number of sensory-motor mappings. Therefore, in order to quantify the learning capacity of a network under this closed-loop design, we can gradually add sensory-motor mappings into the closed loop and evaluate network's ability to learn them simultaneously. By minimizing the overlap of probe responses, Type II learning failure could be avoided (or reduced) when adding an additional sensory-motor mapping.

Besides investigating how many goals or tasks the network can learn, it is also important to understand how much information the network can store, and for how long. One way to study this is to reapply the same task (i.e. the switch of sensory mappings in simulation, see Chapter 5) after different delays from when it is learned previously, and see whether the network can learn it again in a more efficient way. Thus, we can distinguish whether the network is able to recall its past experience, or simply re-learn the task from scratch. If the network can retrieve what has been learned, then we can also evaluate the duration of memory storage by quantifying the frequency of successful recalls after different delays.

Simulated and living networks were embodied with an animat in Chapters 5 and 6, where interactions with its environment were extremely limited. The significance of environmental interactions in learning can be further investigated by embodying a simulated or living network with an actual robot situated in a physical environment, which supplies more realistic, complex and rich sensory inputs and noise.

7.2.5 Goal-directed learning in MEA cultures and neuronrehabilitation

Goal-directed learning was demonstrated in living MEA cultures with an adaptive training feedback, where we hypothesize that directing plasticity using training stimuli contingent on the motor output is more efficient than blindly forcing plasticity, for example, via a large tetanic stimulation or open-loop deep brain stimulation (DBS)

(Chapter 6). Results from our controlled *in vitro* model encourage an *in vivo* investigation of how targeted electrical stimulation of the brain, contingent on the activity of the body, could treat aberrant neural activity. This requires determining the abilities and limitations of electrical stimuli to induce neuronal plasticity, optimizing training parameters, and applying closed-loop algorithms to achieve multiple simultaneous desired motor outputs.

In Chapter 6 we found that the learning curves increased (Figure 6.4), but success did not approach 100%, and some trials showed no learning (Figure 6.3). This can be further investigated by: (1) Extending training period instead of stopping after 2 hours, or by using a set of criteria to determine when to stop training; (2) Using a larger set of possible patterned training stimulations (PTSs) to induce a greater range of plasticity, but with the tradeoff of potentially longer training to find an appropriate sequence of PTSs; (3) Using different spatiotemporally structured PTSs.

We have attempted to investigate what spatiotemporal structures of PTSs made them successful in shaping network dynamics into a desired state. However, no conclusive correlations were found between the structure of PTSs, the location of probe stimulation, and the desired angle (data not shown). Even though this validates the use of the adaptive training algorithm to select training stimuli, a better understanding of why certain PTSs worked and why others failed might improve the construction of PTS pool, and lead to more effective training.

In order to find a more effective training stimulation pattern, the study in Appendix H needs to be extended by a more thorough investigation on a wider range of possible combinations of stimulation parameters. I hypothesize that the amount of network plasticity could be controlled by the spatiotemporal complexity (STC, see its definition and calculation in Appendix I) of training stimuli. By measuring network plasticity induced by stimuli with different STC in simulated networks, this relationship might be established.

7.3 The gap between our closed-loop system and the neurocomputer

We have shown the cultured network's capability to learn to move in desired directions (Chapter 5 and 6). But can we eventually develop a neurocomputer that we trust for piloting our flights, or controlling our nuclear power plants? What are the components that are necessary, even if not sufficient, for achieving these dreams? Here, I will discuss some open questions for filling the gap between our closed-loop system and a more brain-like neurocomputer.

7.3.1 How to include more biological learning?

In Chapters 5 and 6, we have demonstrated that the network could learn the desired association between sensory inputs and motor outputs with an adaptive training algorithm. With this adaptive training algorithm, the probability of selecting different training stimuli was stored and updated as a part of the closed loop. Therefore, a part of adaptability/learning actually occurred outside the biological network (but within the embodied system). If there is more learning programmed in the computer than in the biological networks, then the neurocomputer can never outperform the artificial neural networks or other artificial algorithms. Therefore, if we know how to include more biological learning, or how to utilize the learning capacity of biological networks, we can evaluate the benefits of incorporating live neurons into a computational device.

7.3.2 How to include different forms of learning?

Goal-directed learning shown in Chapters 5 and 6 demonstrates cultured networks' ability to learn to discriminate different sensory inputs and different goals, that is, to learn different modes of behavior depending on signals or cues from the environment. Including other learning components would help scale our embodied cultured network to a more useful system. For example, if the embodied culture can generalize different sensory inputs or environmental cues that have similar meaning, then

the control for each action does not need to be stored and recalled when needed, and thus the behavior of the system can go beyond experience. Also, if the system can generalize inputs with noise, then it can be fault-tolerant. Furthermore, if the network can develop its own idea of the past experience without external supervision, or can be "aware" of what is learned, then it might acquire offline improvement of what is learned.

7.3.3 How to remove the limitation of pre-determined embodiment?

In Chapters 5 and 6, we embodied a cultured network with a pre-determined body and sensory-motor mappings, which places limitations on the system's capability. For example, our brains are evolved together with our bodies and are optimized to control two hands. If we connect our brains to control four hands or two wings, the performance will be inadequate. However, we cannot conclude that our brains are unintelligent, just that intelligence cannot be demonstrated through the wrong body. Therefore, we need to find the "optimal" body and sensory-motor mappings that connect the cultured network and the body so that the hybrid system could show its maximal intelligence. However, it is extremely difficult to test every possible body and mapping on a cultured network. Not only it will be a time-consuming process, but also that different bodies and mappings cannot be evaluated on the same network due to the network's non-stationary dynamics. I propose a possible approach to find an optimal way to embody the network, which is described in Section 7.4.

7.3.4 How to implement more complex sensory inputs and motor outputs?

In order to encode more sensory inputs that have different meanings to the network, we need to construct feedback stimuli with greater resolution spatially and temporally. Another way to increase the resolution of feedback stimuli is to pattern the morphology of the network, so that stimuli that introduce similar effects on the non-patterned network could have more distinct or more independent meanings in the

patterned network. For activity decoding, in order to generate more distinct motor outputs, we need to access network activity in more detail. These require different technologies than conventional MEA system. Some possible options are described in Section 7.4.

7.3.5 How to maintain the neurocomputer?

Even if we could train an embodied neuronal culture to learn a complex goal, whether we can maintain the biological condition of the network so that the system can continuously perform the required task determines the usefulness of the system. The longest lifespan of a MEA culture in our lab is about two years. Thus, the fundamental questions are how to extend the lifespan of a culture and maintain its performance, or how to transfer its learning to a new network, which is analogous to copying data from an old computer to a new one.

7.4 Future work: a step toward the neurocomputer

The closed-loop design in Chapters 5 and 6 was an educated guess, the result of much trial and error. Population coding with center of activity (CA) is a subset of potential motor mappings, and the applications of RBS, PTS, and context-control probing sequence (CPS) are just one combination of all possible mappings for sensory feedback. A better closed-loop design might exist to evaluate the true capabilities of the embodied cultured network. Here I provide a heuristic for automated discovery of successful mappings, and further optimization of mappings.

7.4.1 Overview

In order to verify the true capabilities of the embodied cultured network, we need to find the "optimal" body and sensory-motor mappings that connect the network and the body. This is analogous to our brains, which are optimized through evolution to control our bodies, where its true intelligence cannot be demonstrated through a wrong body or a wrong control mechanism. In this proposal, I present a system for discovering optimal

sensory-mappings and bodies in an embodied cultured network and verify its maximal capability of adaptive learning, which is one of the most attractive properties of the brain.

Inspired by concurrent evolution of the brain and the body, I propose to use an evolutionary algorithm, the genetic algorithm (GA) (Holland, 1975), to search for an optimal way to embody a cultured network, in order to answer two specific questions:

1. Whether living neurons can be utilized to accomplish any complicated engineering goal, such as problem solving (Section 7.4.2).
2. What is the maximal capability of the cultured network to learn a user-defined goal (Section 7.4.3).

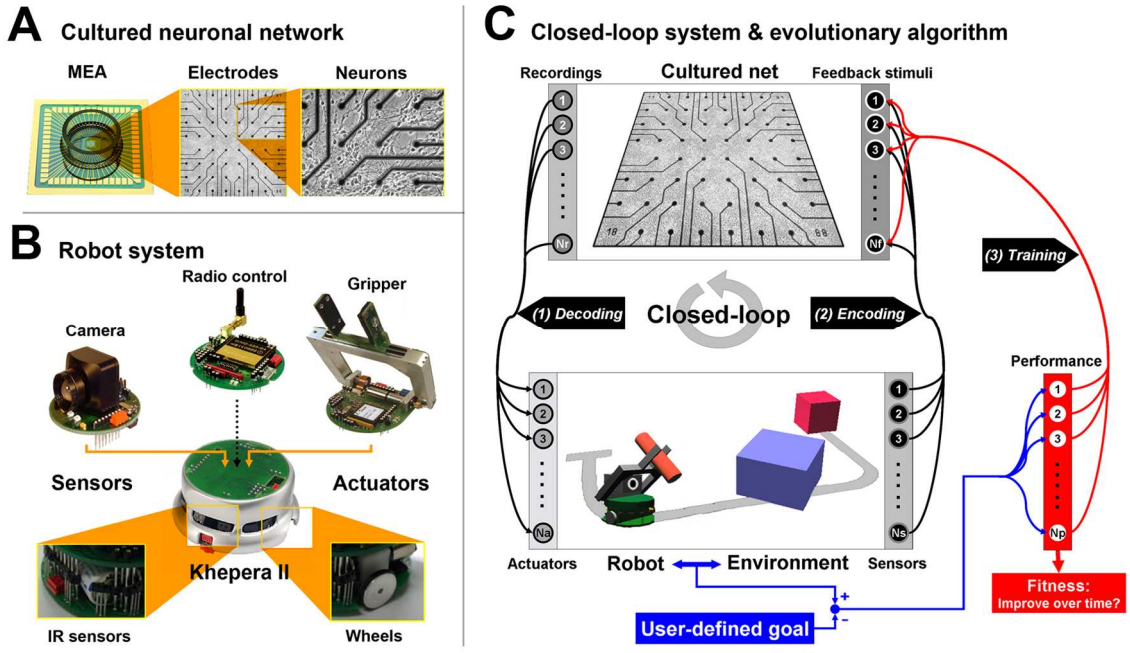

Figure 7.1. Searching for optimal mappings in embodied cultured neuronal networks: A. A cultured network on an MEA. **B.** Khepera robot and its sensors and actuators. **C.** Using evolutionary algorithm for global optimization of three mappings: *(1) Decoding*, *(2) Encoding*, and *(3) Training*.

This is possibly the first attempt to use a *living* neural network to demonstrate complex motor learning. Additionally, unlike in most artificial neural network studies, where learning usually occurs only in the connection weights, one could target another important parameter: *timing*, which was found critical for the brain to continuously

coordinate the body (Swadlow, 1985). Furthermore, the proposed system will continuously process the network activity, interact with the environment, and feed back the sensory information. This preserves the real-time contingency between the embodied network and its surroundings, which is essential for high-level behavior displayed in brains.

7.4.2 Optimize sensory-motor mappings for a complex adaptive goal-directed behavior

I propose to use GA to search for optimal sensory-motor mappings to embody a cultured network with the Khepera robot[xvi] in order to show complex adaptive behavior in a physical environment. The robot will be equipped with two types of sensors (a color video camera and 8 infra-red proximity sensors), and with two types of actuators (two wheels and a gripper) (Figure 7.1B). The goal is to *learn to move to a target through a used-defined track, and identify and remove various obstacles blocking the way* (Figure 7.1C, bottom). This behavioral goal might involve various fascinating elements, such as motor-sequence learning, pattern recognition, and planning, etc.

Three mappings (sets of parameters) need to be optimized by GA (Figure 7.1C):

(1) *Decoding*: how motor mappings continuously translate activity recorded from the network into motor commands for the actuators.

(2) *Encoding*: how sensory inputs are used to construct stimuli fed back into the network.

(3) *Training*: how the training stimuli are instructed according to the robot performance.

[xvi] K-team. http://www.k-team.com.

Each connection in a mapping, which can be portrayed as the artificial neural network extended from the cultured network, is represented by two parameters (a weight w, and a time delay Δt). For example, the output from actuator k at time t, $M_k(t)$, is constructed by a linear combination of recorded activities with different time lags (multiple-input linear filter):

$$M_k(t) = \sum_{i=1}^{Nr} w_{i,k} \cdot A_i\left(t - \Delta t_{i,k}\right) \qquad \text{[Equation 7.1]}$$

where $A_i(t)$ represents the activity from recorder i, and Nr represents the total number of recorders (Figure 7.1C); $w_{i,k}$ and $\Delta t_{i,k}$ represent the weight and the time delay of the connection from A_i to M_k, respectively. In GA, one possible set of parameters which represents the whole-system mappings is defined as a "parent". Robot performance under each parent is evaluated by two fitness functions: (1) whether the goal is achieved within a fixed period of time, and (2) whether the behavior is improved over time. Best-ranking parents are selected to reproduce "offspring" by genetic operations (crossover and mutation), which will become the next parents. The process is iterated until a "solution" is found or other termination conditions are reached.

7.4.2.1 Narrow down the search of optimal mappings by simulation

Due to the characteristic slow convergence of GA, one could first narrow down the search by using a simulation. A biologically-inspired simulated network, which has shown many properties similar to those exhibited in cultured networks (Chao et al., 2005; Chao et al., 2007c), will be embodied with a simulated Khepera robot[xvii], which can amplify searching efficiency by bypassing the restriction of real-time controllability of

[xvii] Webots. http://www.cyberbotics.com.

the real robot. The simulated network I constructed (see Chapter 2) can run in the scale of real-time, which might not be fast enough for searching optimal mappings in the enormous solution domain. This could be solved by moving the model from simulator CSIM, which is in MATLAB platform, to C++, or by using a faster computer or a computer cluster.

7.4.2.1.1 Alternatives

If no solution converges from GA, one could use an alternative method: memetic algorithm (Moscato, 1989), which is a population-based approach for heuristic search in optimization problems. For some problem domains they are orders of magnitude faster than traditional GA (Moscato, 1989).

7.4.2.2 Optimize mappings for living cultured networks with the real robot

Starting from a smaller set of solutions obtained by the simulation, I propose to use GA to search for optimal mappings for living cultures to control the Khepera robot to learn the goal behavior. Due to non-stationary dynamics in living networks, the performance of "bad" parents might be "good" in the future. Thus, GA will be modified to preserve a minimal probability for each possible solution being selected in order to ensure its availability in future iterations. The experimental setup to interface a living culture and the Khepera robot includes two components:

7.4.2.2.1 Feedback stimulation

I propose to use the light-addressable stimulation technique (Suzurikawa et al., 2007), which can overcome the limitations of fixed electrode numbers and densities in conventional MEAs, in order to increase the spatial resolution of stimulation and thus widen the exploration for solution in *Encoding* and *Training* mappings (the total number of nodes in Feedback stimuli, *Nf*, see Figure 7.1C).

7.4.2.2.2 Recording

I propose to use both the conventional MEA which provides high temporal resolution, and the calcium imaging which provides high spatial resolution. The comparison of results from these two recording systems should shed lights on how the nervous system utilizes spatiotemporal precision for motor mappings.

7.4.3 Evaluate the maximal learning capability with evolvable bodies

Evolvable organisms, whose morphology and functions (sensors and actuators) were coded by a graphic representation (Figure 7.2), were used to demonstrate interesting behaviors, such as swimming and jumping (Sims, 1994; Zykov et al., 2005). I propose to use GA to optimize the proposed evolvable sensory-motor mappings together with this evolvable body, and verify whether the goal behavior can be achieved more effectively and efficiently as compared to the results from Section 7.4.2. Furthermore, without restricting the pre-determined body, one could gradually increase the complexity of the task and verify the maximal learning capability of the system.

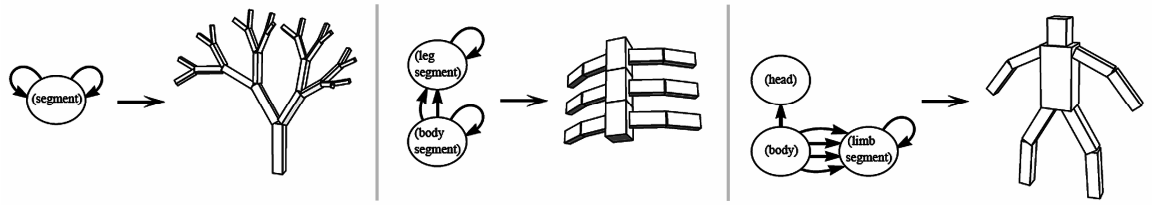

Figure 7.2. Evolvable bodies: Using graphic representation to construct different bodies. (Figure edited from K. Sims, 1994)

7.4.4 Expected results and impacts

Without specific knowledge about how living neural networks self-organize to control a body to learn a goal, global optimization methods, such as evolutionary

algorithms, allow a thorough search for possible solutions. This enables the utilization of living neurons for an engineering purpose (e.g. control a robot to achieve a goal). Furthermore, by finding the optimal combinations of a body and sensory-motor mappings, we can verify the maximal learning capacity (or even true intelligence) of the embodied cultured network, which can elucidate the possibility of the neurocomputer as the agent to future intelligent machines. The knowledge gained from the optimal mappings could also provide insights about learning and memory in the nervous system, which could further lead to direct development of an electronic computer based on the operational principles of biological brains.

APPENDIX A

PARAMETERS FOR THE SIMULATED NETWORKS IN NEURAL CIRCUIT SIMULATOR (CSIM)[xviii]

The parameters used in Neural Circuit SIMulator (CSIM) (Natschlager et al., 2003) and their implementations were shown below:

A.1 General simulation parameters

Parameter	Value	in CSIM
Integration time step	100 μsec	dt
Recording time step for APs	100 μsec	MexRecorder:spikes:dt
Recording time step for synaptic weights	10- 500 msec	MexRecorder:W:dt

A.2 Network parameters

Parameter	Value	Reference value
# of neurons	1,000	——
# of synaptic connection	~50,000	——
Synapses per neuron	50 ± 15	——
% of inhibitory neurons	30	20 (Song et al., 2000) 25 (Izhikevich et al., 2004)
% of self-firing neurons	30	~30 (Latham et al., 2000a; Latham et al., 2000b)

[xviii] http://www.lsm.tugraz.at/csim/index.html

A.3 Neuron parameters

A.3.1 LIF neuron

Parameter	Value	Reference value	in CSIM
$V_{resting}$	-70 mV		LifNeuron:Vresting
V_{init}	-70 mV		LifNeuron:Vinit
V_{thresh}	-54 mV		LifNeuron:Vthresh
V_{reset}	-60 mV		LifNeuron:Vreset
$T_{refract}$	3 msec		LifNeuron:Trefract
C_m	3e-8 F		LifNeuron:Cm
R_m	1e6 ohm		LifNeuron:Rm
τ_m	30 msec		——

A.3.2 Self-firing

Parameter	Value	Reference value	in CSIM
I_{noise} **(self-firing)**	30 nA	By optimization	LifNeuron:Inoise
I_{noise} **(non-self-firing)**	10 nA	By optimization	LifNeuron:Inoise

A.4 Synapse parameters

A.4.1 General

Parameter	Type	in CSIM
Type of excitatory synapses	STDP + frequency-dependent	DynamicStdpSynapse
Type of inhibitory synapses	Frequency-dependent	DynamicSpikingSynapse

A.4.1 Frequency-dependent

A.4.1.1 Excitatory

Parameter	Value	Reference value	in CSIM
R_0	100%	——	DynamicStdpSynapse:r0
U	0.5	~0.6 (Markram et al., 1998a) 0.5 (Izhikevich et al., 2004)	DynamicStdpSynapse:U
u_0	0.5	——	DynamicStdpSynapse:u0
D	800 msec	~800 msec (Markram et al., 1998a) 800 msec (Izhikevich et al., 2004)	DynamicStdpSynapse:D
F	1 sec	1 sec (Izhikevich et al., 2004)	DynamicStdpSynapse:F
τ	3 msec	5- 6 msec (Izhikevich et al., 2004)	DynamicStdpSynapse:tau

A.4.1.2 Inhibitory

Parameter	Value	Reference value	in CSIM
R_0	100%	——	DynamicSpikingSynapse:r0
U	0.5	~0.6 (Markram et al., 1998a) 0.2 (Izhikevich et al., 2004)	DynamicSpikingSynapse:U
u_0	0.5	——	DynamicSpikingSynapse:u0
D	800 msec	~200 msec (Markram et al., 1998a) 700 msec (Izhikevich et al., 2004)	DynamicSpikingSynapse:D
F	1 sec	20 msec (Izhikevich et al., 2004)	DynamicSpikingSynapse:F
τ	3 msec	~2 msec (Abbott et al., 1997)	DynamicSpikingSynapse:tau

A.4.2 STDP (excitatory synapses only)

Parameter	Value	Reference value	in CSIM
A_+	0.5	0.5% (Song et al., 2000) 0.4% (Izhikevich et al., 2004)	DynamicStdpSynapse:Apos
A_-	0.5*1.05%	0.5*1.05% (Izhikevich et al., 2004) 0.4% (Izhikevich et al., 2004)	DynamicStdpSynapse:Aneg
τ_+	20 msec	20 msec (Izhikevich et al., 2004) ~13 msec (Froemke and Dan, 2002) 15 msec (Izhikevich et al., 2004)	DynamicStdpSynapse:taupos
τ_-	20 msec	20 msec (Izhikevich et al., 2004) ~34 nsec (Froemke and Dan, 2002) 20 msec (Izhikevich et al., 2004)	DynamicStdpSynapse:tauneg
W_{up}	0.1	0.5 (Izhikevich et al., 2004)	DynamicStdpSynapse:Wex
W_{low}	0	0 (Izhikevich et al., 2004)	
μ_+	1	——	DynamicStdpSynapse:mupos
μ_-	1	——	DynamicStdpSynapse:muneg
τ_{pre}	34 msec	28 msec (Froemke and Dan, 2002)	DynamicStdpSynapse:tauspre
τ_{post}	75 msec	88 msec (Froemke and Dan, 2002)	DynamicStdpSynapse:tauspost

APPENDIX B

CALCULATIONS OF THE STATISTICS FOR EXPERIMENTS IN SIMULATIONS AND LIVING CULTURES

The evoked responses within 100 msec (to include all evoked responses) after the stimuli of random probing sequences (RPSs) were used for calculations of the statistics compared in Chapter 3. The dimensionalities of different statistics are shown in Table B.1. For those statistics that include temporal information (FRH, MI, SCCC, JPSTH, and CAT), responses within 100 msec were binned by a 5 msec moving time bin with 500 μsec time step. 500 μsec time step was used to obtain fine temporal resolution, since it was less than the duration of an action potential. 5 msec bin size was used to acquire action potentials on multiple electrodes within a single bin. Also, the same binning parameters were used for all statistics in simulations and in living cultures for fair comparison of their performance.

B.1 Simulations

B.1.1 Firing rate (FR)

This most commonly used statistic quantifies the intensity of the evoked responses. During each simulation, stimuli at each electrode occurred multiple times (10.0 ± 3.1 trials) in one RPS. FR for evoked responses to each stimulation electrode was calculated by averaging the number of spikes counted at each recording electrode over trials, producing a 60-dimensional vector.

B.1.2 Firing rate histogram (FRH)

FRH expands on FR by including temporal information. FRH from recording electrode Ek to the probing stimulus at electrode P_i, $FRH_{E_k}^{P_i}$, was the average number of

spikes counted in a 5 msec moving time window with 500 μsec time step over trials, which resulted in a 1 by 191 vector. FRH for evoked responses to stimulation electrode P_i was defined by joining $FRH_{E_k}^{P_i}$ from 60 recording electrodes together, which formed an 11,460-dimensional (191∗60) vector.

B.1.3 Center of activity trajectory (CAT)

The definition of CAT is described in Section 3.2 (Equations 3.1 and 3.2). The X and Y components are both 1 by 191 vectors. By appending two components together, CAT for evoked responses to each stimulation electrode was a 382-dimensional (191∗2) vector.

B.1.4 Mutual information (MI)

MI quantifies the statistical dependence, including higher order moments in addition to 2nd order, between responses at different locations (Moddemeijer, 1989; Brunel and Nadal, 1998; Paninski, 2003). MI between two recording electrodes E_k and E_j for stimulation electrode P_i is defined as the mutual information between two distributions: $FRH_{E_k}^{P_i}$ and $FRH_{E_j}^{P_i}$. Let $FRH_{E_k}^{P_i} = \{A_n\}_{n=1}^{191}$ and $FRH_{E_j}^{P_i} = \{B_m\}_{m=1}^{191}$, where A_n and B_m represent elements in *FRH*s. Then the MI between $FRH_{E_k}^{P_i}$ and $FRH_{E_j}^{P_i}$ is defined as:

$$I(FRH_{E_k}^{P_i}, FRH_{E_j}^{P_i}) = \sum_{n,m} P_{X,Y}(A_n \times B_m) \ln \frac{P_{X,Y}(A_n \times B_m)}{P_X(A_n) \times P_Y(B_m)} \qquad \text{[Equation B.1]}$$

where P_X and P_Y represent the marginal probabilities of $FRH_{E_k}^{P_i}$ and $FRH_{E_j}^{P_i}$, and $P_{X,Y}$ represents the joint probability of $FRH_{E_k}^{P_i}$ and $FRH_{E_j}^{P_i}$. MI was estimated by using the

histogram-based mutual information methods described by Moddemeijer (Moddemeijer, 1989). In this study, the MATLAB codes from Rudy Moddemeijer's group were used[xix]. MI provides a non-directional connectivity map, which represents the dependence between activities at different pairs of electrodes. By joining the MI from every pair of electrodes, MI for evoked responses to each stimulation electrode was a 1,770-dimensional (60∗59/2) vector.

B.1.5 Shift-predictor corrected cross-correlogram (SCCC)

The corrected cross-correlogram (Michalski et al., 1983; Eggermont, 1992; Brody, 1999; Franco et al., 2004; Ventura et al., 2005) removes the peak in the original cross-correlogram that is due to co-stimulation of the neurons, and measures the association between neurons. For each pair of recording electrodes, the "raw" cross-correlogram was constructed by averaging the cross-correlograms between two spike trains from the two electrodes over trials. The "shift predictor" was constructed by averaging the cross-correlograms between all possible pairs of spike trains from the two electrodes but from different trials. SCCC was then the raw cross-correlogram minus the shift predictor. In this study, the algorithm described by George Gerstein's group was used[xx].

With the same binning resolution used for FRH, SCCC between each pair of recording electrodes was a (191∗2-1)-dimensional vector which represents the correlations sequence at different lags. Therefore, SCCC for evoked responses to each stimulation electrode was a 674,370-dimensional ((191∗2-1)∗60∗59/2) vector.

[xix] http://www.cs.rug.nl/~rudy/papers/abstracts/RM8902.html
[xx] http://mulab.physiol.upenn.edu/crosscorrelation.html

B.1.6 Joint peri-stimulus time histogram (JPSTH)

The JPSTH quantifies the causality between responses at different locations (Gerstein and Perkel, 1969; Aertsen et al., 1989; Ventura et al., 2005). JPSTH finds the fixed delay between sequences of spikes recorded at different pairs of neurons (electrodes) over multiple trials, which can depict causal relationships between them. Similar to SCCC, the shift-predictor was applied on the "raw" JPSTH to eliminate the time-locked stimulus-induced covariation due to co-stimulation. In this study, the algorithm and MATLAB codes from George Gerstein's group were used[xxi]. The results can provide directional information about the connectivity. With the same binning resolution used for FRH, JPSTH between each pair of recording electrodes was 191∗191-dimensional. Therefore, JPSTH for evoked responses to each stimulation electrode was a 64,571,370-dimensional (191∗191∗60∗59/2) vector.

B.1.7 Center of activity trajectory with electrode locations shuffled (CAT-ELS)

The electrode locations, E_k, were randomly shuffled. Then CAT-ELS was calculated according to Equations 3.1 and 3.2 (in Section 3.2) by using these shuffled electrode locations. For each network, the electrode locations were shuffled 10 times and 10 different corresponding CAT-ELSs were generated.

B.2 Experiments in living cultures

B.2.1 Firing rate (FR)

The number of spikes was counted at each recording electrode for each probe response and averaged every block. Thus, for each stimulation electrode, a 60-dimensional FR vector was obtained for every 240 seconds ("block", see Section 3.2).

[xxi] http://mulab.physiol.upenn.edu/jpst.html

B.2.2 Firing rate histogram (FRH)

For evoked responses to each stimulus, the FRH was calculated by using a 5 msec moving time window with time step of 500 μsec. Thus, for each stimulation electrode, an 11,460-dimensional (191∗60) FRH vector was obtained for every block.

B.2.3 Center of activity trajectory (CAT)

Let $FRH_{E_k}^{P_i}$ be the average responses over each block, recorded at electrode E_i to stimulation electrode P_i. CAT for stimulation electrode P_i was then calculated from the $FRH_{E_k}^{P_i}$ by using Equation 3.1 and 3.2 (in Section 3.2). Thus, for each stimulation electrode, a 382-dimensional (191∗2) CAT vector was obtained for every block.

B.2.4 Shift-predictor corrected cross-correlogram (SCCC)

With the same binning resolution used for FRH, SCCC between each pair of recording electrodes was calculated for every block. Thus, for each stimulation electrode, a 674,370-dimensional ((191∗2-1)∗60∗59/2) SCCC vector was obtained for every block.

B.2.5 Center of activity trajectory with electrode locations shuffled (CAT-ELS)

CAT-ELS was calculated by the same shuffling procedure used in simulations. For each experiment, the electrode locations were shuffled 10 times and 10 different corresponding CAT-ELSs were generated. The dimensionality of CAT-ELS was the same as CAT.

Table B.1. The dimensionality of the statistics

Statistics	Dimensionality*	
	Simulations	Experiments in living cultures
FR	60	60
FRH	11,460	11,460
MI	1,770	-
CAT	382	382
CAT-ELS	382	382
SCCC	674,370	674,370
JPSTH	64,571,370	-

* The dimensionality is defined as the length of the statistic calculated from evoked responses to *one* stimulation electrode in one simulation or in one block (for experiments in living cultures).

APPENDIX C

EXPERIMENTAL SETUPS FOR LIVING MEA CULTURES

This appendix describes the detailed protocols for experiments with living MEA cultures, mentioned throughout Chapters 2 to 6, which include cell culture techniques and setups of recording and stimulation systems.

C.1 Cell culture techniques

C.1.1 Cell dissociation

E18 rat cortices from time-pregnant Sasco Sprague-Dawley rate (Charles River) were dissected and preserved in Hibernate E (Brainbits) at 4ºC. Cortices were put in 2.5U/ml papain (Roche 108014) in Segal's medium (Banker and Goslin, 1998a) for 20 minutes in a 37ºC water bath. Cells then were dissociated by triturating 2-3 passes through a 1mL pipette tip, and stored in Neurobasal medium (Invitrogen) with B27 (Invitrogen), 0.5 mM Glutamax (Invitrogen), and 10% horse serum (Hyclone). To remove debris, dissociated cells were passed through a 40μm cell strainer (Falcon) and centrifuged at 150 xg onto 5% bovine serum albumin (BSA) in phosphate buffered saline (PBS). The pellet of cells was re-suspended in Neurobasal medium.

C.1.2 MEA coating and cell plating

MEAs were pre-coated with poly-ethylene-imine (PEI, Sigma 94832) and a 20μL drop of laminin (Invitrogen L2020). The drop of laminin was placed on the center of the MEA to cover the electrode grid of the size of 1.4 mm by 1.4 mm. 50,000 cells (~7000 cells/mm^2) were dropped on pre-coated MEAs. After 30 minutes of incubation, 1mL of Neurobasal medium was added into MEAs, and was replaced by feeding medium adapted from Jimbo et al. (Jimbo et al., 1998c) after 24 hours. Adapted Jimbo's medium

contained Dulbecco's modified Eagle's medium (DMEM, Irvine Scientific), 10% horse serum, 0.5mM glutamax, and 1% sodium pyruvate (Sigma).

C.1.3 Culture maintenance

Cultures were maintained in MEAs sealed with gas-permeable teflon membrane (Potter and DeMarse, 2001) inside an environmentally controlled incubator (at 35 ºC, 65% RH, 5% CO_2, and 9% O_2). The culture medium was exchanged with fresh feeding medium once a week.

C.2 MEA recording and stimulation

C.2.1 Electrical recording

Data acquired through MCCard (Multichannel Systems) was recorded and visualized by using our publicly available acquisition and analysis software, Meabench (Potter et al., 2006). The spike detection was performed in real-time by identifying signals that cross a threshold of 5X RMS noise. Real-time artifact suppression tools (SALPA) allowed the detection of spikes as soon as 2 msec after an electrical stimulus (Wagenaar and Potter, 2002).

C.2.2 Electrical stimulation

We delivered biphasic stimuli (monopolar) at 500 mV and 400 us per phase by using our custom-made 60-channel stimulation board (RACS) (Wagenaar et al., 2004; Wagenaar and Potter, 2004). The stimulator was controlled using real-time Linux with stimulation sequences coded by C++ or MATLAB.

APPENDIX D

NETWORK PLASTICITY IN SPONTANEOUS BURSTS[xxii]

Besides the plasticity found in stimulus-evoked responses described in Chapter 3, network plasticity in spontaneous bursts was also discovered in living cortical cultures. Three different statistics were used to quantify the dynamics of spontaneous bursts: center of activity trajectory (CAT), burst activity matrix (BAM), and burst initiation probability (BIP). The ability of these statistics to capture the underlying changes in network synaptic connectivity was further verified in the simulated network.

D.1 Experiment protocols

Details of the experiment protocols are described elsewhere (Madhavan et al., 2007b). Briefly, we used tetanic stimulation to induce functional changes in spontaneously bursting dissociated cultures. Spontaneous activity was recorded for 3 hours (*Pre* period). Tetanization consisted of a train of stimuli at 20 Hz, was applied simultaneously on two electrodes lasting for 15 minutes, followed by another recording of spontaneous activity for 3 hours (*Post* period). The tetanization was unusually long, compared to other studies (see Table 1.1), in order to increase the likelihood of inducing plasticity.

[xxii] Partial results from: Radhika Madhavan, Zenas C. Chao, and Steve M. Potter (2007): *Plasticity of recurring spatiotemporal activity patterns in dissociated cortical networks*. Physical Biology, **4**, 181-193.

D.2 Spatiotemporal structure of spontaneous bursts

D.2.1 Center of activity trajectory (CAT)

CAT quantifies the dynamics of the spatial asymmetry of the activity distribution (described in Chapter 3). Measured from stimulus-evoked responses, CAT was capable of detecting more pronounced network functional plasticity following tetanus than the alternate statistics in both simulated and living networks (see Chapter 3). Additionally, tetanus-induced changes in CAT of spontaneous bursts were found in the simulated network (Figure 4.1). Similar to the results found in the simulated network, different types of spontaneous bursts were observed in living MEA cultures, each with a specific CAT pattern. Occurrences of different types of bursts were stable without any external stimulation (in *Pre* period), changed after the tetanus, and stabilized at a different set of bursts (in *Post* period) after a transition period (Figure D.1). These dynamics were consistent with the results found in the simulated networks (Figure D.1, and also see Chapter 4).

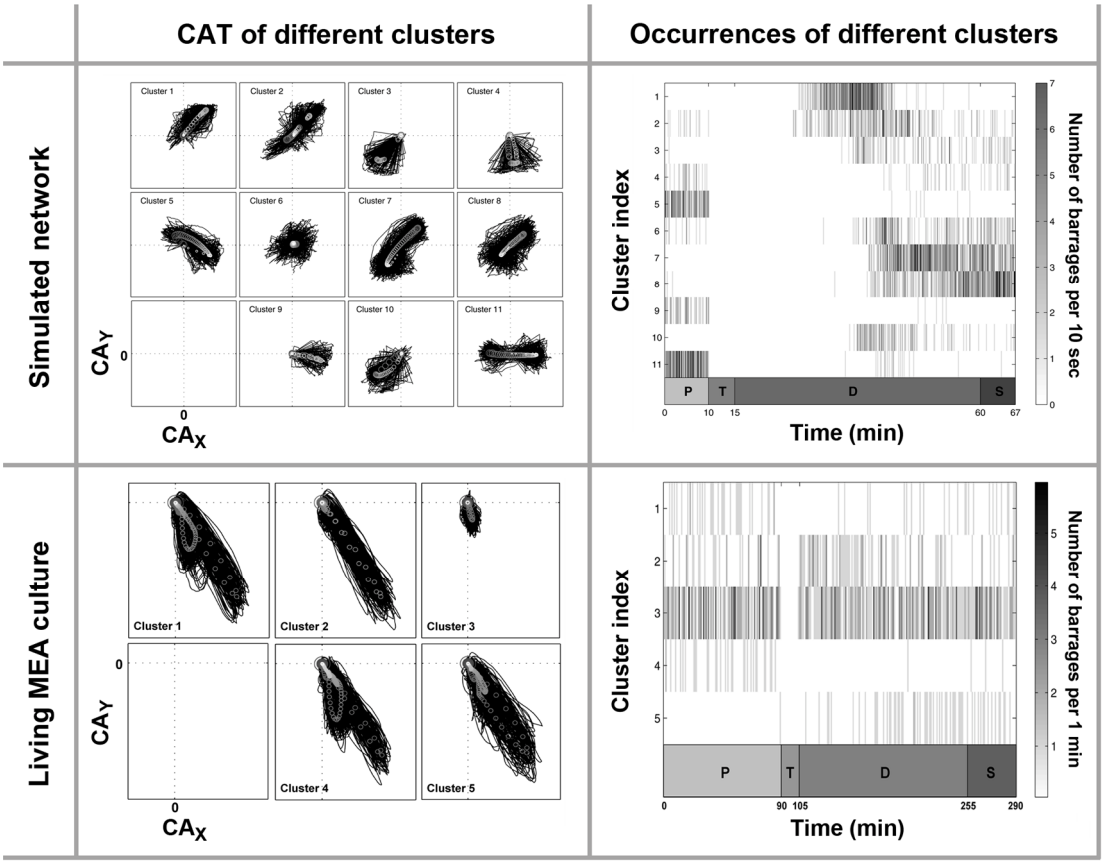

Figure D.1. Comparisons of tetanus-induced changes in CAT of spontaneous bursts in simulated and living networks: Different kinds of spontaneous bursts occurred in different periods in both simulated (**Top**) and living networks (**Bottom**). The same representation is used as in Figure 4.1.

D.2.2 Burst activity matrix (BAM)

The detailed calculation of BAM is described elsewhere (Madhavan et al., 2007b). Briefly, BAM for each burst was constructed by appending 60 firing rate histograms (FRH, see Appendix B), calculated from the 60 recording electrodes, together to form a 1 by 60*N* vector, where *N* is the number of time bins in FRH. Unlike CAT, a population statistic that significantly reduces the dimensionality of the spatiotemporal structure of a burst, BAM preserves the detailed firing patterns recorded at each electrode during a burst.

Similar to the clustering result from CAT (Figure D.1), BAMs of bursts were clustered based on the similarity measure described by Beggs and Plenz (Beggs and Plenz, 2004; Madhavan et al., 2007b), where different types of bursts (called "avalanches") were discovered. Furthermore, occurrences of bursts with different BAM structures were stable for hours without external stimuli (in *Pre* period), and changed after the tetanus (Figure D.2), which is consistent with the results shown by using CAT (Figure D.1).

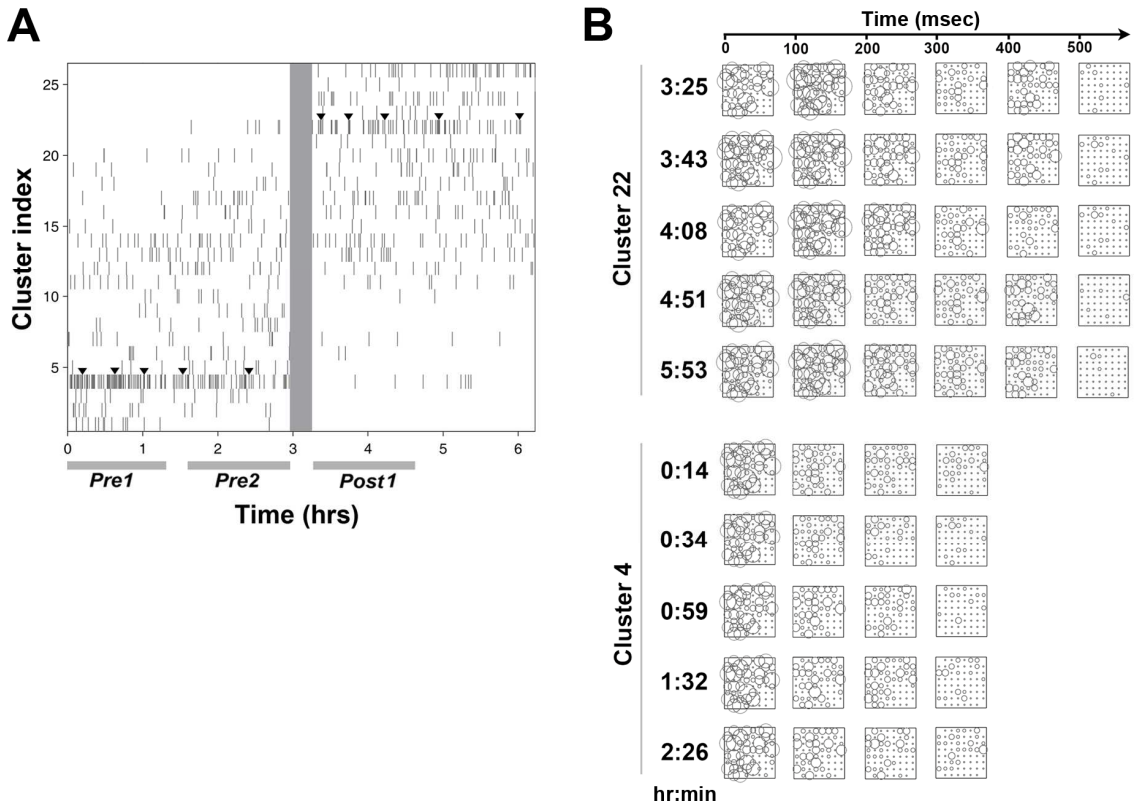

Figure D.2. Tetanus-induced changes in occurrences of spontaneous bursts with different BAM structures: A. The type of spontaneous bursts changed after the tetanus. Each stroke represents the occurrence of a spontaneous burst with a specific BAM structure (the belonging cluster is indicated on y-axis). The grey bar indicates period of tetanization. The arrowheads indicate the timing of the different BAM clusters (clusters 22 and 4) shown in B. **B.** The BAMs of bursts in two different clusters. Each frame of BAM was shown in the original coordinates of an MEA. BAMs shared similar structure within a cluster, and were different across clusters. The sizes of the circles represent the number of spikes in that particular electrode for a particular time bin.

D.3 Initiation sites of spontaneous bursts

D.3.1 Burst initiation probability (BIP)

Bursts originate from various sites in the network, termed 'burst initiation sites', and then propagate to the entire network (Maeda et al., 1998b; Eytan and Marom, 2006). In addition to CAT and BAM, burst initiation properties were also used as a measure to quantify the tetanus-induced change. The burst initiation site is defined as the electrode that records the first spike at the burst onset, and the burst initiation probability (BIP) is defined as the spatial probability distribution of burst initiation sites over the 60 recording electrodes (Madhavan et al., 2007b). BIP was found stable before the tetanus (in *Pre* period), and changed across the tetanus (Figure D.3).This indicates that the tetanus induced changes in network functional connectivity, which was also demonstrated in the simulated network (see Section D.3.2).

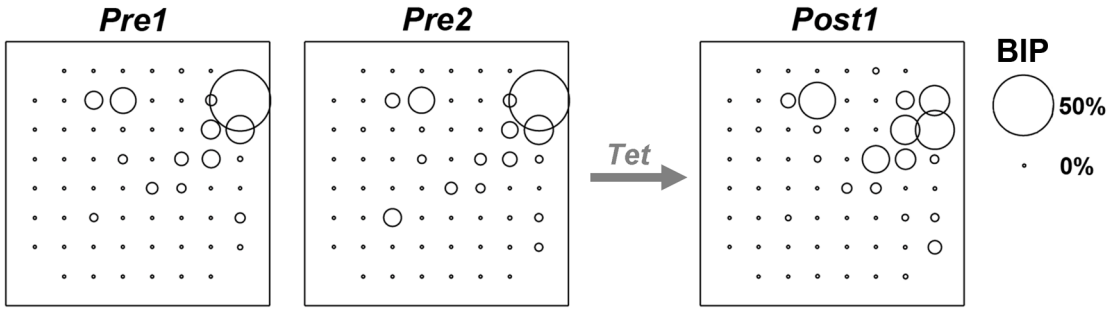

Figure D.3. Tetanus-induced changes in the spatial distribution of BIP: The probability of neurons around an electrode initiating a burst is shown by the different sizes of the circles (right). The spatial distribution (shown in the original coordinates of an MEA) of BIP did not change much before the tetanus (*Pre1* and *Pre2* periods, indicated in the bottom of Figure D.2A), and changed significantly across the tetanus (from *Pre2* to *Post1*).

D.3.2 BIP and underlying synaptic connectivity

Eytan et al. (2006) identified early-to-fire neurons during the onsets of the burst and these initiation areas were found to be characterized by high neuronal density and recurrent excitatory and inhibitory connections (Feinerman et al., 2007). This correlation

was verified in the simulated network (Figure D.4). In simulation, the neurons that initiated bursts were identified in different 10-min periods, and BIP was calculated for each period. The burst rate decreased immediately after the tetanus, and gradually returned to the level before the tetanus after 10 minutes, but with a different spatial distribution of burst-initiating neurons. The corresponding underlying network synaptic connectivity during these periods was measured (Figure D.3). The network synaptic weights were "frozen" from a randomly-selected time frame from each 10-min period used to calculate BIP. On each frozen network synaptic state, a single spike was delivered at each neuron (a probe), one at a time, and the number of other neurons evoked by the spike input was measured to quantify the outward connectivity of that neuron. Intuitively, this quantity measures how extensively each neuron connects to others functionally at that synaptic state. Furthermore, the Gaussian noise for the fluctuation of membrane potentials for all neurons (see Chapter 2) was turned off to avoid any bias from self-firing neurons.

The network connectivity was highly correlated to the burst initiation sites (Figure D.3), which suggests that BIP could be a direct indicator of network synaptic connectivity. The number of outward synaptic connections for each presynaptic neuron was also measured (Figure D.4), and the correlation between the spatial distribution of the synaptic connection and BIP (or functional connectivity) was absent. This suggests that the tetanus-induced changes in BIP or network connectivity were more related to network synaptic strengths (functional connectivity) than to the morphology of network synaptic connections (morphological connectivity).

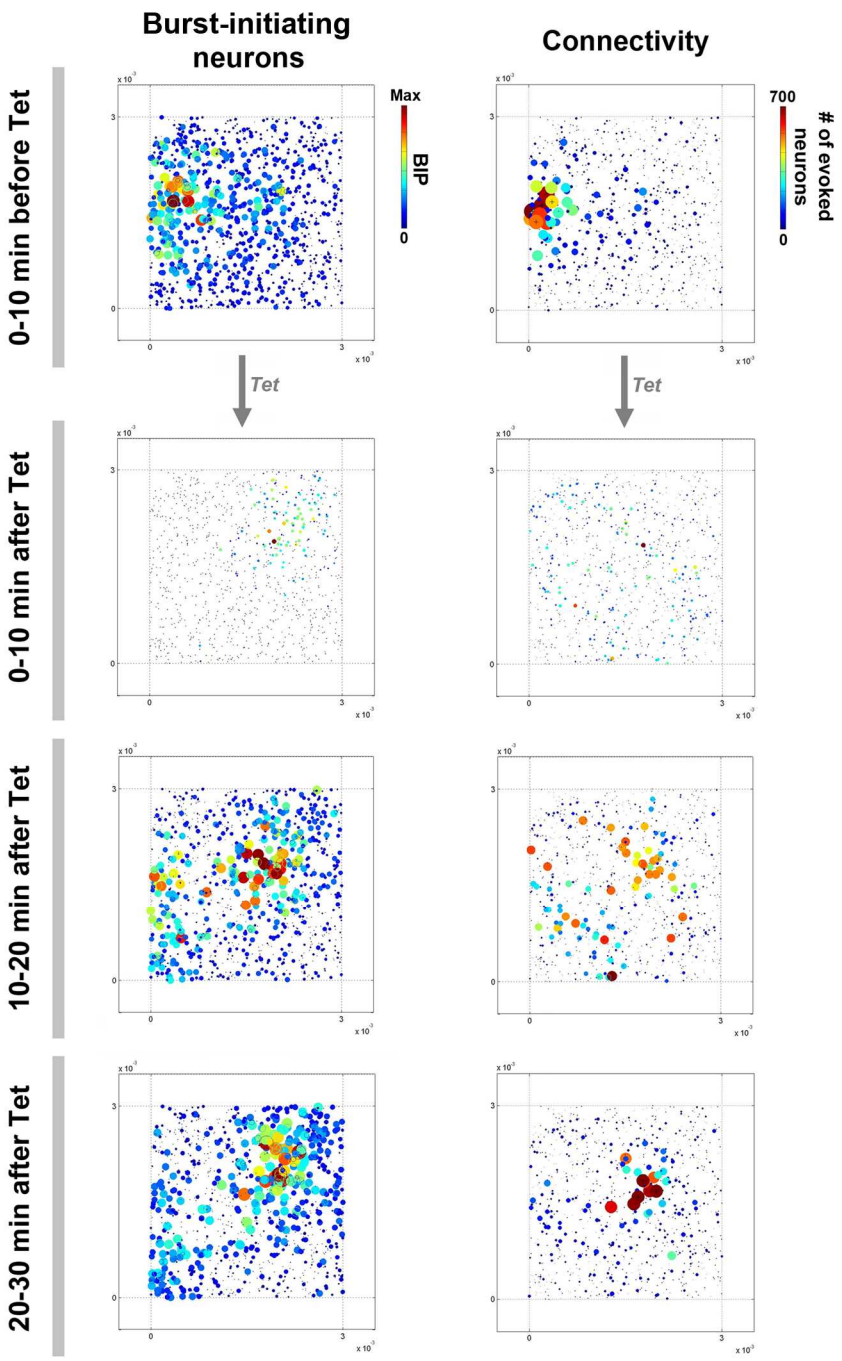

Figure D.4. The distribution of burst-initiating neurons revealed the underlying network connectivity: The spatial distribution of BIP was measured over time across a tetanus in the simulated network (**Left)**, and its dynamics were highly-correlated with the network connectivity, which measures how extensively each neuron connects to others (**Right**).

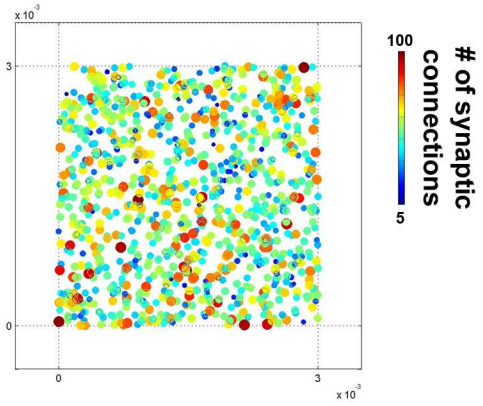

Figure D.5. Insignificant correlation between tetanus-induced changes in BIP and the topology of network synaptic connections: The number of synaptic connections, morphological connections with no concern to their weights, from each neuron was measured. The neurons that had more synaptic connections to other neurons were not necessary the neurons initiating bursts (compare to Figure D.4).

D.4 Burst-induced plasticity

Spontaneous bursts can be used as an indicator of network plasticity. They also can *induce* network plasticity. Changes in connectivity across a burst were measured by delivering stimuli at each neuron (with frozen synaptic states) immediately before and after the burst (see detailed methods described in Section D.3.2). Examples of connectivity before and after a randomly-selected burst are shown in Figure D.6. The connectivity of the network immediately before the randomly-selected burst was different from the connectivity immediately after the burst, where formation and deletion of strong synapses (weight> 0.075) were observed.

Burst-induced plasticity maintained network synaptic weights while in equilibrium (see Chapters 4). The spatiotemporal structure of spontaneous bursts played an important role in this stabilizing effect on the network synaptic weights distribution during the steady state (Figure D.7). In order to evaluate this in a simulated network, the spiking pattern recorded from a series of spontaneous bursts during a 10-min period was shuffled and replayed into the same initial network. Two shuffling methods were used: (1) "Burst order shuffling" preserved the spatiotemporal structure of each spontaneous burst,

but shuffled their occurring order (the structure of a longer time scale). (2) “Spike swapping” repeatedly exchanged the neuron indices of randomly-selected pair of spikes, which retained the same spike times and the same distribution of total number of spikes at each neuron, but removed the original correlations between spike times (Rolston et al., 2007). No significant difference between the synaptic weights distributions measured from the original burst sequence and after burst order shuffling (Figure D.7). This suggests that the order of different spontaneous bursts played no significant role in the stabilizing effect on network synaptic state. However, the stabilizing effect was absent after spike swapping, where the center of weights (CW) drifted away from the initial state. This indicates the significant contribution of the spatiotemporal structure of different spontaneous bursts to the stabilizing effect on network synaptic state.

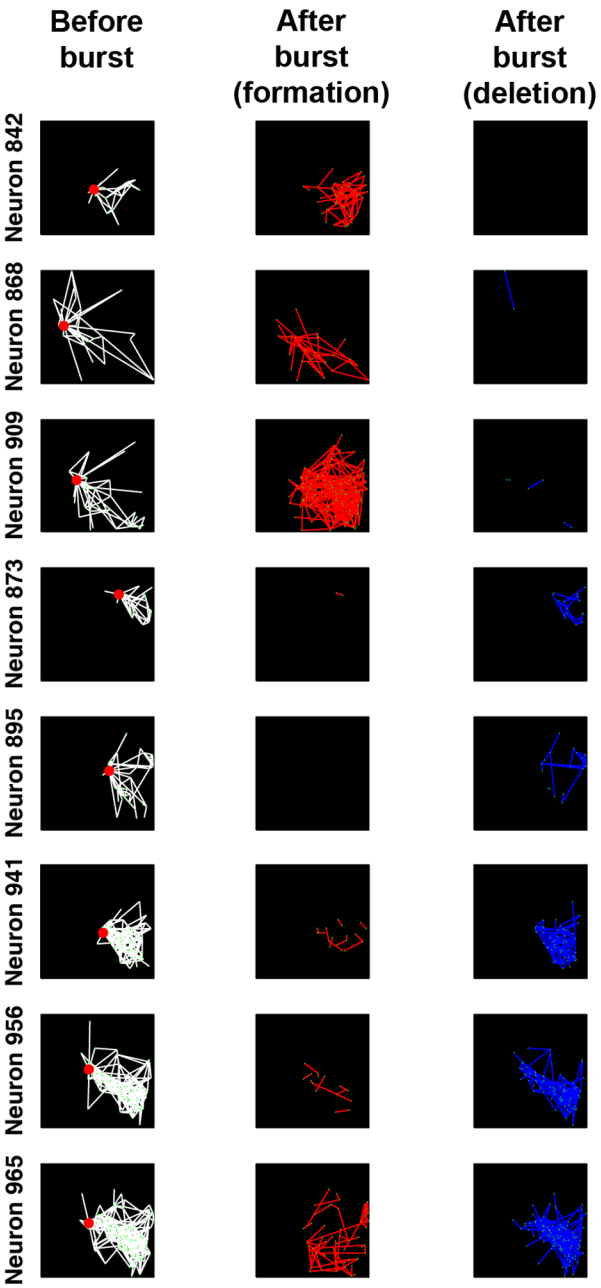

Figure D.6. Spontaneous bursts induced formation and deletion of different synapses: Changes in the network connectivity across a spontaneous burst demonstrated burst-induced plasticity in a simulated network. **Left.** The connectivity of 8 randomly-selected neurons immediately before the burst. Red circles represent the neuron that received the test stimulus (see detailed methods in Section D.2.2), white lines indicate the activated synaptic connections, and small green dots indicate the neurons in which APs were evoked. **Middle.** The new strong synaptic connections (weight> 0.075) formed immediately after the burst. **Right.** The strong synaptic connections deleted immediately after the burst.

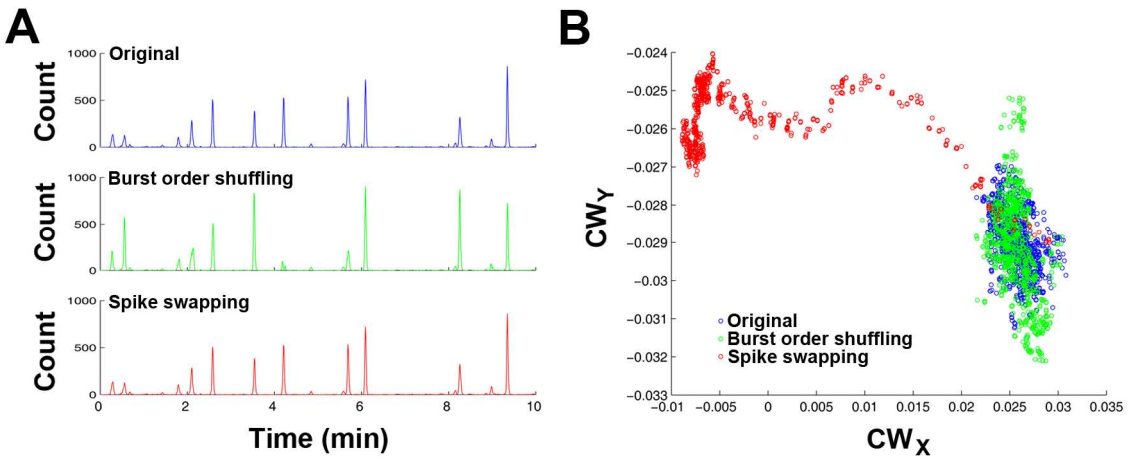

Figure D.7. The spatiotemporal structure of spontaneous bursts plays crucial role in the stabilizing effects on network synaptic weights: A. Firing rate histograms of a 10-min period for the original recording, after burst order shuffling, and after spike swapping. Each peak represents a spontaneous burst. Burst order shuffling retained the structure of each burst, while changed the order of bursts. Spike swapping altered the spatiotemporal structure of each burst, while maintaining the same network-wide firing rate (the histogram after spike swapping was identical to the original histogram). **B.** The center of weights (CW) measured from the three simulations. Burst order shuffling induced similar network plasticity as in the original recording, where both stabilized the network synaptic weights. However, CW drifted away after spike swapping, which suggests the significant role of the spatiotemporal structure of bursts in the stabilizing effect on network synaptic weights.

APPENDIX E

NETWORK PLASTICITY IN THE TIMING OF DIRECT ELECTRICALLY-EVOKED ACTION POTENTIALS (DAPS)[xxiii]

E.1 Introduction

The precise temporal control of neuronal action potentials is essential for regulating many brain functions. From the viewpoint of a neuron, the specific timings of afferent synaptic inputs determines whether or not and when to fire an action potential. Plasticity of the timing of direct electrically-evoked action potentials (dAPs) was found in MEA cultures, where changes in latency of evoked action potentials adapted to different repetitive patterned stimuli (up to 4 msec or 40% after minutes of stimulation, and 13 msec or 74% after hours of stimulation). The changes did not occur when the same stimulation was repeated while blocking synaptic activity, which indicates that plasticity of the timing of dAPs depended on the occurrence of synaptic activity.

Several cellular mechanisms may cause changes in the latency of dAPs, such as fluctuations in membrane potentials (Lipski, 1981) and neural intrinsic excitability (Daoudal and Debanne, 2003; Zhang and Linden, 2003; Xu et al., 2005), which affects the delay that a stimulus evokes an action potential at the cell body. A detailed investigation on these mechanisms in a simulated network is shown in Section E.3. However, the activity-dependent plasticity in the timing of dAPs we found lasted for a much longer term (Bakkum et al., 2007), and thus was unlikely due to these short-term mechanisms. We hypothesized a new form of plasticity might be involved, plasticity in

---

[xxiii] Under review as: Douglas J. Bakkum, Zenas C. Chao,and Steve M. Potter (2007): *Long-term activity-dependent plasticity of action potential propagation in cortical networks*. PLoS One.

axonal propagation, which affects the duration that a signal propagates from the evoked neuron to the recording site. Elucidating the cellular mechanisms of this different form of plasticity is left to future work, but possibilities include non-uniform changes in ion channel properties (Ganguly et al., 2000), in the geometry of varicosities and branch points (Goldstein and Rall, 1974) or axonal arbors, in the proximity of glia (Ishibashi et al., 2006b), and in lipid membrane composition (Bedlack et al., 1994).

E.2 dAP in living networks

Stimulation by one electrode evokes neural responses that can be recorded in a subset of the rest of the electrodes. Of these, dAPs have been observed up to 25 msec later and can be distinguished from subsequent synaptically-evoked action potentials (sAPs) based on their high reliability of occurrence (> 80%), low jitter (160 μs), and consistency of waveform (Lipski, 1981; Marom and Shahaf, 2002; Wagenaar et al., 2004) (Figure E.1). dAPs are presynaptic as they persist when synaptic activity is blocked using fast neurotransmitter receptor antagonists (Wagenaar et al., 2004). We quantified changes in the timing of dAPs by measuring their latencies after a stimulus (Figure E.1C).

By varying a simple low frequency stimulation pattern every 40 minutes, we induced changes in the timing of dAPs. Each stimulation pattern consisted of alternatively stimulating two electrodes at 2-sec intervals (Figure E.2A). The second electrode, termed probe, was fixed and used throughout, while the location of a preceding context electrode was moved spatially every 40 minutes to make each new pattern. Interestingly, we found dAPs evoked by the probe stimuli changed via gradual shifts and jumps in latency (up to 4 msec or 40%), but not when the stimulation was repeated in the presence of antagonists of NMDA-R, AMPA-R, and GABA-R (Figure E.2B). This suggests that plasticity of the timing of dAPs depended on the occurrence of synaptic activity.

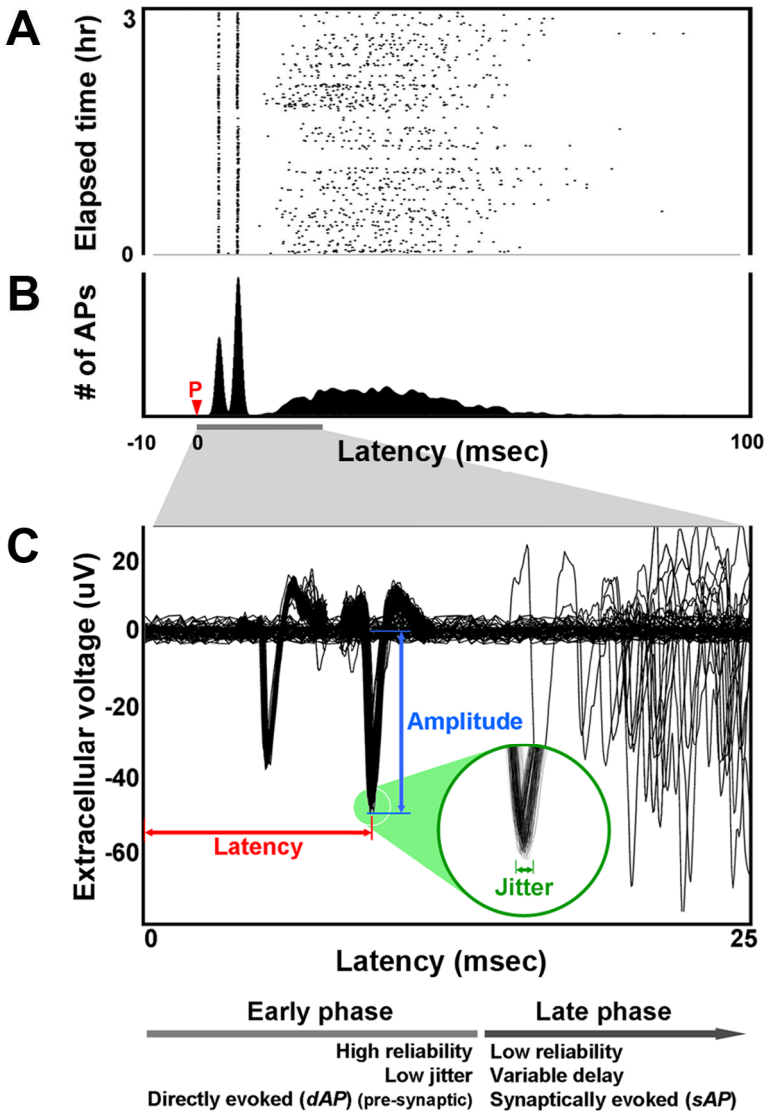

Figure E.1. Directly-evoked action potentials (dAPs) and synaptically-evoked action potentials (sAPs): Neural activity recorded on one electrode in response to stimulation at another consists of an early dAP-phase and a later sAP-phase. **A.** The raster plot (1 dot per action potential) shows the first 100 msec of neural responses to 3 hours of periodic 1/4 Hz probe stimulation (P). The firing rate histogram (**B**) and overlaid extracellular voltage traces across all trials (**C**) emphasize the consistency of the early phase with respect to the later phase. The sharp peaks in the histogram arise from the trains of two dAPs. A dAP is characterized by its low jitter, high reliability, and consistency of waveform.

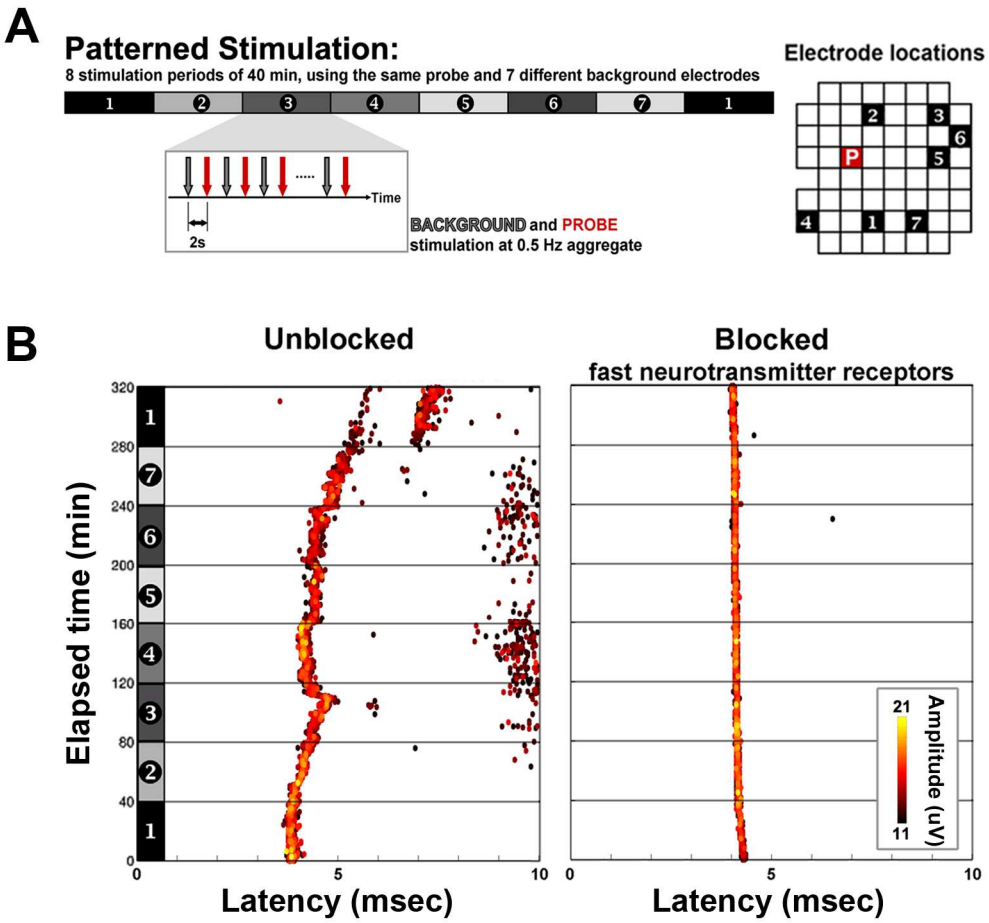

Figure E.2. The timing of dAPs depended on ongoing neural activity and stimulation pattern: A. Experiment protocol. 1/4 Hz probe stimuli (red) produced dAPs whose latencies were investigated for plasticity. A context electrode (gray) was stimulated 2 seconds prior to each probe stimulus, and its location was shifted every 40 minutes to produce different patterns of stimulation (numbers and shaded bars). Right: electrode locations for data in B. **B.** Example raster plots of a given dAP recorded on one electrode in response to probe stimulation of another electrode in culture media (left, Unblocked) and when blocking synaptic activity (right, Blocked). Ongoing neural activity modified latency (x-axis) and amplitude (color).

E.3 dAP in simulated networks

Here I used the simulated network to investigate how synaptic activity affects plasticity of the timing of dAPs found in living cortical cultures.

E.3.1 STDP and membrane potential fluctuations

By delivering a similar patterned stimulation used in living networks (Figure E.2A), similar changes in the timing of dAPs were observed in the simulated network

(compare left panels in Figures E.3A and E.2B). These changes in a single neuron is shown in Figure E.3B. However, these changes were absent when the STDP property in excitatory synapses was removed (Figure E.3C), or synaptic connections were removed, which is analogous to adding synaptic blockers (Figure E.3D). This supports the conclusion found in living networks, where synaptic activity was required for plasticity in the timing of dAPs.

In order to eliminate the possibility that changes in the timing of dAPs were due to the variation of neurons' membrane potentials, which directly affect their excitability, the Gaussian noise introduced to mimic fluctuations in membrane potentials were removed. Without random noise, but with STDP, gradual changes in the timing of dAPs across trials remained (right panel in Figure E.3A).

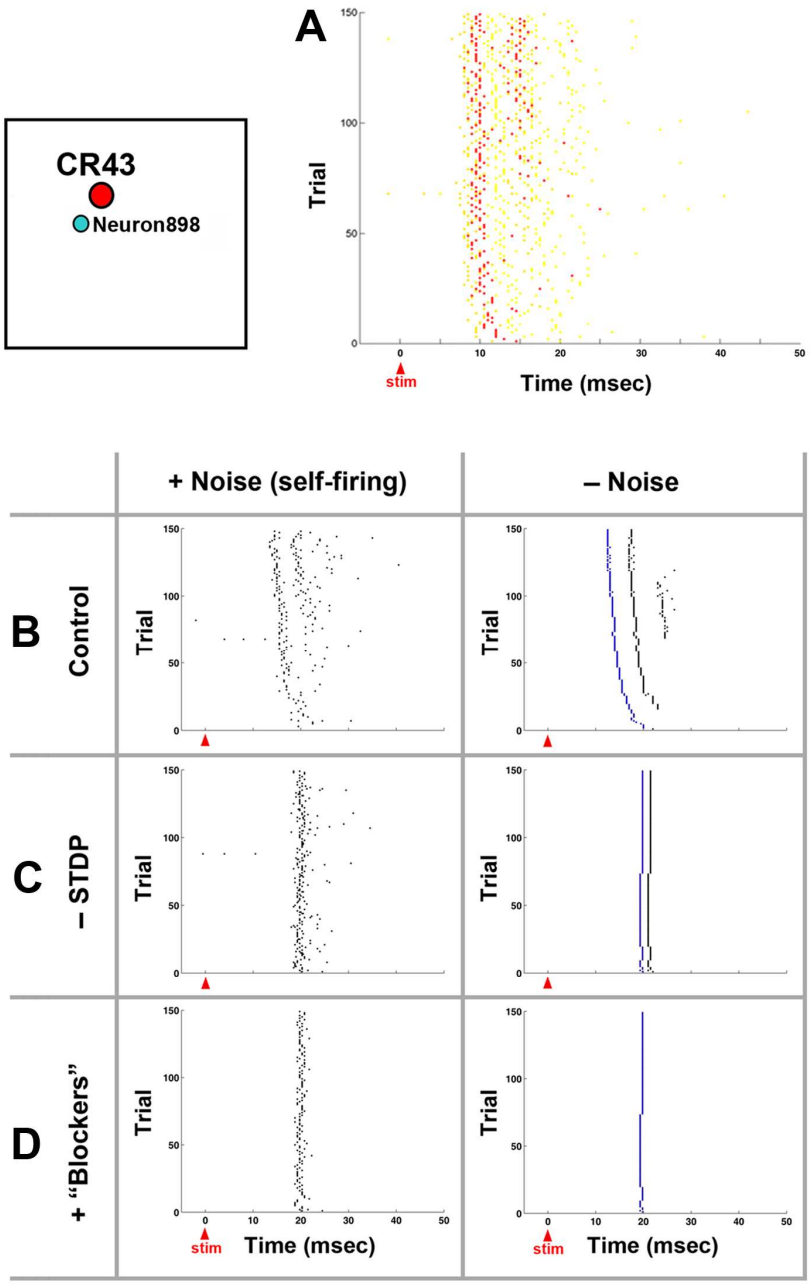

Figure E.3. Significant role of STDP in activity-dependent plasticity of the timing of dAPs in a simulated network: Activity-dependent plasticity of the timing of dAPs was associated with STDP but not with the fluctuation of neurons' membrane potentials. **A.** Plasticity in the timing of dAPs was observed in the simulated network. The raster plot of probe responses recorded at electrode CR43 are shown. Two different colors (red and yellow) represent responses at two neurons near the electrode. **B.** Stimulation-induced changes in dAP timing were observed in the simulated network only with STDP synapses. The raster plot of probe responses recorded at neuron 898 were shown. **C.** Plasticity of dAP timing was absent when removing the STDP property in excitatory synapses (frequency-dependent property, see Section 2.2.2.2.2, remained). **D.** Plasticity of dAP timing was absent when removing all synaptic connections, which is analogous to adding synaptic blockers. Without the Gaussian noise on neurons' membrane potentials (see the right panels in B, C, and D), only the stimulus-evoked activity remained in the network. dAPs, the responses that remained after adding "blockers" (right column), were indicted in blue.

E.3.2 Synaptic-strength dependent plasticity of the timing of dAPs

In simulation, synaptic plasticity was an essential element for activity-dependent plasticity of the timing of dAPs (Figure E.3). In order to understand how a synaptic input affects the timing of a direct non-synaptic response, I used a simple network consisting of two leaky integrate-and-fire (LIF) neurons connected by one non-STDP synapse (Figure E.4A). A neuron (*N1*) was connected to a target neuron (*N2*) through a synapse (*Syn12*), where its synaptic weight was controlled by the experimenter. Spike inputs *S1* and *S2* were delivered at *N1* and *N2*, respectively, with various inter-pulse intervals (IPIs). *S2* represents the direct stimulus on *N2*.

With IPI= 10 msec, the relation between the synaptic weight of *Syn12* and timings of responses in *N2* is shown in Figure 4B. The latency of non-synaptic responses to *S2* decreased when the weight of *Syn12* increased. This demonstrated the influence of synaptic inputs, or synaptic plasticity in the network, on the timing of dAPs. The postsynaptic current (PSC) of *Syn12* on *N2* was higher with a greater synaptic weight (Figure E.4C), which affected the membrane potential of *N2* and thus its timing of firing. Relations between the synaptic weight and the timing of responses with different IPIs are shown in Figures E.4D and E.4E. The latency of dAP depended not only on the synaptic weight but also the relative timing between the external stimulus (through *S2*) and the synaptic input (through *S1*).

With one synaptic input, the change in dAP latency varied up to 5 msec (see Figure E.4D). Furthermore, the timing of the synaptic input regulated not only the timing of dAP but also its dependency on the weight of the synaptic connection (Figure E.4D). With multiple synaptic inputs per neuron, as in living cortical cultures, the maximal change in dAP latency was even more (data not shown). In addition, a rich dynamics of changes in the timing of dAPs under different combinations of synaptic weights and timings of synaptic inputs was found.

These simulation experiments indicate that synaptic plasticity could affect plasticity in the timing of non-synaptic responses. The possible mechanism is that different dynamics of synaptic inputs (measured as postsynaptic currents, PSC) induce different levels of membrane potentials, and directly change the excitability of neurons.

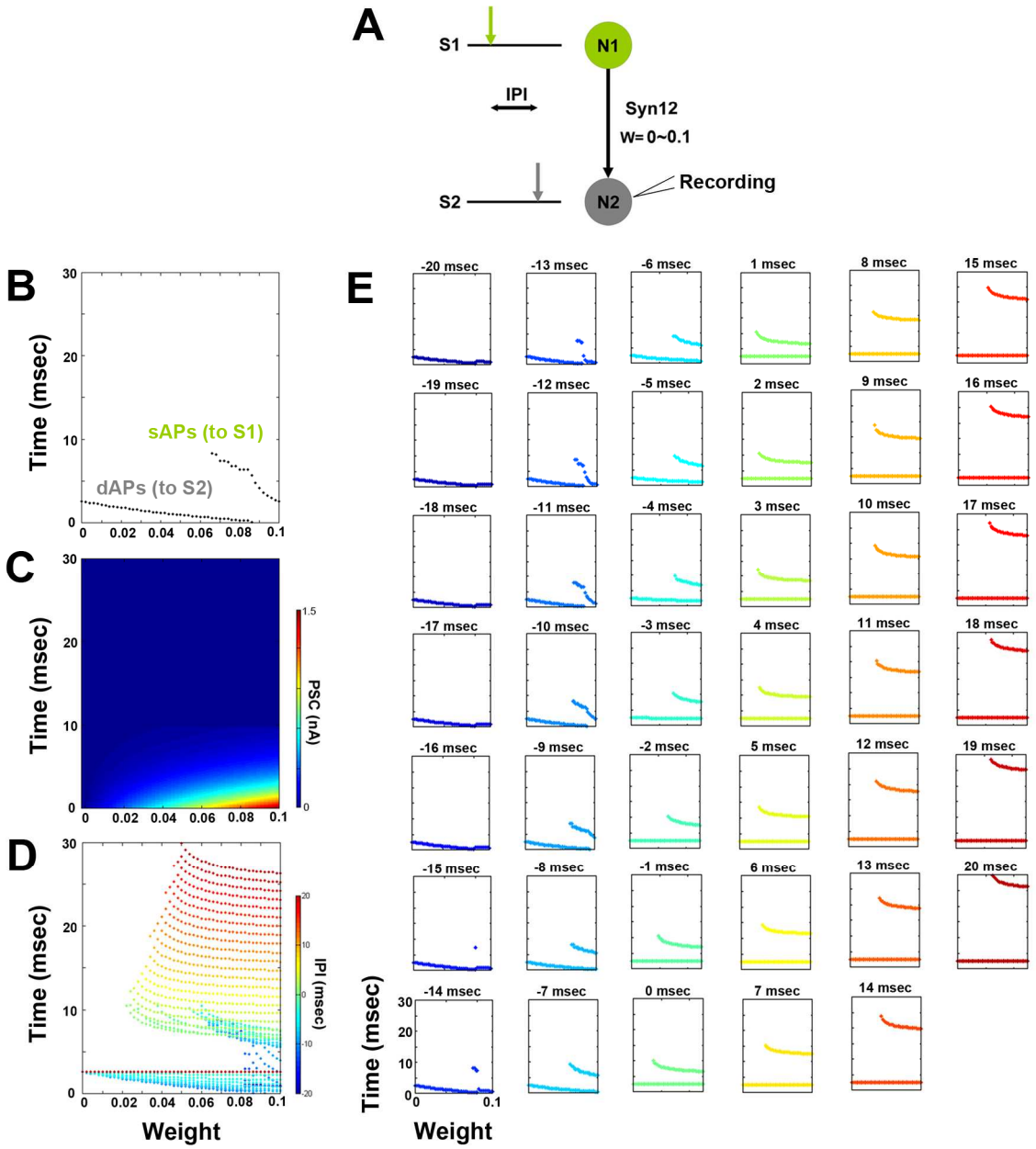

Figure E.4. Plasticity of the timing of dAPs depended on the timing of synaptic inputs: The latency of dAP depended not only on the weight of the synaptic input but also the relative timing between the external stimulus and the synaptic input. **A.** The structure of the simple network. **B.** The relation between the synaptic weight of *Syn12* and timings of responses in *N2* with IPI= -10 msec. dAPs (responses to S2) and sAPs (responses to S1) are indicated. **C.** The corresponding postsynaptic current (PSC) of *Syn12* on *N2*. **D.** The relation between synaptic weights and timings of responses with different IPIs. **E.** The separated plots of different IPIs shown in D. The same color representation is used.

APPENDIX F

STABILIZING TETANUS-INDUCED PLASTICITY BY REDUCING OCCURRENCES OF SPONTANEOUS BURSTS IN LIVING NETWORKS[xxiv]

Random background stimulation (RBS) of aggregated frequency of 1 Hz helped maintain the stability of network synaptic weights after tetanization in simulated networks (Chapter 4). A higher aggregated frequency (~ 3 Hz) was found to have the same effect (Chapter 5). We hypothesized that the network synaptic weights drifted after a tetanization because of the ongoing spontaneous activity, consisting of mostly spontaneous network bursts. In both simulated networks and living cultured networks, spontaneous bursts were reduced at least 10 times by RBS (Figure 4.4), and so was the drift.

In another study, we found that tetanus-induced plasticity, measured in center of activity trajectories (CATs), was stabilized and maintained in living MEA cultures by reducing the occurrence of spontaneous bursts (Madhavan et al., 2007c) (Figure F.1). A burst-control stimulation protocol consisting of a group of electrodes cyclically stimulated with an aggregated frequency of 50 Hz was found to completely eliminate spontaneous bursts (Wagenaar et al., 2005). Although different mechanisms might be involved in RBS and the burst-control stimulation (see Section 5.4.3), these results from living networks support the hypothesis that spontaneous bursts are involved in the drift of network synaptic strengths after stimulus-induced changes.

[xxiv] To be submitted as: Radhika Madhavan, Zenas C. Chao, and Steve M. Potter (2007): *Electrical control of population bursting aids functional plasticity in cortical networks*.

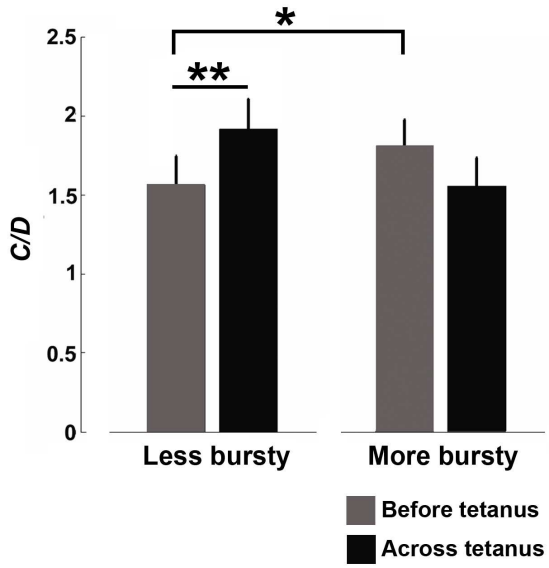

Figure F.1. Tetanus-induced changes maintained by reducing the occurrence of spontaneous bursts in living networks: The change-over-drift ratio (or C/D, which quantifies the dynamics of CAT of network responses, see definition in Section 3.2.2.3) before tetanus in less-bursty experiments (n= 8 experiments) was significantly lower than that in more-bursty experiments (n= 6 experiments) (*, p-value< 0.05). This indicates that the drift in network responses was reduced by "quieting" spontaneous bursts. Furthermore, C/D across tetanization was significantly higher than C/D before tetanization in less-bursty experiment (**, p-value< 0.05), whereas this significance was absent in more-bursty experiments. This indicates that tetanus-induced plasticity was stabilized by reducing the occurrence of spontaneous bursts. This stabilizing effect was maintained at least for 2 hours after the tetanization (Madhavan et al., 2007c).

APPENDIX G

CONTEXT-CONTROL PROBING SEQUENCE (CPS) MINIMIZES THE VARIABILITY IN PROBE RESPONSES

The evoked responses to the last stimulus (probe) in context-control probing sequences (CPSs) were used to generate motor commands for the animat (in Chapters 5 and 6). We found that by controlling the stimulation context (the stimuli before the probe) with inter-pulse interval (IPI) between 200 to 400 msec, the variability in the probe responses could be minimized in both simulated networks and living MEA cultures (Figure G.1).

In 5 stimulated networks and a living MEA culture, we delivered pairs of stimuli at two randomly selected electrodes. The stimuli at the first electrode (context) served as the context of the stimuli at the second electrode (probe). IPIs (time intervals from the context stimuli to the corresponding probe stimuli) were randomized between 100 msec and 2 seconds, and the time intervals between the probe stimuli and the next context stimuli were fixed at 2 seconds. By binning the IPIs with 100 msec moving window and 10 msec step, we grouped the IPIs into 181 groups. The variability of CAs of the probe responses, whose corresponding IPIs belonged to the same group, was calculated. The variability was defined as:

$$Variability = \sqrt{\mathrm{var}(CA_X) + \mathrm{var}(CA_Y)} \qquad \text{[Equation G.1]}$$

For each experiment, the variability calculated from different IPI bins was normalized by removing the mean then dividing by the standard deviation. The mean ± SEM of the normalized variability from 20 experiments in 5 simulated networks (4 different stimulation pairs in each network) is shown in the left panel. The mean ± SEM

of the normalized variability from 4 experiments in a living MEA culture (4 different stimulation pairs) is shown in the right panel. The relation between normalized variability and IPI was fitted with a 6 degree polynomial (red curves) and the 90% confidence intervals (red dotted curves) were calculated. The minimum of the normalized variability was found between 200 to 400 msec in both simulated networks and the living MEA culture.

Compared to stimulating with random IPI, fixing IPI can reduce response variability. Using the same stimulation sequence, but instead of analyzing the responses per IPI, responses were analyzed for randomly-selected IPIs. The average normalized variability from 1000 different random samplings is shown as the black horizontal lines. The results indicate that by controlling IPI and the context electrode, the variability in probe responses can be reduced with a minimum between 200 and 400 msec IPIs.

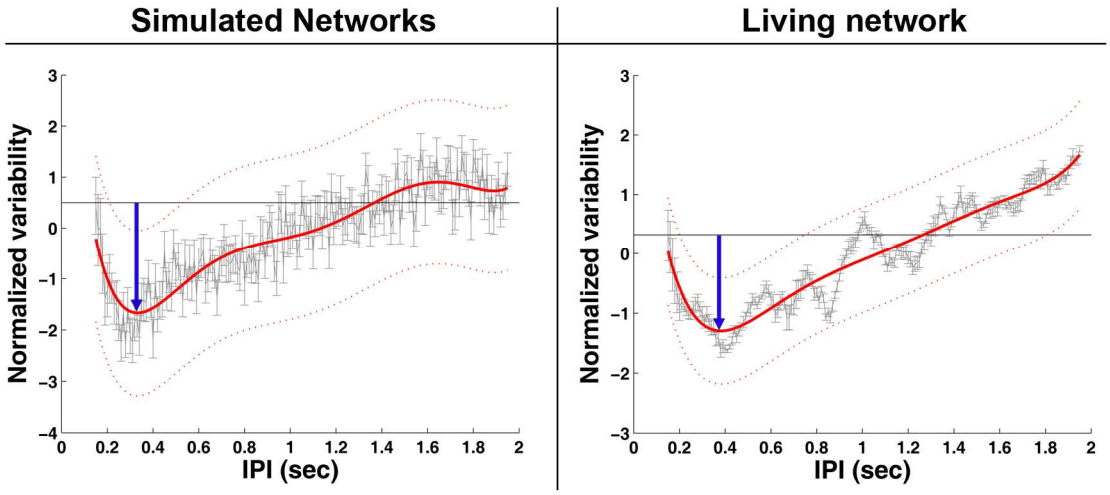

Figure G.1. Relation between variability of probe responses and IPI in simulated and living networks: The minimal variability in CAT of probe responses occurred with IPIs between 200 and 500 msec in both simulated networks (**Left**) and living MEA cultures (**Right**). Blue arrows indicate expected reduction in the variability of probe responses, when using optimal IPIs, compared to using randomly-timed stimuli preceding a probe.

APPENDIX H

EFFECTS OF PATTERNED TRAINING STIMULATION (PTS) ON NETWORK SYNAPTIC WEIGHTS

The purpose of this study is to validate the design of patterned training stimulation (PTS) described in Chapters 5 and 6 by showing that network synaptic weights could be shaped differently with different stimulation parameters. This demonstrates the feasibility of using paired stimuli to "direct" network synaptic connectivity, or to train the network to exhibit desired dynamics. However, limited combinations of parameters were tested here. In order to answer the questions mentioned above, a more thorough investigation on a wider range of possible combinations of stimulation parameters and network connectivity is needed.

H.1 Introduction

Paired stimulation of monosynaptically connected neurons induces both long-term potentiation (LTP) and long-term depression (LTD) of synapses through spike-timing-dependent plasticity (STDP). Firing of a postsynaptic neuron immediately after a presynaptic neuron results in LTP of synaptic transmission, and the reverse order of firing results in LTD (Desmond and Levy, 1983; Gerstner et al., 1996; Markram et al., 1997; Bi and Poo, 1998). However, much remains unknown about how cellular plasticity scales to affect network population dynamics. Here, I investigated how different stimulation protocols affect the network-wide synaptic properties in a biologically-inspired simulated network (Chapter 2). Among possible stimulation patterns, I explored a subset of those: periodic stimulation delivered at two electrodes with different frequencies, phases, and electrode locations. Understanding effects of different stimulation patterns on network synaptic properties could help answer some important questions: (1) Whether different stimulation patterns have different effects on "shaping" the network? If so, how? (2) Whether these effects are network-specific or more universal? (3) How to determine these stimulation parameters in order to obtain the maximal or desired changes in network synaptic properties?

H.2 Methods

A simulated network consisting of 1,000 leaky integrate-and-fire (LIF) neurons that exhibits activity patterns similar to those found in cultured cortical neurons was used (described in Chapter 2). The effects of three stimulation parameters (frequency, phase, and electrode locations) for periodic paired stimulation on network synaptic weights were evaluated in several examples.

H.2.1 Stimulation frequency

Stimulation were applied at two electrodes simultaneously (phase= 0) with frequencies of 1, 2, 4, 5, 6, 8, 10, 15, 20, 25, 30, 50 or 100 Hz. Two stimulation electrodes were selected to be close to each other (electrodes CR13 and CR15, in column-row order) in this experiment; a different selection with electrodes far apart was also tried (see Section H.2.3). For each frequency, a 2-min simulation was performed with the same initial set of synaptic weights. In addition, the self-firing property was turned off by removing the Gaussian noise on neurons' membrane potentials (see Chapter 2) to prevent unpredictable drifts in network synaptic weights caused by spontaneous activity (see Chapter 4). The network was first run for 30 seconds without stimulation (*Pre* period), where all synaptic weights remained unchanged and were used as the control baseline. Then paired stimuli with a chosen frequency were delivered for 30 seconds, followed by a 60-sec period without stimulation (*Post* period).

In order to evaluate the effects of different stimulation frequencies, four quantities were calculated from network synaptic weights:

Summation of synaptic weights

In order to monitor the dynamics of overall changes in network synaptic weights during stimulation, the summation of synaptic weights of excitatory synapses, $\sum(W_{EX})$,

was measured over time. Weights of inhibitory synapses were excluded from the calculation since they were fixed at a constant (see Chapter 2).

Center of weights (CW)

In addition to overall changes in network synaptic weights, CW (see Section 4.2.2.5 and Equations 4.1 and 4.2) was also measured to evaluate changes in the asymmetry of the network synaptic weights distribution.

Percentage change of synaptic weights

The percentage change of $\sum(W_{EX})$ between *Pre* and *Post* periods was calculated, which is similar to the calculation used for describing spike-timing-dependent plasticity (STDP) between two neurons (see Equation 2.3):

$$\Delta\Sigma(W_{EX}) = \frac{\Sigma(W_{EX})_{Post} - \Sigma(W_{EX})_{Pre}}{\Sigma(W_{EX})_{Pre}} \times 100\% \qquad \text{[Equation H.1]}$$

Summation of absolute normalized changes of synaptic weights

Different than $\sum(W_{EX})$, the summation of absolute normalized changes of individual excitatory synaptic weights was measured:

$$\Sigma\left|\Delta W / W\right| = \sum_{n}\left|\frac{W_n^{t+1} - W_n^{t}}{W_n^{t}}\right| \qquad \text{[Equation H.2]}$$

where W_n^t represents the synaptic weight of synapse n at time step t, and $|\cdot|$ represents the absolute value. If each pair of stimuli evoked the same activity pattern (spikes arrived at synapses with the same timing after each stimulation pair), then $\Delta W/W$ for each synapse, and thus $\sum|\Delta W/W|$, will be a constant due to the STDP rule (see Chapter 2). The

dynamics of stimulation-induced effects on synaptic weights, such as decay or saturation, can be quantified by the time course of $\sum|\Delta W/W|$.

H.2.2 Stimulation phase

The stimuli were applied at two electrodes at 10 Hz with phase differences between –50 to 50 msec. Two electrodes (electrodes CR22 and CR72, see Figure H.3A) were used in this experiment, a different selection was also tested (see Section H.2.3 and Figure H.7A). For each stimulation phase, a 14-sec simulation was performed with the same initial set of synaptic weights and with the self-firing property turned off. The network was first run for 2 seconds without stimulation (*Pre* period). Then stimulation was applied for 10 seconds (100 pairs of stimuli), followed by another 2-sec period without stimulation (*Post* period).

Due to insignificant differences found between different stimulation phases by using $\sum(W_{EX})$-related measures (data not shown), CW and three other CW-related measures were used to evaluate effects of the stimulation phase on network synaptic weights. The CW-related measures were:

Normalized changes of CW components

The normalized changes of the X and Y components of CW were calculated to quantify the stimulation-induced changes in CW trajectories (CWTs) between *Pre* and *Post* periods:

$$\Delta CW_X / CW_X = \frac{CW_X^{Post} - CW_X^{Pre}}{CW_X^{Pre}}$$

$$\Delta CW_Y / CW_Y = \frac{CW_Y^{Post} - CW_Y^{Pre}}{CW_Y^{Pre}}$$

[Equation H.3]

where CW_X^{Post} and CW_Y^{Post} represent the X and Y components of CW in the *Post* period, respectively.

Changing distance of CW

The distance between the start point and the end point of CWT (from *Pre* to *Post*) was measured to quantify the magnitude of the change in the asymmetry of the network synaptic weights distribution across stimulation.

Changing direction of CW

The angle of the vector pointing from CW in *Pre* period to CW in *Post* period was measured to quantify how network synaptic weights redistributed spatially. For example, the angle of $\pi/4$ radius indicates that network synaptic weights shifts north after stimulation.

H.2.3 Locations of stimulation electrodes

In order to investigate how locations of stimulation electrodes affect the results found in Sections H.2.1 and H.2.2, the experiments in Sections H.2.1 and H.2.2 were repeated with different electrode pairs: from electrodes pair (CR13, CR15) in Section H.2.1 to (CR13, CR86), and from electrodes pair (CR22, CR72) in Section H.2.2 to (CR22, CR77) (see Figure H.7A), respectively.

H.3 Results

H.3.1 Network synaptic properties vs. stimulation frequency

The time courses of $\sum(W_{EX})$ and CW are shown in Figures H.1B and H.1C, respectively. The percentage changes of $\sum(W_{EX})$ between *Pre* and *Post* periods, $\Delta\sum(W_{EX})$, is shown in Figure H.1D.

The stimulation frequency of 1 Hz caused a decrease in the summation of weights about 4% (Figure H.1D), and frequencies between 2 and 8 Hz caused opposite effects (5 Hz stimulation caused the most increase of about 10%). These results showed that stimulation caused a network-wide increase of synaptic weights (network-wide potentiation) within a particular frequency bandwidth; otherwise, network-wide depression occurred. Interestingly, at 2 Hz, $\sum(W_{EX})$ first increased and then decreased during the stimulation (t= 30- 60 sec) (Figure H.1B), which indicates that the same stimulation pair induced different effects over time (see detailed analysis in Figure H.2). Furthermore, CWTs pointed to the west side for the potentiation cases with frequencies between 2 and 8 Hz (bluish trajectories in Figure H.1C), and pointed to the northeast direction for high frequency stimulation (> 20 Hz). This suggests that stimulation of different frequencies also caused different changes in the spatial distribution network synaptic weights.

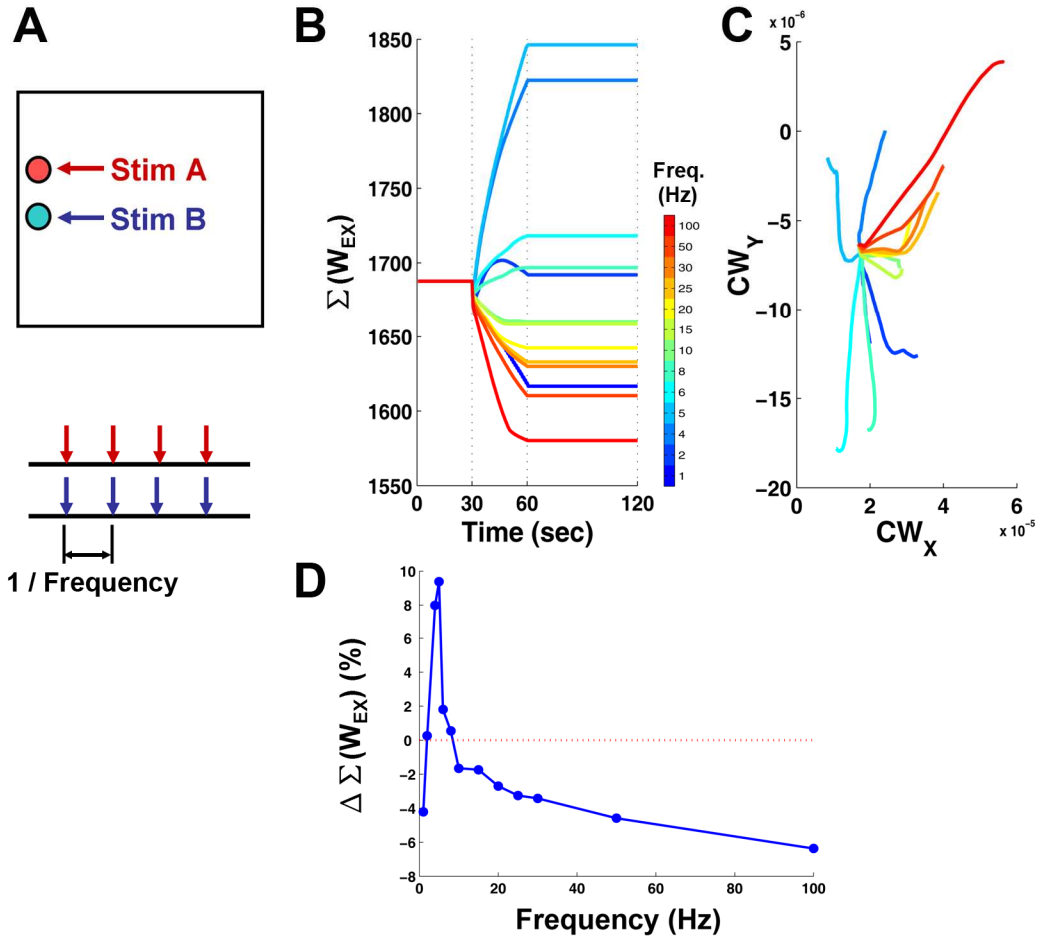

Figure H.1. Paired stimulation with different frequencies induced different changes in network synaptic weights: Simultaneous stimulation at electrodes CR13 and CR15 with different frequencies (**A**), delivered between t=30 to 60 sec, induced different magnitudes (**B**) and different asymmetries (**C**) of network synaptic weights. The color code is shared in B and C, which represents the stimulation frequency (indicated by the colorbar). In C, CWTs under different stimulation frequencies started from the same point that represents the initial network synaptic weights. **D.** The percentage change of $\sum(W_{EX})$ showed a peak at 5 Hz and decreased as stimulation frequency increased.

An example, with 5 Hz stimulation, of the time course of the summation of absolute normalized changes of excitatory synaptic weights, $\sum|\Delta W/W|$, is shown in Figure H.2A. During the 30 seconds of stimulation, $\sum|\Delta W/W|$ continuously decreased over time and approached a steady value, $\sum_{steady}$, in the end. Each time course of $\sum|\Delta W/W|$ was fitted with an exponential function (R-square> 0.89 for all frequencies). The half-life ($\tau_{1/2}$) and $\sum_{steady}$ for each stimulation frequency are shown in Figures H.2B and H.2C, respectively.

The transition of $\sum|\Delta W/W|$ in the beginning of stimulation suggests that the same stimulation pair evoked different activity patterns over time. The convergence of $\sum|\Delta W/W|$ to a steady value suggests that the effect of periodic stimulation on network synaptic weights gradually became stable. The values of $\tau_{1/2}$ show the fastest convergence rate occurred between 2 and 10 Hz (Figure H.2B). The value of $\sum_{steady}$ peaked around 5 Hz, and decreased as the frequency increased.

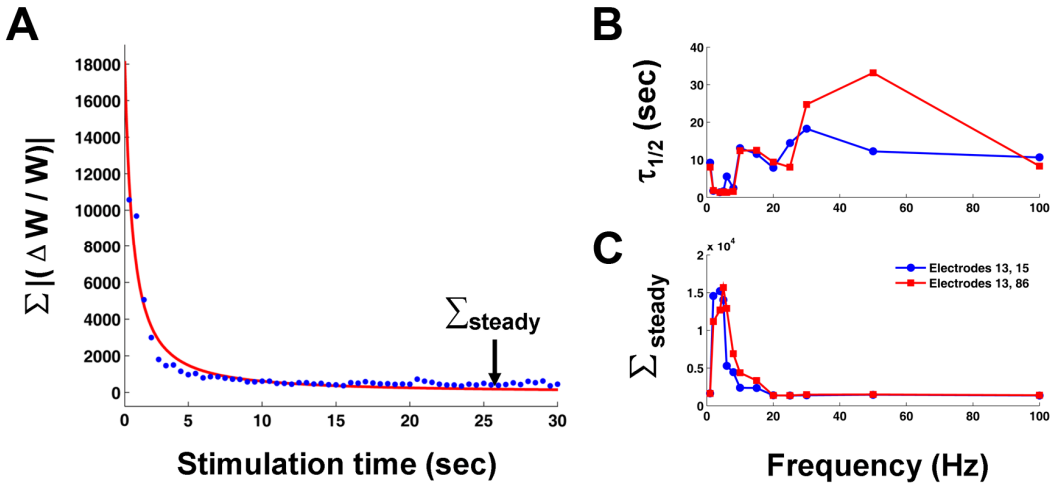

Figure H.2. Stimulation frequency around 5 Hz induced the fastest and the highest plasticity: A. During the 30 seconds of 5 Hz stimulation, $\sum|\Delta W/W|$ showed an exponential decay and approached a steady value, $\sum_{steady}$, in the end. Independent to the two different selections of electrodes, 5 Hz stimulation showed the shortest half-life ($\tau_{1/2}$) (**B**) and the highest final change ($\sum_{steady}$) (**C**).

H.3.2 Network synaptic properties vs. stimulation phase

Stimulation with different phases induced different spatial redistributions of network synaptic weights. CWTs from 10 Hz stimulation with different phases are shown in Figure H.3. The normalized changes of the X and Y components of CW between *Pre* and *Post* periods, $\Delta CW_X/CW_X$ and $\Delta CW_Y/CW_Y$, are shown in Figure H.4A. For each CWT, the vector that pointed from the start point to the end point of the trajectory was measured to quantify the change of CW. The changing distance and direction of each vector were calculated and plotted versus the stimulation phase (Figure H.4B). The

maximal magnitude of the CW change was found with the phase of ± 20 msec. This suggests that the simultaneous paired stimulation, such as some tetanization protocols, was not the optimal stimulation protocol for inducing asymmetric synaptic weights redistribution.

With 10 Hz stimulation, the induced CW change with phase= +50 msec was different from that with phase= –50 msec (compare the left and right points in Figures H.4B and H.8B), even though the stimulation patterns were the same except that the stimulation started/ended at different electrodes. This implies that stimulation with the same frequency, duration, and phase caused different effects when started/ended at different electrodes. This emphasizes the sensitivity of network plasticity to the stimulation history, and further suggests that the network memorizes the history of the stimulation sequence.

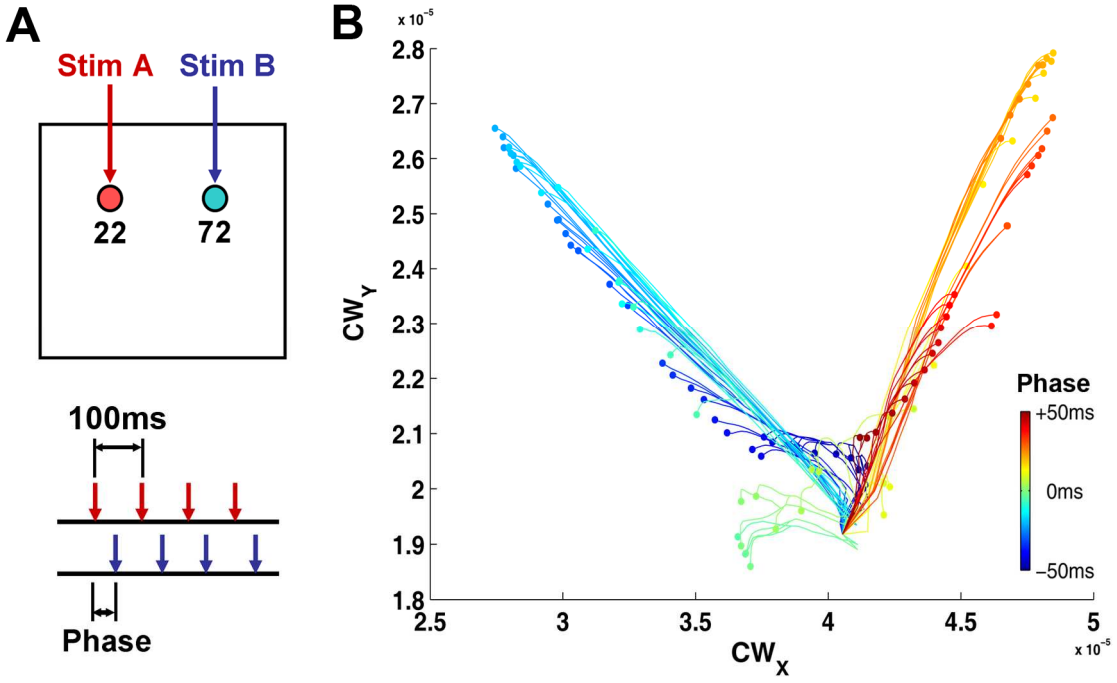

Figure H.3. Paired stimulation with different phases induced different changes in network synaptic weights distribution: A. The location of the stimulation electrodes (electrodes CR 22 and CR72) in an MEA (black square). Stimulation was delivered at 10 Hz with different phases. **B.** CWTs were used to quantify changes in the asymmetry of the network synaptic weights distribution.

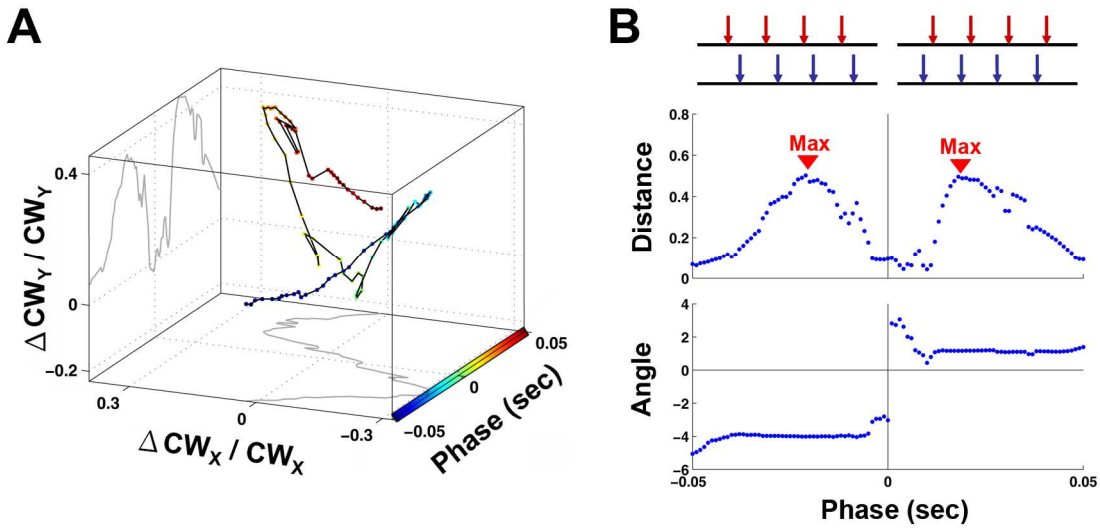

Figure H.4. Effects of the stimulation phase on CWTs: A. The relation between the stimulation phase and the normalized changes of CW components, which are projected at the X and Y planes (grey curves). **B.** The changing distance and direction of CWTs showed an asymmetric relationship with the stimulation phase. The maximal magnitude of CW changes occurred at phase= ± 20 msec (indicated by red triangles).

In addition to CW which measures the population changes in synaptic weights, the individual weight change of each synapse across the stimulation was measured (Figure H.5). Excitatory synaptic weights were summed at the corresponding postsynaptic neurons. The neurons that received positive and negative overall synaptic inputs are shown separately. In order to understand the underlying mechanisms, further verification of the propagation of individual signals within different pathways is needed.

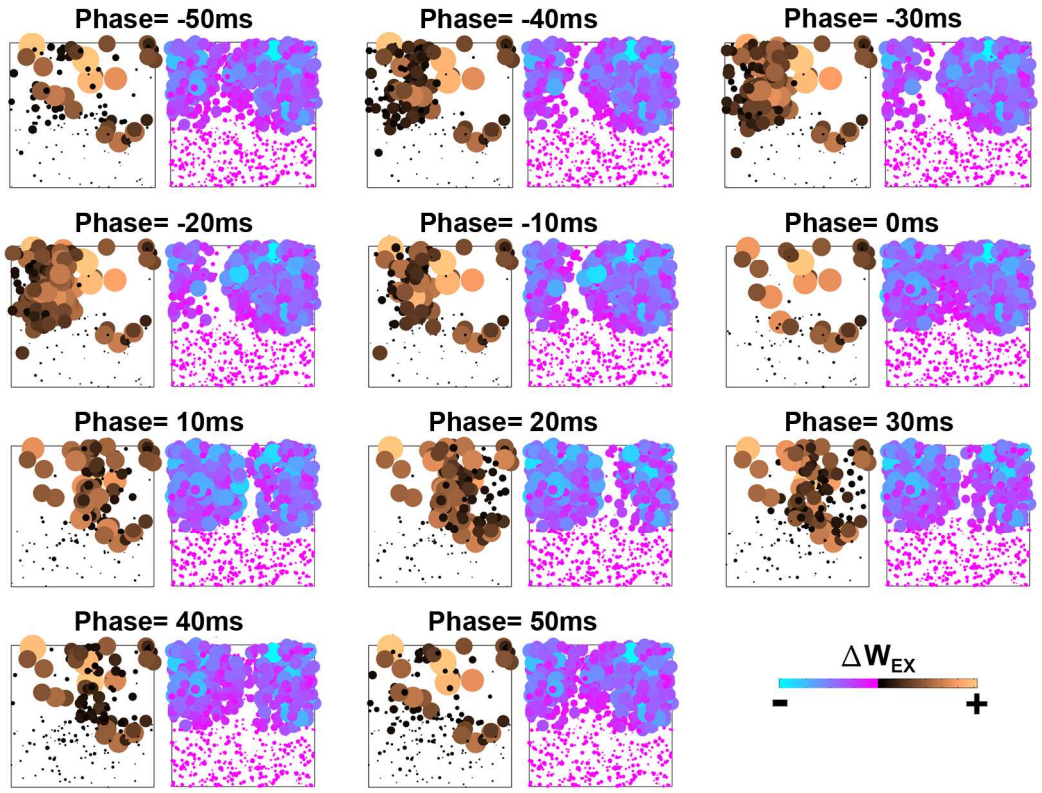

Figure H.5. Potentiation and depression of individual neurons: Excitatory synaptic weights were summed at the corresponding postsynaptic neurons. The neurons that received positive (potentiation) and negative (depression) overall synaptic inputs are shown separately. The magnitudes of potentiation and depression are indicated by filled circles with different sizes and colors.

H.3.3 Network synaptic properties vs. stimulation electrodes

The frequency experiments and the phase experiments were performed on the same network but with a different electrode pair (CR13 and CR86). Results from the frequency experiment are shown in Figure H.6 (compare to Figure H.1), and results from the phase experiment are shown in Figures H.7 and H.8 (compare to Figures H.3 and H.4, respectively). Significant differences were found with different stimulation electrodes. Interestingly, the measures of $\tau_{1/2}$ and $\sum_{steady}$ appeared to be similar for the frequency experiments when two different electrode pairs were used (see Figures H.2B and H.2C). However, in order to verify whether this finding is independent of the choice of

stimulation electrodes (or further to verify that whether this is independent of the connectivity of networks), more experiments are needed.

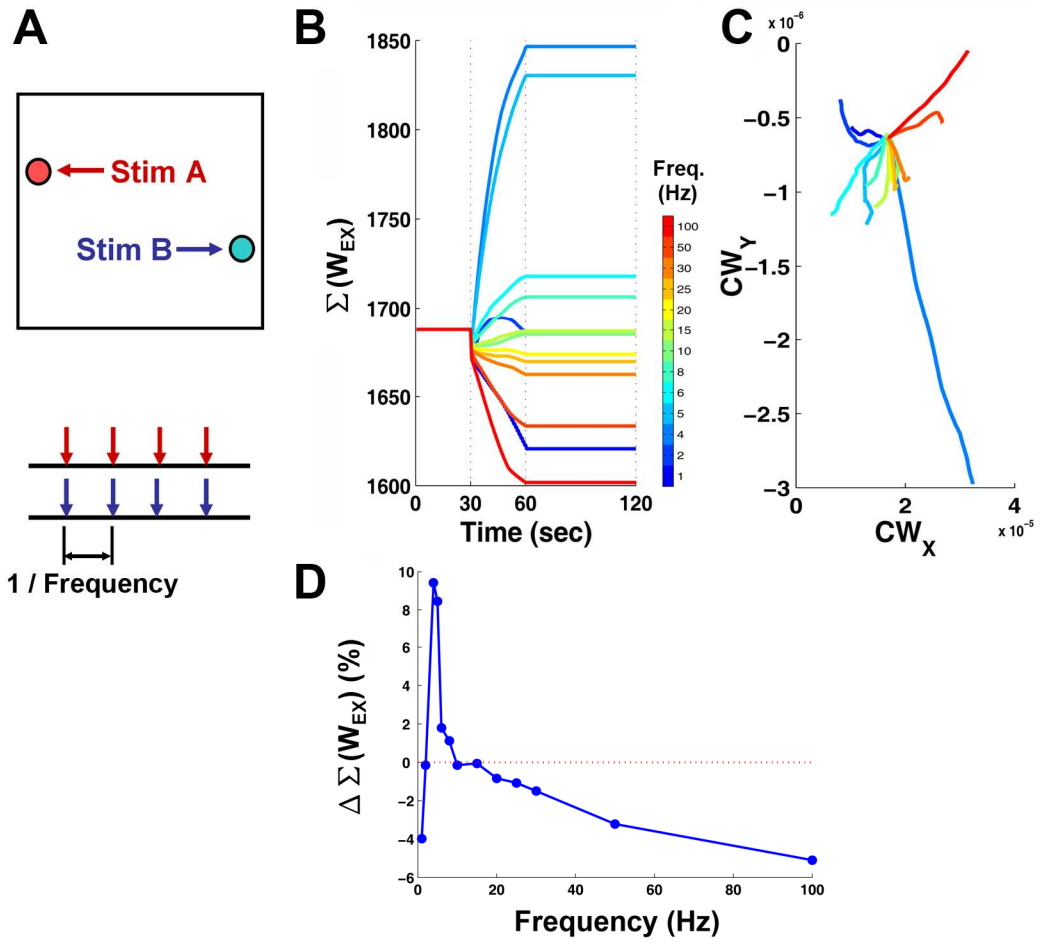

Figure H.6. Paired stimulation with different electrodes showed different frequency dependencies: The same representation as in Figure H.1 is used. The frequency effects on network synaptic weights were dependent on the selection of stimulation electrodes, in this case, CR13 and CR 86 (compare to Figure H.1).

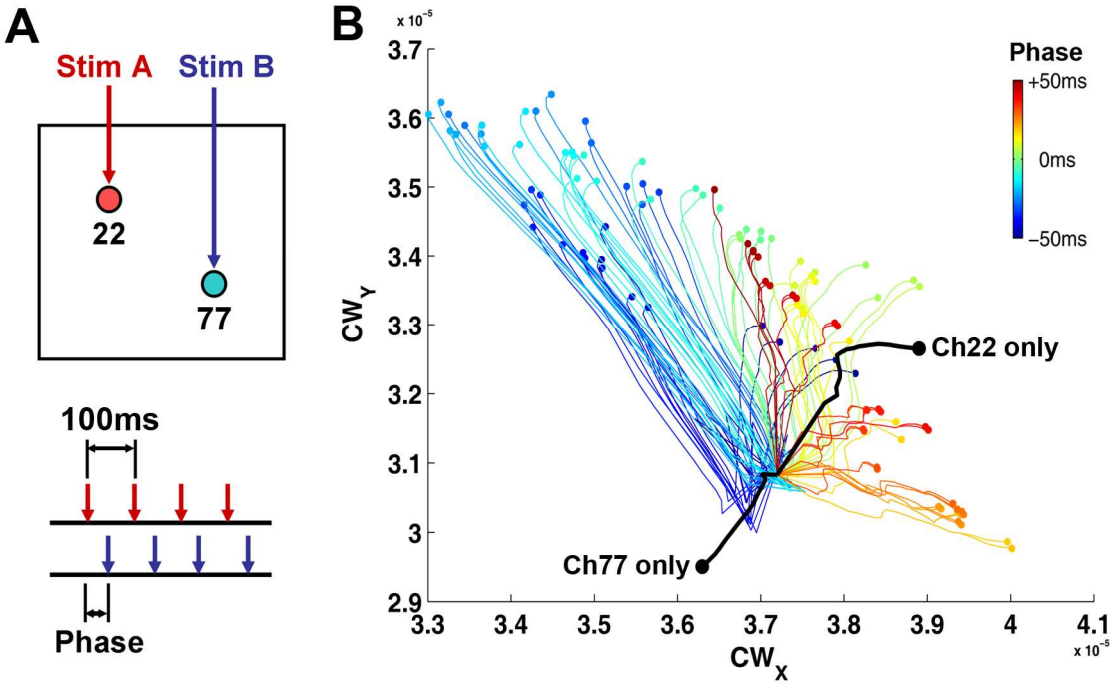

Figure H.7. Paired stimulation with different electrodes showed different phase dependencies: The same representation as in Figure H.3 is used. The phase effects on CWTs were dependent on the selection of stimulation electrodes (compare to Figure H.3). CWTs of stimulation with only one electrode (electrode CR22 or CR77) are also shown for comparison.

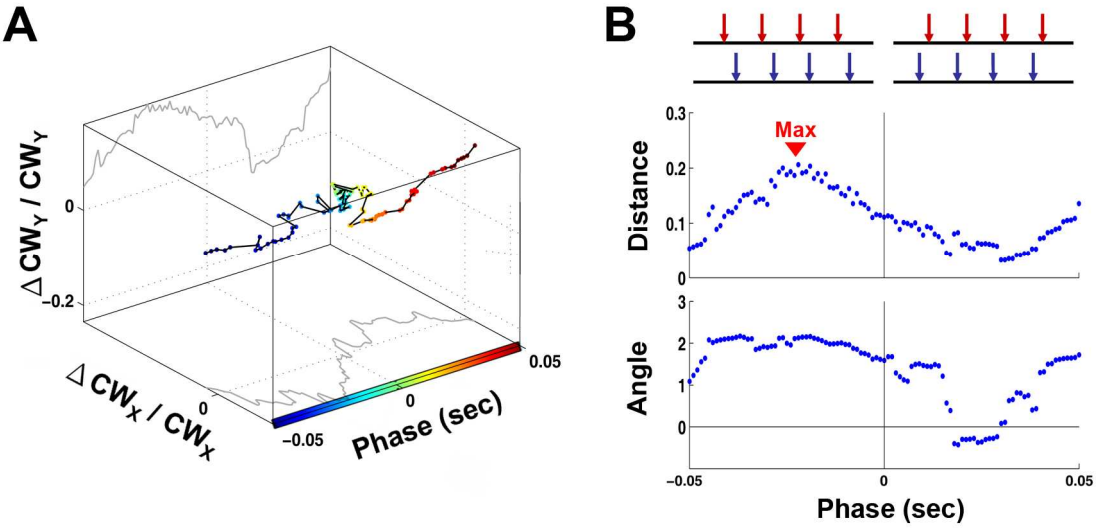

Figure H.8. Asymmetric effects of the stimulation phase on CWTs: The same representation as in Figure H.4 is used. The phase effects on the changing distance and direction of CWTs were dependent on the selection of stimulation electrodes (compare to Figure H.4).

H.4 Discussions

This study is a proof of concept to demonstrate that the network can be shaped into a variety of possible synaptic states by using paired stimulation with different stimulation parameters. The main purpose is to validate the use of patterned training stimulation (PTS) to direct network plasticity (see Chapters 5 and 6). These experiments were performed on *one* network (starting from the same initial network synaptic state for each experiment), so whether these results can be extended as universal phenomena remains unknown. A more systematical investigation of different combinations of stimulation parameters and network connectivity is needed.

For two different selections of electrodes, the frequency that required the least time to saturate the effect on the network synaptic change ($\tau_{1/2}$) and to induce the maximal steady change ($\sum_{steady}$) was found between 2 and 10 Hz (Figures H.2B and H.2C), where the inter-pair intervals were between 200 and 500 msec. This is analogous to the inter-PTS interval, which was selected to be between 200 and 400 msec (2.5 to 5 Hz) for the closed-loop design (see Chapter 5). Moreover, different stimulation phases and electrode pairs were found to shape the network synaptic weights distribution differently, which validates the design of PTS with different inter-PTS intervals ($PTS_{\Delta t}$, analogous to the stimulation phase) and electrode locations (PTS-E1 and PTS-$E2_k$) described in Chapter 5.

APPENDIX I

SPATIOTEMPORAL COMPLEXITY OF STIMULATION PATTERNS

In order to quantify the complexity of the spatiotemporal structure of a stimulation sequence, I will use a measure called spatiotemporal complexity (STC), an information-based measure (Parrott, 2005). STC is applied to a cube of data, which could be a stack of successive spatial "images" in raster format, such as a series of stimuli applied at a 2-D MEA (Figure I.1). The result is thus a cube of binary data of dimensions N_l by N_w by t cells, where N_l and N_w are the length and width of the landscape and t is the number of time slices. The measure is then calculated by counting the number of non-zero contents (blue dots in Figure I.1) in a moving time cube, or a counting cube (red cubes in Figure I.1), whose dimensions are considerably smaller than the dimensions of the data cube.

For all of the different possible numbers counted, $M_i \in [0, \ldots, N]$, the relative frequency of occurrence is computed and the spatiotemporal complexity of the data is calculated as follows:

$$STC = \frac{-\sum_{i=0}^{N} p_i \cdot \ln(p_i)}{\ln(N)} \qquad 0 < STC < 1 \qquad \text{[Equation I.1]}$$

where p_i = relative frequency of M_i. Division by ln(N) serves to normalize the measure.

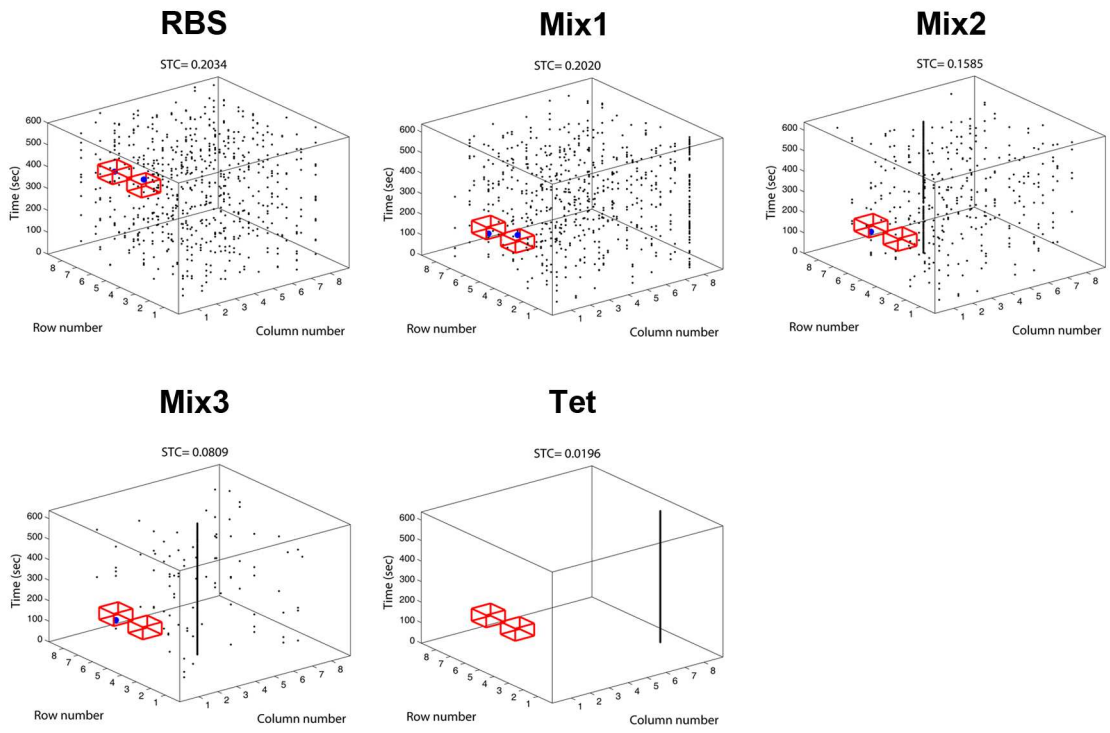

Figure I.1. Stimulation with different spatiotemporal patterns: 3-D representations of 1-min stimulation patterns from random background stimulation (RBS) to one-channel tetanization (Tet) on an 8 by 8 grid of electrodes. Each dot represents a stimulus. Examples of counting cubes are shown as red cubes, and the stimuli counted within them are shown as blue dots.

The value of STC ranges from 0 for the completely ordered case where only one occupation level is observed (equivalent to data of solid zeros or ones) to 1 for the most complex case (equivalent to observing all occupation levels with equal frequency). Unlike the Shannon entropy for temporal series, the random case does not receive the highest value of STC, since, for data of randomly distributed 1's and 0's, the average occupation of a given counting cube is $N/2$ and unoccupied or fully occupied counting cubes are very unlikely. Thus, for completely random spatiotemporal data, the distribution of relative occupation frequencies is normal, giving rise to intermediate values of STC. At the other extreme, a very "clumpy" mosaic, with large-sized regularly shaped patches would have high frequencies of fully occupied or completely empty counting cubes and few intermediate cases. This type of distribution would tend to have lower values of STC, being closer to the completely ordered case. The highest values of

STC correspond therefore to very "complex" spatiotemporal patterns that consist of irregular patches of various sizes. For this type of spatiotemporal dynamics, all occupation levels of counting cubes are likely and the frequency distribution is more uniform.

I calculated STC from various 1-min stimulation patterns: random background stimulation (RBS), one-channel tetanization (Tet), and mixtures of RBS and Tet with various levels (Mix1 to Mix3) (Figure I.1), where the number of stimuli in different stimulation patterns was identical. The results are shown in Figure I.2. STC was higher if a stimulation sequence included a larger proportion of RBS and a smaller proportion of tetanization.

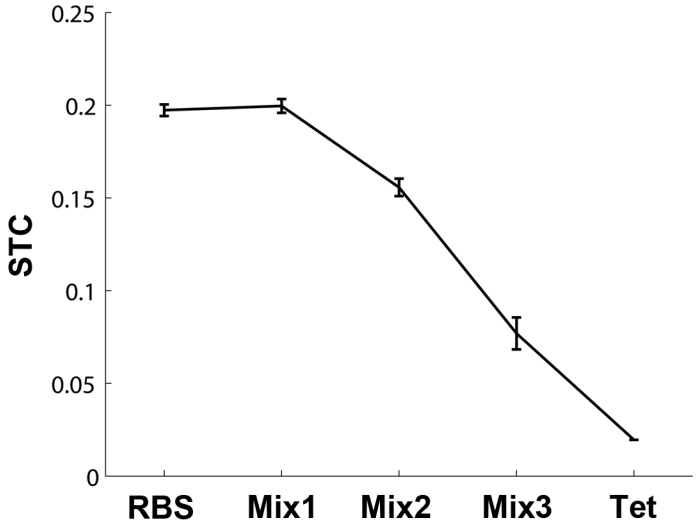

Figure I.2. STC of different stimulation patterns: STC was higher if a stimulation sequence included a larger proportion of RBS and a smaller proportion of tetanization (mean and SEM are shown, n= 50 different sequences for each type of stimulation).

I hypothesize that the amount of network plasticity could be controlled by the spatiotemporal complexity of training stimuli (see Section 7.2.5), where STC becomes useful for describing the high-dimensional spatiotemporal pattern of stimuli with a single value. By measuring network plasticity induced by stimuli with different STC in

simulated or living networks, this relationship might be established. For example, one could plot various plasticity measures (see Appendix H) versus the STC of plasticity-inducing stimuli for simulated networks, or plot C/D of CAT (see Chapter 3) versus the STC of plasticity-inducing stimuli for living networks.

REFERENCES

Abbott LF, Varela JA, Sen K, Nelson SB (1997) Synaptic Depression and Cortical Gain Control. Science 275:221-224.

Aertsen AM, Gerstein GL, Habib MK, Palm G (1989) Dynamics of neuronal firing correlation: modulation of "effective connectivity". J Neurophysiol 61:900-917.

Ahissar E, Abeles M, Ahissar M, Haidarliu S, Vaadia E (1998) Hebbian-like functional plasticity in the auditory cortex of the behaving monkey. Neuropharmacology 37:633-655.

Ahissar E, Vaadia E, Ahissar M, Bergman H, Arieli A, Abeles M (1992) Dependence of Cortical Plasticity on Correlated Activity of Single Neurons and on Behavioral Context. Science 257:1412-1415.

Aviel Y, Mehring C, Abeles M, Horn D (2003) On embedding synfire chains in a balanced network. Neural Comput 15:1321-1340.

Bakkum DJ, Chao ZC, Potter SM (2007) Long-term activity-dependent plasticity of action potential propagation in cortical networks. PLoS One Under review.

Bakkum DJ, Shkolnik AC, Ben-Ary G, Gamblen P, Demarse TB, Potter SM (2004) Removing some 'A' from AI: embodied cultured networks. In: Embodied Artificial Intelligence (Iida F, Steels L, Pfeifer R, eds), pp 130-145: Springer-Verlag.

Balleine BW, Dickinson A (1998) Goal-directed instrumental action: contingency and incentive learning and their cortical substrates. Neuropharmacology 37:407-419.

Banker G, Goslin K (1998a) Culturing Nerve Cells: MIT Press.

Banker G, Goslin K (1998b) Culturing Nerve Cells, 2nd Edition. Cambridge, Mass.: MIT Press.

Bao S, Chang EF, Davis JD, Gobeske KT, Merzenich MM (2003) Progressive Degradation and Subsequent Refinement of Acoustic Representations in the Adult Auditory Cortex. Journal of Neuroscience 23:10765-10775.

Baruchi I, Ben-Jacob E (2004) Functional holography of recorded neuronal networks activity. Neuroinformatics 2:333-352.

Baruchi I, Ben-Jacob E (2007) Towards neuro-memory-chip: Imprinting multiple memories in cultured neural networks. PHYSICAL REVIEW E Phys Rev E 75:050901.

Bedlack RS, Jr., Wei MD, Fox SH, Gross E, Loew LM (1994) Distinct electric potentials in soma and neurite membranes. Neuron 13:1187-1193.

Beggs J, Plenz D (2004) Neuronal avalanches are diverse and precise activity patterns that are stable for many hours in cortical slice cultures. J Neuroscience 24:5216-5229.

Betz WJ (1970) Depression of transmitter release at the neuromuscular junction of the frog. The Journal of Physiology 206:629-644.

Bi G, Poo M (1998) Synaptic modifications in cultured hippocampal neurons: Dependence on spike timing, synaptic strength, and postsynaptic cell type. J Neurosci 18:10464-10472.

Biswal B, Dasgupta C (2002) Stochastic neural network model for spontaneous bursting in hippocampal slices. Phys Rev E Stat Nonlin Soft Matter Phys 66:051908.

Bliss TV, Lømo T (1973) Long-lasting potentiation of synaptic transmission in the dentate area of the anaesthetized rabbit following stimulation of the perforant path. J Physiol (Lond) 232:331-356.

Bliss TV, Collingridge GLA (1993) A synaptic model of memory: long-term potentiation in the hippocampus. Nature 361:31-39.

Blum NA, Carkhuff BG, Charles Jr HK, Edwards RL, Meyer RA (1991) Multisite microprobes for neural recordings. Biomedical Engineering, IEEE Transactions on 38:68-74.

Bonhoeffer T, Staiger V (1988) Optical recording with single cell resolution from monolayered slice cultures of rat hippocampus. Neurosci Lett 92:259-264.

Brody CD (1999) Correlations Without Synchrony. Neural Computation 11:1537-1551.

Brooks R (1999) In: Cambrian intelligence, the early history of the new AI: The MIT press.

Brown EN, Kass RE, Mitra PP (2004) Multiple neural spike train data analysis: state-of-the-art and future challenges. Nature Neuroscience 7:456-461.

Brunel N, Nadal J-P (1998) Mutual Information, Fisher Information, and Population Coding. Neural Computation 10:1731-1757.

Bucher V, Brunner B, Leibrock C, Schubert M, Nisch W (2001) Electrical properties of a light-addressable microelectrode chip with high electrode density for extracellular stimulation and recording of excitable cells. Biosens Bioelectron 16:205-210.

Buonomano DV (1998) Cortical plasticity: from synapses to maps. Annual Review of Neuroscience 21:149-186

Caminiti R, Johnson PB, Burnod Y, Galli C, Ferraina S (1990) Shifts of preferred directions of premotor cortical cells with arm movements performed across the workspace. Experimental Brain Research 83:228-232.

Canepari M, Bove M, Maeda E, Cappello M, Kawana A (1997) Experimental analysis of neuronal dynamics in cultured cortical networks and transitions between different patterns of activity. Biological Cybernetics 77:153-162.

Carmena JM, Lebedev MA, Crist RE, O'Doherty JE, Santucci DM, Dimitrov DF, Patil PG, Henriquez CS, Nicolelis MAL (2003) Learning to Control a Brain–Machine Interface for Reaching and Grasping by Primates. PLoS Biology 1:1-16.

Celikel T, Szostak VA, Feldman DE (2004) Modulation of spike timing by sensory deprivation during induction of cortical map plasticity. Nat Neurosci 7:534-541.

Chao ZC, Bakkum DJ, Potter SM (2007a) Shaping embodied neural networks for adaptive goal-directed behavior. PLoS Computational Biology Under review.

Chao ZC, Bakkum DJ, Potter SM (2007b) Feedback training of electrical stimuli in a cortical network: learning and neurorehabilitation. Ready to submit.

Chao ZC, Bakkum DJ, Potter SM (2007c) Region-specific network plasticity in simulated and living cortical networks: comparison of the center of activity trajectory (CAT) with other statistics. J Neural Eng 4:1-15.

Chao ZC, Bakkum DJ, Wagenaar DA, Potter SM (2005) Effects of random external background stimulation on network synaptic stability after tetanization—A modeling study. Neuroinformatics 3:263-280.

Chase VD, York N (1999) Team develops biological computer. Nature Medicine 5:722.

Chornoboy ES, Schramm LP, Karr AF (1988) Maximum likelihood identification of neural point process systems. Biological Cybernetics 59:265-275.

Corbit LH, Balleine BW (2003) The role of prelimbic cortex in instrumental conditioning. Behav Brain Res 146:145-157.

Corey JM, Wheeler BC, Brewer GJ (1991) Compliance of hippocampal neurons to patterned substrate networks. Journal of Neuroscience Research 30:300-307.

Costanzo RM (2000) Rewiring the Olfactory Bulb: Changes in Odor Maps following Recovery from Nerve Transection. Chemical Senses 25:199-205.

Cozzi L, D'Angelo P, Chiappalone M, Ide AN, Novellino A, Martinoia S, Sanguineti V (2005) Coding and decoding of information in a bi-directional neural interface. Neurocomputing 65:783-792.

Daoudal G, Debanne D (2003) Long-Term Plasticity of Intrinsic Excitability: Learning Rules and Mechanisms. Learning & Memory 10:456-465.

Darbon P, Scicluna L, Tscherter A, Streit J (2002) Mechanisms controlling bursting activity induced by disinhibition in spinal cord networks. European Journal of Neuroscience 15:671-683.

David O, Cosmelli D, Friston KJ (2004) Evaluation of different measures of functional connectivity using a neural mass model. Neuroimage 21:659-673.

Davies DL, Bouldin DW (1979) A cluster separation measure. IEEE Trans Pattern AnalMachine Intell 1:224-227.

del Castillo J, Katz B (1954) Statistical factors involved in neuromuscular facilitation and depression. The Journal of Physiology 124:574-585.

Delaney KR, Zucker RS, Tank DW (1989) Calcium in motor nerve terminals associated with posttetanic potentiation. Journal of Neuroscience 9:3558-3567.

DeMarse TB, Wagenaar DA, Blau AW, Potter SM (2001) The Neurally Controlled Animat: Biological Brains Acting with Simulated Bodies. Autonomous Robots 11:305-310.

Demas J, Eglen SJ, Wong ROL (2003) Developmental Loss of Synchronous Spontaneous Activity in the Mouse Retina Is Independent of Visual Experience. Journal of Neuroscience 23:2851-2860.

Desmond NL, Levy WB (1983) Synaptic correlates of associative potentiation/depression: an ultrastructural study in the hippocampus. Brain Res 265:21-30.

Dobkin BH, Firestine A, West M, Saremi K, Woods R (2004) Ankle dorsiflexion as an fMRI paradigm to assay motor control for walking during rehabilitation. Neuroimage 23:370-381.

Eggermont J (1992) Neural interaction in cat primary auditory cortex. Dependence on recording depth, electrode separation, and age. J Neurophysiol 68:1216-1228.

Ermentrout GB, Kopell N (1998) Fine structure of neural spiking and synchronization in the presence of conduction delays. 95:1259-1264.

Eytan D, Marom S (2006) Dynamics and Effective Topology Underlying Synchronization in Networks of Cortical Neurons. Journal of Neuroscience 26:8465-8476.

Eytan D, Brenner N, Marom S (2003) Selective adaptation in networks of cortical neurons. J Neurosci 23 9349-9356.

Feinerman O, Segal M, Moses E (2007) Identification and Dynamics of Spontaneous Burst Initiation Zones in Unidimensional Neuronal Cultures. Journal of Neurophysiology 97:2937-2948.

Fellous J-M, Tiesinga PHE, Thomas PJ, Sejnowski TJ (2004) Discovering Spike Patterns in Neuronal Responses. J Neuroscience 24:2989-3001.

Fields RD (2005) Myelination: An Overlooked Mechanism of Synaptic Plasticity? The Neuroscientist 11:528-531.

Fisher SA, Fischer TM, Carew TJ (1997) Multiple overlapping processes underlying short-term synaptic enhancement. Trends Neurosci 20:170-177.

Fortune ES, Rose GJ (2000) Short-Term Synaptic Plasticity Contributes to the Temporal Filtering of Electrosensory Information. Journal of Neuroscience 20:7122-7130.

Franco L, Rolls ET, Aggelopoulos NC, Treves A (2004) The use of decoding to analyze the contribution to the information of the correlations between the firing of simultaneously recorded neurons. Exp Brain Res 155:370-384.

Froemke RC, Dan Y (2002) Spike-timing-dependent synaptic modification induced by natural spike trains. Nature 416:433-438.

Ganguly K, Kiss L, Poo M (2000) Enhancement of presynaptic neuronal excitability by correlated presynaptic and postsynaptic spiking. Nat Neurosci 3:1018-1026.

Garaschuk O, Hanse E, Konnerth A (1998) Developmental profile and synaptic origin of early network oscillations in the CA1 region of rat neonatal hippocampus. The Journal of Physiology 507:219-236.

Garcia PS, Calabrese RL, Ellis RT, Deweerth SP, Ditto WL (2001) Computing with neuronal dynamics. American Physical Society, Annual March Meeting, March 12-16, 2001 Washington State Convention Center Seattle, Washington Meeting ID: MAR01, abstract# N23 007.

Georgopoulos A, Schwartz A, Kettner R (1986) Neuronal population coding of movement direction. Science 233:1416-1419.

Georgopoulos AP (1994) Population Activity in the Control of Movement. In: Selectionism and the Brain, pp 103-119. San Diego: Academic Press.

Gerstein G, Perkel D (1969) Simultaneously recorded trains of action potentials: analysis and functional interpretation. Science 164:828-830.

Gerstner W, Kempter R, van Hemmen JL, Wagner H (1996) A neuronal learning rule for sub-millisecond temporal coding. Nature 383:76-78.

Gibbs JW, Sombati S, DeLorenzo RJ, Coulter DA (1997) Physiological and pharmacological alterations in postsynaptic GABA(A) receptor function in a hippocampal culture model of chronic spontaneous seizures. Journal of Neurophysiology 77:2139-2152.

Goldstein SS, Rall W (1974) Changes of action potential shape and velocity for changing core conductor geometry. Biophys J 14:731-757.

Gross GW (1979) Simultaneous single unit recording in vitro with a photoetched laser deinsulated gold multimicroelectrode surface. IEEE Trans Biomed Eng 26:273-279.

Gross GW, Kowalski JM (1999) Origins of activity patterns in self-organizing neuronal networks in vitro. Journal of Intelligent Material Systems and Structures 10:558-564.

Gross GW, Rhoades BK, Kowalski JK (1993a) Dynamics of burst patterns generated by monolayer networks in culture. In: Neurobionics: An Interdisciplinary Approach to Substitute Impaired Functions of the Human Nervous System (Bothe HW, Samii M, Eckmiller R, eds), pp 89-121. Amsterdam: North-Holland.

Gross GW, Rieske E, Kreutzberg GW, Meyer A (1977) A new fixed-array multi-microelectrode system designed for long-term monitoring of extracellular single unit neuronal activity in vitro. Neuroscience Letters 6:101-105.

Gross GW, Rhoades BK, Reust DL, Schwalm FU (1993b) Stimulation of monolayer networks in culture through thin-film indium-tin oxide recording electrodes. Journal of Neuroscience Methods 50:131-143.

Gutig R, Aharonov R, Rotter S, Sompolinsky H (2003) Learning Input Correlations through Nonlinear Temporally Asymmetric Hebbian Plasticity. Journal of Neuroscience 23:3697.

Hochbruck M, Lubich C, Selhofer H (1998) Exponential Integrators for Large Systems of Differential Equations. SIAM Journal on Scientific Computing 19:1552-1574.

Hodgkin AL, Huxley AF (1990) A quantitative description of membrane current and its application to conduction and excitation in nerve. Bulletin of Mathematical Biology 52:25-71.

Holland JH (1975) Adaptation in natural and artificial systems, University of Michigan press. Ann Arbor, MI.

Horn D (1998) Memory Maintenance via Neuronal Regulation. Neural Computation 10:1-18.

Houde JF, Jordan MI (1998) Sensorimotor Adaptation in Speech Production. Science 279:1213.

Hu B, Karnup S, Zhou L, Stelzer A (2005) Reversal of Hippocampal LTP by Spontaneous Seizure-Like Activity: Role of Group I mGluR and Cell Depolarization. Journal of Neurophysiology 93:316-336.

Huang H, Wolf SL, He J (2006) Recent developments in biofeedback for neuromotor rehabilitation. J Neuroengineering Rehabil 3:11.

Ikegaya Y, Aaron G, Cossart R, Aronov D, Lampl I, Ferster D, Yuste R (2004) Synfire chains and cortical songs: temporal modules of cortical activity. Science 304:559-564.

Ishibashi T, Dakin KA, Stevens B, Lee PR, Kozlov SV, Stewart CL, Fields RD (2006a) Astrocytes Promote Myelination in Response to Electrical Impulses. Neuron 49:823-832.

Ishibashi T, Dakin KA, Stevens B, Lee PR, Kozlov SV, Stewart CL, Fields RD (2006b) Astrocytes promote myelination in response to electrical impulses. Neuron 49:823-832.

Izhikevich EM (2004) Which model to use for cortical spiking neurons? Neural Networks, IEEE Transactions on 15:1063-1070.

Izhikevich EM (2005) Polychronization: Computation with Spikes. Neural Computation 18:245-282.

Izhikevich EM, Gally JA, Edelman GM (2004) Spike-Timing Dynamics of Neuronal Groups. Cerebral Cortex 14:933-944.

Jackson A, Mavoori J, Fetz EE (2006) Long-term motor cortex plasticity induced by an electronic neural implant. Nature 444:56-60.

Jahanshahi M, Ardouin CMA, Brown RG, Rothwell JC, Obeso J, Albanese A, Rodriguez-Oroz MC, Moro E, Benabid AL, Pollak P (2000) The impact of deep brain stimulation on executive function in Parkinson's disease. Brain 123:1142-1154.

Jimbo Y, Kawana A (1992) Electrical stimulation and recording from cultured neurons using a planar electrode array. Bioelectrochemistry and Bioenergetics 29:193-204.

Jimbo Y, Robinson HPC, Kawana A (1998a) Strengthening of synchronized activity by tetanic stimulation in cortical cultures: Application of planar electrode arrays. IEEE Trans Biomed Eng 45:1297-1304.

Jimbo Y, Tateno T, Robinson HPC (1998b) Simultaneous induction of potentiation and depression in cortical network activity. Eur J Neurosci 10:222.

Jimbo Y, Tateno T, Robinson HPC (1999) Simultaneous induction of pathway-specific potentiation and depression in networks of cortical neurons. Biophysical Journal 76:670-678.

Jimbo Y, Kawana A, Parodi P, Torre V (1998c) The dynamics of a neuronal culture from dissociated cortical neurons of neonatal rats. European Journal of Neuroscience 10:403-403.

Johansen-Berg H, Dawes H, Guy C, Smith SM, Wade DT, Matthews PM (2002) Correlation between motor improvements and altered fMRI activity after rehabilitative therapy. Brain 125:2731-2742.

Kam L, Shain W, Turner JN, Bizios R (2001) Axonal outgrowth of hippocampal neurons on micro-scale networks of polylysine-conjugated laminin. Biomaterials 22:1049-1054.

Kamioka H, Maeda E, Jimbo Y, Robinson HPC, Kawana A (1996) Spontaneous periodic synchronized bursting during formation of mature patterns of connections in cortical cultures. Neuroscience Letters 206:109-112.

Karniel A, Kositsky M, Fleming KM, Chiappalone M, Sanguineti V, Alford ST, Mussa-Ivaldi FA (2005) Computational analysis in vitro: dynamics and plasticity of a neuro-robotic system. Journal of Neural Engineering 2:S250-S265.

Katz LC, Shatz CJ (1996) Synaptic Activity and the Construction of Cortical Circuits. Science 274:1133.

Kawaguchi H, Fukunishi K (1998) Dendrite classification in rat hippocampal neurons according to signal propagation properties - Observation by multichannel optical recording in cultured neuronal networks. Experimental Brain Research 122:378-392.

Kempermann G (2002) Why New Neurons? Possible Functions for Adult Hippocampal Neurogenesis. Journal of Neuroscience 22:635-638.

Krahe R, Gabbiani F (2004) Burst firing in sensory systems. Nature Reviews Neuroscience 5:13-23.

Krichmar J, Edelman G (2002) Machine psychology: autonomous behavior, perceptual categorization and conditioning in a brain-based device. Cereb Cortex 12:818-830.

Krichmar JL, Nitz DA, Gally JA, Edelman GM (2005) Characterizing functional hippocampal pathways in a brain-based device as it solves a spatial memory task. Proceedings of the National Academy of Sciences 102:2111-2116.

Kudoh SN, Taguchi T (2005) Interaction and intelligence in living neuronal networks interfaced with moving robot. Proceedings of SPIE 6036:60360S.

Kudrimoti HS, Barnes CA, McNaughton BL (1999) Reactivation of Hippocampal Cell Assemblies: Effects of Behavioral State, Experience, and EEG Dynamics. Journal of Neuroscience 19:4090-4101.

Latham P, Richmond B, Nelson P, Nirenberg S (2000a) Intrinsic dynamics in neuronal networks. I. Theory. J Neurophysiol 83:808-827.

Latham PE, Richmond BJ, Nirenberg S, Nelson PG (2000b) Intrinsic dynamics in neuronal networks. II. Experiment. Journal of Neurophysiology 83:828-835.

Leahy RM, Mosher JC, Spencer ME, Huang MX, Lewine JD (1998) A study of dipole localization accuracy for MEG and EEG using a human skull phantom. Electroencephalogr Clin Neurophysiol 107:159-173.

Lee A, Wilson M (2002) Memory of sequential experience in the hippocampus during slow wave sleep. Neuron 36:1183-1194.

Lee BS (1950) Effects of Delayed Speech Feedback. The Journal of the Acoustical Society of America 22:824.

Legendy CR, Salcman M (1985) Bursts and recurrences of bursts in the spike trains of spontaneously active striate cortex neurons. Journal of Neurophysiology 53:926-939.

Lewicki MS (1998) A review of methods for spike sorting: the detection and classification of neural action potentials. Network: Computation in Neural Systems 9:R53 - R78.

Li Y, Zhou W, Li X, Zeng S, Liu M, Luo Q (2007) Characterization of synchronized bursts in cultured hippocampal neuronal networks with learning training on microelectrode arrays. Biosensors and Bioelectronics 22:2976-2982.

Liepert J, Bauder H, Miltner WHR, Taub E, Weiller C (2000) Treatment-Induced Cortical Reorganization After Stroke in Humans. Stroke 31:1210-1216.

Lipski J (1981) Antidromic activation of neurones as an analytic tool in the study of the central nervous system. J Neurosci Methods 4:1-32.

Madhavan R, Mehta B, Potter SM (2007a) Artificial sensory background stimulation induces altered GABA expression in cortical cultures. Ready to submit.

Madhavan R, Chao ZC, Potter SM (2007b) Plasticity of recurring spatiotemporal activity patterns in dissociated cortical networks. Physical Biology 4:181-193.

Madhavan R, Chao ZC, Potter SM (2007c) Electrical control of population bursting aids functional plasticity in cortical networks. Ready to submit.

Maeda E, Kuroda Y, Robinson HPC, Kawana A (1998a) Modification of parallel activity elicited by propagating bursts in developing networks of rat cortical neurones. European Journal of Neuroscience 10:488-496.

Maeda E, Kuroda Y, Robinson HPC, Kawana A (1998b) Modification of parallel activity elicited by propagating bursts in developing networks of rat cortical neurones. Eur J Neurosci 10:488-496.

Maher MP, Pine J, Wright J, Tai YC (1999) The neurochip: a new multielectrode device for stimulating and recording from cultured neurons. Journal of Neuroscience Methods 87:45-56.

Manjarrez E, Vazquez M, Flores A (2007) Computing the center of mass for traveling alpha waves in the human brain. Brain Res 1145:239-247.

Marinaro M, Scarpetta S (2004) Effects of noise in a cortical neural model. Phys Rev E Stat Nonlin Soft Matter Phys 70.

Markram H, Wang Y, Tsodyks M (1998a) Differential signaling via the same axon of neocortical pyramidal neurons. In, pp 5323-5328: National Acad Sciences.

Markram H, Lubke J, Frotscher M, Sakmann B (1997) Regulation of synaptic efficacy by coincidence of postsynaptic APs and EPSPs. Science 275:213-215.

Markram H, Gupta A, Uziel A, Wang Y, Tsodyks M (1998b) Information processing with frequency-dependent synaptic connections. Neurobiology of Learning and Memory 70:101-112.

Marom S, Shahaf G (2002) Development, learning and memory in large random networks of cortical neurons: Lessons beyond anatomy. Quarterly Reviews of Biophysics 35:63-87.

Martinerie J, Adam C, Le Van Quyen M, Baulac M, Clemenceau S, Renault B, Varela FJ (1998) Epileptic seizures can be anticipated by non-linear analysis. Nature Medicine 4:1173-1176.

Martinoia S, Sanguineti V, Cozzi L, Berdondini L, van Pelt J, Tomas J, Le Masson G, Davide F (2004) Towards an embodied in vitro electrophysiology: the NeuroBIT project. Neurocomputing 58:1065-1072.

McIntyre C, Grill W (2002) Extracellular stimulation of central neurons: influence of stimulus waveform and frequency on neuronal output. J Neurophysiology 88:1592-1604.

Mehring C, Hehl U, Kubo M, Diesmann M, Aertsen A (2003) Activity dynamics and propagation of synchronous spiking in locally connected random networks. Biol Cybern 88:395-408.

Meister M, Wong RO, Baylor DA, Shatz CJ (1991) Synchronous bursts of action potentials in ganglion cells of the developing mammalian retina. Science 252:939-943.

Merzenich M, Sameshima K (1993) Cortical plasticity and memory. Curr Opin Neurobiol 3:187-196.

Meyer JA, Wilson SW (1991) From Animals to Animats: Proceedings of the First International Conference on Simulation of Adaptive Behavior. Cambridge: MIT Press.

Michalski A, Gerstein GL, Czarkowska J, Tarnecki R (1983) Interactions between cat striate cortex neurons. Experimental Brain Research 51:97 - 107.

Miles R, Wong RK (1987) Inhibitory control of local excitatory circuits in the guinea-pig hippocampus. The Journal of Physiology 388:611-629.

Moddemeijer R (1989) On Estimation of Entropy and Mutual Information of Continuous Distributions. Signal Processing 16:233-246.

Mongillo G, Amit D (2001) Oscillations and irregular emission in networks of linear spiking neurons. J Comput Neurosci 11:249-261.

Moore SD, Barr DS, Wilson WA (1993) Seizure-like activity disrupts LTP in vitro. Neurosci Lett 163:117-119.

Morris KF, Baekey DM, Nuding SC, Dick TE, Shannon R, Lindsey BG (2003) Invited Review: Neural network plasticity in respiratory control. J Appl Physiol 94:1242-1252.

Morrison SJ, Csete M, Groves AK, Melega W, Wold B, Anderson DJ (2000) Culture in reduced levels of oxygen promotes clonogenic sympathoadrenal differentiation by isolated neural crest stem cells. Journal of Neuroscience 20:7370-7376.

Moscato P (1989) On evolution, search, optimization, genetic algorithms and martial arts: Towards memetic algorithms. Caltech Concurrent Computation Program, C3P Report 826.

Murphy TH, Blatter LA, Wier WG, Baraban JM (1992) Spontaneous synchronous synaptic calcium transients in cultured cortical neurons. J Neurosci 12:4834-4845.

Mussa-Ivaldi FA, Miller LE (2003) Brain-machine interfaces: computational demands and clinical needs meet basic neuroscience. Trends Neurosci 26:329-334.

Nádasdy Z (2000) Spike sequences and their consequences. J Physiol (Paris) 94:505-524.

Nádasdy Z, Hirase H, Czurkó A, Csicsvari J, Buzsáki G (1999) Replay and Time Compression of Recurring Spike Sequences in the Hippocampus. J Neuroscience 19:9497-9507.

Natschlager T, Markram H, Maass W (2003) Computer models and analysis tools for neural microcircuits. In: Neuroscience Databases. A Practical Guide (Kotter R, ed), pp 123-138. Boston: Kluwer Academic Publishers.

Nimchinsky EA, Sabatini BL, Svoboda K (2002) Structure and function of dendritic spines. Annual Review of Physiology 64:313-353.

Novellino A, D'Angelo P, Cozzi L, Chiappalone M, Sanguineti V, Martinoia S (2007) Connecting Neurons to a Mobile Robot: An In Vitro Bidirectional Neural Interface. Computational Intelligence and Neuroscience 2007.

O'Donovan MJ, Chub N, Wenner P (1998) Mechanisms of spontaneous activity in developing spinal networks. Journal of Neurobiology 37:131-145.

Okatan M, Wilson MA, Brown EN (2005) Analyzing Functional Connectivity Using a Network Likelihood Model of Ensemble Neural Spiking Activity. Neural Computation 17:1927-1961.

Paninski L (2003) Estimation of Entropy and Mutual Information. Neural Computation 15:1191-1253.

Parnavelas JG, Lynch G, Brecha N, Cotman CW, Globus A (1974) Spine loss and regrowth in hippocampus following deafferentation. Nature 248:71-73.

Parrott L (2005) Quantifying the complexity of simulated spatiotemporal population dynamics. Ecological Complexity 2:175-184.

Parsons TD, Kleinfeld D, Raccuia-Behling F, Salzberg BM (1989) Optical recording of the electrical activity of synaptically interacting Aplysia neurons in culture using potentiometric probes. Biophysical Journal 56:213-221.

Parsons TD, Salzberg BM, Obaid AL, Raccuia-Behling F, Kleinfeld D (1991) Long-term optical recording of patterns of electrical activity in ensembles of cultured Aplysia neurons. J Neurophysiol 66:316-333.

Perlmutter JS, Mink JW (2006) Deep brain stimulation. Annu Rev Neurosci 29:229-257.

Pesaran B, Pezaris J, Sahani M, Mitra P, Andersen R (2002) Temporal structure in neuronal activity during working memory in macaque parietal cortex. Nature Neuroscience 5:805-811.

Pine J (1980) Recording action potentials from cultured neurons with extracellular microcircuit electrodes. J Neurosci Methods 2:19-31.

Potter SM (1996) Vital imaging: Two photons are better than one. Current Biology 6:1595-1598.

Potter SM (2000) Two-Photon Microscopy for 4D Imaging of Living Neurons. In: Imaging Neurons: A Laboratory Manual (Yuste R, Lanni F, Konnerth A, eds), pp 20.21-20.16. Cold Spring Harbor: CSHL Press.

Potter SM, DeMarse TB (2001) A new approach to neural cell culture for long-term studies. J Neuroscience Methods 110 17-24.

Potter SM, Fraser SE, Pine J (1997) Animat in a Petri Dish: Cultured Neural Networks for Studying Neural Computation. Proc 4th Joint Symposium on Neural Computation, UCSD:167-174.

Potter SM, Wagenaar DA, DeMarse TB (2006) Closing the Loop: Stimulation Feedback Systems for Embodied MEA Cultures. In: Advances in network electrophysiology using multi-electrode arrays (Taketani M, Baudry M, eds), pp 215-242. Kluwer, New York: Springer.

Potter SM, Lukina N, Longmuir KJ, Wu Y (2001) Multi-site two-photon imaging of neurons on multi-electrode arrays. SPIE Proceedings 4262:104-110.

Pouget A, Dayan P, Zemel R (2000) Information processing with population codes. Nat Rev Neurosci 1:125-132.

Prater JF (1998) Vagus nerve stimulation therapy for partial-onset seizures: a randomized active-control trial. Neurology 51:48-55.

Rambani K, Booth M, Brown E, Raikov I, Potter S (2005) Custom-made multiphoton microscope for long-term imaging of neuronal cultures to explore structural and functional plasticity. In: SPIE International Symposium, Photonics West 2005. San Jose, California USA.

Reger BD, Fleming KM, Sanguineti V, Alford S, Mussa-Ivaldi FA (2000) Connecting brains to robots: The development of a hybrid system for the study of learning in neural tissues. In: Proc. of the VIIth Intl. Conf. on Artificial Life, pp 263-272.

Reich DS, Victor JD, Knight BW, Ozaki T, Kaplan E (1997) Response Variability and Timing Precision of Neuronal Spike Trains In Vivo. J Neurophysiol 77:2836-2841.

Riva Sanseverino E, Galletti C, Maioli MG (1973) Responses to moving stimuli of single cells in the cat visual areas 17 and 18. Brain Res 55:451-454.

Rolston JD, Wagenaar DA, Potter SM (2007) Precisely-timed spatiotemporal patterns of neural activity in dissociated cortical cultures. Neuroscience 148:294-303.

Rosenkranz JA, Grace AA (1999) Modulation of Basolateral Amygdala Neuronal Firing and Afferent Drive by Dopamine Receptor Activation In Vivo. Journal of Neuroscience 19:11027-11039.

Ruaro ME, Bonifazi P, Torre V (2005) Toward the neurocomputer: Image processing and pattern recognition with neuronal cultures. IEEE Trans Biomed Eng 52:371-383.

Sakata JT, Brainard MS (2006) Real-Time Contributions of Auditory Feedback to Avian Vocal Motor Control. Journal of Neuroscience 26:9619.

Schaal S, Ijspeert A, Billard A, Vijayakumar S, Hallam J, Meyer J, eds (2004) From animals to animats 8 : Proceedings of the Eighth International Conference on the Simulation of Adaptive Behavior: Bradford Books

Schachter S, Saper C (1998) Vagus Nerve Stimulation. Epilepsia 39:677-686.

Scherg M (1990) Fundamentals of dipole source potential analysis. Advances in audiology 6:40-69.

Segal M (1983) Rat hippocampal neurons in culture: Responses to electrical and chemical stimuli. J Neurophys 50:1249-1263.

Segev R, Ben-Jacob E (2000) Generic Modeling of Chemotactic Based Self-Wiring of Neural Networks. Neural Networks 13:185-199.

Segev R, Benveniste M, Shapira Y, Ben-Jacob E (2003) Formation of electrically active clusterized neural networks. Phys Rev Lett 90:168101.

Shahaf G, Marom S (2001) Learning in Networks of Cortical Neurons. Journal of Neuroscience 21:8782-8788.

Sharma J, Angelucci A, Sur M (2000) Induction of visual orientation modules in auditory cortex. Nature 404:841-847.

Sheffler LR, Chae J (2007) Neuromuscular electrical stimulation in neurorehabilitation. Muscle & nerve 35:562-590.

Shefi O, Golding I, Segev R, Ben-Jacob E, Ayali A (2002) Morphological characterization of in vitro neuronal networks. Physical Review E 66:021905.

Shkolnik A (2003) Neurally controlled simulated robots: applying cultured neurons to handle and approach/avoidance task in real time, and a framework for studying learning in vitro. In: Dept. of Mathematics and Computer Science. Atlanta: Emory University.

Sims K (1994) Evolving virtual creatures. Proceedings of the 21st annual conference on Computer graphics and interactive techniques:15-22.

Song S, Miller KD, Abbott LF (2000) Competitive hebbian learning through spike-timing-dependent synaptic plasticity. Nature Neuroscience 3:919-926.

Steriade M (1996) Coherent oscillations and short-term plasticity in corticothalamic networks. J Physiol 497:19-29.

Steriade M, McCormick DA, Sejnowski TJ (1993) Thalamocortical oscillations in the sleeping and aroused brain. Science 262:679.

Sur M, Garraghty P, Roe A (1988) Experimentally induced visual projections into auditory thalamus and cortex. Science 242:1437-1441.

Suzurikawa J, Takahashi H, Kanzaki R, Nakao M, Takayama Y, Jimbo Y (2007) Light-addressable electrode with hydrogenated amorphous silicon and low-conductive passivation layer for stimulation of cultured neurons. Applied Physics Letters 90:093901.

Swadlow HA (1985) Physiological properties of individual cerebral axons studied in vivo for as long as one year. Journal of Neurophysiology 54:1346-1362.

Tateno T, Jimbo Y (1999) Activity-dependent enhancement in the reliability of correlated spike timings in cultured cortical neurons. Biological Cybernetics 80:45-55.

Timofeev I, Grenier F, Bazhenov M, Sejnowski TJ, Steriade M (2000) Origin of Slow Cortical Oscillations in Deafferented Cortical Slabs. Cerebral Cortex 10:1185-1199.

Tscherter A, Heuschkel MO, Renaud P, Streit J (2001) Spatiotemporal characterization of rhythmic activity in rat spinal cord slice cultures. European Journal of Neuroscience 14:179-190.

Uesaka N, Hayano Y, Yamada A, Yamamoto N (2007) Interplay between Laminar Specificity and Activity-Dependent Mechanisms of Thalamocortical Axon Branching. Journal of Neuroscience 27:5215.

Valverde P (1967) Apical dendritic spines of the visual cortex and light deprivation in the mouse. Experimental Brain Research 3:337-352.

Van Pelt J, Wolters PS, Corner MA, Rutten WLC, Ramakers GJA (2004) Longterm characterization of firing dynamics of spontaneous bursts in cultured neural networks. IEEE Trans Biomed Eng 51:2051-2062.

Ventura Vr, Cai C, Kass RE (2005) Trial-to-Trial Variability and Its Effect on Time-Varying Dependency Between Two Neurons. J Neurophysiol 94:2928-2939.

Wagenaar D, Pine J, Potter S (2004) Effective parameters for stimulation of dissociated cultures using multi-electrode arrays. J Neuroscience Methods 138:27-37.

Wagenaar D, Pine J, Potter S (2006a) Searching for plasticity in dissociated cortical cultures on multi-electrode arrays. Journal of Negative Results in BioMedicine 5:16.

Wagenaar D, Madhavan R, Pine J, Potter S (2005) Controlling Bursting in Cortical Cultures with Closed-Loop Multi-Electrode Stimulation. J Neuroscience 25:680-688.

Wagenaar DA, Potter SM (2002) Real-time multi-channel stimulus artifact suppression by local curve fitting. J Neuroscience Methods 120:113-120.

Wagenaar DA, Potter SM (2004) A versatile all-channel stimulator for electrode arrays, with real-time control. J Neural Eng 1:39-44.

Wagenaar DA, Nadasdy Z, Potter SM (2006b) Persistent dynamic attractors in activity patterns of cultured neuronal networks. Physical Review E 73:51907.

Wagenaar DA, Pine J, Potter SM (2006c) An extremely rich repertoire of bursting patterns during the development of cortical cultures. BMC Neurosci 7.

Wilson M, McNaughton B (1993a) Dynamics of the hippocampal ensemble code for space. Science 261:1055-1058.

Wilson MA, McNaughton BL (1993b) Dynamics of the hippocampal ensemble code for space. Science 261:1055-1058.

Wojtowicz JM, Atwood HL (1985) Correlation of presynaptic and postsynaptic events during establishment of long-term facilitation at crayfish neuromuscular junction. Journal of Neurophysiology 54:220-230.

Wong ROL, Meister M, Shatz CJ (1993) Transient period of correlated bursting activity during development of the mammalian retina. Neuron 11:923-938.

Xu J, Kang N, Jiang L, Nedergaard M, Kang J (2005) Activity-Dependent Long-Term Potentiation of Intrinsic Excitability in Hippocampal CA1 Pyramidal Neurons. Journal of Neuroscience 25:1750-1760.

Yang G, Masland RH (1992) Direct visualization of the dendritic and receptive fields of directionally selective retinal ganglion cells. Science 258:1949-1952.

Zhang W, Linden DJ (2003) The other side of the engram: experience-driven changes in neuronal intrinsic excitability. Nature Reviews Neuroscience 4:885-900.

Zucker RS (1989) Short-term plasticity. Annu Rev Neurosci 12:13-31.

Zykov V, Mytilinaios E, Adams B, Lipson H (2005) Self-reproducing machines. Nature 435:163-164.

VITA

ZENAS C. CHAO

Zenas was born in Hsinchu, Taiwan. He received this B.S. in Life Science and Chemistry from the National Tsing Hua Univeristy, Hsinchu, Taiwan and received honors from Phi Tau Phi Scholastic Honor Society of America Scholarship. After his graduation, he went to military service for two years. During this period, a devastated earthquake, which the people of Taiwan refer to it as 921, occurred. During his duty of relieving victims of the disaster, Zenas encountered his first doubt of being a scientist, which was his only dream since childhood. However, he still entered the Institute of Biomedical Sciences, Academia Sinica, Taipei, Taiwan in 2000, developing analytical tools for fMRI research. While still in confusion, he joined the Georgia Institute of Technology in 2001 to pursue a PhD in Bioengineering. During his PhD, Zenas published a series of journal articles and conference papers focusing on different parts of his design of closed-loop control of embodied cultured networks for goal-directed learning. He also was involved in several other publications on different forms of long-term plasticity in cultured networks, and gave several successful oral presentations in various conferences worldwide (SIMEA 2006, BMES 2006, and NER 2007). However, gradually Zenas realized his true enthusiasm is creating stories instead of proving them. He has published a series of short Taiwanese novels since 2003, and started filming in 2005. His future plan is to become a novelist, a script writer, and a film maker. His famous quote is “I’ll send you an invitation to the red carpet”.